PRODUCTION OF ALCOHOL DISPERSION CONTAINING CALCIUM HYDROXIDE AND MAGNESIUM HYDROXIDE NANOPARTICLES FOR DOLOMITE FORMATION AND CONSOLIDATION

A THESIS SUBMITTED TO
THE GRADUATE SCHOOL OF NATURAL AND APPLIED SCIENCES
OF
MIDDLE EAST TECHNICAL UNIVERSITY

BY

FULYA KARAHAN DAĞ

IN PARTIAL FULFILLMENT OF THE REQUIREMENTS
FOR
THE DEGREE OF DOCTOR OF PHILOSOPHY
IN
ARCHAEOMETRY

FEBRUARY 2021

Approval of the thesis:

PRODUCTION OF ALCOHOL DISPERSION CONTAINING CALCIUM HYDROXIDE AND MAGNESIUM HYDROXIDE NANOPARTICLES FOR DOLOMITE FORMATION AND CONSOLIDATION

submitted by **FULYA KARAHAN DAĞ** in partial fulfillment of the requirements for the degree of **Doctor of Philosophy** i**n Archaeometry, Middle East Technical University** by,

Prof. Dr. Halil Kalıpçılar
Dean, Graduate School of **Natural and Applied Sciences** _____

Prof. Dr. Gülay Ertaş
Head of the Department, **Archaeometry** _____

Assoc. Prof. Dr. Ayşe Tavukçuoğlu
Supervisor, **Archaeometry, METU** _____

Prof. Dr. Emine Nevin Caner-Saltık
Co-Supervisor, **Architecture, METU** _____

Examining Committee Members:

Prof. Dr. Asuman Günal Türkmenoğlu
Geological Engineering, METU _____

Assoc. Prof. Dr. Ayşe Tavukçuoğlu
Architecture, METU _____

Prof. Dr. Sinan Turhan Erdoğan
Civil Engineering, METU _____

Prof. Dr. Meriç Bakiler
Conservation and Restoration of Cultural Property,
Mimar Sinan Fine Arts Universtiy _____

Prof. Dr. Başak İpekoğlu
Architectural Restoration, Izmir Institute of Technology _____

Date: 12.02.2021

I hereby declare that all information in this document has been obtained and presented in accordance with academic rules and ethical conduct. I also declare that, as required by these rules and conduct, I have fully cited and referenced all material and results that are not original to this work.

Name, Last name : Fulya Karahan Dağ

Signature :

ABSTRACT

PRODUCTION OF ALCOHOL DISPERSION CONTAINING CALCIUM HYDROXIDE AND MAGNESIUM HYDROXIDE NANOPARTICLES FOR DOLOMITE FORMATION AND CONSOLIDATION

Karahan Dağ, Fulya
Doctor of Philosophy, Archaeometry
Supervisor: Assoc. Prof. Dr. Ayşe Tavukçuoğlu
Co-Supervisor: Prof. Dr. Emine Nevin Caner-Saltık

February 2021, 172 pages

Dolostone ($CaMg(CO_3)_2$ - calcium magnesium carbonate) has been a commonly-used building stone in the construction of many historical structures since the ancient periods. Those structures show deterioration problems in time and need conservation treatments. Repairs with incompatible materials are known to damage the original stone. In the context of dolomite conservation, there is a necessity to develop a consolidation material and treatment method that is compatible with the dolomite. The study aims to consolidate the dolostone by synthesizing dolomite within its deteriorated parts. For that purpose, alcohol dispersion of $Ca(OH)_2$ and $Mg(OH)_2$ nanoparticles was produced from the dolostone itself. This dispersion was allowed to react with CO_2 in a desiccator. The carbonation process was followed in petri dishes prior to consolidation treatment. It is found that the carbonation process is affected by relative humidity (RH) and CO_2 partial pressure (pCO_2) in the desiccator, and Mg:Ca ratio of the dispersion. The most effective dolomite formation is achieved by the carbonation process of $Ca(OH)_2$ and $Mg(OH)_2$ nanoparticles under high RH (90-95%) and high CO_2 partial pressure (pCO_2 ~ 0.4 atm) conditions in ethanol dispersion where Mg:Ca ratio is ~1. It is important not to disturb that system in the desiccator at least for 10 days for dolomitization. The carbonation products formed

in petri dishes were followed by means of XRD, FTIR, and SEM analyses. Afterwards, the deteriorated dolostone sample was treated with alcohol dispersion of $Ca(OH)_2$ and $Mg(OH)_2$ nanoparticles, and kept in a desiccator under high RH and high CO_2 partial pressure conditions for carbonation. The formation of dolomite aggregates having 100-200 nm size within the matrix of dolostone was confirmed by SEM analysis. Average UPV_{direct} value of the treated dolostone sample increased from ~1844 m/s to 2158 m/s. The carbonation products could join two broken dolostone pieces together, which shows its strong adhesion property. The production of this specific nano-consolidation material from the dolostone itself, the description of the consolidation treatment for dolostone, and the success in dolomite synthesis in the laboratory under the appropriate carbonation conditions are expected to provide an important contribution to stone conservation practices.

Keywords: Dolomite Synthesis, Dolostone, Calcium Hydroxide and Magnesium Hydroxide Nanoparticles, Alcohol Dispersion, Stone Consolidation

ÖZ

KALSİYUM HİDROKSİT VE MAGNEZYUM HİDROKSİT NANO TANELİ ALKOL DİSPERSİYONU ÜRETİMİ İLE DOLOMİT OLUŞTURMA VE SAĞLAMLAŞTIRMA

Karahan Dağ, Fulya
Doktora, Arkeometri
Tez Yöneticisi: Doç. Dr. Ayşe Tavukçuoğlu
Ortak Tez Yöneticisi: Prof. Dr. Emine Nevin Caner-Saltık

Şubat 2021, 172 sayfa

Dolomit taşı ($CaMg(CO_3)_2$ – kalsiyum magnezyum karbonat), antik dönemlerden beri birçok tarihi yapının yapımında yaygın olarak kullanılan önemli bir yapı taşıdır. Bu yapılar zamanla bozulma sorunları gösterebilir ve korunmaya ihtiyaç duyarlar. Dolomit taşının korunmasında, taşın bünyesine uygun olmayan malzemeler ve kimyasallar ile yapılan sağlamlaştırma işlemlerinin özgün taşa zarar verdiği bilindiğinden, taşın yapısı ile uyumlu bir sağlamlaştırma malzemesinin kullanılması gereği şarttır. Bu çalışmada, yıpranmış dolomit taşının bozulmuş kısımlarında yine dolomit sentezleyerek sağlamlaştırılması hedeflenmiştir. Bunun için, taşın kendisinden üretilmiş $Ca(OH)_2$ ve $Mg(OH)_2$ nanotaneli alkol dispersiyonu hazırlanmıştır. Bu dispersiyon, desikatör içerisinde CO_2 ile reaksiyona sokularak karbonatlaşma işleminin gerçekleşmesi sağlanmıştır. Taşa uygulama yapmadan önce, karbonatlaşma işlemi petri kaplarında izlenmiştir. Karbonatlaşma işleminin, desikatördeki bağıl nem ve CO_2 kısmi basıncından ve dispersiyonun Mg:Ca oranından etkilendiği görülmüştür. En etkili dolomit oluşumu, $Ca(OH)_2$ ve $Mg(OH)_2$ nanotanelerinin, yüksek bağıl nem (90-95%) ve yüksek CO_2 kısmi basıncı (pCO_2~0.4 atm) altında, Mg:Ca oranının yaklaşık 1 olduğu etil alkol

dispersiyonunda karbonatlaşması ile sağlanmıştır. Dolomitleşme için desikatörde oluşan sistemin en az 10 gün rahatsız edilmemesi gereklidir. Petri kabında oluşan ürünler XRD, FTIR ve SEM ile takip edilmiştir. Daha sonra $Ca(OH)_2$ ve $Mg(OH)_2$ nanotaneli alkol dispersiyonu yıpranmış dolomit taşının içine nüfuz ettirilerek, yüksek bağıl nem ve yüksek CO_2 basıncı altındaki desikatöre konmuş ve solüsyonun taşın içinde karbonatlaşması sağlanmıştır. Karbonatlaşma işlemi sonucunda, 100-200 nm boyutunda dolomit agregalarının taşın içerisinde oluştuğu SEM ile gözlemlenmiştir. Yıpranmış taşın ortalama ultrasonik hızı yaklaşık 1844 m/s'den 2158 m/s'ye yükselmiştir. Bunlara ek olarak, oluşan karbonatlaşma ürünlerinin, yani dolomitin, iki kırık parçayı bir arada tutabilecek kadar güçlü yapıştırma özelliği olduğu görülmüştür. Dolomit taşının kendisinden başlayarak bu özgün sağlamlaştırma malzemesinin üretilebilmesinin, sağlamlaştırma uygulamasının tariflenebilmesinin ve laboratuvar ortamında dolomit sentezinin başarılmasının, taş koruma uygulamalarına büyük katkı sağlaması beklenmektedir.

Anahtar Kelimeler: Dolomit Sentezi, Dolomit Taşı, Kalsiyum Hidroksit, Magnezyum Hidroksit, Nanotaneli Alkol Solüsyonu, Taş Sağlamlaştırma

to my grandparents & family

ACKNOWLEDGMENTS

I would like to present my sincere thanks to my supervisors Prof. Dr. Emine N. Caner Saltık and Assoc. Prof. Dr. Ayşe Tavukçuoğlu for their guidance and support throughout my Ph.D. studies at METU. They always encouraged me to go further in my studies. I learned how to develop in the study by asking relevant questions from them.

Special thanks to Prof. Dr. Mustafa Tokyay and Prof. Dr. Asuman Günal Türkmenoğlu for their valuable comments and ideas we discussed during thesis monitoring committee meetings.

I also thank all of my friends from METU Materials Conservation laboratory due to their friendship and support. Especially, Fatıma Erol's support was worthy of note.

Throughout my Ph.D. education, I worked as a research assistant and then as an instructor at the Graduate School of Natural and Applied Sciences (GSNAS). I would like to thank my directors for encouraging me to continue my studies and providing me flexible working hours to do my experimental work at the laboratory. Moreover, thanks to second-floor colleagues at GSNAS for showing understanding. Especially, I would like to thank Münevver Gün for her support when I was at the laboratory.

I would like to thank my family, especially my daughter Duru Deniz Dağ and my son Aras Dağ, for the time I took from them. Also, to my husband Bülent Dağ for his support and taking care of the home and kids.

I would like to thank my mother, Leyla Karahan, for helping me take care of my children and rising them while I was studying, and thanks to Adalet Dağ for her support.

TABLE OF CONTENTS

ABSTRACT v

ÖZ…. vii

ACKNOWLEDGMENTS x

TABLE OF CONTENTS xi

LIST OF TABLES xvi

LIST OF FIGURES xvii

CHAPTERS

1 INTRODUCTION 1

1.1 Argument 3

1.2 Aims and Objectives 5

1.3 Disposition 6

2 LITERATURE REVIEW 9

2.1 Characteristics and Formation of Dolomite 10

2.1.1 Dolomite Occurrence in Nature 10

2.1.2 Dolomite Problem: Kinetic Factors Inhibiting Its Formation 12

2.1.3 Thermodynamic Factors and Suggested Reaction Mechanisms for Dolomitization Process 14

2.2 Precursor Minerals in Dolomite Formation and Some of Their Basic and Thermodynamic Properties 15

2.2.1 Calcium Carbonate Minerals and The Effect of Magnesium on the Crystallization of Calcite and Aragonite 16

2.2.2 Magnesium Carbonate Minerals 18

2.2.3 Calcium-Magnesium Carbonate Minerals 22

2.2.4 Thermodynamic Properties of Some Minerals Formed in Ca-Mg-CO_2-H_2O System 23

2.3 Crystallography of Dolomite and Its Verification by XRD 25

2.4 Some Studies on Dolomite Formation and Arguments Concerning Mechanisms, Conditions, and Analyses 28

2.5 Dedolomitization-Dissolution of Dolomite 33

2.6 Some Characteristics at Nanoscale and Use of Hydroxide Nanoparticles as Consolidants for the Conservation of Cultural Heritage 35

2.7 Carbonation Process of Hydroxide Nanoparticles 37

3 MATERIALS AND METHODS 39

3.1 Major Analytical Equipment and Tools Used for the Analyses 39

3.2 Dolostone Used in the Study 42

3.3 Preparation and Examination of Alcohol Dispersion of $Mg(OH)_2$ Nanoparticles 48

3.4 Carbonation of $Mg(OH)_2$ Nanoparticles Dispersed in Ethanol 48

3.5 Preparation and Examination of Alcohol Dispersion of $Ca(OH)_2$ and $Mg(OH)_2$ Nanoparticles 49

3.5.1 Calcination of Midyat Dolostone 49

3.5.2 Slaking of CaO and MgO 50

3.5.3 Dispersion and Stability of $Ca(OH)_2$ and $Mg(OH)_2$ Nanoparticles in Ethanol 50

3.6 Carbonation of $Ca(OH)_2$ and $Mg(OH)_2$ Nanoparticles Dispersed in Ethanol 51

3.6.1 Carbonation of $Ca(OH)_2$ and $Mg(OH)_2$ Nanoparticles Under High Relative Humidity (90-95%) and High CO_2 Partial Pressure ($p(CO_2)$~0.4 atm) Conditions 52

3.7 Carbonation of $Ca(OH)_2$ on Nesquehonite 54

3.8 Preparation of Control Samples and Mixtures for XRD and FTIR Analyses ……...54

3.9 Consolidation Experiments 55

3.9.1 Consolidation Experiments with Dolostone and Evaluation of Effectiveness of Consolidation Treatment 55

3.9.2 Adhesive Property of Carbonation Products 59

4 RESULTS 61

4.1 Analyses of Preparation Stages of $Mg(OH)_2$ Nanoparticles from Magnesite ……...61

4.2 Carbonation of $Mg(OH)_2$ Nanoparticles 63

4.3 Analyses of the Preparation Stages of Alcohol Dispersion of $Ca(OH)_2$ and $Mg(OH)_2$ Nanoparticles from Midyat Dolostone 66

4.3.1 Stability of Alcohol Dispersion of $Ca(OH)_2$ and $Mg(OH)_2$ Nanoparticles and the Changes in the Mg:Ca Ratio of the Solution 72

4.4 Carbonation Experiments of $Ca(OH)_2$ and $Mg(OH)_2$ Nanoparticles..... 76

4.4.1 Carbonation of $Ca(OH)_2$ and $Mg(OH)_2$ Nanoparticles at Room Condition..... 77

4.4.2 Carbonation of $Ca(OH)_2$ and $Mg(OH)_2$ Nanoparticles at High Relative Humidity and Low CO_2 Partial Pressure Conditions 77

4.5 Carbonation of $Ca(OH)_2$ and $Mg(OH)_2$ Nanoparticles at High Relative Humidity and High CO_2 Partial Pressure Conditions Using Alcohol Dispersion with Mg:Ca ratio ~2: Set-1 78

4.5.1 XRD Analyses 78

4.5.2 FTIR Analyses 84

4.5.3 SEM and EDAX Analyses 87

4.5.4 XRD and FTIR Analyses of Control Mixtures 96

4.6 Carbonation of $Ca(OH)_2$ and $Mg(OH)_2$ Nanoparticles at High Relative Humidity and High CO_2 Partial Pressure Conditions Using Alcohol Dispersion with Mg:Ca ratio ~1: Set 2 101

4.6.1 XRD Analyses 102

4.6.2 FTIR Analyses 110

4.6.3 Stereomicroscope Images 112

4.6.4 SEM Analyses 112

4.7 Carbonation of $Ca(OH)_2$ nanoparticles on Nesquehonite 121

4.8 Consolidation Treatment of Deteriorated Dolomite with Alcohol Dispersion of $Ca(OH)_2$ and $Mg(OH)_2$ Nanoparticles 122

4.8.1 Microstructure of Dolomite Before and After Consolidation Treatment 122

4.8.2 Basic Physico-mechanical Properties of Deteriorated Dolomite Before and After Consolidation Treatment 133

4.8.3 Adhesive Property of the Treatment by Injection of Alcohol Dispersion Through the Crack of Broken Dolomite Cube 136

5 DISCUSSION 139

5.1 Carbonation Characteristics of $Mg(OH)_2$ Nanoparticles Dispersed in Ethanol 140

5.2 Characteristics of Alcohol Dispersion of $Ca(OH)_2$ and $Mg(OH)_2$ Nanoparticles 140

5.3 Carbonation Characteristics of $Ca(OH)_2$ and $Mg(OH)_2$ Nanoparticles Dispersed in Ethanol in Relation to Changes in Relative Humidity and CO_2 Partial Pressure 142

5.4 Carbonation of $Ca(OH)_2$ and $Mg(OH)_2$ Nanoparticles in Alcohol Dispersion with Mg:Ca ratio ~2 (set-1) 143

5.5 Carbonation of $Ca(OH)_2$ and $Mg(OH)_2$ Nanoparticles in Alcohol Dispersion with Mg:Ca ratio ~1 (set-2): Towards Dolomite Formation 146

5.5.1 Towards Dolomitization 147

5.5.2 Effect of Mg:Ca Ratio on Dolomitization 152

5.6 Consolidation of Deteriorated Dolostone with the Alcohol Dispersion of $Ca(OH)_2$ and $Mg(OH)_2$ Nanoparticles 152

5.7 Production Specifications of the Alcohol Dispersion of $Ca(OH)_2$ and $Mg(OH)_2$ Nanoparticles from Dolostone 153

6 CONCLUSION 155

REFERENCES 157

CURRICULUM VITAE 171

LIST OF TABLES

TABLES

Table 1. Activity and Enthalpy of hydration values of corresponding ions in seawater chemistry at 25ºC 15
Table 2. Some thermodynamic properties of some calcium and magnesium minerals: solubility products were measured in the concentrated salt solution. 23
Table 3. Standard free energies of formations of some minerals in the Ca-Mg-CO_3 system 23
Table 4 Gibb's free energies of formations of some minerals in the Ca-Mg-CO_3 system 24
Table 5. Unit cell and XRD information for ideal dolomite versus calcite(CuKα radiation). * Denotes dolomite ordering peaks. 27
Table 6. Peak locations and d-values of XRD traces of Midyat Dolostone.*denotes dolomite ordering peaks 43
Table 7. Physical and Physicomechanical Properties of Midyat dolostone. 47
Table 8. XRD data of synthesized nesquehonite 65
Table 9. Mg:Ca ratio versus time according to the intensity of **second intense peak**s of brucite and portlandite in XRD traces 75
Table 10. Comparision of XRD traces of Midyat Dolomite(MD) versus Synthesized Dolomite (SD) 110
Table 11. Direct UPV Measurement of a weathered dolostone sample with 5x5x5 cm^3 dimensions before (bt) and after (at) treatment. 134

LIST OF FIGURES

FIGURES

Figure 1. Representation of rhombohedral unit cell of dolomite 10
Figure 2. Probable stability relations in the system MgO-CO_2-H_2O between 0ºC and 100 ºC as a function of pCO_2 and assuming aH_2O = 1 19
Figure 3. Crystal structure of nesquehonite in projections parallel to b.Drawings were obtained using the ATOMS program..... 20
Figure 4. Phase diagram of the system $CaCO_3$-$MgCO_3$-H_2O for zero ionic strength at 25ºC. The metastable phases occurring in the system are indicated in italics. The black dot corresponds to the conditions of seawater..... 24
Figure 5. Powder XRD patterns (CuKα) comparing dolomite and calcite from 20 to 55.8 2θ. A) Bonneterre dolomite (Cambrian, Missouri) exhibiting cation ordering. Dolomite peaks are labeled with their corresponding Bravais-Miller indices, with the ordering reflections indicated by an asterisk. B) Optical-grade calcite for comparison showing lack of dolomite ordering reflections.. 26
Figure 6. X-ray diffraction patterns of dolomite and very high magnesium calcite. Dolomite from the 'back reef' facies of the Bonneterre Dolomite (Cambrian) Missouri (up). HMC from a coralline algae (Goniolithon sp.) San Salvador Island, Bahamas(down). Calcite reflections are labeled. Note the pronounced shift of the 104 reflection towards a lower d-value. This shift is caused by a contraction of the calcite unit cell resulting from Mg^{2+} substitution for Ca^{2+}. Broadening of the reflections relative to those in calcite may be due to the exceptionally small crystallite size that is typical of HMC precipitated by coralline algae 28
Figure 7. Comparision of XRD reflections of standard dolomite with a series of products made in low-temperature (25–45 ºC) microbial experiments. 32
Figure 8. Representation of Direct UPV Measurement 41
Figure 9. Location of Yolbaşı town in Midyat-Mardin, in Turkey..... 42
Figure 10. XRD traces of dolostone sample taken from Midyat-Yolbaşı quarries: D-Dolomite 43

Figure 11. FTIR spectrum of Midyat dolostone 44
Figure 12. Stereomicroscopic view of macro-pores of Midyat dolostone in a cross-section at 20x magnification 44
Figure 13. Photographic image of Midyat dolostone samples where veins appear (up) and Stereomicroscope image of the vein and orange colors around veins (down) . 45
Figure 14. The insoluble acid part of Midyat dolostone, filtered and dried. 46
Figure 15. SEM-EDAX image of acid-insoluble part of the dolostone sample at 500x magnification: showing the presence of silicon, aluminum, and iron. 46
Figure 16. SEM-EDAX image of acid-insoluble part of the dolostone sample at 5000x magnification: showing the presence of oxides of titanium and silicon 47
Figure 17. SEM images of Midyat dolostone pores: The general view of a big pore (400x) left; detailed views of crystals inside the pores: (10000x) middle and (40000x) right 48
Figure 18. Pulverization and calcination stages of dolostone. 50
Figure 19. Application methods of alcohol dispersion of $Ca(OH)_2$ and $Mg(OH)_2$ nanoparticles for consolidation/treatment of deteriorated dolostone sample 56
Figure 20. Representation of carbonation process of dolostone samples in desiccator with high RH and high CO_2 partial pressure. 56
Figure 21. x(front)-x'(back) faces of dolostone cube with around 5*5*5 cm^3 dimensions 58
Figure 22. y(front)-y'(back) faces of dolostone cube with around 5*5*5 cm^3 dimensions 58
Figure 23. z(front)-z'(back) faces of dolostone cube with around 5*5*5 cm^3 dimensions 58
Figure 24.Broken dolostone cube before treatment with alcohol dispersion of $Ca(OH)_2$ and $Mg(OH)_2$ nanoparticles 59
Figure 25. XRD analysis of calcination product of $MgCO_3$: P: Periclase (MgO) .. 62
Figure 26. XRD trace of slaked product of MgO: B: Brucite ($Mg(OH)_2$), P: Periclase (MgO) 62

Figure 27. Stereomicroscope images of nesquehonite crystals formed after carbonation of $Mg(OH)_2$ at high relative humidity and high CO_2 partial pressure: 10x (up) and 30x (down)..... 64
Figure 28. XRD analysis of carbonation product of $Mg(OH)_2$ at the 10th day: N: Nesquehonite ($MgCO_3.3H_2O$) 65
Figure 29. FTIR Spectrum of nesquehonite synthesized from $Mg(OH)_2$ nanoparticles. 66
Figure 30. XRD traces of products formed after calcination of dolostone 67
Figure 31. XRD traces of slaking products of CaO and MgO. B: Brucite ($Mg(OH)_2$), P: Portlandite ($Ca(OH)_2$)..... 68
Figure 32. FTIR Spectrum of $Ca(OH)_2$ and $Mg(OH)_2$ hydroxide nanoparticles in dry state before dispersion in alcohol..... 69
Figure 33. FTIR Spectrum of $Ca(OH)_2$ and $Mg(OH)_2$ hydroxide nanoparticles after dispersion in alcohol 70
Figure 34. SEM image of $Ca(OH)_2$ and $Mg(OH)_2$ nanoparticles in the form of aggregates: 80000x. Smaller particles belong to $Mg(OH)_2$, and bigger particles belong to $Ca(OH)_2$ 70
Figure 35. SEM-EDAX of large clusters belonging to $Ca(OH)_2$:EDAX analysis of yellow squared part. 71
Figure 36. SEM-EDAX of smaller clusters belonging to $Mg(OH)_2$: EDAX analysis of red squared part. 71
Figure 37. XRD traces of $Ca(OH)_2$ and $Mg(OH)_2$ nanoparticles dispersed in ethanol, in the beginning-no settlement: P: Portlandite $Ca(OH)_2$ and B: Brucite $Mg(OH)_2$ 73
Figure 38. XRD traces of $Ca(OH)_2$ and $Mg(OH)_2$ nanoparticles dispersed in ethanol, after 4 hours of settlement: P:Portlandite $Ca(OH)_2$ and B:Brucite $Mg(OH)_2$..... 73
Figure 39. XRD traces of $Ca(OH)_2$ and $Mg(OH)_2$ nanoparticles dispersed in ethanol ,after 24 hours of settlement: P:Portlandite $Ca(OH)_2$ and B:Brucite $Mg(OH)_2$..... 74
Figure 40. XRD traces of $Ca(OH)_2$ and $Mg(OH)_2$ nanoparticles dispersed in ethanol, after 44 hours of seetlement: P:Portlandite $Ca(OH)_2$ and B:Brucite $Mg(OH)_2$ 74

Figure 41. XRD traces of $Ca(OH)_2$ and $Mg(OH)_2$ nanoparticles dispersed in ethanol, after 72 hours of settelement: P:Portlandite $Ca(OH)_2$ and B:Brucite $Mg(OH)_2$ 75
Figure 42. Mg:Ca ratio in the alcohol dispersion vs time of settlement.....76
Figure 43. Carbonation of $Ca(OH)_2$ and $Mg(OH)_2$ nanoparticles dispersed in ethanol, at room condition for 4 weeks. B: Brucite; C: Calcite; P: Portlandite 77
Figure 44. Carbonation of $Ca(OH)_2$ and $Mg(OH)_2$ nanoparticles dispersed in ethanol, at high RH and low CO_2 pressure for 4 weeks. C: Calcite, N: Nesquehonite.....78
Figure 45. XRD traces of carbonation products of $Ca(OH)_2$ and $Mg(OH)_2$ nanoparticles dispersed in ethanol, at high RH and high CO_2 pressure for 3 hours. P: Portlandite, B:Brucite, C: Calcite.....79
Figure 46. XRD traces of carbonation products of $Ca(OH)_2$ and $Mg(OH)_2$ nanoparticles dispersed in ethanol, at high RH and high CO_2 pressure for 1 day. P: Portlandite, B: Brucite, C: Calcite.....80
Figure 47. XRD traces of carbonation products of $Ca(OH)_2$ and $Mg(OH)_2$ nanoparticles dispersed in ethanol, at high RH and high CO_2 pressure for 3 days. N: Nesquehonite, C: Calcite, D: Dolomite.....80
Figure 48. XRD traces of carbonation products of $Ca(OH)_2$ and $Mg(OH)_2$ nanoparticles dispersed in ethanol, at high RH and high CO_2 pressure for 7 days. N: Nesquehonite, C: Calcite, D: Dolomite.....81
Figure 49. XRD traces of carbonation products of $Ca(OH)_2$ and $Mg(OH)_2$ nanoparticles dispersed in ethanol, at high RH and high CO_2 pressure for 17 days. N: Nesquehonite, C: Calcite, D: Dolomite.....82
Figure 50. XRD traces of carbonation products of $Ca(OH)_2$ and $Mg(OH)_2$ nanoparticles dispersed in ethanol, at high RH and high CO_2 pressure for 21 days. N: Nesquehonite, C: Calcite, D: Dolomite.....82
Figure 51. XRD traces of carbonation products of $Ca(OH)_2$ and $Mg(OH)_2$ nanoparticles dispersed in ethanol, at high RH and high CO_2 pressure for 28 days. N: Nesquehonite, C: Calcite, D: Dolomite.....83

Figure 52. XRD traces of carbonation products of $Ca(OH)_2$ and $Mg(OH)_2$ nanoparticles dispersed in ethanol, at high RH and high CO_2 pressure for 58 days. N: Nesquehonite, C: Calcite, D: Dolomite. 83
Figure 53. XRD traces of carbonation products of $Ca(OH)_2$ and $Mg(OH)_2$ nanoparticles dispersed in ethanol, at high RH and high CO_2 pressure for 7 months. N: Nesquehonite, C: Calcite, D: Dolomite. 84
Figure 54. FTIR Spectrum of standard calcite. 85
Figure 55. FTIR Spectrum of Midyat dolomite 85
Figure 56. FTIR Spectrum of the mixture of standard calcite and dolomite. 86
Figure 57. FTIR spectrum of carbonation products of $Ca(OH)_2$ and $Mg(OH)_2$ nanoparticles after 28 days. 87
Figure 58. FTIR spectrums of control mixture of dolomite and calcite (blue), nesquehonite (green) and carbonation products (red) 87
Figure 59. SEM images of carbonation products at the 7th day: calcite aggregates 5000x (up, left), 20000x (up, right), 80000x (down). 88
Figure 60. SEM image of carbonation products at the 7th day: Nesquehonite aggregates with calcite aggregates associated with it: 1000x (up, left), 5000x (up, right), 20000x (down) 89
Figure 61. SEM images of carbonation products in the 17th day: calcite or dolomite aggregates 5000x (up, left), 20000x (up, right), 80000 (down). 90
Figure 62. SEM images of carbonation products on the 17th day: nesquehonite, and calcite aggregates 1000x(left), and closer view showing aggregates of calcite or dolomite nanoparticles 10000 (right). 91
Figure 63. SEM EDAX results of the red squared region, nanoparticle aggregates on nesquhonite. 91
Figure 64. SEM images of carbonation products on the 21st day: general view 1000x (up, left), 5000x (up, right), closer view showing nanoparticles aggregates of dolomite having sizes around 100-500 nm10000x (down) 92

Figure 65. SEM-EDAX analysis of nesquehonite needle itself (up, yellow squared part of Fig.63), and of the aggregates of nanoparticles next to nesquehonite needle (down, red squared part of Fig 63) on the 21st day. 93
Figure 66. SEM images of carbonation products at 28th day 200x (up, left), 5000x of elongated aggregate (up, right) showing newly formed crystals on nesquehonite, 5000x of smaller aggregates belonging to calcite or dolomite (down). 94
Figure 67. SEM image of carbonation products at 58th day: A dissociated nesquehonite aggregate 500x(up), SEM-EDX analysis of crystals near nesquehonite (green squared part) showing very close Mg:Ca ratio (down). 95
Figure 68. XRD traces of Calcite and Nesquehonite mixtures with the ratios a) Ca:Nes-0.8:0.2, b) Ca:Nes-0.6:0.4 97
Figure 69. FTIR of Calcite and Dolomite mixture with a ratio of 0.2:0.8. 99
Figure 70. FTIR of Calcite and Dolomite mixture with a ratio of 0.4:0.6 99
Figure 71. FTIR of Calcite and Dolomite mixture with a ratio of 0.5:0.5. 100
Figure 72. FTIR of Calcite and Dolomite mixture with a ratio of 0.6:0.4 100
Figure 73. FTIR of Calcite and Dolomite mixture with a ratio of 0.8:0.2. 101
Figure 74. XRD traces of carbonation products in petri dish, upper layer, 1 day of carbonation 103
Figure 75. XRD traces of carbonation products in petri dish, bottom layer, 1 day of carbonation 103
Figure 76. XRD traces of carbonation products in petri dish, upper layer, 2 days of carbonation 104
Figure 77. XRD traces of carbonation products in petri dish, bottom layer, 2 days of carbonation 104
Figure 78. XRD traces of carbonation products in petri dish, upper layer, 3 days of carbonation 105
Figure 79. XRD traces of carbonation products in petri dish, bottom layer, 3 days of carbonation 105
Figure 80. XRD traces of carbonation products in petri dish, upper layer, 4 days of carbonation 106

Figure 81. XRD traces of carbonation products in petri dish, bottom layer, 4 days of carbonation 106
Figure 82. XRD traces of carbonation products in petri dish, upper layer, 5 days of carbonation 107
Figure 83. XRD traces of carbonation products in petri dish, bottom layer, 5 days of carbonation 107
Figure 84. XRD traces of carbonation products in petri dish, upper layer, 10 days of carbonation 108
Figure 85. XRD traces of carbonation products in petri dish, bottom layer, 10 days of carbonation 108
Figure 86. XRD traces of synthesized dolomite compared with Midyat dolostone sample (red). 109
Figure 87.FTIR spectra of dolomite formed at the upper layer at the tenth day... 111
Figure 88. FTIR spectrum of dolomite formed at the upper layer (black) and FTIR spectrum of Midyat dolomite (blue) 111
Figure 89. Stereomicroscope images of carbonation products in petri dish (left: 10x, right: 50x magnification) 112
Figure 90. SEM image of carbonation products of upper layer at the first day. Hydroxide particles seems as aggregates integrated within each other (40000x-up and 100000x-down) 113
Figure 91. SEM image of carbonation products of upper layer at the second day. In that layer hydroxide nanoparticles seems to be carbonated as aggregates of calcite, dolomite (or maybe magnesium calcite) and nesquehonite (10000x-up and 40000x-down) 114
Figure 92. Closer view of aggregates having calcite, dolomite and nesquehonite aggregates integrated within each other (100000x magnification) 115
Figure 93. SEM image of carbonation products of upper layer at the tenth day. showing dolomite aggregates (at 10000x magnification) 116
Figure 94. Closer view showing dolomite aggregates around 500 nm and smaller ones down to around 100 nm (200000x magnification) 117

Figure 95. Another view of the upper layer at the tenth day: SEM images of carbonation products showing dolomite aggregates (up:5000x, down: 50000x magnification).....118
Figure 96. Closer SEM view showing dolomite aggregates around 500 nm and smaller ones having down to around 25-50 nm particles. 119
Figure 97. EDAX analysis of nanoparticle aggregates at the upper layer (at 200000x).(yellow squared part).....120
Figure 98. SEM images of carbonation products in petri dish at the bottom layer at the tenth day: 500x (left), 5000x (middle), 100000x (right). 120
Figure 99. EDAX analysis of aggregates at the bottom layer (at 100000x).....121
Figure 100. XRD traces of carbonation products of $Ca(OH)_2$ nanoparticles added onto nesquehonite crystals for two months. 121
Figure 101. Stereomicroscope images of the main crack of dolostone sample before treatment: 10x (up) and 145x (down). 123
Figure 102. Stereomicroscope images of cracks of dolostone sample after treatment: 10x (up), 40x (middle), 145x (bottom). 124
Figure 103. SEM image of dolostone sample before treatment: 50000x (dolomite grain, from cross-section). 125
Figure 104. EDAX analysis of dolomite grain of untreated dolostone (at 50000x). 125
Figure 105. SEM image of dolostone surface after consolidation treatment: 2000x (dolomite layer) 126
Figure 106. Closer view to the surface of treated dolomite sample (up-10000x and down-40000x).....127
Figure 107. A general view from the cross-section surface of the treated dolostone sample. The red arrow at the right of the image corresponds to the side from where alcohol dispersion was applied: 1000x.....128
Figure 108. SEM view of the cross-section surface from the area close to the treatment surface (10000x-up, 20000x-down) 129

Figure 109. Another SEM view from the cross-section surface of treated dolostone sample:10000x-up, 50000x-down) 130
Figure 110. SEM view of the cross-section surface of treated dolostone sample showing the newly formed dolomite crystals on original dolomite crystals' edges and integration of them at 100000x magnification. 131
Figure 111. SEM view of the cross-section surface from the area close to the treatment surface (100000x-up, 200000x-down showing newly formed dolomite particles around 100-200nm) 132
Figure 112. Broken dolostone sample after consolidation treatment with alcohol dispersion of nanoparticles; broken parts joined together. 137

CHAPTER 1

INTRODUCTION

Cultural heritage is very important for a nation because it represents the history and culture of the past. It provides maintenance of identity in a fast-changing world for future generations. Historical structures are precious for their architectural and aesthetic values. Those structures present several decay problems in time, and they cannot fulfill the purpose for which they were built so, they need conservation treatments. In the conservation of cultural heritage, the critical issues are to identify the problems that the historical structure or material suffers, and to offer a solution or action for conservation. In the context of stone conservation issues, when consolidation treatment is needed, it is necessary to choose consolidation materials that have similar properties with the original material. The treatment is expected to be compatible and provide long-term durability. Therefore, the characteristics of the material, its state of conservation, the degradation mechanism, and the environmental factors affecting deterioration should be well analyzed before any treatment.

In the conservation of cultural heritage, the use of compatible materials has been gaining importance recently. Especially, alcohol dispersions of nanoparticles have been studied for various conservation purposes since nanoparticles can easily penetrate through the stone in alcohol dispersion, and they show enhanced properties due to their small sizes. Especially, hydroxide nanoparticles of calcium, magnesium, barium, strontium, etc., are presented to be effective in the conservation of many historical materials like stone, wood, paper, wall paintings, etc. (Sierra-Fernandez *et al*., 2017). They react with atmospheric CO_2 to form their carbonates and act as a filler or binder.

Dolostone (dolomite-$CaMg(CO_3)_2$) (calcium magnesium carbonate) has been a widely used building stone in the construction of many historical structures and archaeological settlements since the archaeological periods. As an example, Sivas Divriği Ulu Camii and Darüşşifası (13^{th} century), being on World Heritage List since 1985, is one of the medieval examples in Anatolia whose building stone is dolomite (Caner *et al*., 1985; Caner-Saltık, 2009). Those structures may show decay problems in time and need conservation treatments with compatible consolidation materials.

For the consolidation of dolomite, the ideal method is to synthesize dolomite mineral within the weak parts of the stone. On the other hand, dolomite can only be observed in specific geological environments. It is a unique mineral whose synthesis is challenging under normal atmospheric conditions at the laboratory due to kinetic inhibitions, such as the difficulty in the formation of regularly interchanging planes of calcium and magnesium cations between each carbonate anions in a growing dolomite crystal. Many researchers tried to understand the origin and precipitation mechanism of dolomite, and the circumstances under which it is formed. However, there is no exact evidence about its synthesis in the laboratory under atmospheric conditions.

The study deals with the production of a new, remedial, and compatible nanomaterial (alcohol dispersion of $Ca(OH)_2$ and $Mg(OH)_2$ nanoparticles), which can form dolomite after the carbonation process under specific conditions and be used in the consolidation of deteriorated dolomite. The argument and main objectives of the research are explained under the respective subheadings.

The term “dolomite” used in the text refers both to the mineral and the building stone composed of dolomite. In the literature, the terms such as; dolomite rock, dolostone, or dolomitic limestone are also used to distinguish the rock dolomite from the mineral dolomite. In the thesis, dolostone refers to dolomitic rock.

1.1 Argument

For the conservation of historical structures constructed with dolostone, a consolidation material compatible with the dolomite microstructure is needed. To produce such a material, primarily diagnostic investigations have to be done to identify and eliminate the sources of the deterioration problems. Afterwards, comprehensive field and laboratory analyses, conservation treatments targeted to deteriorated zones should be planned and applied to ensure the structure's long-term durability. As one of the conservation treatment, consolidation of stone helps to stabilize degraded or weakened areas by introducing or attaching materials capable of holding them together.

One of the major factors that cause dolostone deterioration is the sulphate (SO_4^{2-}) inclusion to its structure, which gives rise to the formation of sulphate salts within the stone, resulting in serious damage (Lopez-Arce *et al*., 2009). The sulphate source might be sulphate bearing repair materials or air pollution. For instance, as seen in the case of Sivas Divriği Ulu Camii, when cement-based repair mortars are used in contact with dolostone, they form slightly basic conditions (pH~8-9) in damp areas of the monument. At those damp parts, dolomite dissociates and gives out its magnesium. The reaction between Mg^{2+} and SO_4^{2-}gives rise to the formation of $MgSO_4$ salts of epsomite and hexahydrate in damp areas of the monument, which triggers the salt decay mechanism resulting in materials loss in the forms of powdering, scale and flake formations, and breakdowns (Caner *et al*., 1985; Caner - Saltık, 2009).

When Portland cement mortars are used in repairs of dolostone, due to the high solubility of $Ca(OH)_2$ in cement, it dissociates to Ca^{2+} and OH^- ions, the pH of the medium rises, and dolomite gives out its Mg^{2+} ion that reacts with free OH^- ions resulting in dolomite deterioration (Garcia *et al*., 2003; Zhang *et al.*, 2014).

On the other hand, the issue of consolidating the stone using alcohol dispersions of nanoparticles is gaining importance in stone conservation. Calcium hydroxide

($Ca(OH)_2$) nanoparticles/dispersions, in other words, nano-lime dispersions, which are compatible with the texture and composition of the limestone, are produced and tested for their success for the consolidation of limestone ($CaCO_3$), (Dei and Salvadori, 2006; Daniele *et al.*, 2008; Caner, 2011; Daehne and Hern, 2013; Rodriguez-Navarro *et al*., 2013). A nanolime dispersion can penetrate deep within the stone into fine cracks and capillaries and serves as a binder. Therefore, $Ca(OH)_2$ nanoparticles are effective as a consolidation or repair material for limestones. However, for dolomitic limestones, its use may not be so efficient. Although the final product, calcite ($CaCO_3$), has a similar crystal form (rhombohedral) as dolomite, there might still be questions about chemical compatibility. Therefore, the ideal method for consolidation of dolostone is to synthesize dolomite within the weak parts of the dolostone. This method has not been studied yet.

One of the relevant research suggests that $Ca(OH)_2$ and $Mg(OH)_2$ nanoparticles can be synthesized separately and combined in a solution, which can be used for dolostone conservation (Clelazzi *et al*., 2013). However, that suggestion has not been supported by experimental data. Under atmospheric conditions, it is expected that $Ca(OH)_2$ and $Mg(OH)_2$ are carbonated individually, forming calcite and nesquehonite ($MgCO_3$).$3H_2O$, respectively. There is a lack of experimental studies on this issue.

Considering all, the production of an innovative consolidation material, namely, alcohol dispersion of calcium hydroxide ($Ca(OH)_2$) and magnesium hydroxide ($Mg(OH)_2$) nanoparticles, was targeted. The production of those nanoparticles starting from the dolostone itself is considered to be advantageous for a compatible dolostone consolidation. The success in dolomite formation will help the dolostone regain its own microstructure with its own minerals. However, as mentioned before, the formation of dolomite under laboratory conditions is a very challenging research topic because of kinetic inhibitions. In order to achieve such a competency, it is necessary to understand the dolomite formation mechanism in detail, especially in nature. Therefore, this thesis presents a comprehensive literature review of relevant studies to guide the experimental studies. It is hoped that the experimental results

obtained by laboratory analyses towards dolomitization may be helpful to develop knowledge for a new conservation method for deteriorated dolostone.

1.2 Aims and Objectives

The main aim of the study is to produce a new consolidation material compatible with the stone itself for stone conservation purposes, specifically focused on dolomite consolidation treatment. In this regard, the study targets:

- the production of a new generation nano-consolidation material, namely, alcohol dispersion of $Ca(OH)_2$ and $Mg(OH)_2$ nanoparticles, starting from dolostone itself, and
- the synthesis of dolomite mineral within deteriorated parts of the dolostone after treatment.

Throughout the study, the aims and objectives directed towards the main aim are as follows:

- to develop a new consolidation material, alcohol dispersion of $Ca(OH)_2$ and $Mg(OH)_2$ nanoparticles, which can easily penetrate into the tiny cracks and very fine pores through the dolostone surfaces by means of capillary absorption and injection. After its application and carbonation within the deteriorated parts of dolostone, that solution is expected to have a function for dolomite formation,
- to develop a method for the preparation of alcohol dispersion containing $Ca(OH)_2$ and $Mg(OH)_2$ nanoparticles,
- to define the characteristics of alcohol dispersion and the proper carbonation conditions needed for dolomite synthesis within dolostone microstructure, which will be guiding for the application stages of consolidation treatment,
- to achieve proper dolomitization in petri dishes with the use of alcohol dispersion of $Ca(OH)_2$ and $Mg(OH)_2$ nanoparticles under proper carbonation conditions at the laboratory, and to verify the formation of dolomite mineral by means of advanced laboratory analyses and measurable parameters

- to better-understand the dolomite formation mechanism by trials of suitable carbonation conditions applied,
- to verify the dolomite formation within the dolostone samples after consolidation treatment and assess the changes in physical, physicomechanical, and microstructural properties compared to untreated dolostone samples. Particularly, the physicomechanical properties analyses can be guiding for the non-destructive monitoring of treated parts on site.

1.3 Disposition

This thesis is composed of 6 chapters, including Introduction, Literature Survey, Materials and Methods, Results, Discussion, and Conclusion.

In the first chapter, a very brief introduction was written. The argument part describes the importance of the subject and the contribution of the studies conducted on stone conservation. Aims and objectives were presented very briefly. The flow and the content of the thesis were described in the disposition part.

In the second chapter, a Literature survey was presented, including the studies, reviews, and book chapters about the subjects included in the context of this thesis. The characteristics and the formation of the mineral dolomite were presented together with thermodynamic and kinetic factors for dolomitization. Some minerals that can be precursors for dolomite formation and the possible minerals formed in Ca-Mg-CO_2 systems were mentioned together with their basic properties. Crystallography and XRD characteristics of dolomite were given comparatively together with the studies claiming dolomite synthesis and the reviews claiming dolomite synthesis wasn't achieved. Dedolomitization and dissolution of dolomite, some characteristics of materials at the nanoscale, and the use of hydroxide nanoparticles as consolidant were also explained very briefly in relevant sub-headings. The literature survey ends up with information about the carbonation process of hydroxide nanoparticles.

Materials and Methods comprise the third chapter of the thesis. That section starts with the description of the major analytical equipment and tools used for the analyses. Later, dolostone used in the study was described in detail. Experimental procedures were presented in the flow of the stages of the study as; preparation of alcohol dispersions, carbonation experiments, and finally, consolidation experiments of deteriorated dolostone samples.

The fourth chapter, results, present the results of the conducted experiments and analyses together with relevant XRD diagrams, Stereomicroscope and SEM images, SEM-EDAX analyses, and FTIR spectra.

A brief discussion was made based on comparative and combined results obtained from experimental data and analyses together with related literature in the fifth chapter.

Finally, the summary of the study, recommendations, and further studies were presented in the conclusion chapter.

CHAPTER 2

LITERATURE REVIEW

In this chapter, a comprehensive literature review of the relevant studies and subjects focusing on the aim of the thesis is presented. In this context, some topics and studies regarding dolomite, such as its formation in nature, kinetic and thermodynamic factors in dolomite formation, were analyzed in the first stage. When the occurrence of dolomite was investigated in nature, it was realized that dolomite is found in association with some other minerals that can be formed in Ca-Mg-CO_2-H_2O systems. Those minerals, calcium-magnesium carbonate minerals, can be possible precursors for dolomite formation. Therefore, they were mentioned together with some of their basic and thermodynamic properties.

The crystal structure of dolomite will be presented with its XRD traces and compared with XRD traces of calcite to understand and discuss the difference. Moreover, some studies claiming the synthesis of dolomite will be given along with the ideas of other researchers claiming the synthesized products are high magnesium calcite in the light of their XRD traces.

Dolomite dissolution (dedolomitization) was mentioned to figure out the factors that can cause the degradation of dolomite.

The use of nanomaterials is a recent and improving issue in conservation science. Therefore, the literature concerning the use of hydroxide nanoparticles in cultural heritage conservation will be presented by trying to answer the question, “why do nano-sized materials show different properties from their bulk state?”

Finally, the factors affecting the carbonation characteristics of hydroxide nanoparticles will be mentioned.

2.1 Characteristics and Formation of Dolomite

Dolomite, $CaMg(CO_3)_2$ (Calcium-Magnesium Carbonate), is an unusual carbonate mineral. Although up to 50% of the world's carbonate reservoirs are dolomite (Zenger *et al*., 1980), it is hard to understand many aspects of this mineral. It has a rhombohedral unit cell comprising regular alternating planes of Ca^{2+} and Mg^{2+} between CO_3^{2-} planes in a layered superstructure (Figure 1). This unique structure of dolomite makes it hard to be synthesized under laboratory conditions. Dolomite can only be observed in very specific geological environments in nature.

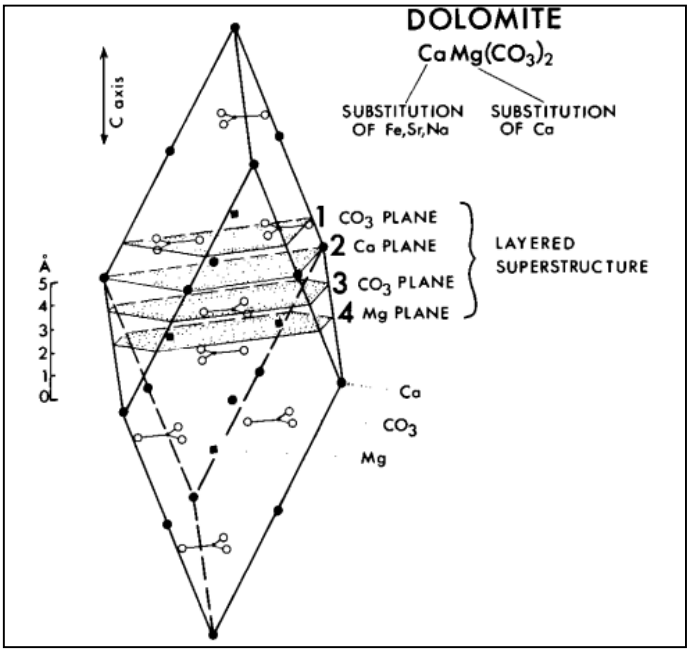

Figure 1. Representation of rhombohedral unit cell of dolomite (Morrow, 1982, p:5).

2.1.1 Dolomite Occurrence in Nature

The formation mechanism of dolomite in nature is uncertain. It can form as a primary precipitate or as a secondary product as a result of a diagenetic replacement as partial replacement of calcium with magnesium in limestone sediments. Large volumes of

dolomite are attributed to subsurface processes or long-term circulation of seawater through platform sediments (Land, 1985; Hardie, 1987). Those formations require sufficient Mg^{2+} and CO_3^{2-} supply, as well as a mechanism to provide the available Mg^{2+} and a proper dolomitization solution (Morrow, 1982). Since dolomite is mainly observed in ancient sediments (Machel, 2004), some of those formations belong to marine sediments formed from ancient sea-water.

It was also realized that there was bacterial mediation where dolomite precipitation occurred. Microbes were thought to control the primary precipitation of dolomite. Therefore, to synthesize dolomite in the laboratory at the Earth's surface temperatures, creating bacterial mediation was necessary (Vasconcelos *et al*., 1995)

Dolomite formation is also observed in nature in some caves. Although caves don't provide suitable conditions for dolomite formation, with the help of bacterial agents, dolomite formation can be triggered (Vasconcelos and McKenzie, 1997; Friedman, 1991). On the other hand, it is questioned whether dolomite is formed through direct precipitation from the cave waters or by the transformation of metastable mineral phases like aragonite ($CaCO_3$), huntite ($CaMg_3(CO_3)_4$), amorphous Ca-Mg carbonates or hydromagnesite ($3MgCO_3.Mg(OH)_2.3H_2O$) (Alonso-Zarza and Martin-Perez, 2008; Martin-Perez *et al*., 2015). Aragonite and huntite transformations at high Mg/Ca ratio were reported for the formation of dolomite (Martin-Perez *et al*., 2012). As an example, in Castanar Cave, Spain, as a result of the sequence of precipitation of minerals and the change in the composition of cave waters, dolomite formation was favored. Calcite and aragonite precipitate first, leaving cave water rich in Mg and Mg-carbonate precipitates as huntite (Alonso-Zarza and Martin-Perez, 2008).

Dolomite formation is thermodynamically favored. However, due to kinetic problems related to Ca, Mg, and CO_3 planes' regular ordering in its structure, its synthesis in the laboratory under ambient conditions is challenging. Those difficulties came up with a "dolomite problem" to be investigated.

2.1.2 Dolomite Problem: Kinetic Factors Inhibiting Its Formation

Starting from the mid-1800s, dolomite has attracted the interest of many researchers, especially of geological scientists. They tried to understand its origin and asked questions like what is dolomite? How does it precipitate? What are the conditions for dolomite formation in geological beds? (Von Morlot, 1847; Skeats, 1905; Van Tuyl, 1918; Steidtmann, 1926; Hewett, 1928; Young, 1933; Riviere, 1939; Landes, 1946; Behre, 1947; Chave, 1952; Graf and Goldsmith, 1956; Fairbridge, 1957; Strakhov, 1958; Medlin, 1959; Baron, 1960; Wells, 1962; Alderman and von der Borch, 1963; Friedman and Sanders, 1967). Those questions came up with the state of "dolomite problem" including more subjects like why dolomite is mainly observed in ancient settings, and there is so little modern dolomite. Therefore, there should be some factors that can control the kinetics of dolomite formation in ancient rocks (Warren, 2000)

Kinetic factors inhibiting dolomite formation include the molecular mechanics of precipitation and difficulties related to the regularly interchanging layers of calcium and magnesium cations between carbonate anions in growing dolomite crystals. Some kinetic factors listed in the literature may be listed as follows:

- Lattice energies of calcium and magnesium ions are very close to each other such that rapid precipitation from supersaturated, concentrated (i.e., saline) solutions hinder the insertion of calcium and magnesium ions into their corresponding planes in the dolomite crystal. Calcium ions make impurities in magnesium layers or vice versa (Lippman, 1973; Folk, 1974). The growth of dolomite crystals is more likely to be achieved by a slow crystallization process, which requires more exposure to the solution.

- In aqueous solution, due to the differences in hydration behavior of ions in the structure of dolomite, precipitation of calcium-rich phases is favored; i.e., there is a strong electrostatic bond between H_2O-Mg^{2+} (20 percent more than H_2O-Ca^{2+}) that inhibits Mg^{2+} to react with calcareous sediments (Lippman, 1973) (Table 1). Therefore, it is difficult for Ca and Mg to settle into their

corresponding planes to form ideal dolomite. In order to overcome the kinetic barrier, seawater may need to be concentrated, heated, cooled, diluted, have its levels of sulfate lowered, increased in CO_3^{2-}concentrations.

- Compared with Ca^{2+} and Mg^{2+} ions, CO_3^{2-}has lower activity/concentration in most natural solutions (such as in lagoonal or tidal areas) that prevents precipitation of magnesium-bearing minerals. Thus, the external addition of CO_3^{2-} might be needed for dolomite precipitation (Lippman, 1973).

The studies to overcome kinetic barrier are numerous, including temperature (e.g., Graf and Goldsmith 1956, Katz and Matthews 1977, Sibley *et al*., 1994); Mg^{2+} /Ca^{2+}ratio of the dolomitizing solution (e.g., Sibley 1990; Kaczmarek and Sibley 2007, 2011); the surface area to volume ratio of the precursor $CaCO_3$ (e.g., Katz and Matthews 1977, Sibley *et al*., 1987); solubility of the precursor $CaCO_3$ (e.g., Gaines 1974, Kaczmarek and Sibley 2014); alkalinity of the fluid (e.g., Land 1967, Morrow and Rickets 1988); molarity of the fluid (e.g., Land 1967); fluid to solid ratio (e.g., Land 1967); presence or absence of sulfate (e.g., Baker and Kastner 1981, Morrow and Rickets 1988); desolvation of Mg ions (e.g., Lippmann 1973, Usdowski 1994, Zhang *et al*., 2012); and presence of microbes and/or organic matter (e.g., Vasconcelos *et al*., 1995, Zhang *et al*., 2012)

Among those studies, Katz and Mathew (1977) explain the dependence of the rate of dolomitization on relatively high temperatures because of the high activation energy for very high magnesium calcite (VHMC) and dolomite (48 and 49-50 kcal/mol, respectively) compared to calcite (10 kcal/mol). Vasconcelos *et al*. (1995) claimed microbes can catalyze dolomite nucleation and growth at low temperatures. On the other hand, Land (1998) presents his studies in the attempt to precipitate dolomite at low temperature, which ended with failure, and concluded that the 'Dolomite Problem' is one of kinetics.

2.1.3 Thermodynamic Factors and Suggested Reaction Mechanisms for Dolomitization Process

Even though dolomite formation is inhibited due to kinetic factors, thermodynamic factors favor its formation. There are mainly two reactions offered for dolomite formation mechanisms. Those reaction mechanisms may be affected by factors that make the dolomitization process favorable, for example, high Mg/Ca ratios, low salinities, high salinities, high $[CO_3^{2-}]$ concentration, large organic content, *etc*. (Folk and Land, 1975; Badiozamani, 1973).

The first suggested reaction for dolomitization can be given by Reaction 1 (Bathurst, 1975):

$2CaCO_3(s)+Mg^{2+}(aq) \rightarrow CaMg(CO_3)_2\ (s)+ Ca^{2+}\ (aq)$.....Reaction 1

Standard free energy change of this reaction (transformation of calcite to ordered dolomite), ΔG^o_r is -1.38 kcal/mol. Marine environments favor the formation of aragonite rather than calcite due to high Mg/Ca ratio, and ΔG^o_r is -1.86 kcal/mol for the transformation of aragonite to ordered dolomite. The value shows a thermodynamic drive towards dolomitization.

The free energy change related to the activity is given below in Equation 1.

$\Delta G^o = \Delta G^o_r + RT\ LnQ$ ……...Equation 1

Where Q(activity ratio)= aCa^{2+}/aMg^{2+} ; R=the gas constant; T=absolute temperature

The smaller the Q value is, the more favorable the transformation of aragonite to ordered dolomite is.

The Q value for sea-water was suggested as 0.16 (Wigley and Plummer, 1976). Thus, seawater seems to be a good choice for dolomite precipitation. Activity and Enthalpy of hydration values of Ca^{2+}, Mg^{2+} and CO_3^{2-} ions in seawater chemistry at 25°C are given in Table 1.

Table 1. Activity and Enthalpy of hydration values of corresponding ions in seawater chemistry at 25°C

Species	Energies of interaction for H_2O dipoles with ions Enthalpy of hydration ΔH in kcal/mole*	Activity**
Ca^{2+}	395	0.00264
Mg^{2+}	473	0.0169
CO_3^{2-}		0.0000047
* Noyes, 1962 ** Garrels and Thompson, 1962		

On the other hand, the second suggested reaction for dolomitization questions that whether dolomite is formed as a result of exchange reaction (insertion of Mg^{2+} ions into the calcium carbonate by exchanging Ca^{2+} (as in Reaction 1) or it is formed by coprecipitation reactions (i.e., the reaction of solution derived from seawater with previously deposited calcium carbonates). In a suggestion given by Lippman (1973), Besides Mg, CO_3^{2-} ions should also be supplied externally, and calcium carbonate dissociates first before dolomite formation (dissolution-precipitation mechanism) (Reaction 2).

$Ca^{2+}(aq) + Mg^{2+}(aq) + 2CO_3^{2-}(aq) \rightarrow CaMg(CO_3)_2\ (s)$……...Reaction 2

ΔG^o_r = -13.24 kcal/mol for this dolomitization process, which indicates a much more favorable reaction than the reaction shown in Reaction 1. At the same time, this reaction doesn't possess any by-products like Ca^{2+} as in Reaction 1. All $CaCO_3$ is consumed so that the Ca^{2+}/ Mg^{2+} ratio will be stable (Morrow, 1982).

2.2 Precursor Minerals in Dolomite Formation and Some of Their Basic and Thermodynamic Properties

In nature, dolomite is found together with some other minerals that can be formed in Ca-Mg-CO_2-H_2O system. Those minerals might exist as Calcium-Carbonate

minerals, Magnesium-Carbonate Minerals, or Ca-Mg-Carbonates. It is important to know their properties to understand the way for dolomitization

2.2.1 Calcium Carbonate Minerals and The Effect of Magnesium on the Crystallization of Calcite and Aragonite

$CaCO_3$ has three forms of crystals, namely, calcite, aragonite, and vaterite. Calcite is the most abundant mineral form of $CaCO_3$. Aragonite is a metastable phase of $CaCO_3$. Higher solubility of aragonite than calcite (Table 2) makes this mineral metastable. That is why aragonite is mostly a precursor of carbonate minerals such as calcite, dolomite, *etc*., which are formed in marine sediments. (Lippman, 1973).

The transformation of aragonite to calcite occurs spontaneously at 25^oC temperature and 1 atm total pressure. The standard free energy of formation of calcite (-269.8 kcal/mol) is lower than the standard free energy of formation of aragonite (-269.6 kcal/mol) (Table 3). However, the stability of mineral phases may change as the conditions change such that minerals' stability changes in sea-water compared with distilled water due to the changes in specific kinds of substances in seawater (Winland,1969). The content of seawater (i.e., Mg/Ca ratio) determines the type of marine organisms. The organisms might be either calcite or aragonite forming organisms. At a high Mg/Ca ratio, aragonite-forming organisms are more likely to appear in seawater (Ries, 2010).

On the other hand, in the experiments conducted under laboratory conditions, at 20^oC in the system of Ca-Mg-CO_3 by Lippmann (1960), Mg/Ca ratio determined the final products precipitated. In these experiments, Magnesium source was $MgSO_4.7H_2O$, Calcium source was $CaSO_4.2H_2O$, and Carbonate was supplied by the dissolution of Potassium cyanate, KOCN, in an aqueous solution yielding potassium and ammonium carbonate. When the Mg/Ca ratio was higher than 2, aragonite was the main product (the amount of KOCN as the CO_3^{2-}source was 1000 mg/L). When the amount of KOCN was doubled, aragonite could only be observed when the Mg/Ca

ratio was higher than 11. Although in these experiments, synthesis of dolomite was attempted. This attempt was failed to yield dolomite. Instead, it provided information about the effect of magnesium amount on calcite crystallization. The formation of aragonite can be attributed to the inhibitory effect of Mg on growing calcite crystals that affect the chemical composition and mineralogy of the phases formed (Fernandez-Diaz, *et al*., 1996). It was concluded that Mg acts as a modifier on calcite morphology rather than co-precipitation. The possible reasons for these formations can be due to several factors;

1. Thermodynamic stability of calcite gets less in the presence of Mg^{2+} ion (Busenberg and Plummer, 1989; Konigsberger and Gamsjager, 1992; Davis *et al*., 2000, 2004; Kulik, 2006). As the Mg content in calcite increases, free energy of formations for magnesian calcites decreases due to the incorporation of disorders (Berner, 1975; Mucci and Morse, 1983) and lattice strain (Glodsmith and Graf, 1958; Goldsmith *et al*.,1961; Althoff, 1977; Bischoff *et al*., 1983; Paquette and Reeder, 1990) in the calcite structure due to the size difference between Ca^{2+} (r = 1.14A˚) and Mg^{2+} (r = 0.86A˚) (Shannon, 1976). At supersaturation with magnesium (like %15 $MgCO_3$), aragonite is a more stable phase than calcite. (Winland, 1969)
2. Mg^{2+} ion is more strongly hydrated than Ca^{2+} and is strongly adsorbed onto the surface of growing calcite crystals. Dehydration of Mg^{2+} ions before incorporation into the calcite lattice creates a barrier for the growth of calcite nuclei (Loste, *et al*., 2003).
3. The supply rate of CO_3^{2-} also plays an important role in the precipitation of $CaCO_3$ in the presence of Mg. At higher temperatures (100 ºC), CO_3^{2-} concentration is more compared with at lower temperatures (20ºC). At high temperatures, using the amount of KOCN (100 mg/l), aragonite was obtained when the Mg/Ca ratio was around 2 (Lippman, 1960).

2.2.2 Magnesium Carbonate Minerals

Magnesium carbonates could be formed where dissolved magnesium is abundant. Magnesium sources may come from weathering and solution of silicate rocks such as serpentinite ($Mg_3Si_2O_5(OH)_4$), peridotite, and dunite ($(Fe, Mg)_2SiO_4$), or carbonates such as magnesian calcite and dolomite. Together with a concentrated water source or temperature changes, magnesium may precipitate as magnesium carbonates at elevated temperatures (Langmiur, 1965).

Magnesium carbonates can show up with various phases in nature, other than magnesite ($MgCO_3$). They tend to form in hydrous forms as barringtonite ($MgCO_3.2H_2O$) (rare abundance), nesquehonite ($MgCO_3.3H_2O$), lansfordite ($MgCO_3.5H_2O$), artinite ($Mg_2(CO_3)OH_2.3H_2O$), and hydromagnesite ($3MgCO_3.Mg(OH)_2.3H_2O$). The formation of those minerals is directly related to CO_2 pressure, pH, temperature, and humidity of the environment, as well as the concentration of anions and cations in aqueous solution, presence of clay minerals, or organic matter. The phases formed under given conditions can control the precipitation kinetics with supersaturation of species in the solution medium.

While Langmiur (1965) states that elevated temperatures (above 50-60 ^oC), high CO_2 pressures (more than atmospheric-$10^{-3.5}$ atm), and high ionic strength in aqueous solution favor magnesite ($MgCO_3$) formation, Hanchen *et al*. (2007) could obtain magnesite (together with minor amounts of brucite and hydromagnesite) at high T (120 ^oC) and high pCO_2 (3 bar). The hydration character of Mg^{2+} ions in the solution is quite high such that before magnesite formation, metastable phases like hydromagnesite precipitates first (Sayles and Fyfe, 1973). At sufficient supersaturation, hydromagnesite coprecipitates with magnesite but transforms into magnesite within a few hours. At lower pCO_2 (1 bar) and low T (25 ^oC), the precipitated product was nesquehonite, which was influenced by Mg^{2+} and CO_3^{2-} ratio (Hanchen *et al*., 2007).

In the system of $MgO\text{-}CO_2\text{-}H_2O$, Mg-carbonate phases were shown as a function of temperature (°C) and partial pressure of carbon dioxide (-log pCO_2 (atm)) (assuming $aH_2O=1$) by Langmuir (1965) (Figure 2). Lansfordite-nesquehonite and nesquehonite-magnesite boundaries are horizontal since hydration/dehydration equilibria change with temperature. The diagram assumes that as the temperature increases, relative humidity decreases, so magnesite could only form at high temperature (where relative humidity ~15%) and pressures greater than atmospheric ($10^{-3.5}$).

Lansfordite and Nesquehonite are mostly abundant in caves and coal mines where CO_2 concentration is high (10 times more than atmospheric conditions) and low-temperature conditions. Nesquehonite was recorded as a spring mineral deposit. Both lansfordite and nesquehonite are identified by weathering of serpentinite rock in Italy (Palache et al., 1951). For example, weathering products on the surface of the Antarctic meteorite were found to be nesquehonite with the reaction of meteoritic minerals with terrestrial water and carbon dioxide at near-freezing temperature (Jull *et al*., 1988; Graddy *et al*., 1989).

Hydromagnesite is secondly abundant among magnesium carbonates under atmospheric CO_2 pressure and typical temperature intervals that could be on the surface (Figure 2). Nesquehonite readily transforms into hydromagnesite above 52 °C (Davies and Bubela, 1973).

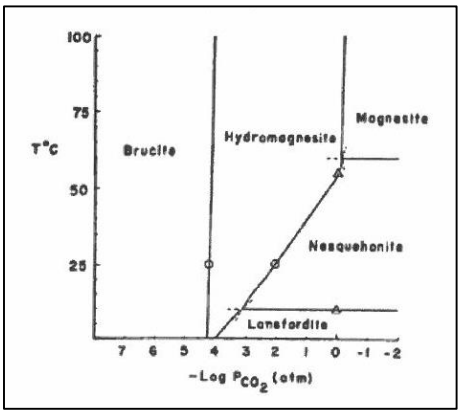

Figure 2. Probable stability relations in the system $MgO\text{-}CO_2\text{-}H_2O$ between 0°C and 100 °C as a function of pCO_2 and assuming $aH_2O = 1$ (Langmiur, 1965, p:248)

2.2.2.1 Nesquehonite

Nesquehonite, $Mg(HCO_3)(OH)\cdot 2H_2O$ or $MgCO_3\cdot 3H_2O$ named after its discovery of local sources in Nesquehoning, Pennsylvania, USA (Kloprogge *et al*., 2003).

Nesquehonite could be synthesized at room temperature with the reactions, which include Mg^{2+} and CO_3^{2-} sources in an aqueous medium. Depending on the drying temperature of the solution, its morphology could be either very thin plates (at RT) or well-crystallized needles (at 50 ºC) (Kloprogge *et al*., 2003).

The crystal structure of nesquehonite is characterized by infinite chains formed by corner-sharing $(MgO_6)^{10-}$ octahedra. Within the chains CO_3^{2-} groups link three $(MgO_6)^{10-}$ octahedra by two common corners and one edge, which causes strong distortions of the involved polyhedra. Chains are interconnected by hydrogen bonds only whereby each Mg atom is coordinated to two water ligands, and one free water molecule locates between the chains (Figure 3) (Giester *et al*., 2000).

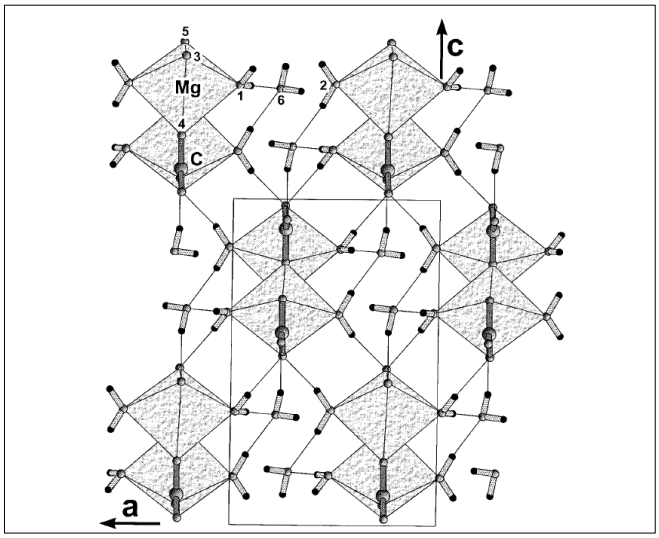

Figure 3. Crystal structure of nesquehonite in projections parallel to b.Drawings were obtained using the ATOMS program (Dowty, 1999)

2.2.2.2 Dolomite Formation from Nesquehonite Precursor

Nesquehonite is a metastable phase of Mg-carbonate minerals. At a certain temperature and CO_2 pressure, it transforms into hydromagnesite in aqueous solutions. Since Mg-carbonates are quite soluble in the aqueous medium, when there is calcium in the medium, the precipitation of calcite (or aragonite/ monohydrocalcite) is strongly affected by the amount of Mg^{2+} ions.

Davies e*t al*. (1975) constructed a laboratory set up (a tank system which allows controlling the conditions) including nesquehonite (as the source of Mg^{2+} and CO_3^{2-}), calcite (crushed calcite about 10 cm thick) and brine (25% solid salt solution) to understand the chemical, mineralogical and biological processes occurring in sediments in laboratory conditions. The experimental results pointed out some critical issues, especially focusing on the formation of precursor phases prior to formation of the final precipitate.

Cores of nesquehonite layers showed nesquehonite with an increasing amount of protohydromagnesite and hydromagnesite growing in the cores. After some time (95 days), nesquehonite peaks were seen less intense, and magnesium-rich dolomite (Ca:Mg-0.43:0.57) was seen on XRD. From this diagenetic transformation, it could be said decomposing the nesquehonite layer gives rise to the formation of dolomite.

The system followed three stages:

- Dissociation period
- Supersaturation period
- Crystallization period

In the dissociation period (Reaction 3), nesquehonite dissolves in contact with brine in two intermediate steps:

$MgCO_3 .3\ H_20 + H_2O = Mg^{2+} + CO_3^{2-} + H^+$

$CO_3^{2-} + H^+ + H_20 = HCO_3^{2-} + OH^-$

Generally written as:

$MgCO_3 .3\ H_20 + H_2O = Mg^{2+} + HCO_3^{2-} + OH^-$……..……..Reaction 3

During the supersaturation step, high Mg^{2+} concentration, low Ca^{2+} concentration, relatively high CO_3^{2-} concentration where OH^- production is slow, result in the precipitation of huntite and dolomite.

The maintenance of high CO_3^{2-} concentration throughout this stage, by the slow decomposition of nesquehonite, may, therefore, be critical for the dolomite formation.

2.2.3 Calcium-Magnesium Carbonate Minerals

Among Ca-Mg-Carbonate minerals, huntite ($CaMg_3(CO_3)_4$) is the most widely encountered mineral associated with dolomite. Therefore, huntite can be a precursor mineral for the formation of dolomite (Lippman, 1973). It was first described by Faust (1953) with the examples of volcanic tuffs at Currant Creek, Nevada. When the occurrence of huntite was investigated, it was realized that there had been an association with magnesite and/or dolomite which transformed to huntite due to the influence of near-surface or meteoric waters. Huntite is known from three different environments (Kinsman, 1967):

- As a cave carbonate which comprises metastable and stable calcium and magnesium minerals (especially in areas where the country rocks are magnesium-rich).
- As a near-surface weathering product of magnesium-rich rock, such as brucite marbles, dolomites, magnesites, or serpentinites.
- As a diagenetic mineral in recent sediment sequences.

Although Kinsman (1967) states that the precipitating solution of huntite is not definitely known, Lippman suggested the below reaction for huntite formation (Reaction 4) (Lippman, 1973)

$CaCO_3$ (solid) + 3 Mg^{2+} +3$CO_3^{2-} \rightarrow CaMg_3(CO_3)_4$ ……..Reaction 4

2.2.4 Thermodynamic Properties of Some Minerals Formed in Ca-Mg-CO_2-H_2O System

To better interpret the formation of minerals concerning the seawater chemistry, the solubilities, standard free energies of formations, and Gibbs free energy of formations for possible minerals formed in Ca-Mg-CO_2-H_2O systems are given in Table 2, Table 3, and Table 4, respectively.

Table 2. Some thermodynamic properties of some calcium and magnesium minerals: solubility products were measured in the concentrated salt solution.

Minerals	Chemical Formula	Solubility products Ksp at 25°C	Reference
Portlandite	$Ca(OH)_2$	$10^{-5.30}$	Zhang *et al*., 2014
Brucite	$Mg(OH)_2$	$10^{-11.07}$	Horn, 1969
Aragonite	$CaCO_3$	$10^{-8.22}$	Garrels & Thompson 1962
Calcite	$CaCO_3$	$10^{-8.35}$	Horn, 1969
Dolomite	$CaMg(CO_3)_2$	$10^{-18,22}$	Horn, 1969
Huntite	$CaMg_3(CO_3)_4$	$10^{-7.8}$	Lippman, 1973
Magnesite	$MgCO_3$	$10^{-8.14}$	Horn, 1969
Hydromagnesite	$3MgCO_3.Mg(OH)_2.3H_2O$	10^{-30}	Lippman, 1973
Nesquehonite	$MgCO_3.3H_2O$	10^{-5}	Lippman, 1973

Table 3. Standard free energies of formations of some minerals in the Ca-Mg-CO_3 system

Minerals	Standard free energies of formations (kcal/mol) $\Delta_f F$	References
Aragonite	-269.6	Garrels *et al*., 1960
Calcite	-269.8	Garrels *et al*., 1960
Dolomite	-520	Garrels *et al*., 1960
Magnesite	-246	Garrels *et al*., 1960
Huntite	-1007.7	Garrels *et al*., 1960
Hydromagnesite	-1108.3	Garrels *et al*., 1960
Nesquehonite	-412.66	Langmuir,1965

Table 4 Gibb's free energies of formations of some minerals in the Ca-Mg-CO_3 system

Minerals	Standard free energies of formations (kJ/mol) $\Delta_f G$	References
Aragonite	-1128.306	Hummel *et al*., 2002
Calcite	-1129.127	Hummel *et al*., 2002
Dolomite (ordered) Dolomite (disordered)	-2161.565 -2158.425	Hummel *et al*., 2002
Magnesite	-1030.6	Hummel *et al*., 2002
Huntite	-4203.4	Woods and Garrels, 1987
Hydromagnesite	-5864.6	Woods and Garrels, 1987
Nesquehonite	-1723.7	Woods and Garrels, 1987

Based on the solubility products determined by Horn (1969), phase diagram of the system $CaCO_3$-$MgCO_3$-H_2O for zero ionic strength at 25°C was given in Figure 4. This phase diagram was prepared according to the minerals formed in various Ca/Mg ratios with respect to CO_2 partial pressure. Seawater conditions indicated by a black dot locates in the dolomite region together with some metastable phases (Lippman, 1973).

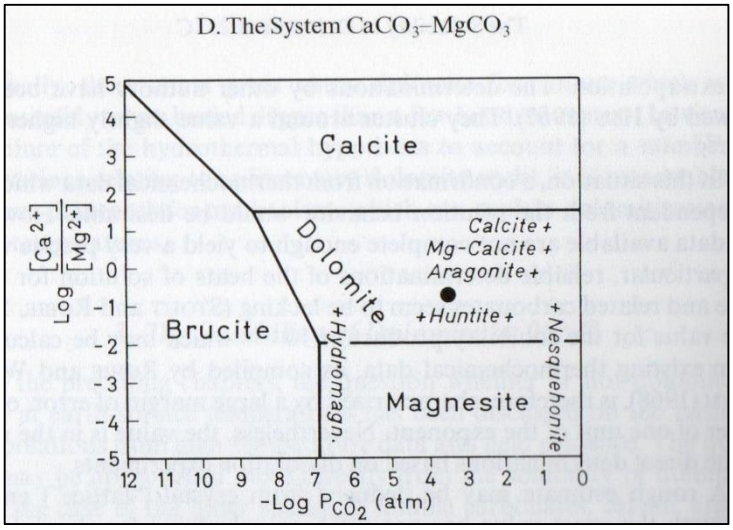

Figure 4. Phase diagram of the system $CaCO_3$-$MgCO_3$-H_2O for zero ionic strength at 25°C. The metastable phases occurring in the system are indicated in italics. The black dot corresponds to the conditions of seawater. (Lippman, 1973, p:158)

2.3 Crystallography of Dolomite and Its Verification by XRD

Dolomite, with the chemical formula $CaMg(CO_3)_2$, is similar in structure to calcite ($CaCO_3$) with planes of carbonate groups (CO_3^{2-}) alternating with planes of cations. In dolomite, planes are alternately Ca^{2+} and Mg^{2+} cations interspersed with CO_3^{2-} oriented normal to *c*-axis. In calcite structure, alternating planes are Ca^{2+} and CO_3^{2-} in which each metal cation is coordinated by six oxygen atoms. The insertion of magnesium atom for half of the calcium atoms makes dolomite with a lower degree of symmetry compared with calcite (Figure 1). Therefore, both dolomite and calcite minerals have a rhombohedron unit cell of rhombohedral shape elongated through the c-axis. They differ in that, while calcite belongs to $R\bar{3}c$ space group minerals, dolomite belongs to $R\bar{3}$ space group due to its lower degree of symmetry.

The charge density difference between Ca^{2+} and Mg^{2+} (due to the large difference in ionic radii) results in a shift of the oxygen atoms towards the Mg^{2+} plane, which reduces the bond length. The difference between Ca-O and Mg-O bond lengths in dolomite is 2.38 ^{o}A and 2.08 ^{o}A, respectively (Reeder, 1983).

Gregg *et al*. (2015) compared XRD data of standard dolomite with near-perfect ordering and calcite (Figure 5 and Table 5). According to the hexagonal unit cell (*hkl*) indices of XRD data of perfectly ordered dolomite, the 101,015 and 021 indices (with XRD peak location ($^{o}2\theta$) at 22.04, 35.31, and 43.78 respectively) show the cation (alternating planes of Ca and Mg) ordering reflections that help to distinguish $R\bar{3}$ (dolomite space group) from that of $R\bar{3}_c$ (calcite space group). These reflections represent planes in the dolomite structure that are characterized by the atomic scattering factor of Ca minus Mg. The reduced XRD peaks belonging to these reflections attributed as poorly ordered dolomite, where Ca^{2+} ions occupying Mg^{2+} positions and vice versa. The absence of these indices in XRD data was noted as there is no cation ordering, and this kind of XRD data belongs to Very High Magnesium Calcite (VHMC) (Figure 6).

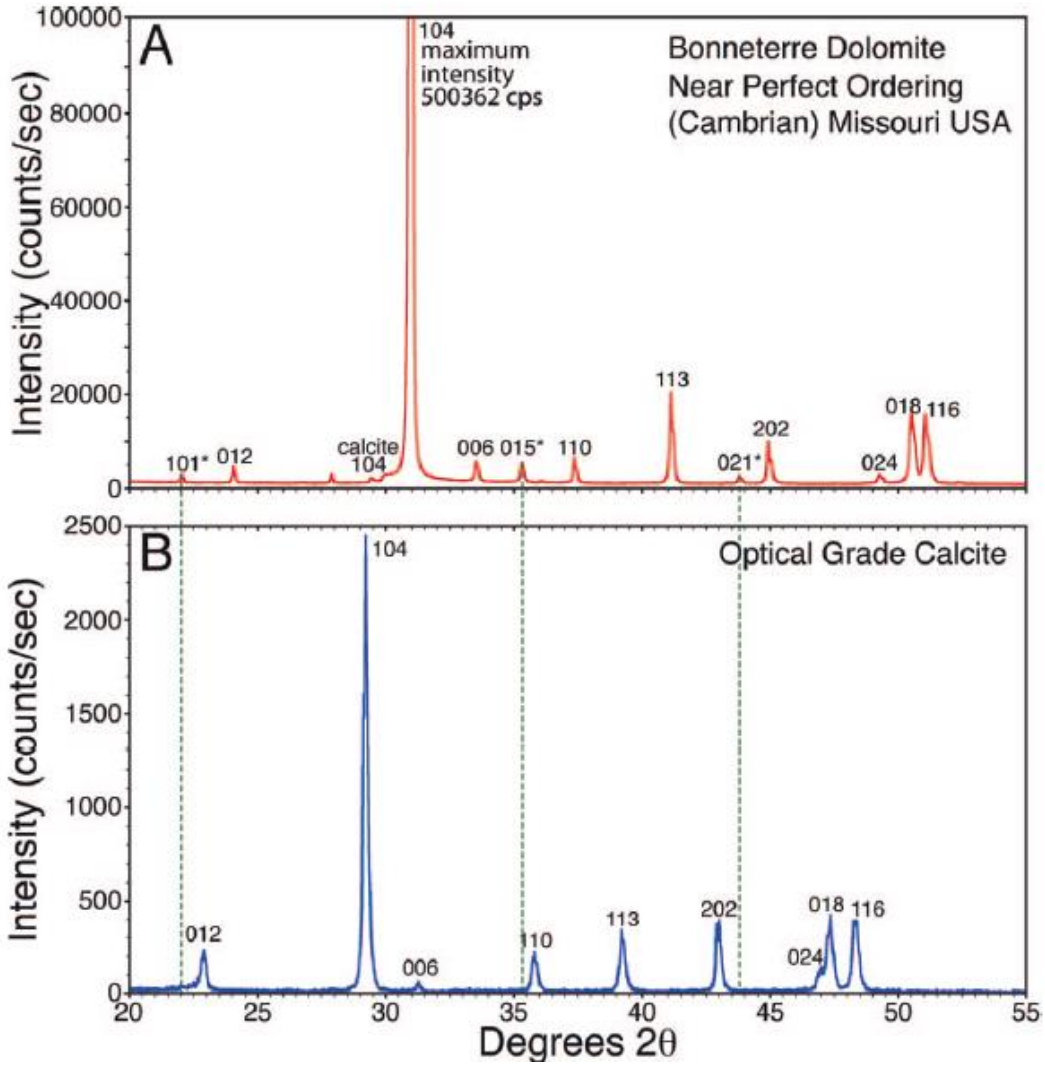

Figure 5. Powder XRD patterns (CuKα) comparing dolomite and calcite from 20 to 55.8 2θ. A) Bonneterre dolomite (Cambrian, Missouri) exhibiting cation ordering. Dolomite peaks are labeled with their corresponding Bravais-Miller indices, with the ordering reflections indicated by an asterisk. B) Optical-grade calcite for comparison showing lack of dolomite ordering reflections. Modified from Gregg *et al*. (2015).

Table 5. Unit cell and XRD information for ideal dolomite versus calcite(CuKα radiation). * Denotes dolomite ordering peaks.

Hexagonal unit cell (hkl) Indıces	~XRD peak location ($^o2\theta$)	d-Spacing (angstroms)	Relative XRD peak intensity
Dolomite-Calcite	Dolomite	Dolomite-Calcite	Dolomite-Calcite
101*-doesn't appear	22.04	4.03	<5*
012	24.10	3.69 - 3.85	5 - 12
104	30.96	2.886 - 3.0359	100 - 100
006	33.54	2.670 - 2.8440	10 - 3
015*-doesn't appear	35.31	2.540	10*
110	37.36	2.405 - 2.4949	10 - 14
113	41.15	2.192 - 2.2848	30 - 18
021*-doesn't appear	43.78	2.066	5*
202	44.99	2.015 - 2.0946	15 - 18
024	49.31	1.848 - 1.9275	5 - 5
018	50.60	1.804 - 1.9127	20 - 17
116	51.14	1.786 - 1.8755	30 - 17
009	51.29	1.781	30
214	63.49	1.465	5

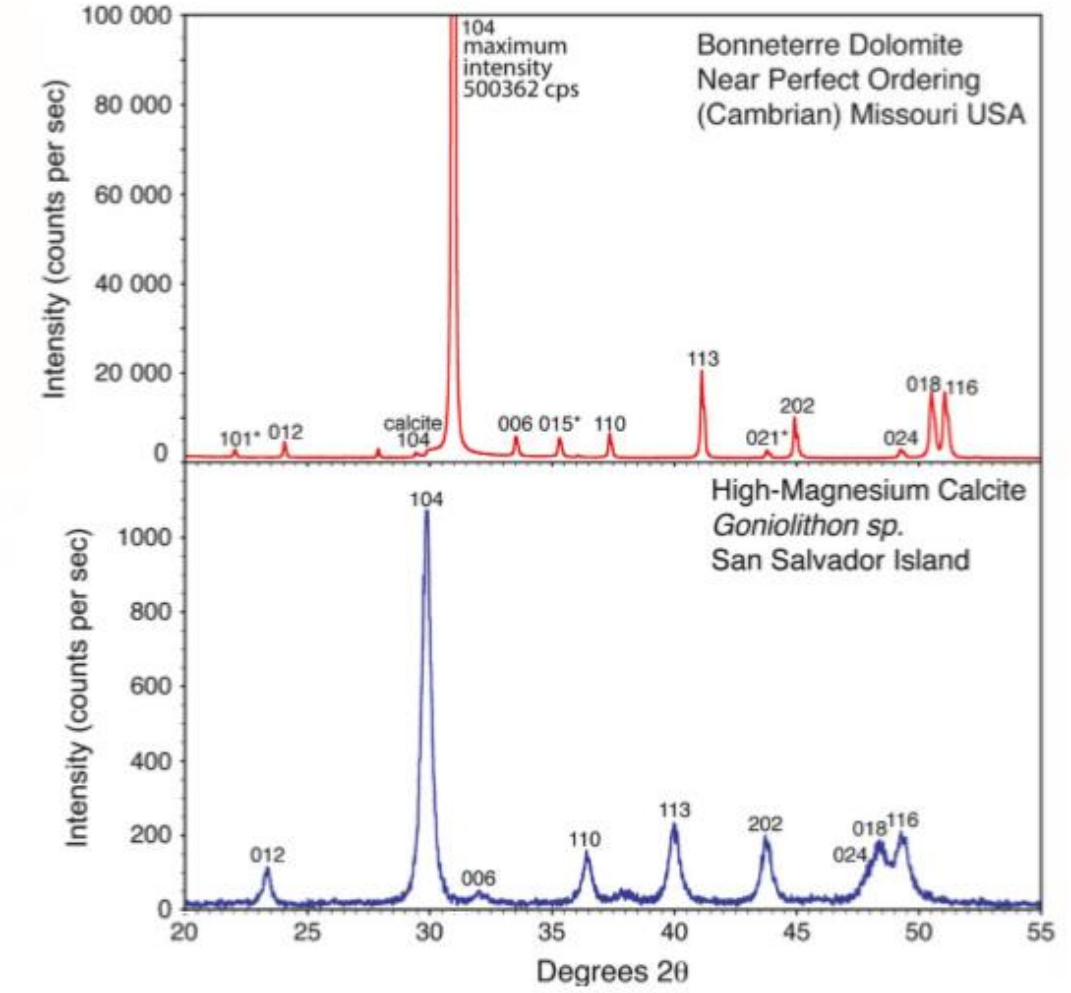

Figure 6. "X-ray diffraction patterns of dolomite and very high magnesium calcite. Dolomite from the 'back reef' facies of the Bonneterre Dolomite (Cambrian) Missouri (up). HMC from a coralline algae (Goniolithon sp.) San Salvador Island, Bahamas(down). Calcite reflections are labeled. Note the pronounced shift of the 104 reflection towards a lower d-value. This shift is caused by a contraction of the calcite unit cell resulting from Mg^{2+} substitution for Ca^{2+}. Broadening of the reflections relative to those in calcite may be due to the exceptionally small crystallite size that is typical of HMC precipitated by coralline algae" Modified from Greg,2015, p:1756.

2.4 Some Studies on Dolomite Formation and Arguments Concerning Mechanisms, Conditions, and Analyses

Among suggested mechanisms on dolomite formation, many researchers agree that the dolomite precipitation follows Ostwald's ripening-step rule. Ostwald's rule states that during the diagenesis of an unstable mineral to a stable form, one or more

intermediate phases are formed that leads to the final precipitate. This process proceeds by a recrystallization mechanism where large crystals grow at the expense of smaller ones. The driving force for this process is the surface energy of the various crystals (Gregg *et al*., 1992, Morse and Casey, 1988)

Sibley *et al*., 1994, showed that dolomite precipitated in the laboratory at elevated temperatures (150-300 ^{o}C). The dolomitization process was in agreement with Ostwald's rule. Precipitation started with very-high-Mg calcite crystallization and then its replacement with dolomite. The dolomitization process details were explained with three successive periods being nucleation, long induction period, and replacement period.

In the nucleation period, nucleation of very high magnesium calcite (VHMC) (35-40 mole %$MgCO_3$) or nonstoichiometric dolomite is followed by nucleation of more stoichiometric dolomite on $CaCO_3$. The composition of the initial precipitate is a function of the solutions' Mg/Ca ratio.

The long induction period corresponds to the post-nucleation growth of dolomite nuclei. Solution variables and substrate surface area change the duration of the induction period.

In the replacement period, there exist two phases. In the first one, $CaCO_3$ is replaced by VHMC or nonstoichiometric dolomite. VHMC nucleates faster than stoichiometric dolomite and therefore begins to replace the reactant first. Afterward, $CaCO_3$ and VHMC and/or nonstoichiometric dolomite are rapidly replaced by stoichiometric dolomite.

This three-phase model is consistent with the Ostwald's ripening and with many characteristics of natural dolomites, including

1. The fact that very Ca-rich dolomite is common only in modern dolomites,
2. There is a direct relationship between the Mg/Ca ratio in the solution and Mg/Ca ratio in the dolomite,

3. The stoichiometry of dolomites in some ancient rocks is directly related to the percentage of dolomite in the rock,
4. The suppression of stoichiometric dolomite nucleation allows the persistence of metastable Ca-Mg-CO_3 phases,
5. Dolomite-limestone contacts are often sharp,
6. Dolomite selectively replaces fine-grained $CaCO_3$,
7. Dolomite crystals often have cloudy centers and clear rims,
8. Dolomite textures are mainly determined by the crystal size of the substrate.

When Wenk *et al.* (1993) investigated the microstructural characteristics of specific dolomite in nature, he concluded that there is no exact evidence on the crystallization mechanism, such as replacement or direct crystallization of calcium magnesium carbonates in nature. He also adds that ordered dolomites are generally not caused by the ordering of a disordered protodolomite, but are the result of direct growth, mainly by dissolution and precipitation.

On the other hand, numerous studies were conducted at low temperatures (25-60 ^{o}C) using microbial mediation. It is stated that microbes can behave as a catalyst in the nucleation and growth of dolomites (Vasconcelos *et al*., 1995; Vasconcelos and MacKenzie, 1997; Neher and Rohrer, 1958; Warthmann *et al*., 2000; Kenward *et al*., 2013). They all claim that the presence of microbes helps to overcome kinetic barriers to dolomitization in low-temperature geologic environments. Their claim is based on the two models. One is the observation that dolomite is present in some modern carbonate depositional settings where microbes are known to be present and potentially active. The second is that dolomite has been produced experimentally at low diagenetic temperatures via microbial mediation under conditions simulating those observed in nature. Microbes have the ability to create nucleation sites for mineral growth or to alter the chemistry of their environments through metabolic activity (Dupraz *et al*., 2009).

Those experimental research results influenced some scientists in the way that "microbial experiments are the only proven approach to produce experimental dolomite under Earth surface conditions'' (Sa´nchez-Roma´n *et al*. 2008). Wright and Wacy (2005) stated that bacterial sulfate reduction could drive dolomite formation by overcoming kinetic constraints at normal temperatures and pressure. Low-temperature experimental studies involving microbes have even led some workers to claim dolomite as a biomineral (Vasconcelos and MacKenzie 2008).

On the other hand, Gregg *et al*. (2015) has criticized those studies of low-temperature dolomite precipitation on the basis of published XRD data belonging to those studies. They called those products synthesized at low temperatures in the laboratory as "laboratory products." They compared XRD data of standard dolomite, which has near-perfect ordering, with XRD data of laboratory products. He pointed out that the specific hexagonal unit cell (*hkl*) indices (the 101,015 and 021 indices) of dolomite that represent the cation ordering reflections are absent for those products and concluded that there is no cation ordering and the synthesized product is Very High Magnesium Calcite (VHMC).

Moreover, Kaczmarek *et al*. (2017) has made a critical review of the XRD data published in studies including microbial dolomitization. He discussed and compared the XRD reflections of standard dolomite with the products synthesized at low-temperature microbial experiments by labeling reflections with *hkl* indices (Figure 7). He stated that the laboratory products display lack of XRD reflections of cation ordering, and the peaks are broader. He also stated that those products don't show the ideal dolomite ordering, and it is more accurate to call them VHMC. Those products help to enlighten the "dolomite problem," and they are potential precursors for dolomite formation. In the long term, if the duration of experiments increases, it is possible to obtain an ordered dolomite structure.

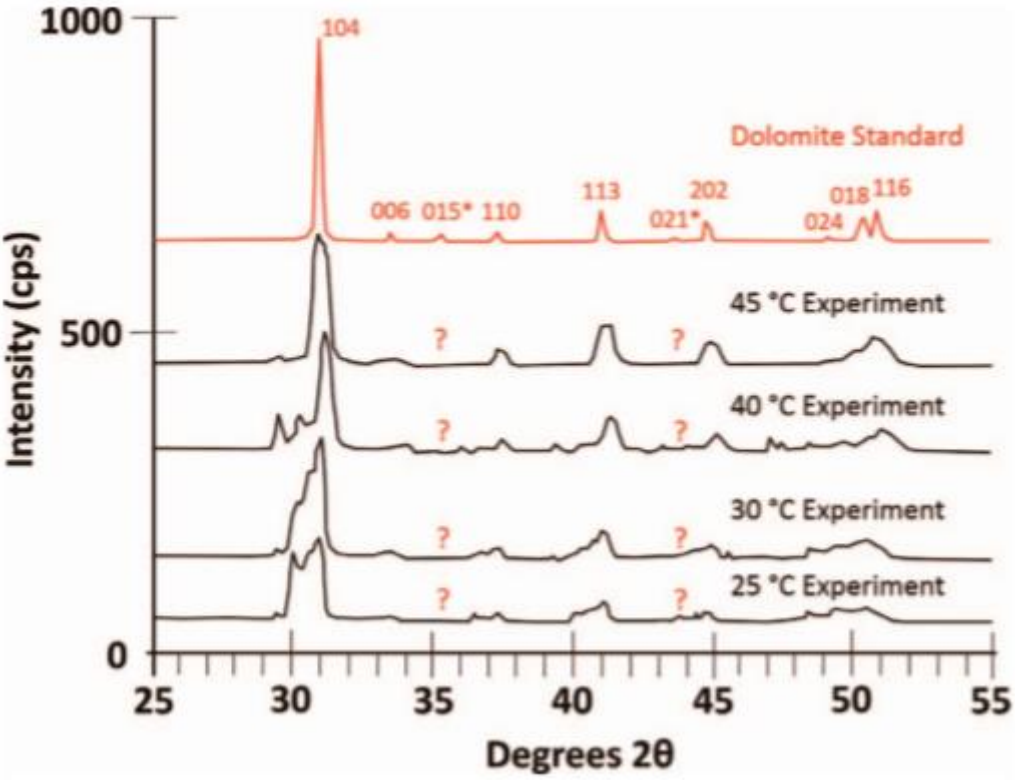

Figure 7. Comparision of XRD reflections of standard dolomite with a series of products made in low-temperature (25–45 ºC) microbial experiments (modified by the author after Vasconcelos *et al.*,1995).

To sum up, despite the numerous studies mentioned above, there is still debate about whether dolomitization is possible at near-surface conditions. Although some claim that they could obtain dolomite in the laboratory, some argue the terminology and structure of the product formed at the laboratory, claiming they are not dolomite but rather high magnesium calcite (HMC). Laboratory products show rhombohedral crystal symmetry of single-phase carbonates, which deviate from the ideal stoichiometry but would transform to dolomite if an equilibrium is established. Graf and Goldsmith (1956) redefined the term protodolomite. Gaines (1977) suggested another definition for protodolomite as metastable Ca-Mg carbonate phases that display weak or incompatible ordering. This author suggested the term pseudodolomite. Greg *et al.* (2015) and Kaczmarek *et al.* (2017) claimed that they

are VHMC having calcite symmetry group $R\bar{3}c$, not dolomite, whereas Vasconcelos *et al*. (1995) claimed they could overcome the kinetic barrier by microbial experiments and the laboratory products are dolomite.

Considering of all above, it can be said that although dolomite formation is thermodynamically favorable, the precipitation of dolomite is inhibited by some mentioned kinetic factors. On the other hand, the behaviour of minerals at the nanoscale can show differences in chemical, physical, thermodynamic, or kinetic properties due to the increase in surface to volume ratio. In this research, starting with bulk dolostone, calcium hydroxide and magnesium hydroxide nanoparticles were studied at the nanoscale and their behaviour under certain conditions (high relative humidity (90-95%) and high CO_2 partial pressure pCO_2=0.4 atm) was examined for nanoparticles' usability as consolidant for deteriorated dolostones. The synthesized dolomite properties will be listed and discussed in this thesis to add our argument to the literature for the synthesized dolomite under those conditions.

2.5 Dedolomitization-Dissolution of Dolomite

Dedolomitization is a term used to define the transformation of dolomite into another, mainly calcite, mineral phase, and formation of a side product. Generally, the process starts with the dissolution of dolomite due to the release of Mg in its structure. There might be various factors that trigger Mg removal like impurities in dolomite, use of dolomite together with a reactive material like portlandite ($Ca(OH)_2$) or gypsum ($CaSO_4$) relative humidity of medium, *etc*. The dissolution rate gets slower as the calcite and brucite grow on dolomite. This reduces the area of dolomite to be dissolved (Garcia *et al*., 2003).

Impurities in the dolomite matrix may be clay minerals which give rise to the expansion of aggregates in the alkali medium. Ion exchange or removal of organic coatings from clay mineral surfaces might increase their water absorption capacity, which causes swelling and pressure that cause expansion (Hadley, 1961).

Inclusions/impurities in the dolomite structure may also cause dedolomitization. Fe-rich dolomites may dissociate due to the liberation of iron from its structure (orange-brownish color may be observed due to hematite formation). Gypsum ($CaSO_4$) in dolomite gives SO_4^{2-} ions to the medium which favors the formation of epsomite salts ($MgSO_4.7H_2O$) by the reaction with Mg^{2+} liberated from dolomite (Jie *et al*., 2011).

When dolomitic rock particles are used as aggregates in portland cement concrete, the dolomitic aggregates in the concrete containing alkali (Na, K), show extensive expansion properties (Garcia *et al*., 2003; Gillott and Swenson, 1969; Hadley, 1961). Dolomite reacts with portlandite in alkaline medium and dissociates according to Reaction 5.

$CaMg(CO_3)_2 + Ca(OH)_2 \rightarrow 2CaCO_3 + Mg(OH)_2$ ……..…Reaction 5

Production of calcite and brucite in dolomite gives rise to volume increase and expansion in dolomite. In this reaction mechanism, the free energy differences between products and reactants at 25 ºC makes the solubility order as:

$Ca(OH)_2 > CaCO_3 > Mg(OH)_2 > CaMg(CO_3)_2$

The dissolution of $Ca(OH)_2$ to Ca^{2+} and $2OH^-$ increases the pH of the medium. The reaction rate is reported to be controlled by the dissolution of dolomite (Zhang *et al*., 2014). Another possibility considered was the alteration of dolomite surface properties by the adsorption of the charged chemical species in solutions OH^-, H^+, Ca^{2+},CO_3^{2-}. At high pH, the surface is negatively charged and at low pH, the surface is positively charged which creates active sites to form complexes and modifying the surface charge. (Garcia *et al*., 2003)

As a result of dedolomitization reaction and formation of several reaction products in alkaline medium, dolomite particles get larger, which causes a breakdown in alkali concrete (Sherwood and Newlon, 1964). Thus, to control the expansion and cracking in concrete with dolomitic limestone aggregates, low concentration of alkali, control of moisture, and temperature should be considered (Gilliot and Swenson, 1969).

2.6 Some Characteristics at Nanoscale and Use of Hydroxide Nanoparticles as Consolidants for the Conservation of Cultural Heritage

Nanoparticles are the particles having dimensions between 1-100nm (10^{-9} – 10^{-7} m) (10^{-7}-10^{-5} cm) (10-1000A^{o}). As we know, a bulk material has constant physical properties regardless of its size. However, at the nanoscale, size-dependent properties may emerge because of their high surface area and a higher number of atoms at the surface. Thus, they behave different, generally show enhanced properties than in their bulk state. A new property may emerge since optical (like colour), electrical (conductivity), physical (hardness, melting point, etc.) or chemical (reactivity, reaction rate, etc.) properties show difference. For example, gold nanoparticles are deep red to black in solutions compared to their red colour in a colloidal state having size 100A^{0}. Gold nanoparticles melt at about 300 ^{o}C at 2.5nm. Whereas normal gold melts at 1064 ^{o}C (Simona *et al*., 2017).

Phase diagrams, diffusion activation energies are also size- and shape-dependent. This property leads to a change in thermodynamics of the materials; so-called "nanothermodynamics" referred to the temperature, T, defined within a nanoparticle. The basic principle is based on the increase of excess surface energy of small systems. In a bulk material, the stable phase is the one with the lowest bulk Gibbs free energy. In the nanoparticle, the surface and interphase energies should also be considered (Wautelet and Shirinyan, 2009). Such that nano-size materials are more continuously exposed to random collisions with surrounding molecules, which creates fluctuating environments. The fundamental laws of thermodynamics of macro-size materials may thus show deviations in nano-size. Gieseler *et al*. (2014) stated that a nanoparticle trapped with laser light temporarily violates the famous second law of thermodynamics.

Due to these functions, in many disciplines, like energy, health, technology, the use of nanotechnology is developing as well as in the conservation of cultural heritage. In cultural heritage, nanotechnology finds its place as nanoparticles for various conservation purposes as consolidants. They can provide better penetration due to

their very small sizes and long-term durability if compatible material is used. There are various hydroxide nanoparticles used as consolidants like calcium, magnesium barium, strontium, *etc*. (Sierra-Fernandez *et al*., 2017).

Studies on synthesis and application of calcium hydroxide nanoparticles as consolidant are numerous (Dei and Salvadori, 2006; Daniele *et al.*, 2008; Daehne and Hern, 2013; Caner, 2011; Rodriguez-Navarro *et al*., 2013). Calcium hydroxide nanoparticles are dispersed in short-chain aliphatic alcoholic solutions (ethanol, propanol) which shows enhanced stability and high penetration depth. Those properties make use of nanodispersed solutions to re-adhere lifted and detached paint layers in wall painting conservation (Blee and Matison, 2008). Moreover, historical structures may have cracks or fissures (about 1mm) formed due to atmospheric conditions or the use of incompatible materials for restoration. When calcium hydroxide nanoparticles are introduced within the stone matrix or pores, they react with atmospheric CO_2 and form very tiny calcite crystals within the stone and acts as a binder material (Daniele *et al.*, 2008; Gomez-Villalba *et al*., 2012). That is why calcium hydroxide nanoparticles are generally preferred to consolidate limestone ($CaCO_3$)-based structures. On the other hand, for the purpose of dolostone ($CaMg(CO_3)_2$) consolidation, the use of calcium hydroxide nanoparticles might be risky. Since the dolomite has alternating planes of Ca^{2+} and Mg^{2+} between planes of CO_3^{2-} anions, the possible increase in Ca^{2+} ion may lead to the dissolution of dolomite (Lopez-Arce *et al.*, 2010).

There are also few studies on the use of magnesium hydroxide nanoparticles. Since they could be usually obtained in a smaller size than calcium hydroxide nanoparticles, magnesium hydroxide nanoparticles are mostly employed for the deacidification of artworks, such as paper, canvas, and wood which can be categorized as low porosity materials (Giorgi *et al*., 2005)

To make a compatible conservation treatment for Ca-Mg carbonates, like dolomite-based structures, which could be consolidated by particles with an average size of

250 nm. a mixture of calcium hydroxide and magnesium hydroxide nanoparticles are preferred (Chelazzi *et al*., 2013).

As an example, for the use of mixture of calcium hydroxide and magnesium hydroxide nanoparticles: The building stone of Pietra d'Angera was dolomite and the structure was degraded as exfoliations or detachments due to water freeze-thaw cycles and acid rain. That monument was also previously consolidated with commercial products like ethyl silicate, salt-rich cement, and silicone resins, which produced physico-chemical incompatibility. Those consolidation materials provided a hard and impermeable surface that could protect the surface but introduced salt crystallization within the stone pores. As a result, degradation has accelerated. For the preparation of consolidation material, calcium hydroxide (via thermo-mechanical treatment of lime) and magnesium hydroxide (via a homogenous phase reaction) nanoparticles were prepared separately. The continuation of the study was not further mentioned (Chelazzi *et al*., 2013).

In this thesis, calcium hydroxide and magnesium hydroxide nanoparticles were obtained starting from the calcination of natural dolomite. They were synthesized as a mixture and dispersed in alcohol. It is expected that under proper carbonation conditions, they will end up with dolomite formation by overcoming kinetic barrier.

2.7 Carbonation Process of Hydroxide Nanoparticles

When hydroxides undergo carbonation process with atmospheric CO_2 under humid conditions, they are carbonated. This reaction mechanism makes it possible to use it as binders to provide adhesion of porous materials by enhancing the material characteristics and durability in restoration works (Doehne and Price, 2010).

The superiority of nanoparticles for consolidation is based on their high surface to volume ratio, which provides more surface area for adhesion. The carbonation process of hydroxide nanoparticles determines the effectiveness of consolidation, as well as the mineral phases, structure, and morphology of the final precipitate. Thus,

to make an effective consolidation, the conditions for carbonation of hydroxide nanoparticles should be optimized.

- Temperature, relative humidity and carbon dioxide enhancement (partial pressure of CO_2) of the environment,
- pore size and amount of water inside the material pores,
- nanoparticles' crystallinity and size,
- the dispersion medium (the type of solvent, pH)

may all affect the carbonation process (Lopez-Arce *et al*., 2013). Alcohols such as ethanol, isopropanol as a dispersion medium are preferred. While temperature and partial pressure of CO_2 are used to correlate phase diagrams for minerals formation, relative humidity and exposure times also affect the mineral phases of the precipitated products. For example, in the precipitation of calcite, according to the relative humidity and dispersion medium, it might precipitate as vaterite or aragonite (Lopez-Arce *et al*., 2011) and only when CO_2 enhancement of environment is high enough, calcium hydroxide could carbonate as calcite (Lopez-Arce and Zornoza-Indart, 2015).

In the carbonation of magnesium hydroxide, under low T (25 ^{o}C) and low pressure (pCO_2 of 10^{-2}) Nesquehonite ($Mg.CO_3.3H_2O$) is the most commonly formed phase of Mg-Carbonates (Zhao *et al*., 2010) if temperature is raised above 52 ^{o}C, nesquehonite readily transforms into hydromagnesite (Davies and Bubela, 1973). Due to the strong hydration behaviour of Mg^{2+}, magnesite formation requires high T and P (Sayles and Fyfe, 1973).

.

CHAPTER 3

MATERIALS AND METHODS

In this section, the main analytical equipment, experimental materials and set-ups, and procedures used during the research are briefly summarized under the following main headings:

- Major Analytical Equipment and Tools Used for the Analyses
- Dolostone Used in the Study
- Preparation and Examination of Alcohol Dispersion of $Mg(OH)_2$ Nanoparticles
- Carbonation of $Mg(OH)_2$ Nanoparticles Dispersed in Ethanol
- Preparation and Examination of Alcohol Dispersion of $Ca(OH)_2$ and $Mg(OH)_2$ Nanoparticles
- Carbonation of $Ca(OH)_2$ and $Mg(OH)_2$ Nanoparticles Dispersed in Ethanol
- Carbonation of $Ca(OH)_2$ on Nesquehonite
- Preparation of Control Samples and Mixtures for XRD and FTIR Analyses
- Consolidation Experiments

The titles are given with respect to the sequence of the individual experimental procedures during the development of the thesis. Before experimental procedures, main analytical methods used for each experimental procedure are mentioned.

3.1 Major Analytical Equipment and Tools Used for the Analyses

Major analytical equipment used for the analyses are mainly X-Ray Powder Diffraction (XRD), Fourier Transform Infrared Spectroscopy (FTIR), Stereomicroscope, Scanning Electron Microscope (SEM), and Direct Ultrasonic Pulse Velocity (UPV_{direct}).

Samples like dolomite pieces, Calcium Hydroxide and Magnesium Hydroxide nanoparticles, carbonation products that were prepared in the powder form were analysed for their mineralogical composition by XRD and FTIR.

Bruker D8 Advance XRD equipment with Sol-X detector and DiffracSuite software were used for XRD analyses. Analyses were conducted with CuK_{α} radiation adjusted to 40 kV and 40mA. The XRD traces were recorded between 5° –70° 2θ range. XRD data was evaluated by EVA software regarding peak location and intensity values.

Dolomite samples to be investigated by XRD were pulverized in agate mortar. When powdered samples were in small amounts, a special sample holder with well polished metallic surface was preferred. The powdered sample was dispersed in ethanol and a few drops were put on a square-shaped glass lamella and replaced on the metallic surface of the holder after the sample dried. This method was mainly used for the XRD analysis of the samples taken from the petri dish, representing the carbonation products of $Ca(OH)_2$ and $Mg(OH)_2$ nanoparticles dispersed in ethanol.

Some samples powdered in agate mortar were analysed by Infrared Spectroscopy using an FTIR instrument Bruker Alpha-P attached with ATR module. The resulting spectrum was Absorbance. Data was saved from 375-4000 cm^{-1}. Samples were scanned 36 times. The sample to be evaluated was inserted on the crystal surface in the powder form and pressed with the ATR-press unit.

Stereomicroscope (Leica Z16 APO A model) was conducted on thick sections of dolomite samples to view the texture, pores, and cracks. Thick sections of dolomite samples were prepared by cutting them with a low speed saw (Buehler Isomet).

SEM (FEI - QUANTA 400F Field Emission SEM model) was used for the microstructural analyses of thick section of stone, and samples in the powder form. Both type of samples were firmly attached on a carbon tape on aluminium SEM sample holder and then coated by gold layer. The powdered samples were firmly attached to the carbon tape, and then nitrogen-gas was blown to the carbon tape by

gun to get rid of the loose particles. The elemental composition of samples were examined by using SEM-EDAX.

UPV_{direct} being an important physicomechanical property was measured to assess the change in dolostone samples' before and after consolidation treatments

For UPV measurements, PUNDIT Plus Pulse Generating Equipment was used with 220 kHz transmitter and receiver probes in the direct transmission mode (Figure 8). The direct ultrasonic velocity of a sample with a known distance can be calculated by inserting the transmitter and receiver probes to two opposing sides of the sample latitudinally. The distance between probes (d) was measured with a sensitive caliper rule in cm. The time that ultrasonic waves pass through the cross direction of the samples (t) was measured in microseconds (μs). Direct ultrasonic velocity was calculated by using Equation 4 (RILEM 1980a, ASTM 1990).

$$UPV = \frac{d}{t}\ m.s^{-1} \quad \text{.....Equation 4}$$

Figure 8. Representation of Direct UPV Measurement

XRD, FTIR, Stereomicroscope, and UPV analyses were conducted at Materials Conservation Laboratory, Department of Architecture. SEM analyses were performed at METU Central Laboratory.

3.2 Dolostone Used in the Study

Dolostone, used in the study, serve two purposes. Firstly, the preparation of $Ca(OH)_2$ and $Mg(OH)_2$ nanoparticles, and secondly, the consolidation treatment experiments. For those purposes, the dolostone, extracted from Yolbaşı quarries locating in Midyat-Mardin, in Turkey's South-Eastern region, was used (Figure 9).

Figure 9. Location of Yolbaşı town in Midyat-Mardin, in Turkey.

It is highly probable that Yolbaşı dolostone quarry formation belongs to the Mardin formation (Gordey, 1971). In the thesis, since dolostone samples were obtained from Midyat-Mardin, they are named as "Midyat dolostone," indicating its source.

The verification and characterization of the mineralogical composition of Midyat dolostone were done by XRD and FTIR analyses (Figure 10&Figure 11). XRD traces of Midyat dolostone sample show that Midyat dolostone is composed of dolomite mineral having its characteristic peaks (Table 6). Moreover, as determined by thin section analyses, it is crystalline dolomite (TUBITAK-CNR–Bilateral Project 213M554).

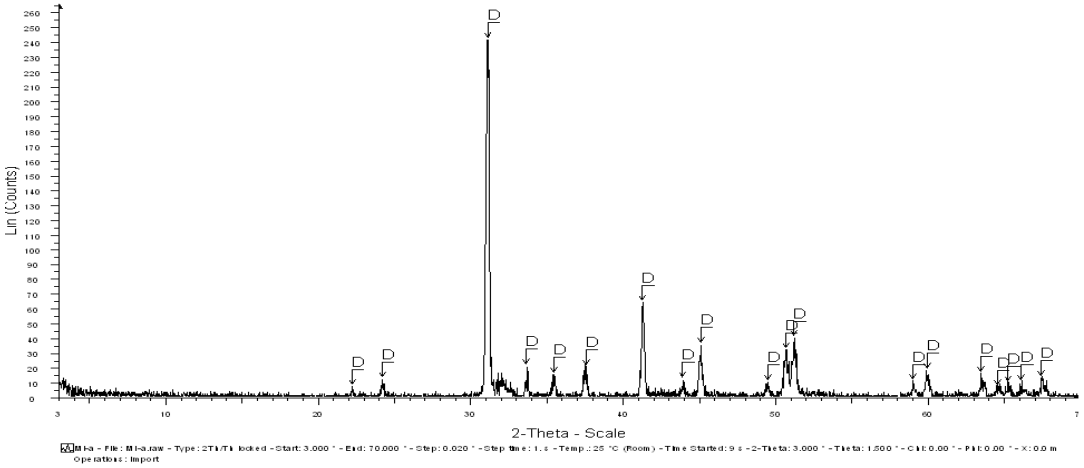

Figure 10. XRD traces of dolostone sample taken from Midyat-Yolbaşı quarries: D-Dolomite

Table 6. Peak locations and d-values of XRD traces of Midyat Dolostone.*denotes dolomite ordering peaks

~XRD peak location (°2θ)	d-Spacing (Angstroms)	Relative XRD peak intensity
Midyat Dolomite		
22.15*	4.00	3.3
24.11	3.69	11.9
31.17	2.87	100
33.67	2.66	8.5
35.41*	2.53	6.5
37.58	2.39	9.9
41.27	2.19	26.5
43.93*	2.06	4.7
45.02	2.01	15.4
49.47	1.84	4.1
50.67	1.80	13.7
51.27	1.78	16.9
59.09	1.56	4.2
59.96	1.54	7.0

In the FTIR spectrum of Midyat dolostone sample, the peak of symmetric deformation of the carbonate group belonging to dolomite appears at 728 cm^{-1}. This peak is the characteristic peak of dolomite that can be used to distinguish it from other carbonates. The band at 877 cm^{-1} shows the asymmetric deformation of carbonate group. The stretching peaks of carbonate group form a band around 1400-1500. Here showing a peak at 1427 cm^{-1} for dolomite (Figure 11).

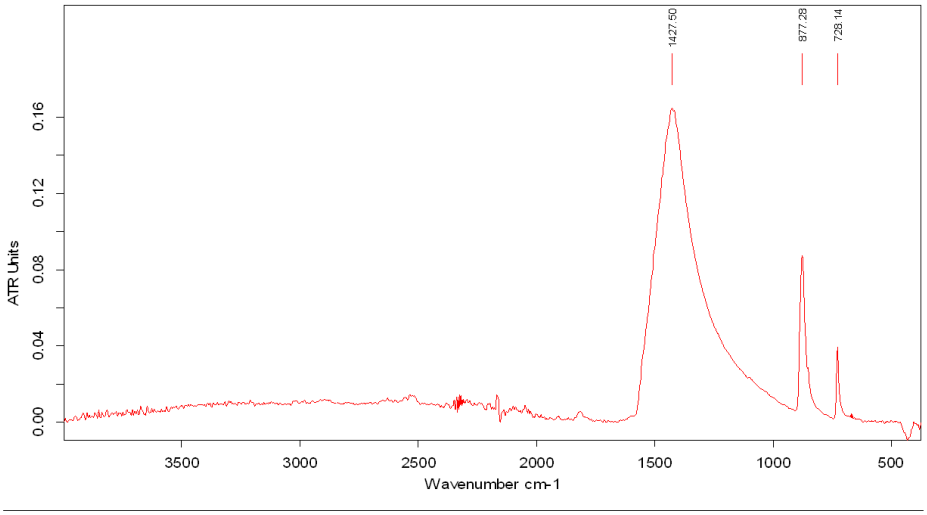

Figure 11. FTIR spectrum of Midyat dolostone

Midyat dolostone is a porous stone having macro-pores of various sizes. (Figure 12).

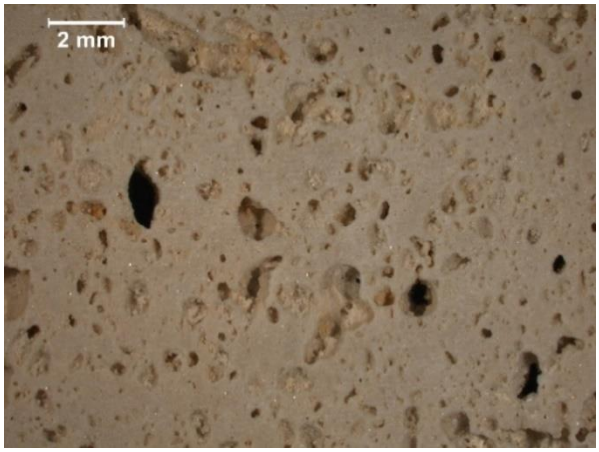

Figure 12. Stereomicroscopic view of macro-pores of Midyat dolostone in a cross-section at 20x magnification

Some dolostone samples show calcite veins and orange-colored impurities around those veins (Figure 13) (TUBITAK-CNR–Bilateral Project 213M554). Orange impurities were identified by the analysis of the acid-insoluble part. In order to determine the percentage of acid-insoluble inclusions, the crushed dolomite sample was treated with 2% HCl to dissolve the carbonate minerals. The acid-insoluble part was filtered through Whatman No.40 filter paper and washed with distilled water, and then the sample was dried on filter paper. The acid-insoluble material on filter paper was analyzed with SEM-EDAX for its elemental composition.

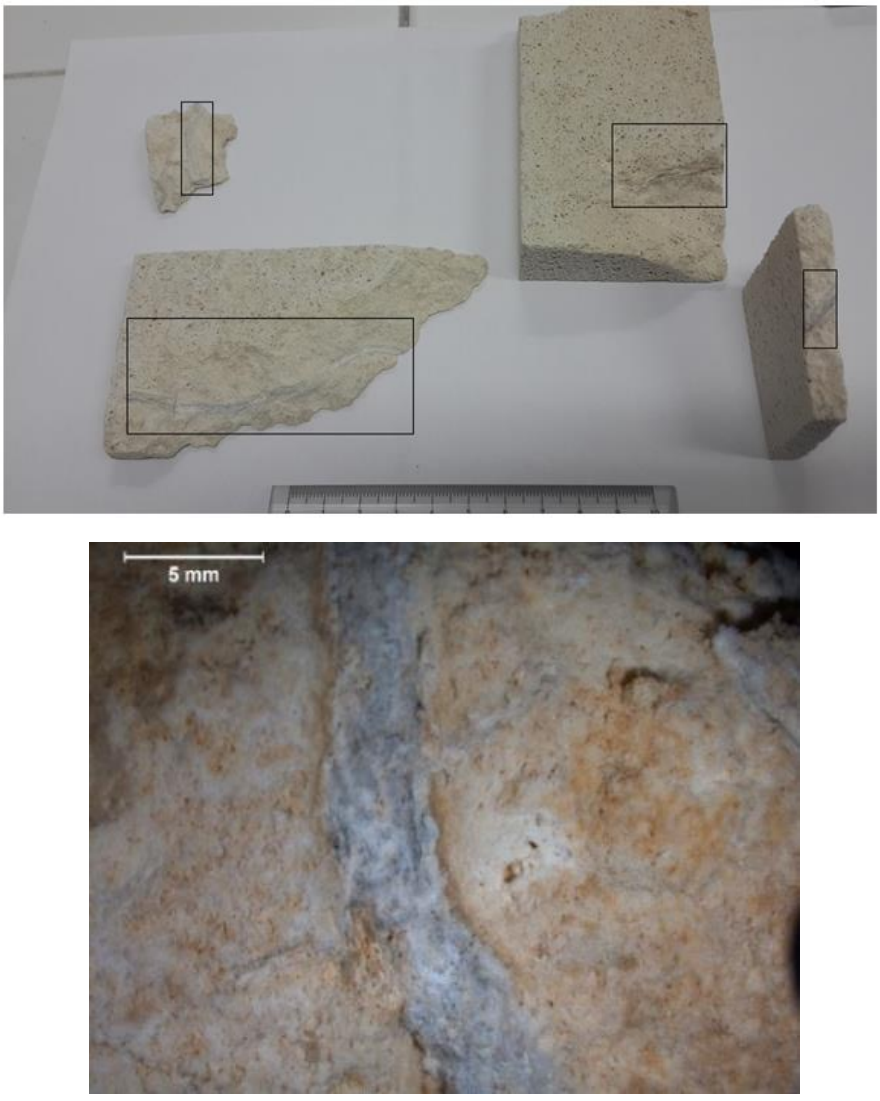

Figure 13. Photographic image of Midyat dolostone samples where veins appear (up) and Stereomicroscope image of the vein and orange colors around veins (down)

The acid-insoluble part of dolostone was less than 1% by weight, collected on filter paper (Figure 14). In EDAX analyses, the presence of silicon (Si), titanium (Ti), iron (Fe), and aluminum (Al) elements are detected (Figure 15&Figure 16). It is concluded that the impurities are most probably composed of iron oxide, titanium oxide, and clay minerals.

Figure 14. The insoluble acid part of Midyat dolostone, filtered and dried.

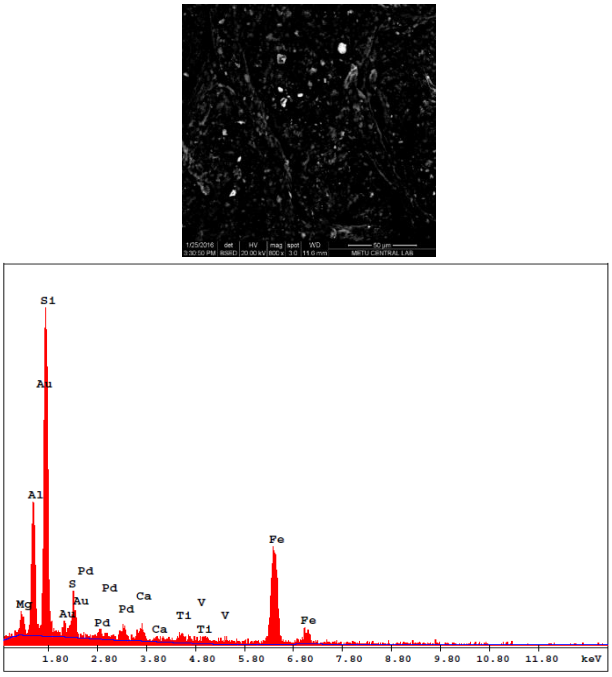

Figure 15. SEM-EDAX image of acid-insoluble part of the dolostone sample at 500x magnification: showing the presence of silicon, aluminum, and iron.

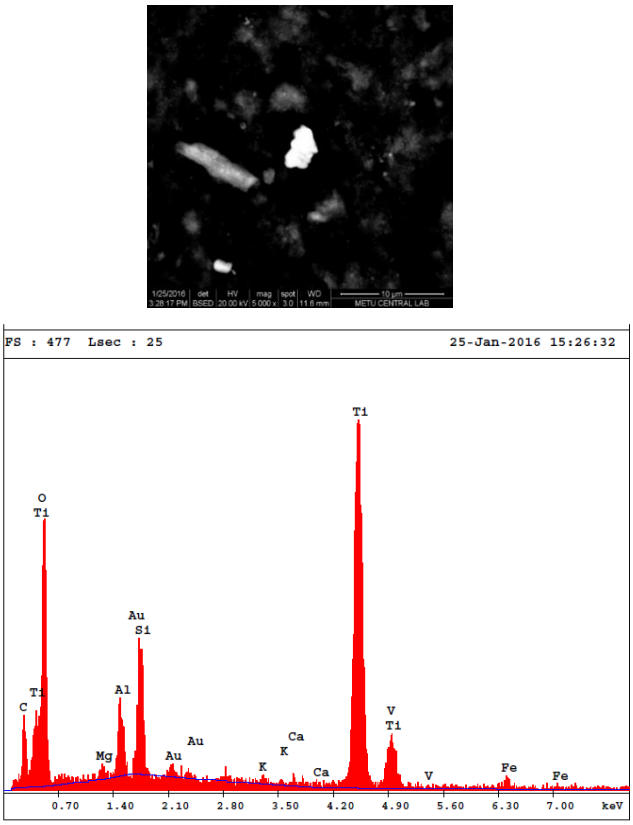

Figure 16. SEM-EDAX image of acid-insoluble part of the dolostone sample at 5000x magnification: showing the presence of oxides of titanium and silicon

Midyat dolostone has bulk density of 1,89±0,02 g/cm^3, and effective porosity of 27,6 ± 0,9% by volume. Due to the heterogeneous distribution of its pores, the average ultrasonic velocity of the stone in the dry state varies between 2600-3200m/s. The calculated modulus of elasticity is in the range of 12-20 GPa (Table 7) (TUBITAK-CNR–Bilateral Project 213M554).

Table 7. Physical and Physicomechanical Properties of Midyat dolostone.

Stone Sample	ρ	φ	UPVdry	Emod
	g.cm^{-3}	volume %	m.s^{-1}	GPa
Midyat dolostone	1,89 ±0,02	27,6 ± 0,9	2600± 200	12 ± 2
			3200 ± 200	20 ± 2

Midyat dolostone has a unique crystal structure, and it has a heterogeneous and porous nature that can be observed from the SEM view of the pores (Figure 17) (TUBITAK-CNR–Bilateral Project 213M554).

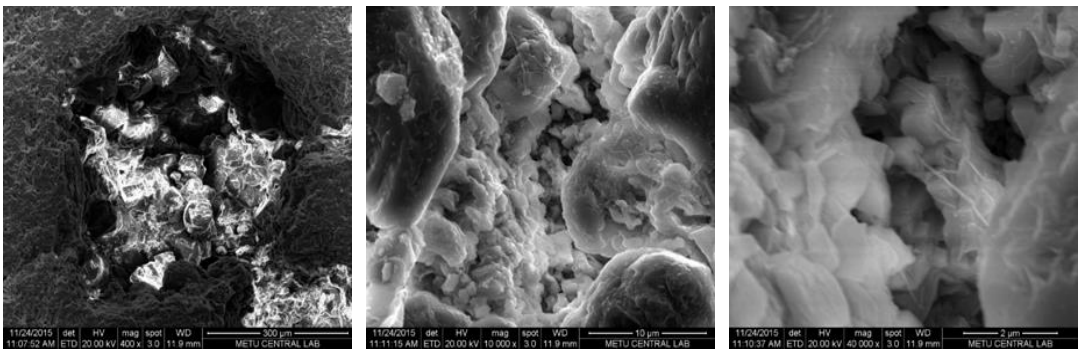

Figure 17. SEM images of Midyat dolostone pores: The general view of a big pore (400x) left; detailed views of crystals inside the pores: (10000x) middle and (40000x) right

3.3 Preparation and Examination of Alcohol Dispersion of $Mg(OH)_2$ Nanoparticles

$Mg(OH)_2$ nanoparticles were produced starting from Magnesite ($MgCO_3$). Magnesite sample, broken and powdered, was calcinated at 600^oC for 4 hours to obtain reactive MgO (periclase). To slake MgO to $Mg(OH)_2$ (brucite), considering exothermic reaction and some of the water evaporation, water was added a bit more than the sufficient amount and stirred in an ultrasonic vibrator. The obtained $Mg(OH)_2$ nanoparticles were then dried and dissolved in ethanol to get alcohol dispersion of $Mg(OH)_2$ nanoparticles. The solution was stirred for 2 hours in an ultrasonic vibrator and 24 hours on magnetic stirrer to satisfy well dispersion. Calcination, and slaking products were examined by XRD.

3.4 Carbonation of $Mg(OH)_2$ Nanoparticles Dispersed in Ethanol

Carbonation of $Mg(OH)_2$ nanoparticles were experimented in order to find out the final product/mineral phase when $Mg(OH)_2$ nanoparticles alone carbonate at high RH and high CO_2 partial pressure. $Mg(OH)_2$ nanoparticles, dispersed in ethanol,

carbonated in petri dish in a desiccator with high RH (90-95%) and high CO_2 partial pressure (pCO_2~0.4 atm) for 10 days.

3.5 Preparation and Examination of Alcohol Dispersion of $Ca(OH)_2$ and $Mg(OH)_2$ Nanoparticles

In the thesis, the consolidant, $Ca(OH)_2$ and $Mg(OH)_2$ nanoparticles dispersed in ethyl alcohol, was produced starting from Midyat dolostone. Since dolomite consists of Ca-Mg carbonate, this consolidant was thought to be useful to provide long term durability by achieving a compatible consolidation of deteriorated dolostone.

$Ca(OH)_2$ and $Mg(OH)_2$ nanoparticles dispersed in ethanol was produced by following the steps in the sub-sections below.

3.5.1 Calcination of Midyat Dolostone

Midyat dolostone samples were broken into small pieces, pulverized into fine powder, and then sieved to seperate the powder below 125μm size. The powder was put in a ceramic crucible and heated to 900ºC in an oven for 4 hours (Figure 18). After 4 hours of heating at 900 ºC, the oven was cooled and the crucible was taken out. Dolomite was expected to release CO_2 to form CaO and MgO according to the Reaction 6.

$$CaMg(CO_3)_2(s) \rightarrow CaO(s) + MgO(s) + CO_2(g)\text{……...……..Reaction 6}$$

The final products were followed by XRD.

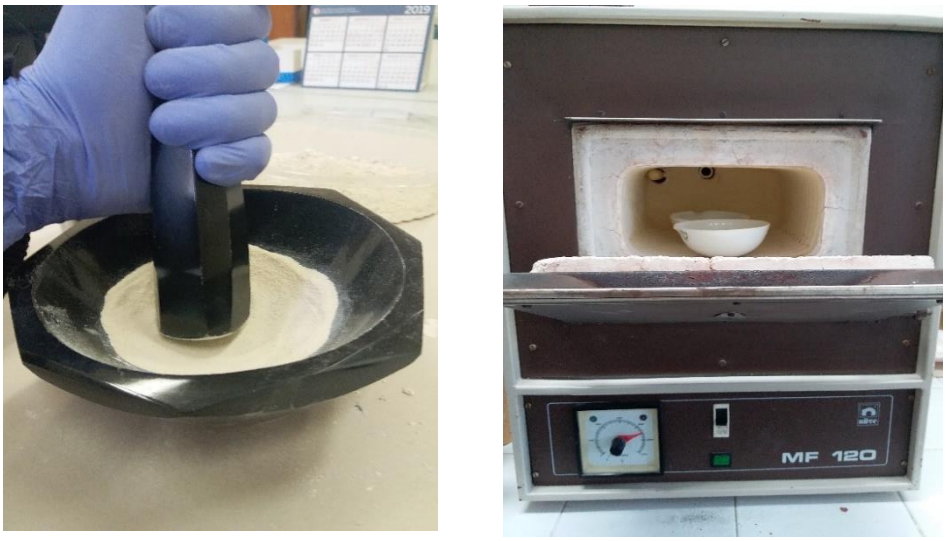

Figure 18. Pulverization and thermal decomposition stages of dolostone.

3.5.2 Slaking of CaO and MgO

Calcination products, CaO (Lime) and MgO (Periclase), were then hydrated with distilled water to produce $Ca(OH)_2$ and $Mg(OH)_2$ nanoparticles (Reaction 7). $Ca(OH)_2$ and $Mg(OH)_2$ nanoparticles were dried in a desiccator containing $CaCl_2$ as desicant. Dried nanoparticles were analyzed with XRD, FTIR, and SEM-EDAX.

$$CaO(s) + MgO(s) + 2H_2O \rightarrow Ca(OH)_2\,(s) + Mg(OH)_2\,(s) \quad \text{……Reaction 7}$$

3.5.3 Dispersion and Stability of $Ca(OH)_2$ and $Mg(OH)_2$ Nanoparticles in Ethanol

5g of dried nanoparticles were dispersed in 100 ml of ethanol to get them in suspension. $Ca(OH)_2$ and $Mg(OH)_2$ nanoparticles in ethanol was then stirred with ultrasonic vibrator for 2 hours followed by magnetic stirring for 24 hours. Dispersion was examined for its stability in $Ca(OH)_2$ and $Mg(OH)_2$ nanoparticles' concentration. the composition of the solution was analyzed by XRD after 0, 4, 24, 44, and 72 hours of relaxation. In the study, it was assumed that dolomite

($CaMg(CO_3)_2$) fully calcinated to CaO and MgO, and they were hydrated as $Ca(OH)_2$ and $Mg(OH)_2$. The ratio of $Mg(OH)_2$: $Ca(OH)_2$ concentrations was described as Mg:Ca ratio of the solution. Under those circumstances, Mg:Ca ratio of the solution was assumed as 1 at the beginning, since Mg:Ca ratio of the original dolomite was assumed as 1.

Two sets of ethyl alcohol dispersion of $Ca(OH)_2$ and $Mg(OH)_2$ nanoparticles were prepared and analyzed to see the effect of Mg:Ca ratio on carbonation experiments.

The first set was prepared by allowing large nanoparticles in the solution to settle. In this way, it was thought that finer nanoparticles suspended in ethyl alcohol solution can be an advantage for stone conservation. The alcohol dispersion of $Ca(OH)_2$ and $Mg(OH)_2$ nanoparticles after 16 hours of settlement was called the first set (Set-1).

In the second set, nanoparticles were well dispersed in ethanol by vigorous stirring. Carbonation of solution was started immediately without any relaxation of that solution, in which the estimated Mg:Ca ratio of the solution was 1 (Set-2).

3.6 Carbonation of $Ca(OH)_2$ and $Mg(OH)_2$ Nanoparticles Dispersed in Ethanol

Carbonation experiments were conducted in petri dishes with set-1 and set-2 solutions, which are described in the previous section. Around 10 ml of alcohol dispersion was poured into petri dishes and put in a desiccator for carbonation process. To identify the most effective carbonation condition, three different conditions were tested with respect to relative humidity and carbon dioxide partial pressure. Firstly, room condition: low RH (35%) and low CO_2 partial pressure (pCO_2 ~ 0.3 mmHg), and secondly, high relative humidity (RH (90-95%) and low CO_2 partial pressure (pCO_2 ~ 0.3 mmHg) conditions were experimented. In the second condition, relative humidity was kept constant with saturated KNO_3 salt solution inserted at the bottom of the desiccator.

Carbonation of $Ca(OH)_2$ and $Mg(OH)_2$ nanoparticles dispersed in ethanol was performed only with set-1 solution under the first and second conditions. The carbonation products were followed by XRD after 4 weeks.

Third condition was high relative humidity (RH (90-95%) and high CO_2 partial pressure (pCO_2 ~ 0.4 atm) condition. The carbonation experiments were conducted both for set-1 and set-2 solutions. The detailed experimental set-up was described in the following sub-section in detail.

3.6.1 Carbonation of $Ca(OH)_2$ and $Mg(OH)_2$ Nanoparticles Under High Relative Humidity (90-95%) and High CO_2 Partial Pressure ($p(CO_2)$~0.4 atm) Conditions

In the experimental set-ups of set-1 and set-2 solutions, the petri dishes were inserted in a desiccator under high relative humidity (90-95%) and high CO_2 partial pressure (pCO_2~0.4 atm).

To keep relative humidity constant at around 95%, a saturated KNO_3 salt solution was inserted at the bottom of the desiccator.

CO_2 was supplied in the desiccator through the reaction of concentrated oxalic acid and sodium bicarbonate in a beaker (4grams of oxalic acid+6.8grams of sodium bicarbonate+200ml of distilled water for 4lt desiccator) (Reaction 8)

$C_2H_2O_4 + 2NaHCO_3 \rightarrow C_2O_4Na_2 + 2CO_2 + 2H_2$…….……Reaction 8

4g 6.8g

0,04 mole 0,08 mole

- The reaction produced 0,08 moles of CO_2 gas (M_W = 44,01 g/mole) which is 3520 mg CO_2 in 4 liters of desiccator.
- To calculate the partial pressure of CO_2 gas in the desiccator, the formula below was used (Equation 6) (Converter Parts Per Million (ppm) from Lenntech calculator)

$$1\ \text{ppm} = \frac{1\ \mu L\ of\ CO_2}{1L\ of\ air} \quad \text{Equation 6}$$

- 44.01 grams (1 mole) of CO_2 occupies 22.4 L
- 3520 mg=3.52 grams of CO_2 occupies 1.79 L=1.79x10^6 µL of CO_2
- The volume of desiccator is 4 liters

$$x\ ppm = \frac{1.79\text{x}10^6 \mu\text{L of } CO_2}{4\text{L of desiccator}}$$

- In 4liters of desiccator, the concentration of 3520 mg of CO_2 (x) is 447.898 ppm
- In the atmosphere, the concentration of carbon dioxide is 450 ppm and it has a partial pressure of $_PCO_2$ = 0.3 mmHg
- 447.898 ppm CO_2 has 299 mmHg partial pressure of CO_2 which is $_PCO_2$ = 0.4 atm (1 atm =760 mmHg)
- -log(0.4) = 0.4

For the first set where the solution was at 16th hour of relaxation (set-1), the carbonation products were examined starting from the very early stages until 7 months (3 hours, 1, 3, 7, 17, 21, 28, 58 days, and 7 months) to observe the order of minerals formed, i.e., to understand whether precursor minerals are formed or there are direct precipitation (dissolution and precipitation) reactions. The carbonation products were analyzed by XRD, and at some stages confirmed with FTIR. Microstructure was analyzed by SEM and EDAX. Samples used for the analyses were taken randomly from the petri dish without any consideration of layering of carbonation products. Importance of layering of products was realized during second set of carbonation experiments.

For the second set, the solution was used right after its preparation without any settlement (set-2), the carbonation products were examined at 1,2,3,4,5 and 10^{th} days by XRD. SEM images of the products at 1^{st},2^{nd}, and 10^{th} days were taken, EDAX analyses were carried out for the 10^{th}-day image. The carbonation products at the 10^{th} day was also examined with FTIR. For the analyses of early days of carbonation,

the lid of the desiccator was opened each day to pick up the sample to be analyzed from petri dish. CO_2 supply was renewed at each opening for the 1^{st},2^{nd}, 3^{rd}, and 4^{th} days. In addition, two separate desiccators having the same experimental conditions containing the petri dishes were opened for the first time at 5^{th} and 10^{th} days to examine the carbonation products. In this way, the system (CO_2, H_2O, and solution) was not disturbed until 5^{th} and 10^{th} days. The XRD and FTIR of the carbonation products at 10^{th} day was compared with that of Midyat dolomite data.

Second set (set-2) carbonation products were examined in two layers in the petri dishes. The conditions in the first layer (upper layer) can be described as being in the solution-air interface. The conditions in the second layer (bottom layer) can be described as being more in the solution-solution interface.

3.7 Carbonation of $Ca(OH)_2$ on Nesquehonite

To understand the dolomite formation mechanism, carbonation of $Ca(OH)_2$ nanoparticles on nesquehonite was experimented. Nesquehonite was obtained by the method described in section 3.4. Nesquehonite was in the solid form and $Ca(OH)_2$ nanoparticles were added on nesquehonite aggregates several times in ethyl alcohol dispersion. Carbonation of $Ca(OH)_2$ on nesquehonite was performed under high relative humidity (RH (90-95%) and high CO_2 partial pressure (pCO_2 ~ 0.4 atm) condition for 2 months. The products formed were analyzed by XRD.

3.8 Preparation of Control Samples and Mixtures for XRD and FTIR Analyses

The expected carbonation products that could be observed at different stages of carbonation process were mainly calcite, dolomite, and nesquehonite. Nesquehonite which was synthesized in the laboratory, and relatively pure minerals of calcite and dolomite that were purchased, served as control samples. They were prepared in powdered form and analyzed by FTIR and XRD to be used as control samples. Since

the carbonation products may appear as mixtures, comtrol mixtures of dolomite-calcite and calcite-nesquehonite with known ratios were prepared from the same samples..

Control mixtures of Calcite (Ca) and Nesquehonite (Nes) were prepared with the ratios: Ca:Nes-0.2:0.8; Ca:Nes-0.4:0.6; Ca:Nes-0.6:0.4; Ca:Nes-0.8:0.2. XRD analyses of those mixtures have been carried out for the identification and observation possibilities of individual Calcite and Nesquehonite in those mixtures. XRD traces were thought to be useful for the identification of carbonation products.

Control mixtures of Calcite (Ca) and Dolomite (Dol) were prepared with the ratios: Ca:Dol-0.2:0.8; Ca:Dol-0.4:0.6; Ca:Dol-0.5:0.5; Ca:Dol-0.6:0.4; Ca:Dol-0.8:0.2. FTIR analyses of those mixtures have been carried out for the observation of dolomite formation even in the presence of very small amounts.

3.9 Consolidation Experiments

Consolidation experiments include a set of experiments to assess the effectiveness of conservation treatment for deteriorated dolostone samples.

3.9.1 Consolidation Experiments with Dolostone and Evaluation of Effectiveness of Consolidation Treatment

Consolidation experiments comprise two steps. First step is the injection or capillary suction of alcohol dispersion of $Ca(OH)_2$ and $Mg(OH)_2$ nanoparticles into the dolostone through the cracks, pores, and capillaries (Figure 19). The second step is the carbonation process of nanoparticles in a desiccator with high relative humidity (90-95%) and high CO_2 partial pressure (pCO_2~0.4 atm) for about 2 months (Figure 20). A Midyat dolostone sample, a cube of 5*5*5 cm^3 dimensions, and thick sections of dolomstone samples (1*1*0.2 cm^3) were used for the consolidation experiments.

The cube sample was chosen randomly between the samples showing natural cracks or defects as shown in the Figure 19.

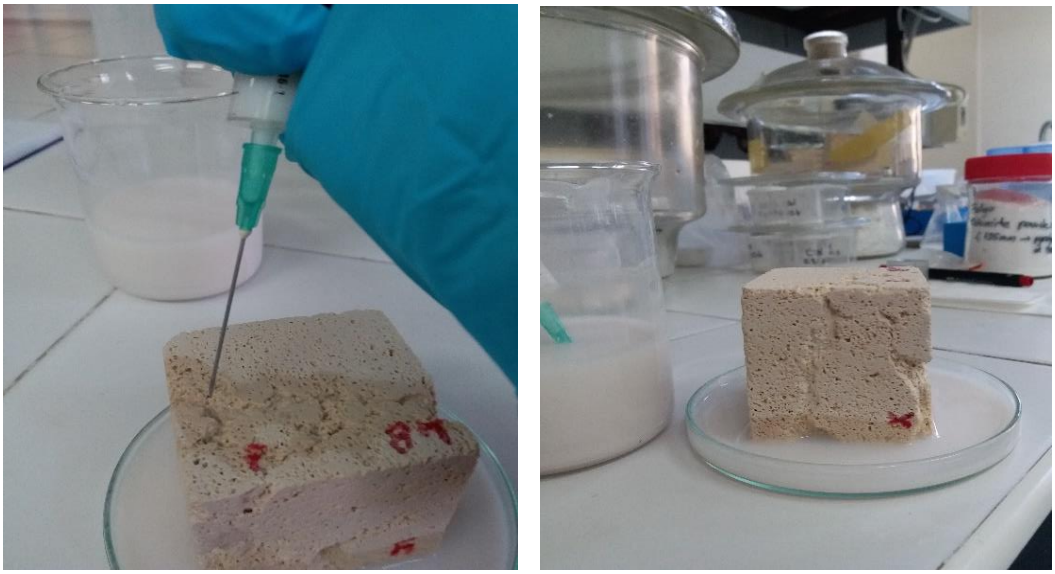

Figure 19. Application methods of alcohol dispersion of $Ca(OH)_2$ and $Mg(OH)_2$ nanoparticles for consolidation/treatment of deteriorated dolostone sample

Figure 20. Representation of carbonation process of dolomite samples in desiccator with high RH and high CO_2 partial pressure.

In order to evaluate the efficiency of the consolidation treatment, changes in physicomechanical and microstructural properties were followed before and after the consolidation treatment. The changes in physicomechanical properties were examined by UPV_{direct} measurements on the cube sample, and the changes in the microstructure of dolomite were analyzed by SEM-EDAX analyses of thick sections and Stereomicroscope images of cube sample.

For UPV_{direct} measurements, from each opposing face of three surfaces of the cube (x-x',y-y',z-z') (Figure 21-Figure 23), 9 points (1a,1b,1c,2a,2b,2c,3a,3b,3c) (27 points in total) were labelled. From each point at least 5 readings were recorded. The UPV readings were recorded as minimum, maximum and average values which are described such that:

- Minimum values are the values read from the weak zones of the dolomite cube.
- Maximum values as the values read from the durable zones of the dolomite cube.
- Average value is the average of UPV_{direct} values measured from 27 points at three surfaces.

Some points where there were no visible cracks were accepted as the characteristic UPV value of the dolostone before treatment; namely; x-x'(2b) and x-x' (3a). UPV values after consolidation treatment were evaluated in comparision to UPV values before treatment as well as with the characteristic UPV value of dolomite (reference readings)

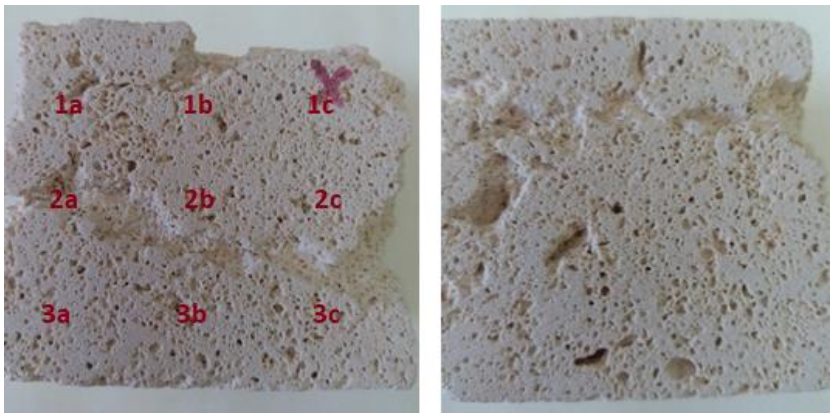

Figure 21. x(front)-x'(back) faces of dolostone cube with around 5*5*5 cm^3 dimensions

Figure 22. y(front)-y'(back) faces of dolostone cube with around 5*5*5 cm^3 dimensions

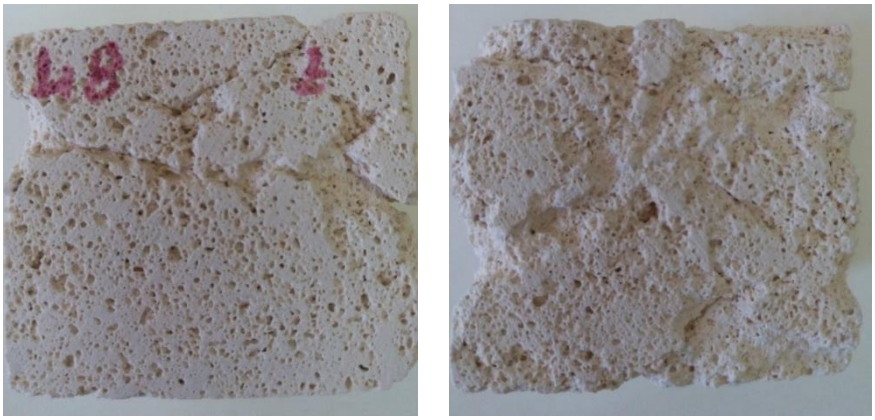

Figure 23. z(front)-z'(back) faces of dolostone cube with around 5*5*5 cm^3 dimensions

3.9.2 Adhesive Property of Carbonation Products

To assess the adhesive (or keeping together) properties of carbonation products of $Ca(OH)_2$ and $Mg(OH)_2$ nanoparticles, a cube sample broken into two (Figure 24) was tied together with a rope. The alcohol dispersion of $Ca(OH)_2$ and $Mg(OH)_2$ nanoparticles was injected through the broken line without taking care of the amount but until a full saturation was ensured. The sample left in a desiccator with high RH (90-95%) and high $p(CO_2)$ (0.4 atm) for carbonation process. The sample was analyzed by visual analyses after 7 months.

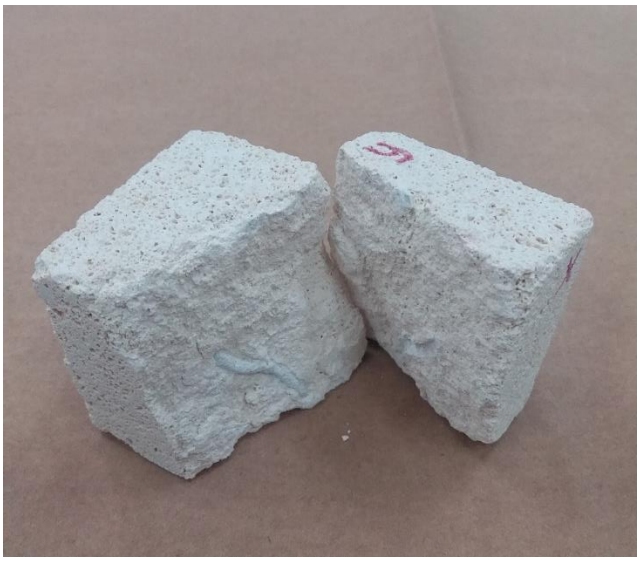

Figure 24.Broken dolostone cube before treatment with alcohol dispersion of $Ca(OH)_2$ and $Mg(OH)_2$ nanoparticles

CHAPTER 4

RESULTS

The results of conducted experiments and analyses are presented in the order of flow of the thesis under the following main topics:

- Analyses of the preparation stages of $Mg(OH)_2$ nanoparticles from magnesite
- Carbonation of $Mg(OH)_2$ nanoparticles
- Analyses of the preparation stages of alcohol dispersion of $Ca(OH)_2$ and $Mg(OH)_2$ nanoparticles from Midyat dolostone, including the stability assessment of the solution
- Carbonation of alcohol disperion of $Ca(OH)_2$ and $Mg(OH)_2$ nanoparticles at different relative humidity, CO_2 partial pressure, and Mg:Ca ratios
- Carbonation of $Ca(OH)_2$ nanoparticles on nesquehonite
- Consolidation treatment of deteriorated dolostone with alcohol dispersion of $Ca(OH)_2$ and $Mg(OH)_2$ nanoparticles

4.1 Analyses of Preparation Stages of $Mg(OH)_2$ Nanoparticles from Magnesite

This part presents the XRD diagrams of the products formed upon calcination of magnesite ($MgCO_3$) and slaking of periclase (MgO) as described in section 3.3. Calcination of $MgCO_3$ yielded MgO (periclase mineral) as seen by the XRD traces (Figure 25).

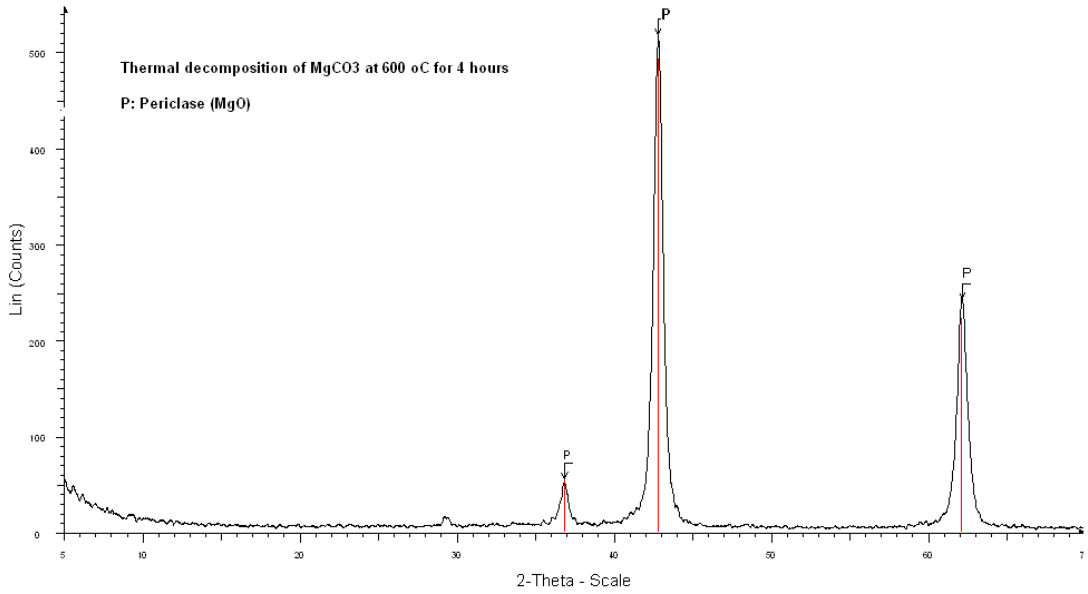

Figure 25. XRD analysis of calcination product of $MgCO_3$: P: Periclase (MgO)

Slaking of periclase formed $Mg(OH)_2$ (brucite) nanoparticles as shown in the XRD traces of dried powder sample (Figure 26). Afterwards, $Mg(OH)_2$ nanoparticles were dispersed in ethanol before its carbonation process.

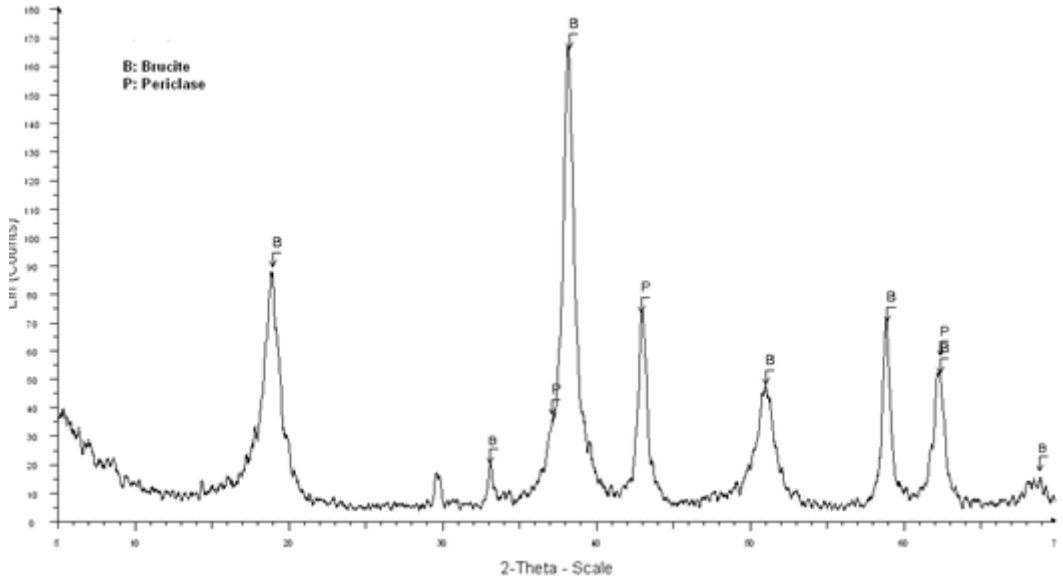

Figure 26. XRD trace of slaked product of MgO: B: Brucite ($Mg(OH)_2$), P: Periclase (MgO)

4.2 Carbonation of $Mg(OH)_2$ Nanoparticles

The carbonation of $Mg(OH)_2$ nanoparticles at high RH (90-95%) and high CO_2 partial pressure ($p(CO_2)$~0.4 atm) resulted in the formation of nesquehonite ($MgCO_3.3H_2O$) at the end of 10 days as characterized by Stereomicroscope, XRD, and FTIR analyses. The stereomicroscope images well revealed the cauliflower like aggregates of nesquehonite crystals of around 2 mm size- a collection of around 1 mm sized needles (Figure 27).

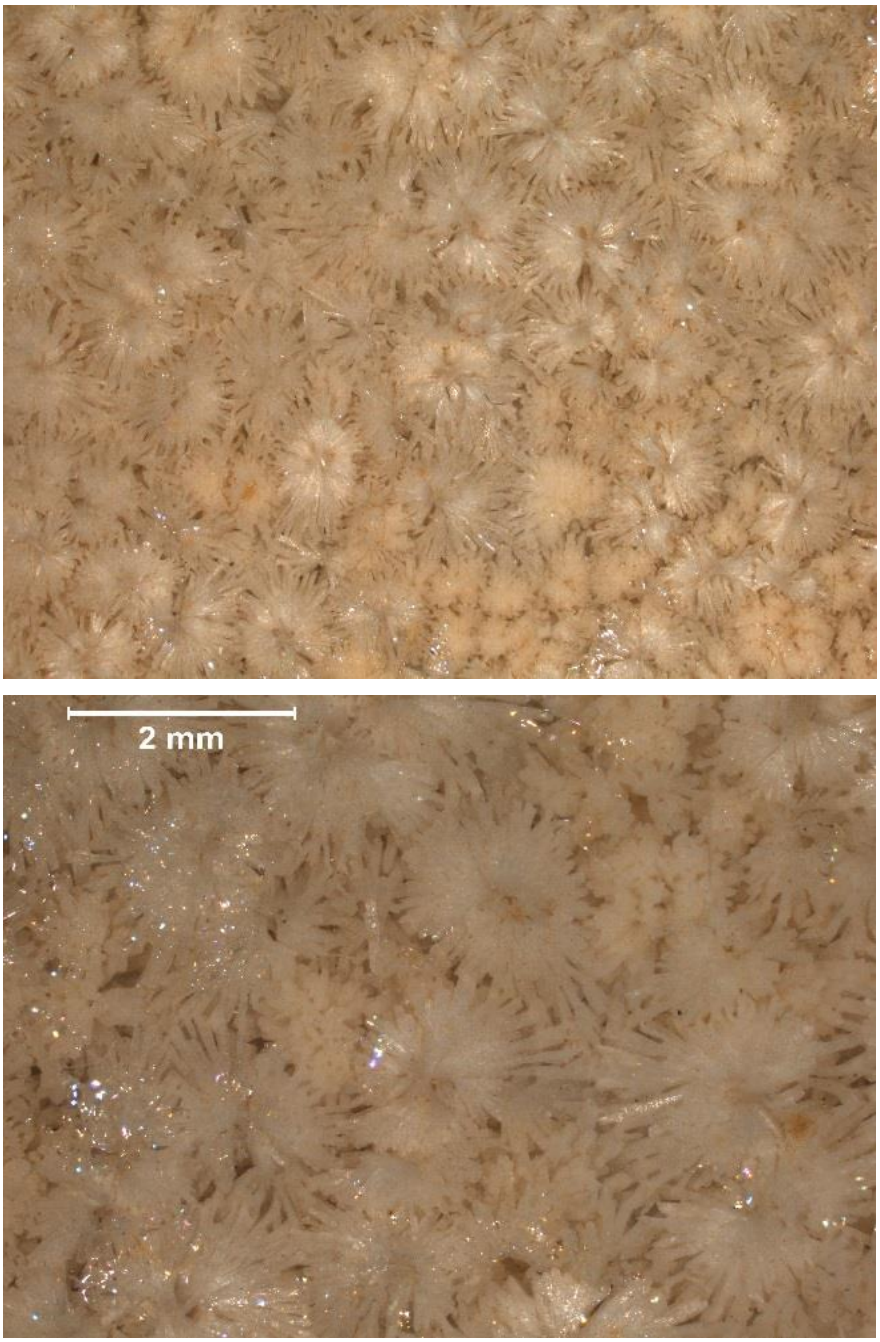

Figure 27. Stereomicroscope images of nesquehonite crystals formed after carbonation of $Mg(OH)_2$ at high relative humidity and high CO_2 partial pressure: 10x (up) and 30x (down).

XRD traces showed the typical peaks of nesquehonite (Figure 28)(Table 8).

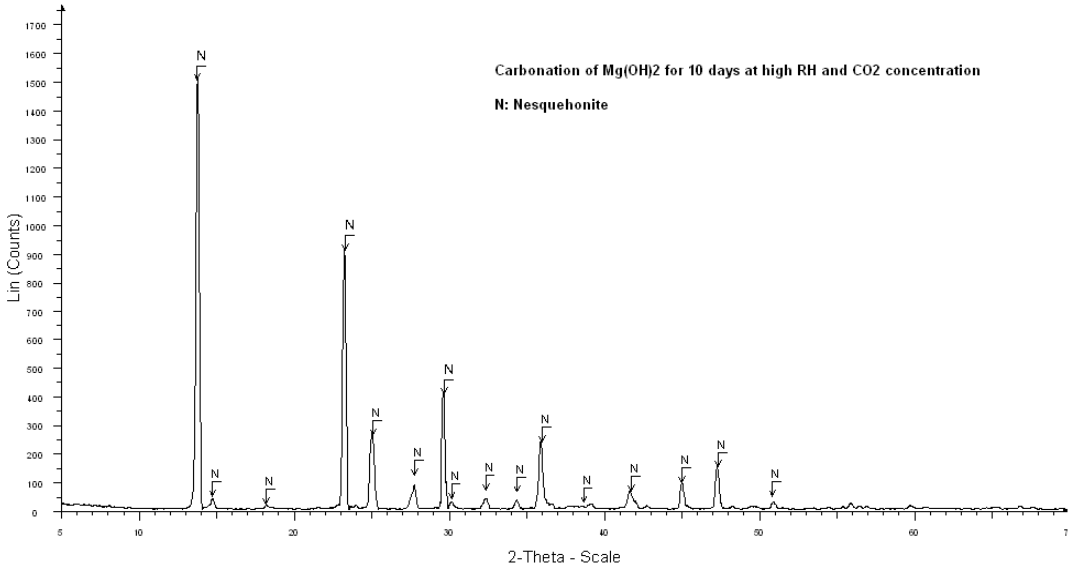

Figure 28. XRD analysis of carbonation product of $Mg(OH)_2$ at the 10th day: N: Nesquehonite ($MgCO_3.3H_2O$)

Table 8. XRD data of synthesized nesquehonite

~XRD peak location ($^o2\theta$)	d-Spacing (Angstroms)	Relative XRD peak intensity
Nesquehonite		
13.74	6.43	100
14.69	6.02	3.9
18.11	4.89	2.7
23.83	3.80	62
25.07	3.55	19.7
27.75	3.21	9.8
29.60	3.01	26.8
34.34	2.61	5.4
36.02	2.49	16.2
41.81	2.16	4.9
45.08	2.00	7.4
47.34	1.92	11.1
50.82	1.79	3

FTIR analysis confirmed its mineralogy (Figure 29). The FTIR spectrum of synthesized nesquehonite displays bending angular mode as splits at 665 and 693 cm^{-1}. Asymmetric deformation of carbonate groups is around 851 cm^{-1}. Symmetrical stretching of carbonate appears at 1099 cm^{-1} as a weak band. Two strong bands belonging to asymmetric stretching of carbonate groups occur around 1406 and 1514 cm^{-1} as splits. Besides, a shoulder is present at around 1450 cm^{-1}. The 1643 cm^{-1} band can be ascribed to an OH-bending mode of water, resulting from the presence of a small amount of absorbed water on the surfaces of the nesquehonite crystals. In addition, the three water molecules of nesquehonite can be recognized from the OH-stretching region between 2500 and 4000 cm^{-1} (Kloprogge et al., 2003) (Figure 29).

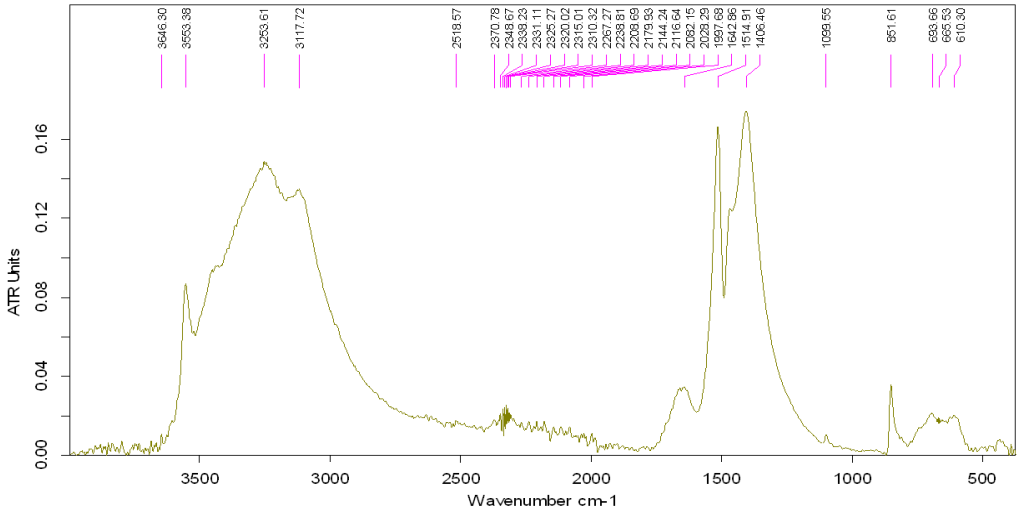

Figure 29. FTIR Spectrum of nesquehonite synthesized from $Mg(OH)_2$ nanoparticles.

4.3 Analyses of the Preparation Stages of Alcohol Dispersion of $Ca(OH)_2$ and $Mg(OH)_2$ Nanoparticles from Midyat Dolostone

The stages of $Ca(OH)_2$ and $Mg(OH)_2$ nanoparticles' preparation include the calcination of Midyat dolostone, and slaking of calcination products, i.e., MgO/CaO mixture. The slaked products were then dispersed in ethanol, and the stability of $Ca(OH)_2$ and $Mg(OH)_2$ nanoparticles in ethanol was analyzed.

Calcination of Midyat dolomite yielded pure Lime (CaO) and Periclase (MgO) as seen in XRD traces (Figure 30).

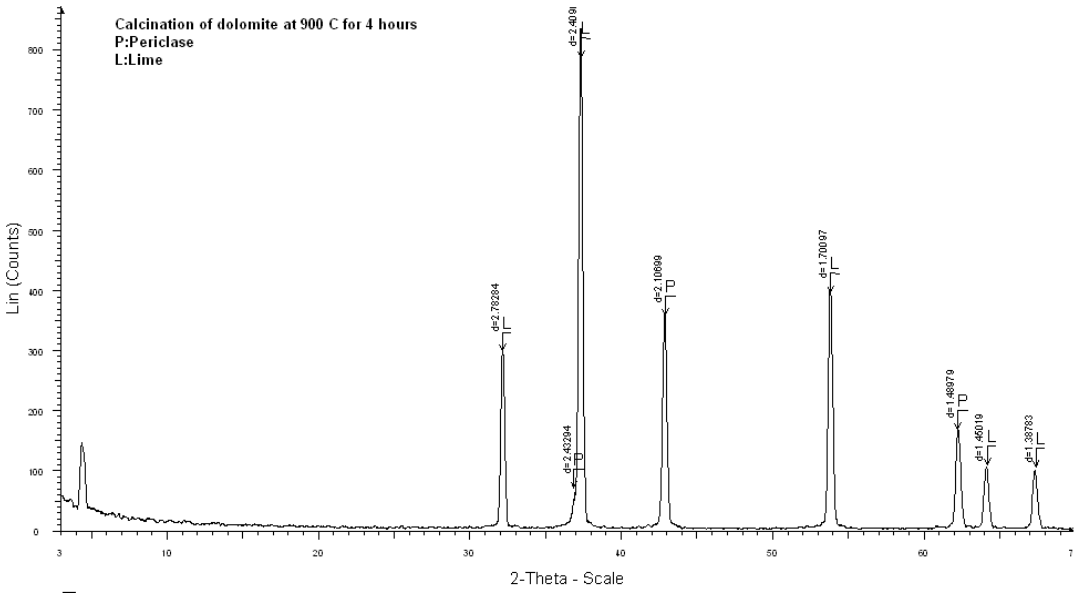

Figure 30. XRD traces of products formed after calcination of dolostone

Slaking of Lime and Periclase yielded Portlandite ($Ca(OH)_2$) and Brucite ($Mg(OH)_2$), respectively as seen in XRD traces (Figure 31).

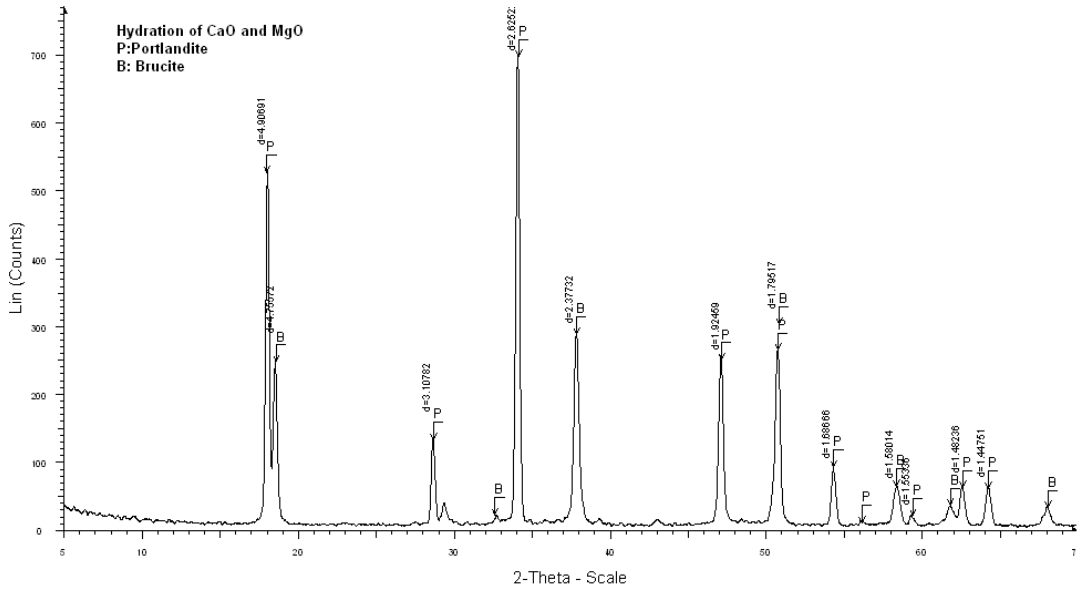

Figure 31. XRD traces of slaking products of CaO and MgO. B: Brucite ($Mg(OH)_2$), P: Portlandite ($Ca(OH)_2$)

$Ca(OH)_2$ and $Mg(OH)_2$ nanoparticles' characterization was also assisted with FTIR analysis in dry state before dispersion in alcohol which could help to separate –OH stretching of $Mg(OH)_2$ and $Ca(OH)_2$ (Figure 32). $Mg(OH)_2$ –OH stretching show very sharp peak at 3693 cm^{-1}, and the other sharp peak at 3642 cm^{-1} is –OH stretching of $Ca(OH)_2$. The bands at 1400-1500 cm^{-1} (stretching modes of carbonate group) and 873 cm^{-1} (bending mode of carbonate) belongs to carbonate groups which indicates that there is some reaction of hydroxides with the atmospheric CO_2, and formation of carbonates during the preparation.

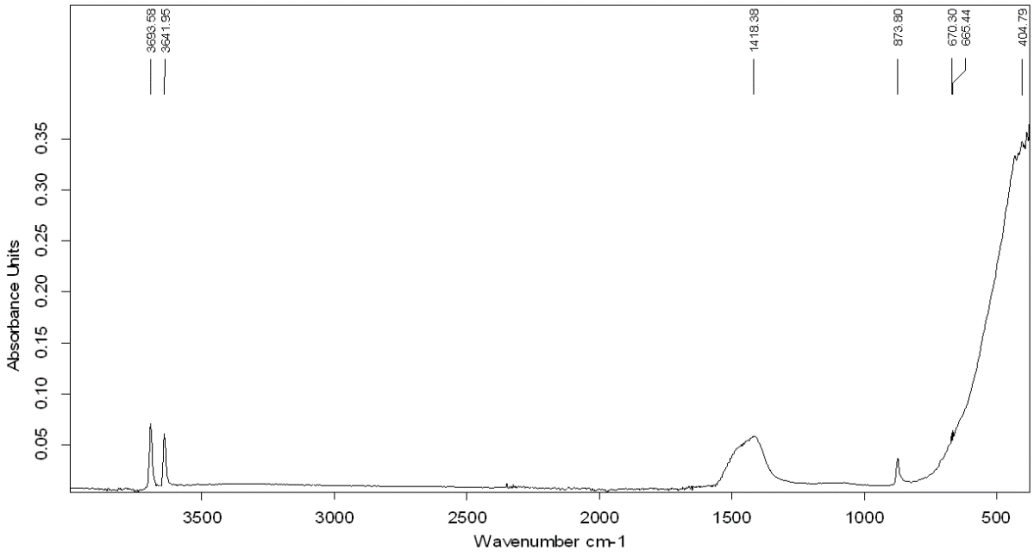

Figure 32. FTIR Spectrum of $Ca(OH)_2$ and $Mg(OH)_2$ hydroxide nanoparticles in dry state before dispersion in alcohol

After $Ca(OH)_2$ and $Mg(OH)_2$ nanoparticles were dispersed in ethanol, FTIR of the dispersion was also analyzed to realize if there is any alkoxide formation (Ca-OR or Mg-OR; -R represents an alkyl group such as $-CH_3$ or $-CH_2CH_3$) due to the reaction between ethanol and hydroxides (Figure 33) Unlike the FTIR of hydroxides in dry state, the peak at 1047 cm^{-1} belongs to C-O stretching mode of ethanol, and the band at 3000-3500 cm-1 belongs to -OH stretching mode of ethanol. The bands at 873 cm^{-1} and 1418 cm^{-1}belongs to carbonate group, showing some carbonation took place. Modes of -C-H stretching couldn't be distinguished. There is no sign of alkoxides formation.

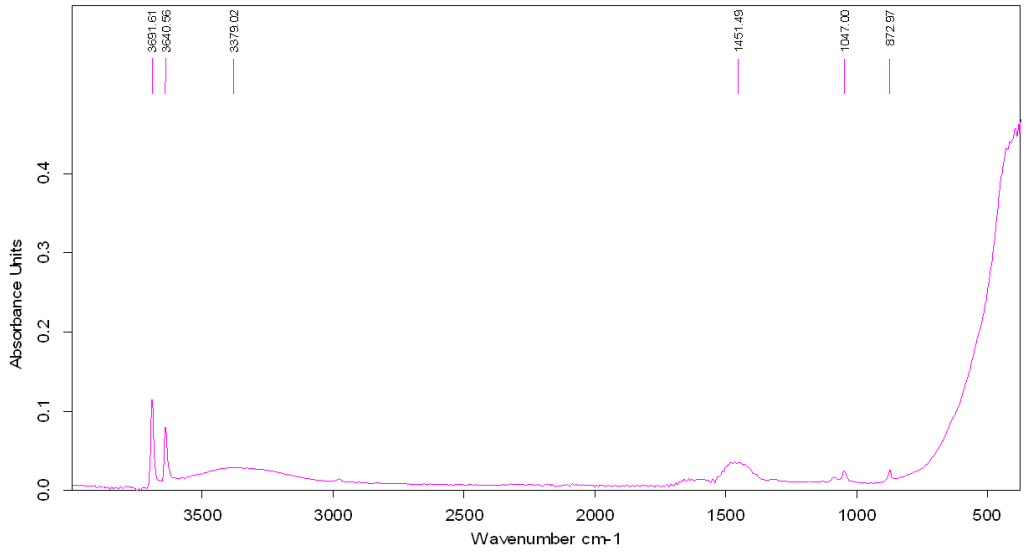

Figure 33. FTIR Spectrum of $Ca(OH)_2$ and $Mg(OH)_2$ hydroxide nanoparticles after dispersion in alcohol

In the SEM images of $Ca(OH)_2$ and $Mg(OH)_2$ nanoparticles at dry state, they appear integrated in the form of aggregates. Aggregates' sizes were between 1-5 µm, and aggregates are composed of nanoparticles clusters in two different size ranges (Figure 34). EDAX analysis of large clusters (around 500nm-1µm) showed that they belong to $Ca(OH)_2$ nanoparticles (Figure 35) and smaller clusters (around 100nm) belong to $Mg(OH)_2$ nanoparticles (Figure 36).

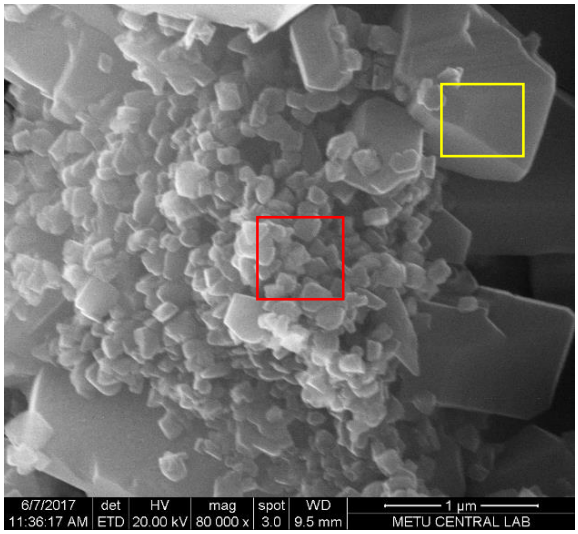

Figure 34. SEM image of $Ca(OH)_2$ and $Mg(OH)_2$ nanoparticles in the form of aggregates: 80000x. Smaller particles belong to $Mg(OH)_2$, and bigger particles belong to $Ca(OH)_2$

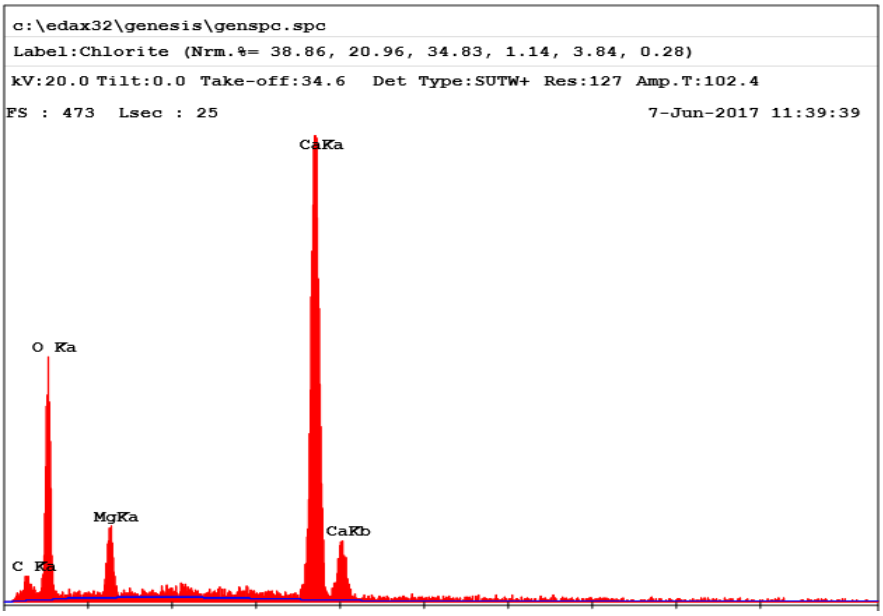

Figure 35. SEM-EDAX of large clusters belonging to $Ca(OH)_2$:EDAX analysis of yellow squared part.

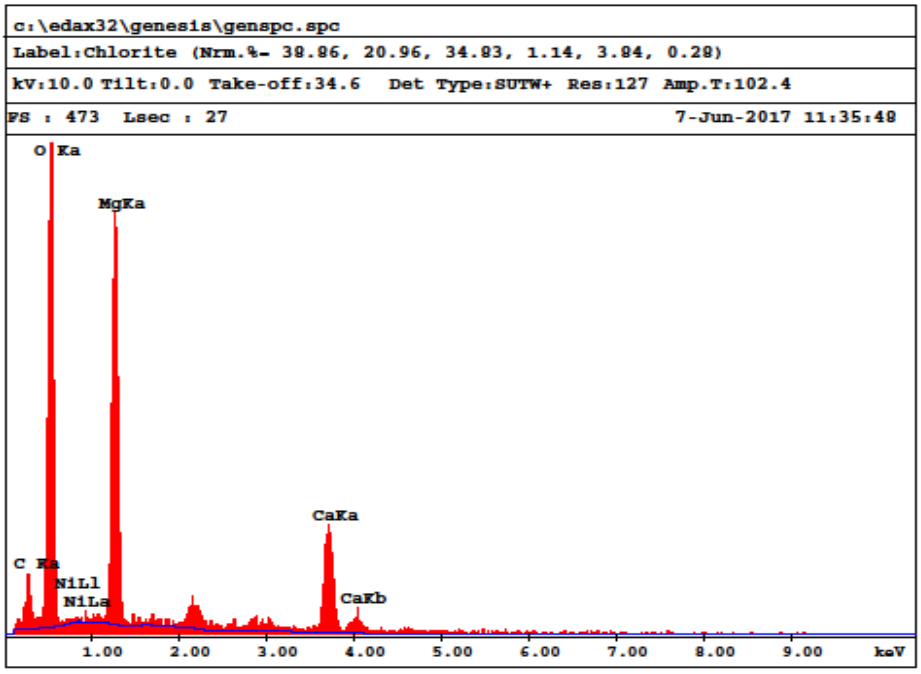

Figure 36. SEM-EDAX of smaller clusters belonging to $Mg(OH)_2$: EDAX analysis of red squared part.

4.3.1 Stability of Alcohol Dispersion of $Ca(OH)_2$ and $Mg(OH)_2$ Nanoparticles and the Changes in the Mg:Ca Ratio of the Solution

Stability of the solution is important in terms of its concentration and the changes in the concentration of individual $Ca(OH)_2$ and $Mg(OH)_2$ nanoparticles. In the beginning, 5g of dried nanoparticles were dispersed in 100 ml of ethanol. To control the change in the concentration of $Ca(OH)_2$ and $Mg(OH)_2$ nanoparticles, the solution was left to rest. The changes in the concentration of $Ca(OH)_2$ and $Mg(OH)_2$ nanoparticles were evaluated according to the XRD traces at the 0^{th}, 4^{th}, 24^{th}, 44^{th}, 72^{nd} hours (Figure 37-Figure 41).

Since the Mg:Ca ratio of the original dolomite used in the preparation of the solution was assumed as 1, the amount of $Ca(OH)_2$ and $Mg(OH)_2$ at the 0th hour was also asuumed to be equal, and Mg:Ca was 1 (Figure 37). At the 4^{th} hour, the amount of $Ca(OH)_2$ (portlandite) has decreased, and peaks of portlandite and brucite came closer (Figure 38). After 24 and 44 hours, the amount of $Mg(OH)_2$ (brucite) in the solution became more abundant(Figure 39&Figure 40), and at 72 hours, brucite was dominant, and portlandite amount was little in the solution (Figure 41). These results confirmed that coarser nanoparticles of $Ca(OH)_2$ settles faster than $Mg(OH)_2$ nanoparticles in the solution, and alcohol dispersion becomes rich in magnesium hydroxide.

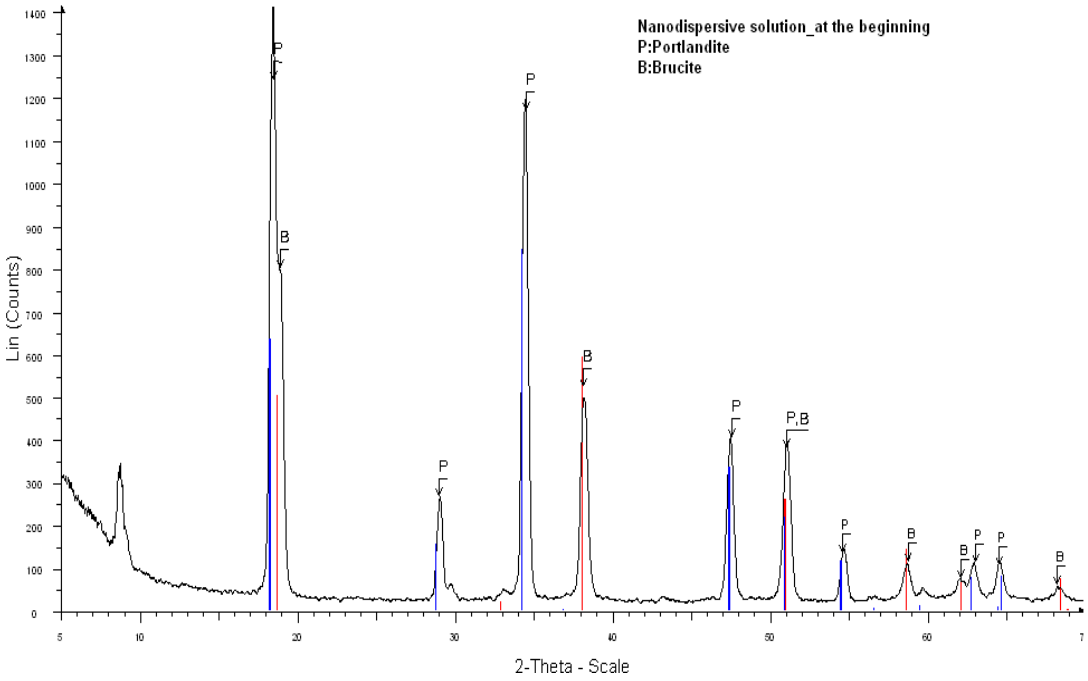

Figure 37. XRD traces of $Ca(OH)_2$ and $Mg(OH)_2$ nanoparticles dispersed in ethanol, in the beginning-no settlement: P: Portlandite $Ca(OH)_2$ and B: Brucite $Mg(OH)_2$

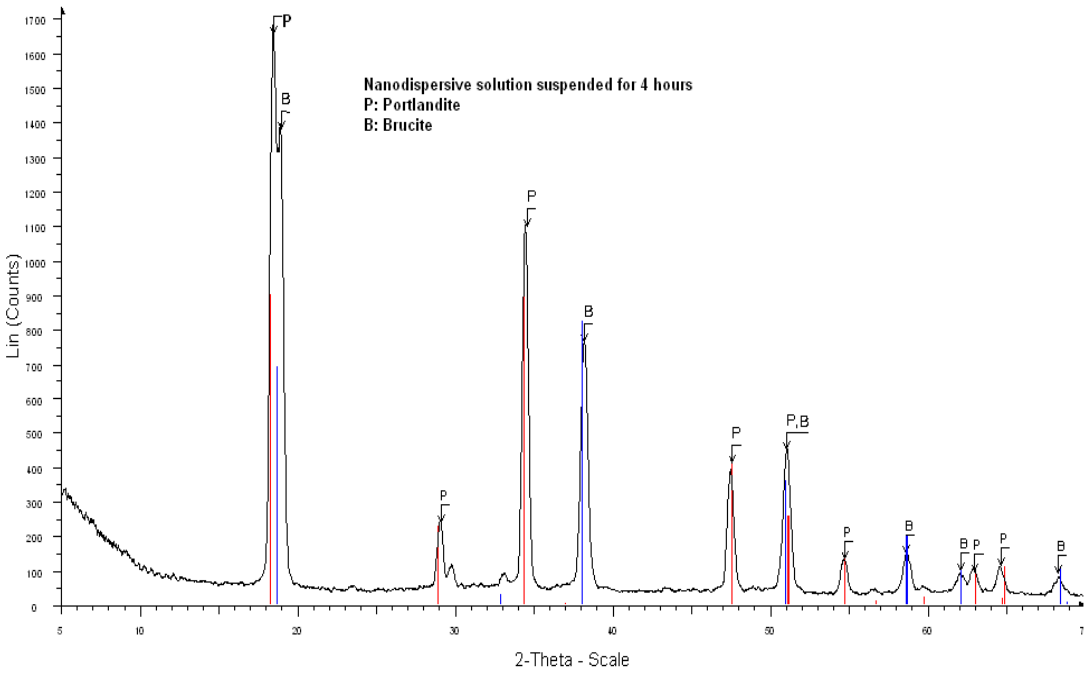

Figure 38. XRD traces of $Ca(OH)_2$ and $Mg(OH)_2$ nanoparticles dispersed in ethanol, after 4 hours of settlement: P:Portlandite $Ca(OH)_2$ and B:Brucite $Mg(OH)_2$

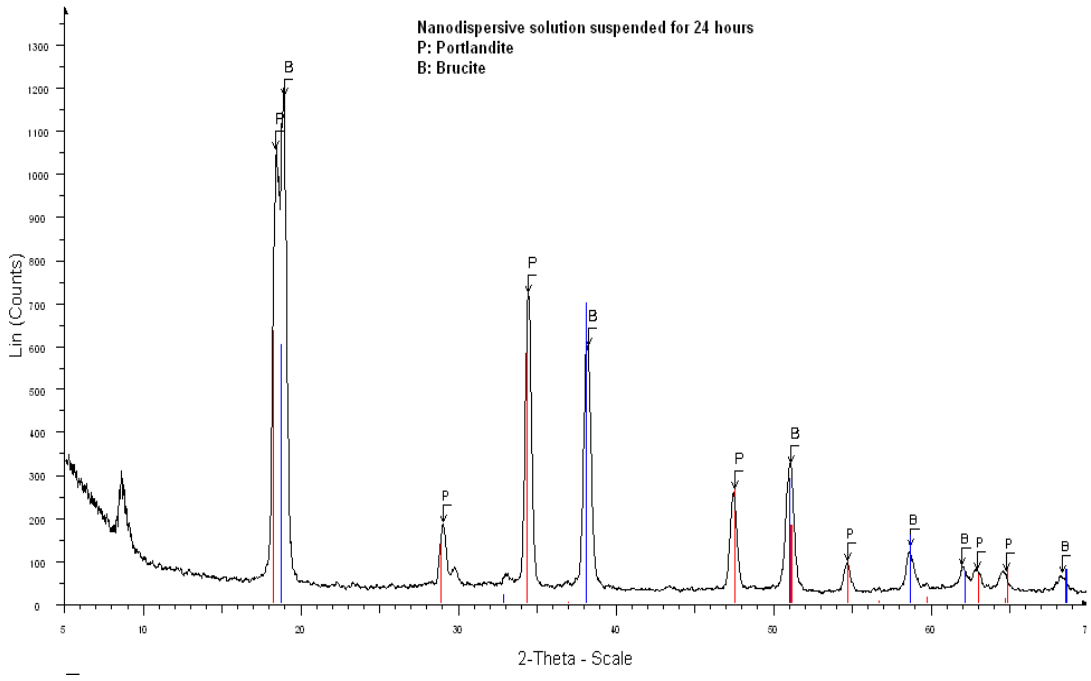

Figure 39. XRD traces of $Ca(OH)_2$ and $Mg(OH)_2$ nanoparticles dispersed in ethanol ,after 24 hours of settlement: P:Portlandite $Ca(OH)_2$ and B:Brucite $Mg(OH)_2$

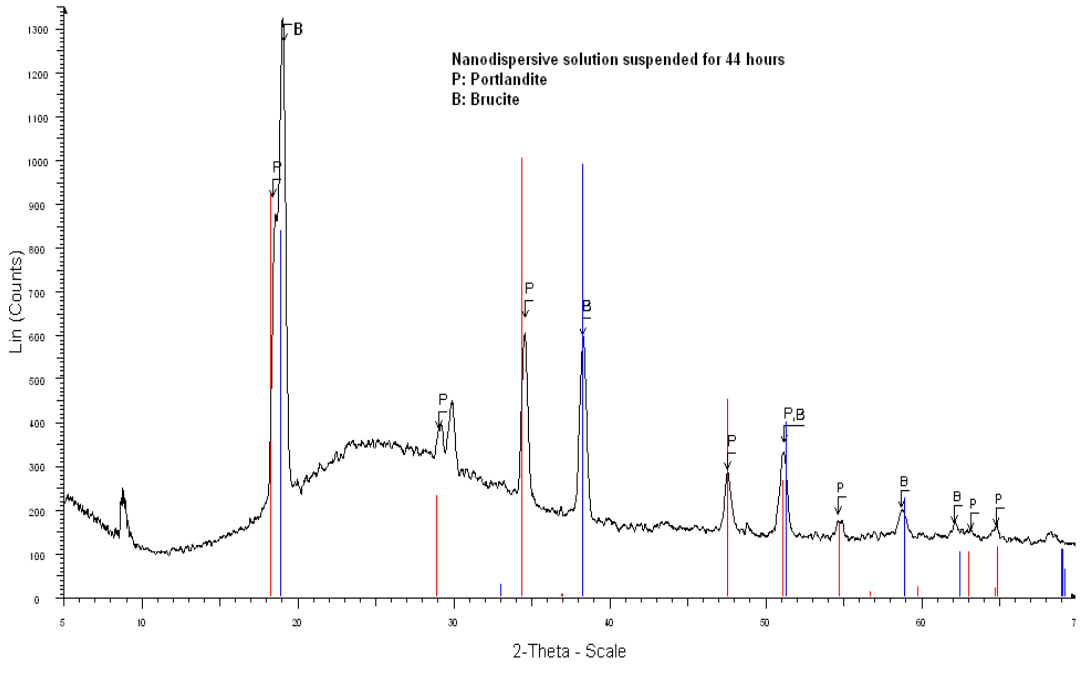

Figure 40. XRD traces of $Ca(OH)_2$ and $Mg(OH)_2$ nanoparticles dispersed in ethanol, after 44 hours of seetlement: P:Portlandite $Ca(OH)_2$ and B:Brucite $Mg(OH)_2$

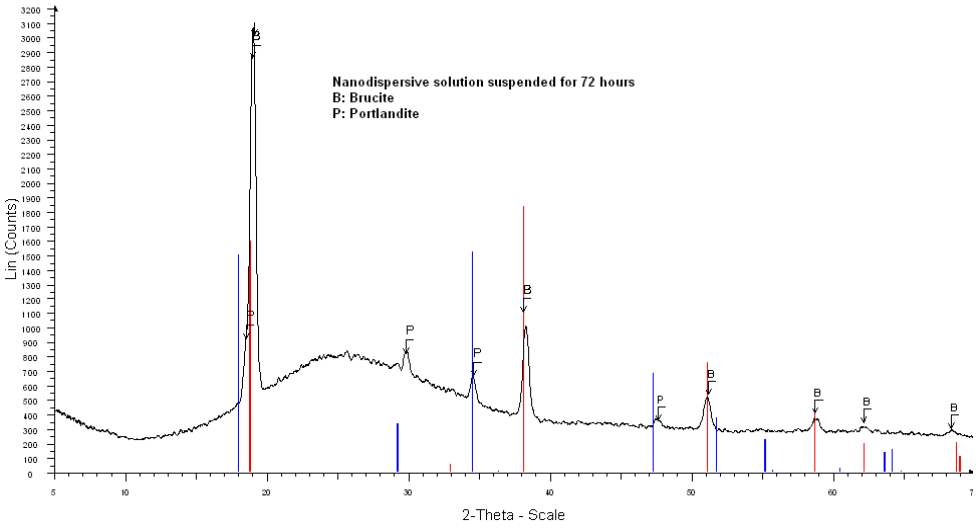

Figure 41. XRD traces of $Ca(OH)_2$ and $Mg(OH)_2$ nanoparticles dispersed in ethanol, after 72 hours of settelement: P:Portlandite $Ca(OH)_2$ and B:Brucite $Mg(OH)_2$

The change in the Mg:Ca ratio of the solution was estimated by the ratio of the second intense peaks of portlandite and brucite in XRD traces (Table 9 and Figure 42). Mg:Ca ratio after 16 hours of resting of the solution was calculated to be around 2.

Table 9. Mg:Ca ratio versus time according to the intensity of **second intense peak**s of brucite and portlandite in XRD traces

Settlement time of dispersion (h)	Mg:Ca ratio	Intensity of portlandite peak (cm) (P)	Intensity of brucite peak (cm) (B)	B/P
0	1	5,5	2,2	0,4
4	1.88	5,1	3,8	0,75
24	2.15	4,2	3,6	0,86
44	2.70	2,5	2,7	1,08
72	5.33	0,8	1,7	2,13

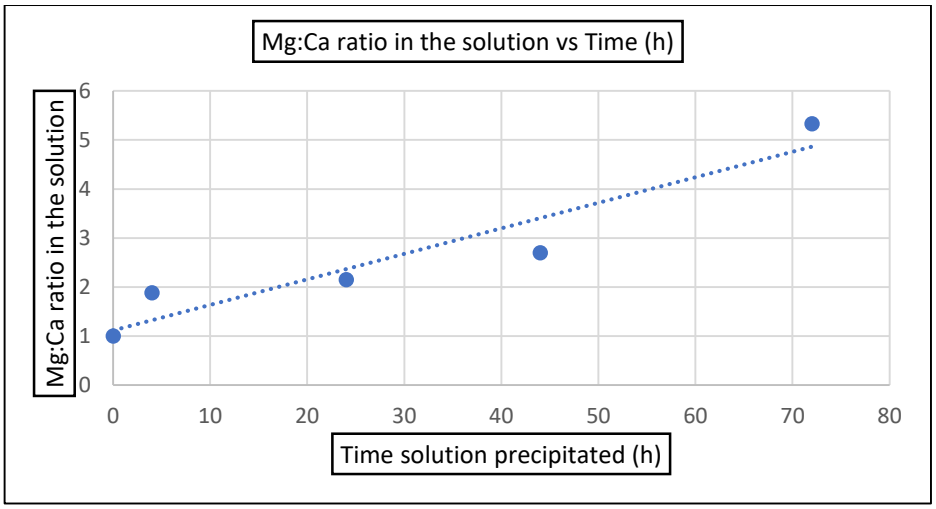

Figure 42. Mg:Ca ratio in the alcohol dispersion vs time of settlement

4.4 Carbonation Experiments of $Ca(OH)_2$ and $Mg(OH)_2$ Nanoparticles

Results of carbonation experiments for set-1 and set 2 are given separately for each run in the related set. In the set-1, Mg:Ca ratio is around 2 in the dispersion. On the other hand, in the set-2 Mg:Ca ratio is around 1. In set-1, carbonation of $Ca(OH)_2$ and $Mg(OH)_2$ nanoparticles were tested for the following conditions:

- room condition (30-35% RH and pCO_2 ~ 0.3 mmHg),
- high relative humidity-low CO_2 partial pressure conditions (90-95% RH and pCO_2 ~ 0.3 mmHg),
- high relative humidity-high CO_2 partial pressure conditions (90-95% RH and pCO_2 ~ 0.4 atm).

In set-2, carbonation was tested only under high relative humidity-high CO_2 partial pressure condition.

4.4.1 Carbonation of $Ca(OH)_2$ and $Mg(OH)_2$ Nanoparticles at Room Condition

At room condition, carbonation products of $Ca(OH)_2$ and $Mg(OH)_2$ nanoparticles dispersed in alcohol are calcite ($CaCO_3$), unreacted portlandite ($Ca(OH)_2$), and brucite ($Mg(OH)_2$), as followed from XRD traces after 4 weeks (Figure 43). $Mg(OH)_2$ nanoparticles did not yet carbonate at that condition.

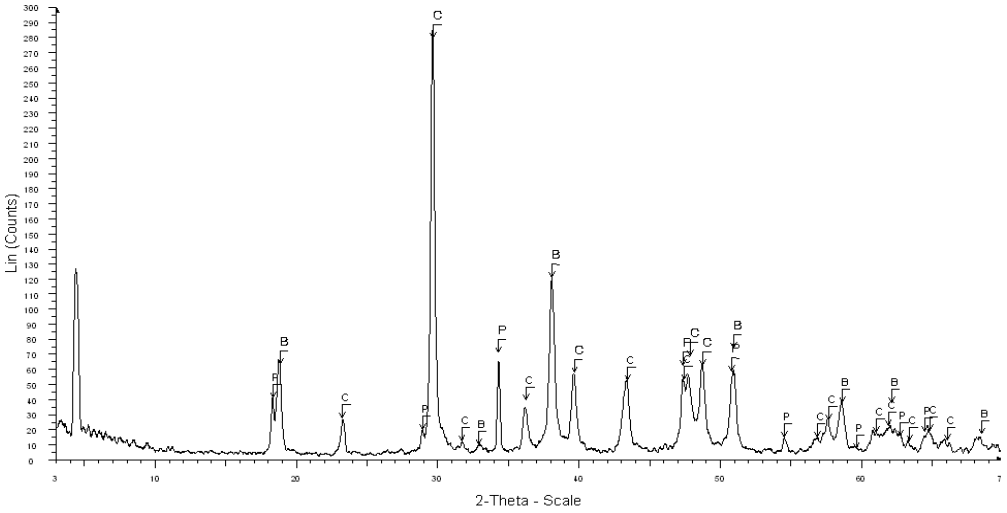

Figure 43. Carbonation of $Ca(OH)_2$ and $Mg(OH)_2$ nanoparticles dispersed in ethanol, at room condition for 4 weeks. B: Brucite; C: Calcite; P: Portlandite

4.4.2 Carbonation of $Ca(OH)_2$ and $Mg(OH)_2$ Nanoparticles at High Relative Humidity and Low CO_2 Partial Pressure Conditions

Under high RH, and low $p(CO_2)$ conditions, carbonation products of $Ca(OH)_2$ and $Mg(OH)_2$ nanoparticles dispersed in ethanol are calcite and nesquehonite ($MgCO_3.3H_2O$), as followed from XRD traces after four weeks (Figure 44). Compared with carbonation products at the room condition, increase in relative humidity favors carbonation of both $Ca(OH)_2$ and $Mg(OH)_2$. Carbonation of individual hydroxides were complete in four weeks.

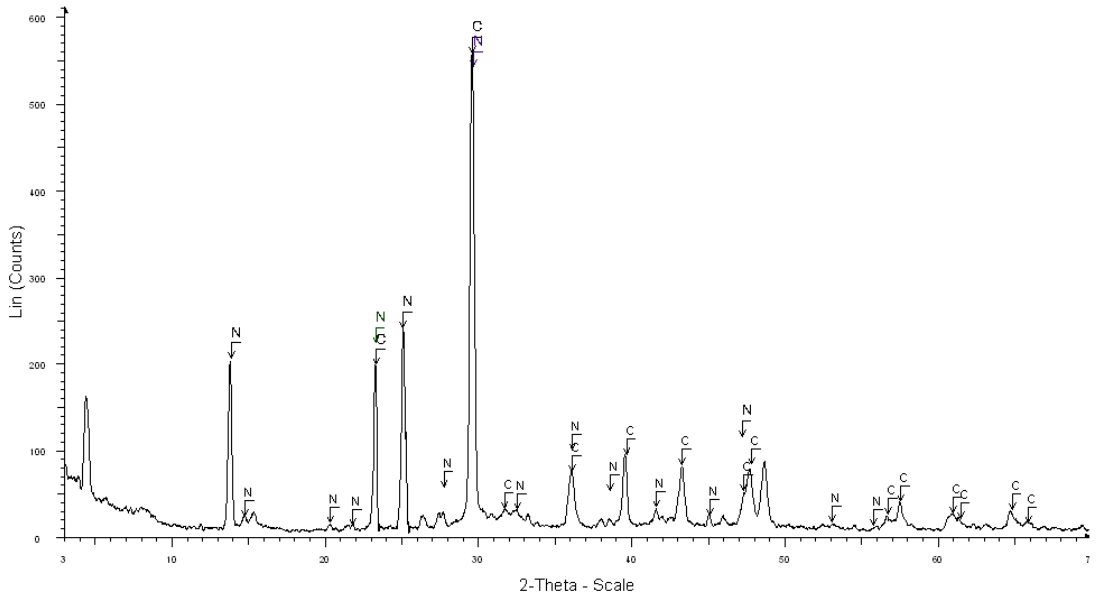

Figure 44. Carbonation of $Ca(OH)_2$ and $Mg(OH)_2$ nanoparticles dispersed in ethanol, at high RH and low CO_2 pressure for 4 weeks. C: Calcite, N: Nesquehonite

4.5 Carbonation of $Ca(OH)_2$ and $Mg(OH)_2$ Nanoparticles at High Relative Humidity and High CO_2 Partial Pressure Conditions Using Alcohol Dispersion with Mg:Ca ratio ~2: Set-1

Under high RH, and high $p(CO_2)$ conditions, the carbonation products of $Ca(OH)_2$ and $Mg(OH)_2$ nanoparticles dispersed in ethanol are nesquehonite (of magnesium hydroxide) and calcite (of calcium hydroxide) with some dolomite as confirmed by XRD, SEM, and FTIR analyses.

4.5.1 XRD Analyses

XRD traces of carbonation products of $Ca(OH)_2$ and $Mg(OH)_2$ nanoparticles dispersed in ethanol at the 3rd hour, 1st, 3rd, 7th, 17th, 21st, 28th, 58th days and 7th month are given in the Figure 45-Figure 53. At the 3rd hour, carbonation of some portlandite ($Ca(OH)_2$) to calcite was observed, and brucite did not carbonate yet (Figure 45). At the end of 1st day, almost all portlandite carbonated to calcite.

However, no carbonation of brucite was observed (Figure 46). All hydroxide particles were observed to be carbonated on the 3rd day. The carbonation products observed were nesquehonite ($MgCO_3.3H_2O$) and calcite ($CaCO_3$). However, just next to the main calcite peak, the main dolomite peak (d=2.87) started to appear as weak and broad peak in XRD traces (Figure 47). Those analyses suggest that carbonation of portlandite is more favorable with respect to brucite carbonation.

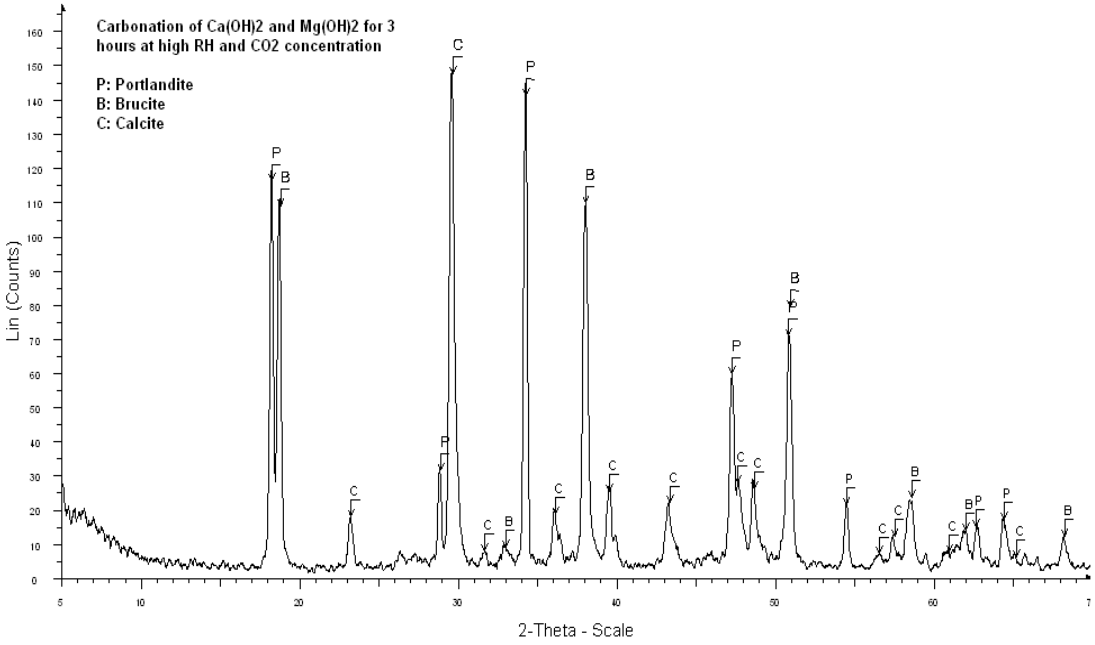

Figure 45. XRD traces of carbonation products of $Ca(OH)_2$ and $Mg(OH)_2$ nanoparticles dispersed in ethanol, at high RH and high CO_2 pressure for 3 hours. P: Portlandite, B:Brucite, C: Calcite.

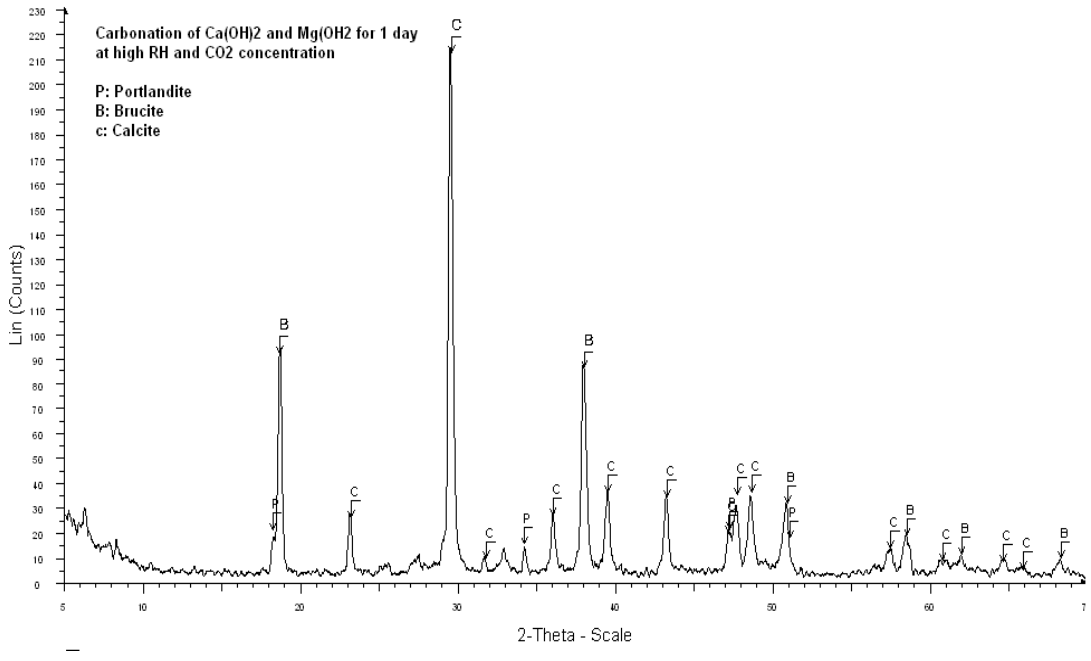

Figure 46. XRD traces of carbonation products of $Ca(OH)_2$ and $Mg(OH)_2$ nanoparticles dispersed in ethanol, at high RH and high CO_2 pressure for 1 day. P: Portlandite, B: Brucite, C: Calcite.

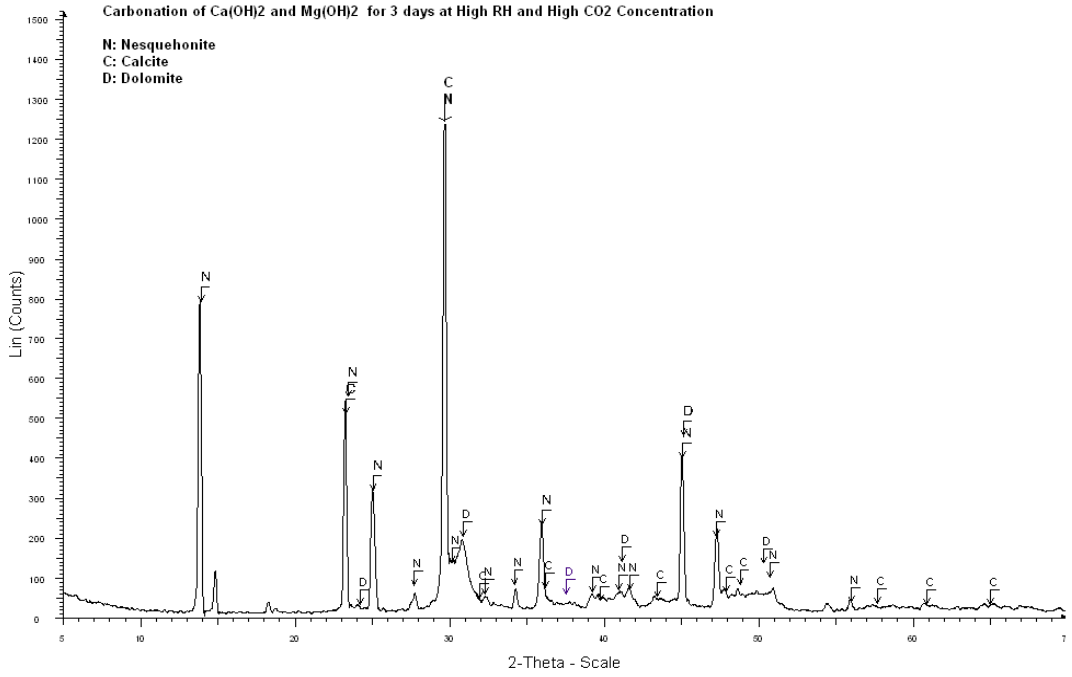

Figure 47. XRD traces of carbonation products of $Ca(OH)_2$ and $Mg(OH)_2$ nanoparticles dispersed in ethanol, at high RH and high CO_2 pressure for 3 days. N: Nesquehonite, C: Calcite, D: Dolomite.

On the 7th day, nesquehonite peaks became higher while the height of major calcite (d=3.03) and dolomite (d=2.86) peaks became closer (Figure 48). Nesquehonite peaks were shorter, and the major dolomite peak became higher on the 17th day (Figure 49). On the 21st, 28th, and 58th days, nesquehonite peaks became more significant while there was little change in calcite and dolomite peak heights (Figure 50-Figure 52). Types of carbonation products were same starting form the 3rd day until 7 months being nesquehonite, calcite, and some dolomite (Figure 53). It is not possible to make semi-quantitative interpretation of carbonation products, since the sampling was random. Later on, it was noticed that there was layering in petri dish due to settlement of alcohol dispersion, and the carbonation products were not homogeneously distributed in petri dish. Therefore, XRD data changed according to where the sample was taken either from the surface or bottom.

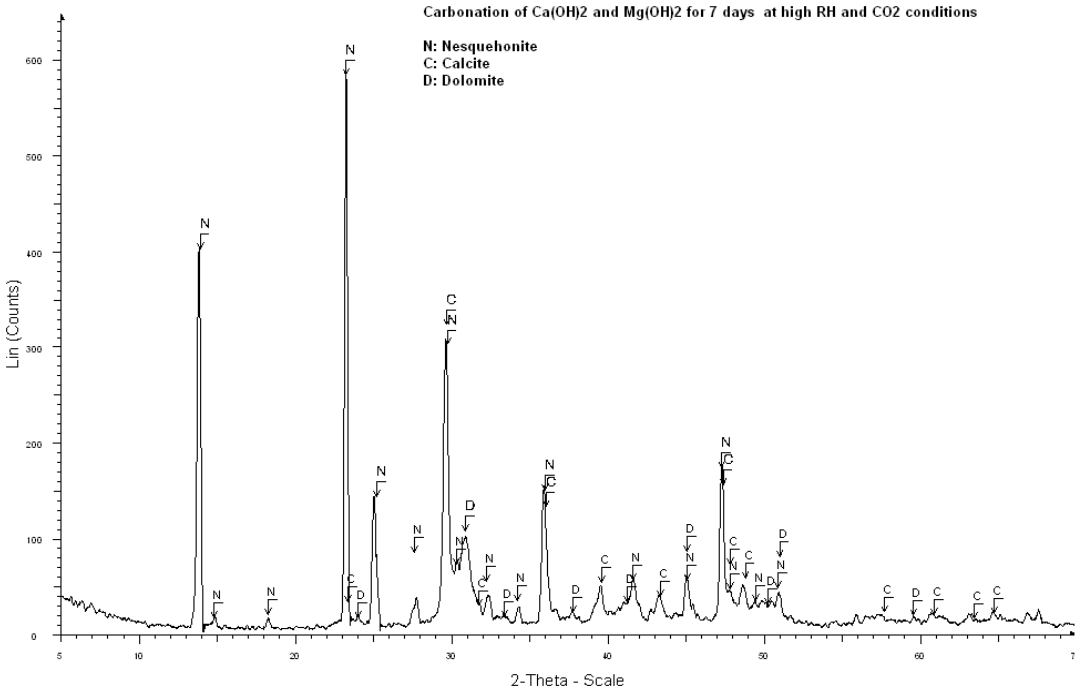

Figure 48. XRD traces of carbonation products of $Ca(OH)_2$ and $Mg(OH)_2$ nanoparticles dispersed in ethanol, at high RH and high CO_2 pressure for 7 days. N: Nesquehonite, C: Calcite, D: Dolomite.

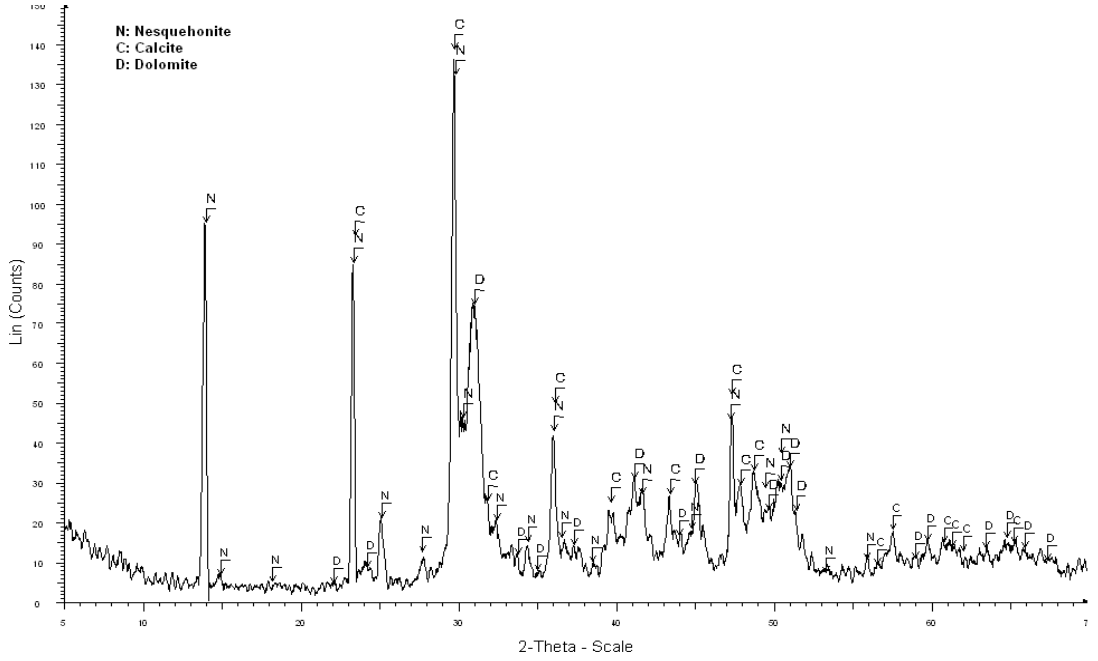

Figure 49. XRD traces of carbonation products of $Ca(OH)_2$ and $Mg(OH)_2$ nanoparticles dispersed in ethanol, at high RH and high CO_2 pressure for 17 days. N: Nesquehonite, C: Calcite, D: Dolomite.

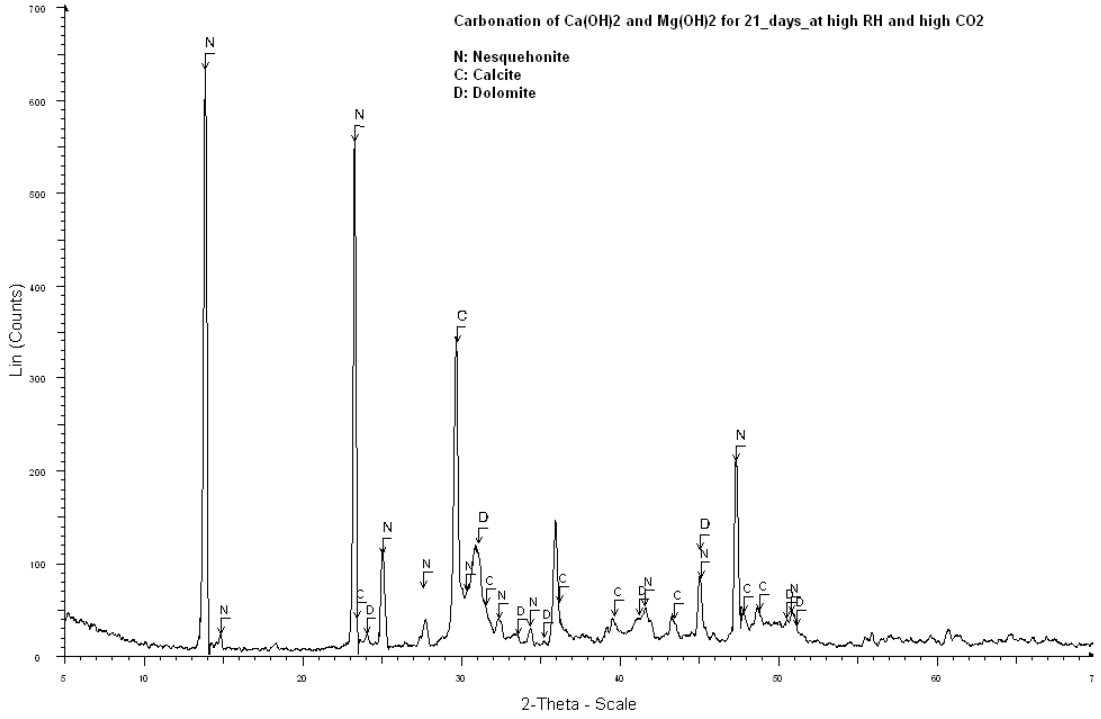

Figure 50. XRD traces of carbonation products of $Ca(OH)_2$ and $Mg(OH)_2$ nanoparticles dispersed in ethanol, at high RH and high CO_2 pressure for 21 days. N: Nesquehonite, C: Calcite, D: Dolomite.

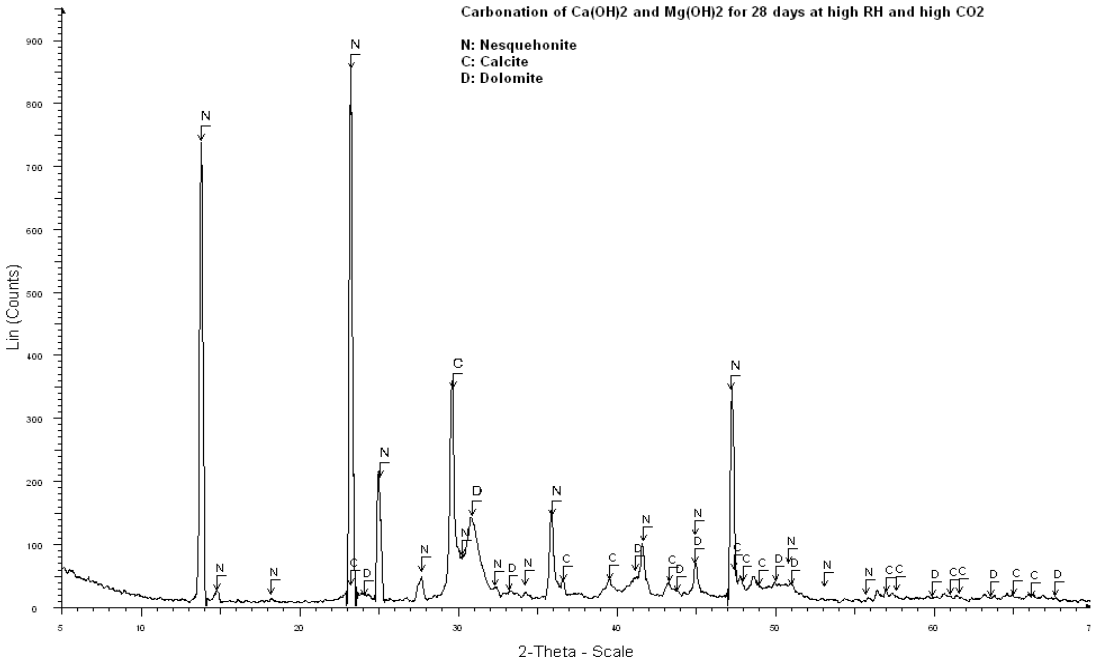

Figure 51. XRD traces of carbonation products of $Ca(OH)_2$ and $Mg(OH)_2$ nanoparticles dispersed in ethanol, at high RH and high CO_2 pressure for 28 days. N: Nesquehonite, C: Calcite, D: Dolomite.

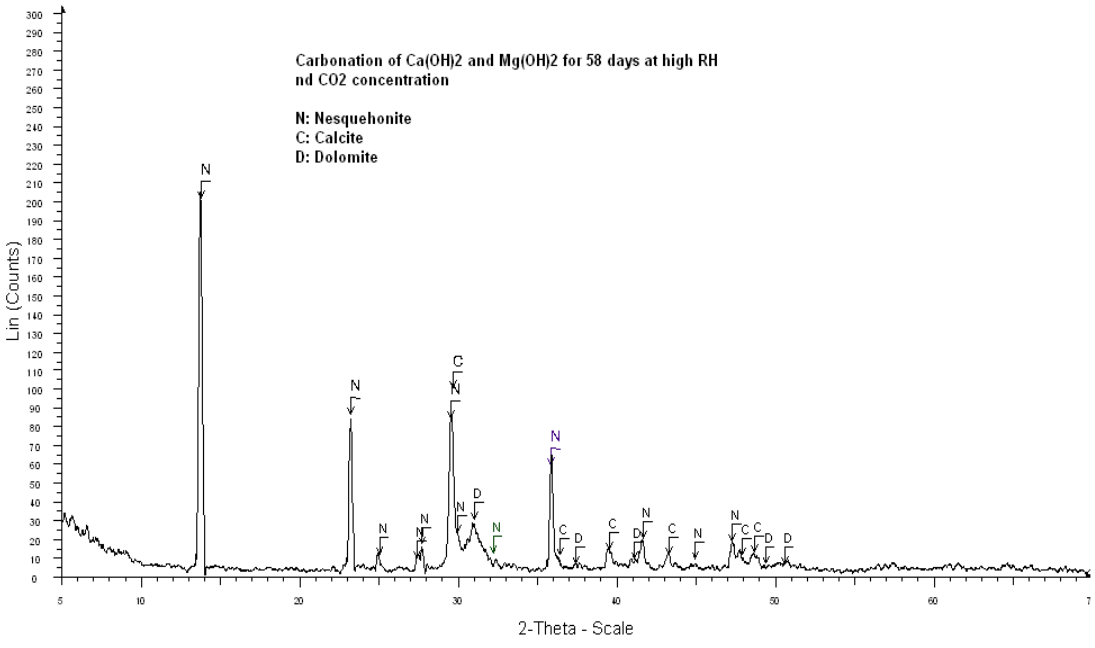

Figure 52. XRD traces of carbonation products of $Ca(OH)_2$ and $Mg(OH)_2$ nanoparticles dispersed in ethanol, at high RH and high CO_2 pressure for 58 days. N: Nesquehonite, C: Calcite, D: Dolomite.

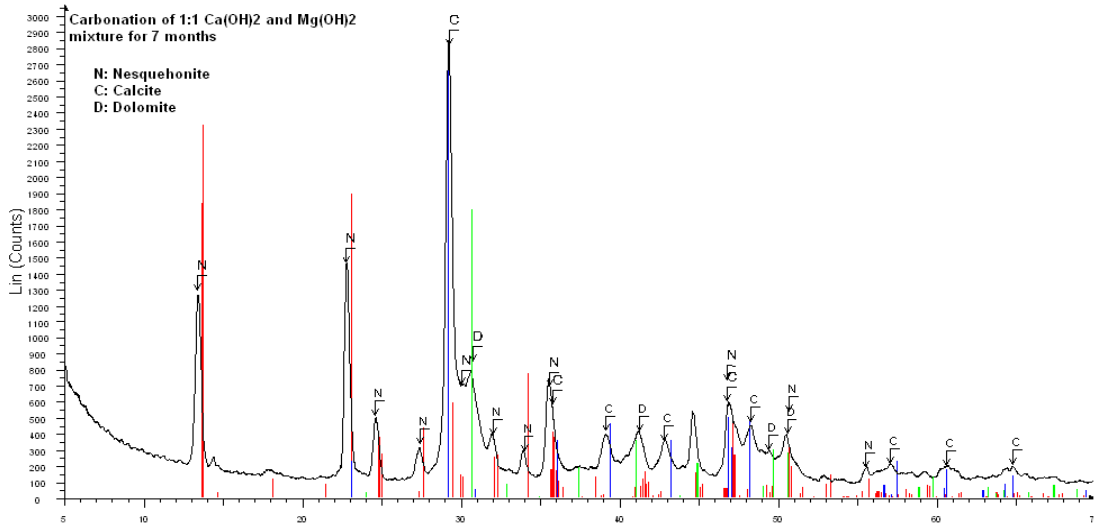

Figure 53. XRD traces of carbonation products of $Ca(OH)_2$ and $Mg(OH)_2$ nanoparticles dispersed in ethanol, at high RH and high CO_2 pressure for 7 months. N: Nesquehonite, C: Calcite, D: Dolomite.

4.5.2 FTIR Analyses

FTIR spectrum provide additional information about carbonation products. FTIR spectra of calcite (prepared as control sample), Midyat dolomite, and their mixtures are given (Figure 54-Figure 56) to distinguish the individual, and overlapping bands in the FTIR spectrum of carbonation products. FTIR spectrum of nesquehonite was already given in Figure 29. FTIR spectrum of carbonation products after 28 days is given in Figure 57. Finally, FTIR spectra of carbonation products were compared with that of calcite, dolomite, and nesquehonite (Figure 58).

In FTIR spectrums of calcite and dolomite, absorption bands at 711 and 727 cm^{-1} show symmetric deformation of carbonate groups that could help to identify and separate calcite and dolomite, respectively (Figure 56). The bands at 871 and 877 cm^{-1} are asymmetric deformation of carbonate groups for calcite and dolomite, respectively (Gunasakaran *et al*., 2006). In the mixture of these two minerals, calcite and dolomite could only be identified from the peaks at 711 and 727 cm^{-1}. The peaks around 870-880 cm^{-1} overlap, and don't help to distinguish calcite and dolomite (Figure 56).

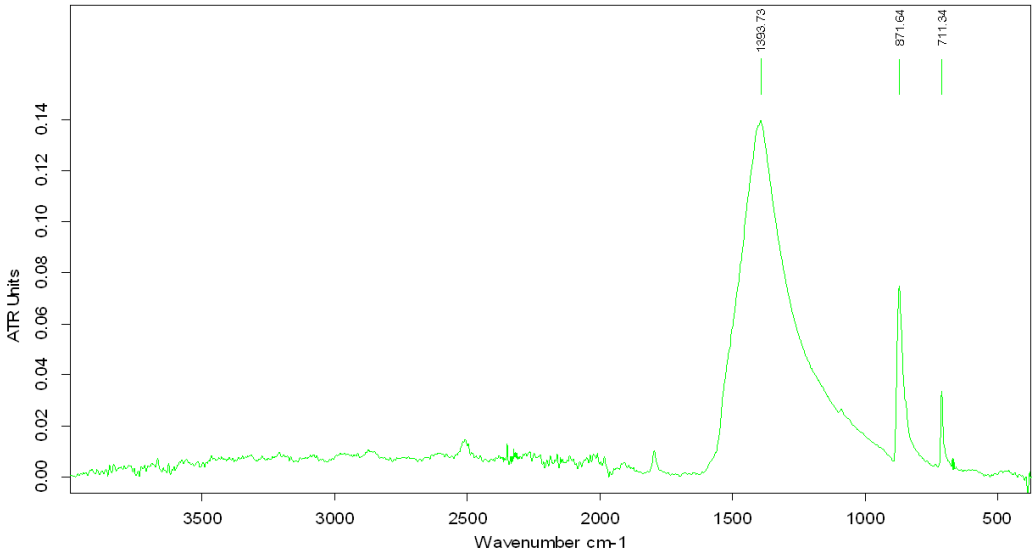

Figure 54. FTIR Spectrum of standard calcite.

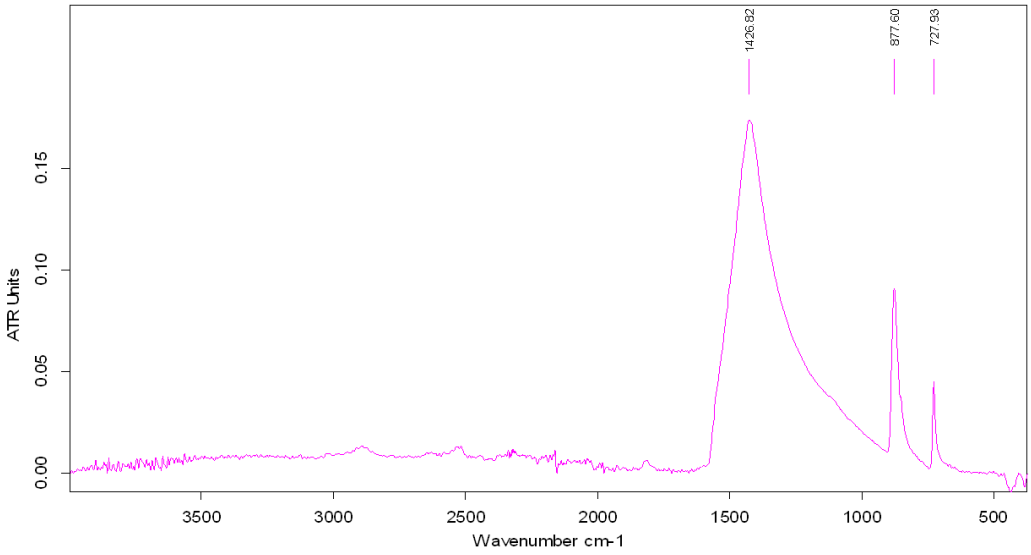

Figure 55. FTIR Spectrum of Midyat dolomite

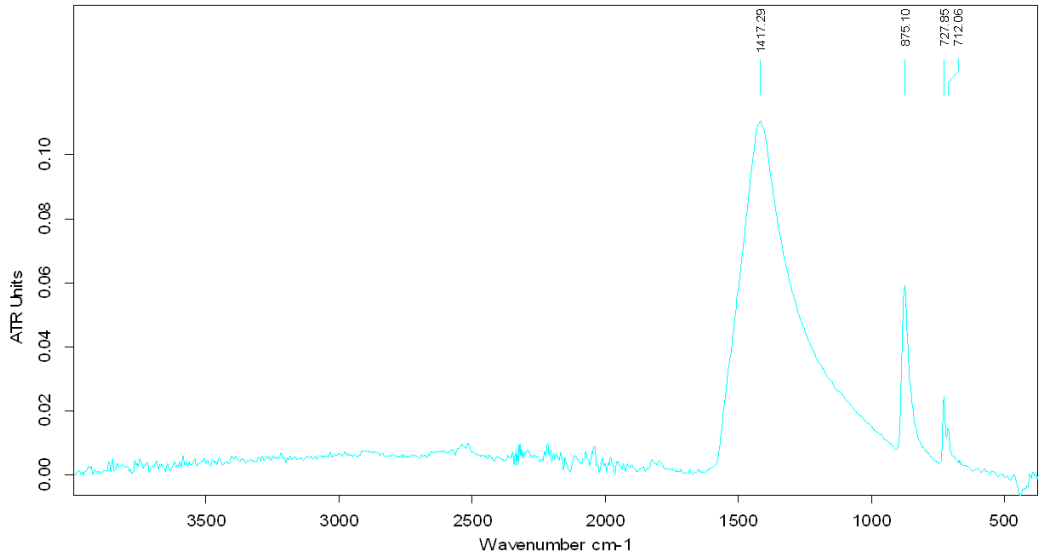

Figure 56. FTIR Spectrum of the mixture of standard calcite and dolomite.

FTIR spectrum of carbonation product of $Ca(OH)_2$ and $Mg(OH)_2$ nanoparticles after 28 days (Figure 57) shows the presence of those three minerals; calcite, dolomite, and nesquehonite. However, the bands of symmetric deformation of carbonate groups of calcite and dolomite around 711-728 cm^{-1} are integrated within each other and show a weak and broadband instead of individual sharp two peaks. All the carbonate stretching peaks overlap around 1400-1500 cm^{-1}. The very broad peak between 2500-4000 cm^{-1} is –OH stretchings of three water molecules of nesquehonite. When FTIR spectra of standard dolomite and calcite mixture (blue), nesquehonite (green), and the sample showing 28 days of carbonation results (red) are compared, the presence of calcite, nesquehonite, and dolomite in the carbonation products can well be identified (Figure 58).

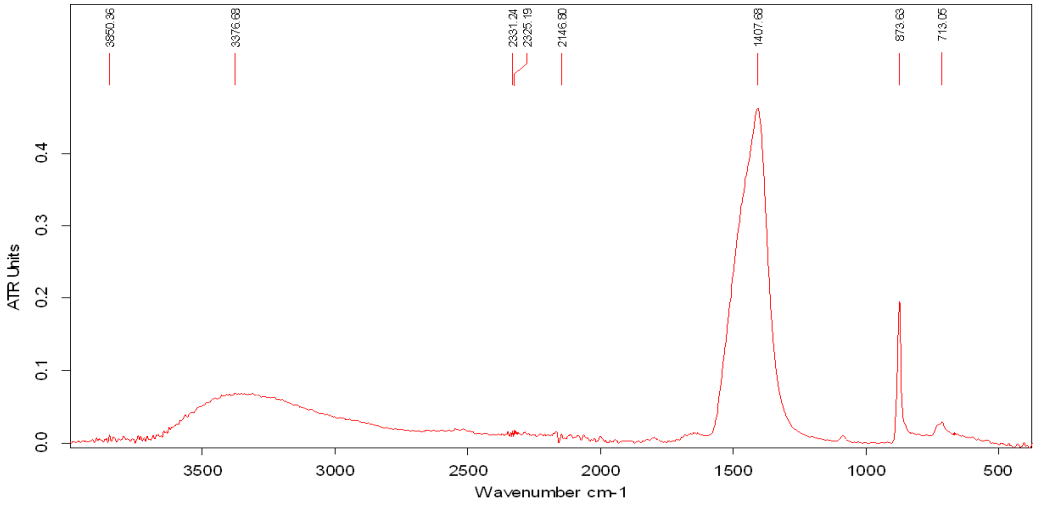

Figure 57. FTIR spectrum of carbonation products of $Ca(OH)_2$ and $Mg(OH)_2$ nanoparticles after 28 days.

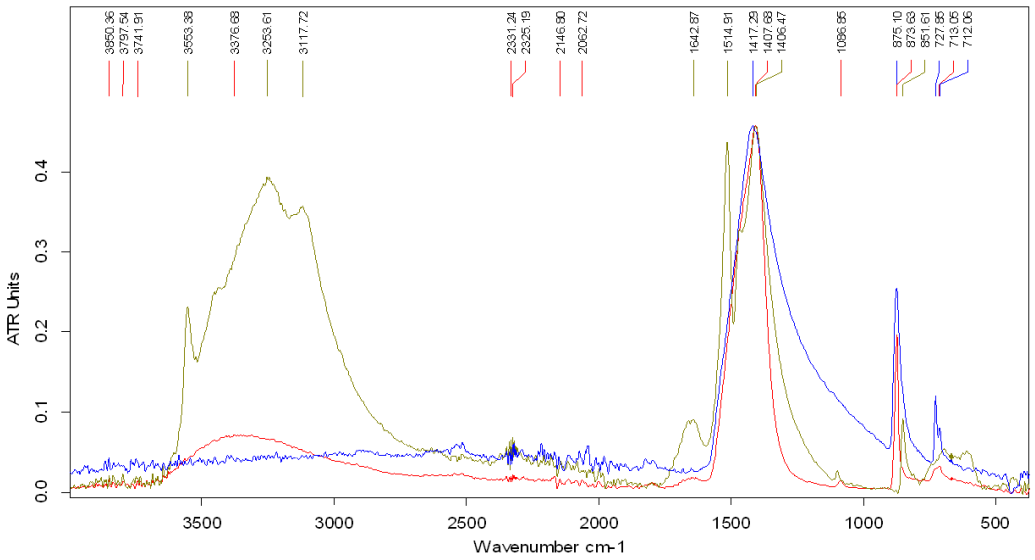

Figure 58. FTIR spectrums of control mixture of dolomite and calcite (blue), nesquehonite (green) and carbonation products (red)

4.5.3 SEM and EDAX Analyses

SEM images of carbonation products of $Ca(OH)_2$ and $Mg(OH)_2$ nanoparticles in alcohol dispersion at the 7th day show the presence of individual calcite (Figure 59)

and nesquehonite aggregates (Figure 60). At 20000x magnification, newly formed dolomite crystals on nesquehonite aggregate can be observed. However, it is hard to make its mineralogical analysis.

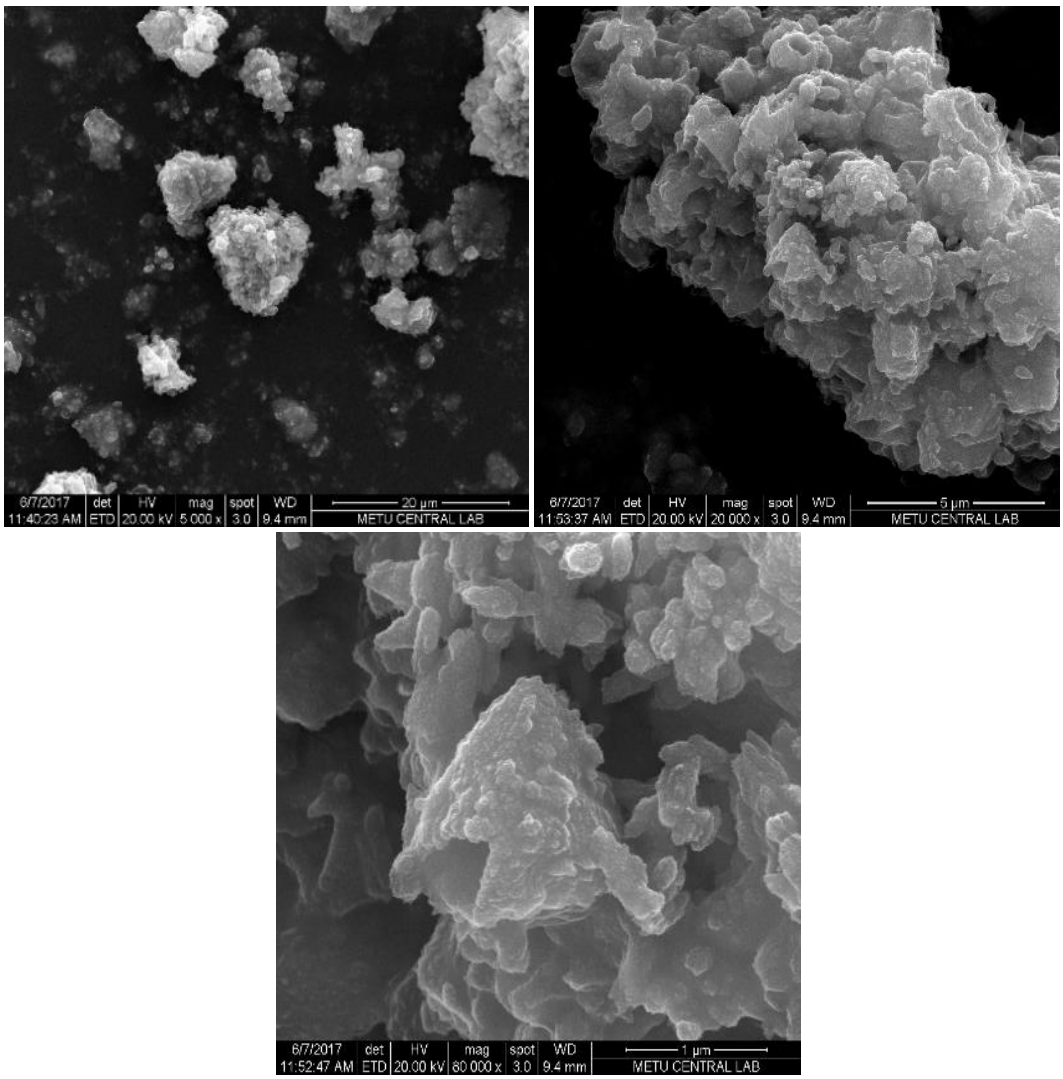

Figure 59. SEM images of carbonation products at the 7th day: calcite aggregates 5000x (up, left), 20000x (up, right), 80000x (down).

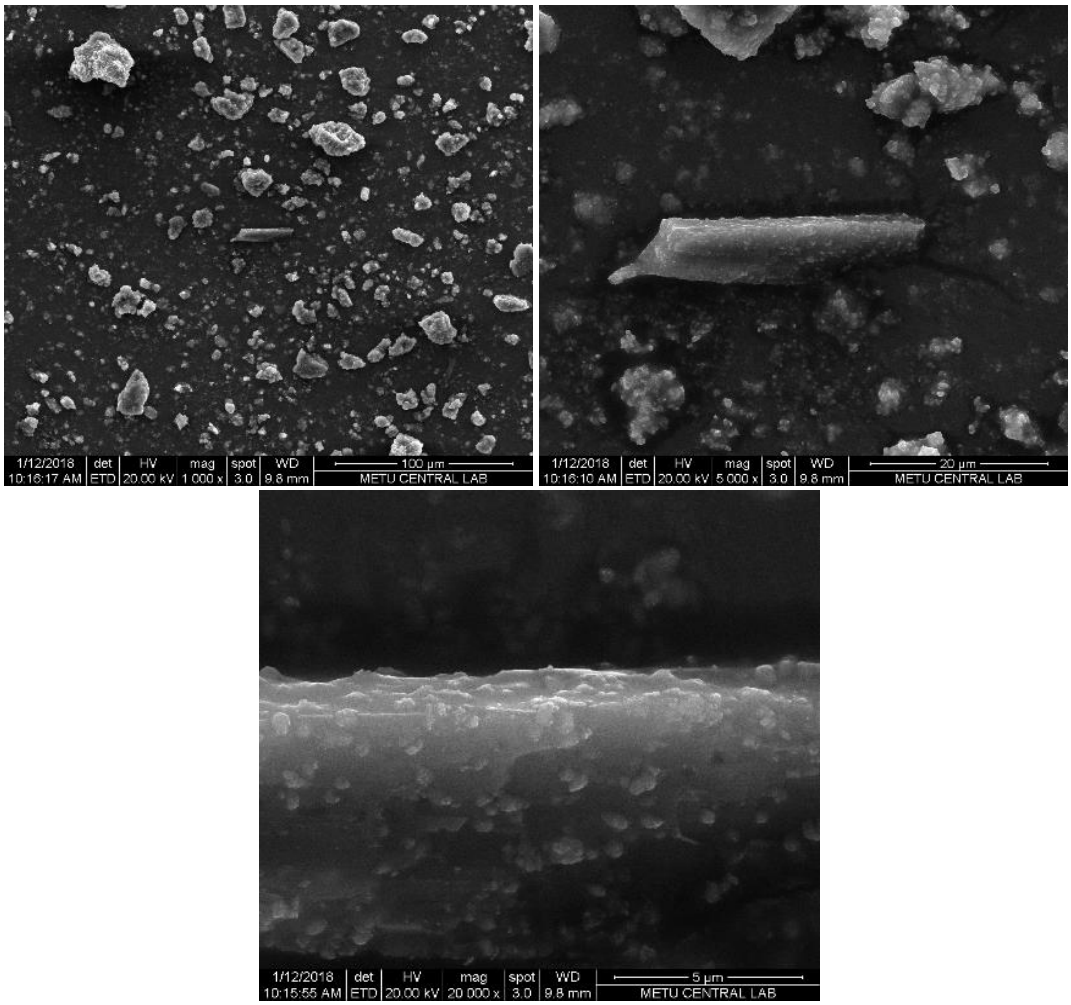

Figure 60. SEM image of carbonation products at the 7th day: Nesquehonite aggregates with calcite aggregates associated with it: 1000x (up, left), 5000x (up, right), 20000x (down)

SEM images of carbonation products at the 17th, 21st, 28th and 58th days show the aggregates of nesquehonite (in the form of rectangular sheets) and calcite (Figure 61-Figure 67). Moreover, many fine aggregates of nanoparticles smaller than 1 μm with sizes around 100-500 nm are observed on/next to the nesquehonite or calcite crystals (Figure 62, Figure 64, and Figure 66). The EDAX analyses of those nanoparticle aggregates indicate that Mg:Ca ratio is almost 1 as in original dolomite (Figure 63, Figure 65, and Figure 67). These results show the formation of dolomite as nanoparticle aggregates in association with calcite and nesquehonite. EDAX analyses of the aggregates on nesquehonite generally shows a higher amount of Mg

since the signals are obtained from the deeper rather than the surface, which might give a signal of whole aggregate.

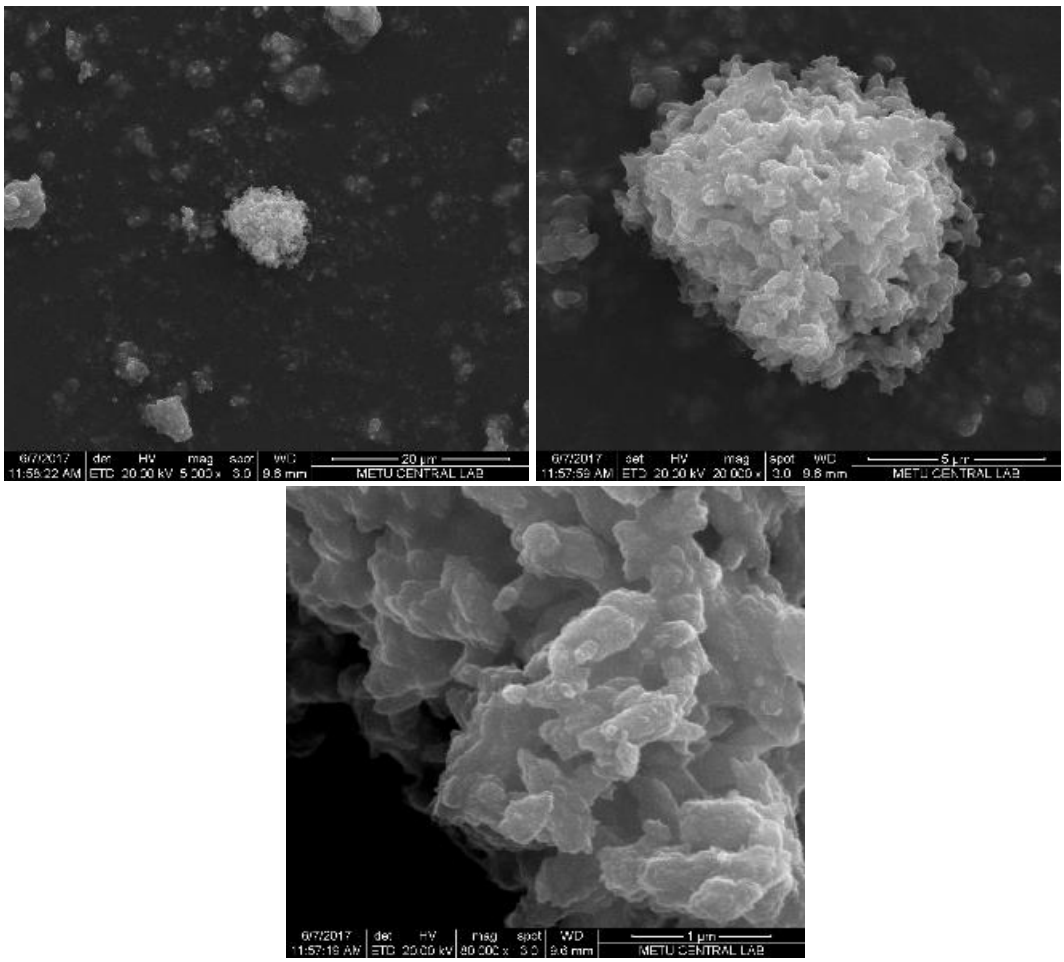

Figure 61. SEM images of carbonation products in the 17th day: calcite or dolomite aggregates 5000x (up, left), 20000x (up, right), 80000 (down).

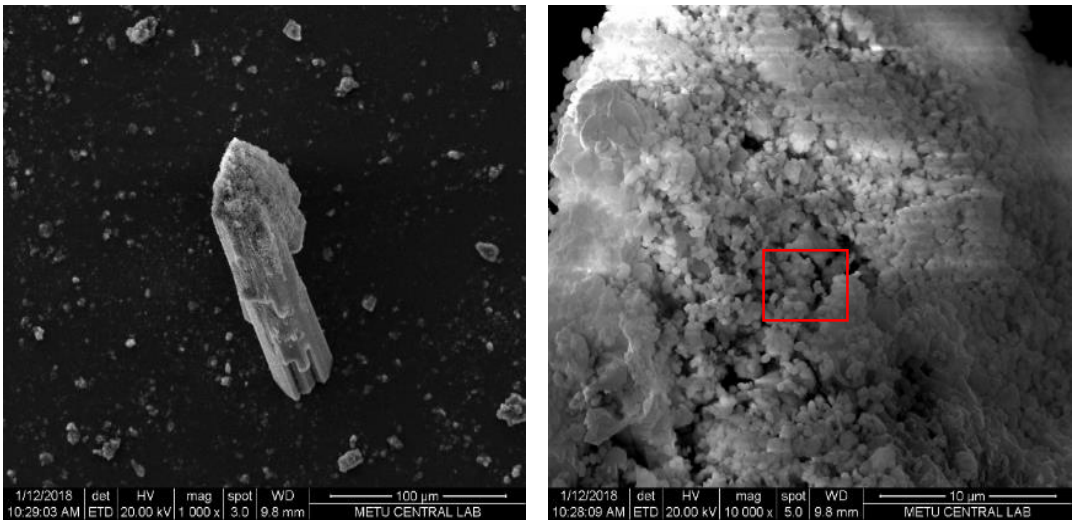

Figure 62. SEM images of carbonation products on the 17th day: nesquehonite, and calcite aggregates 1000x(left), and closer view showing aggregates of calcite or dolomite nanoparticles 10000 (right).

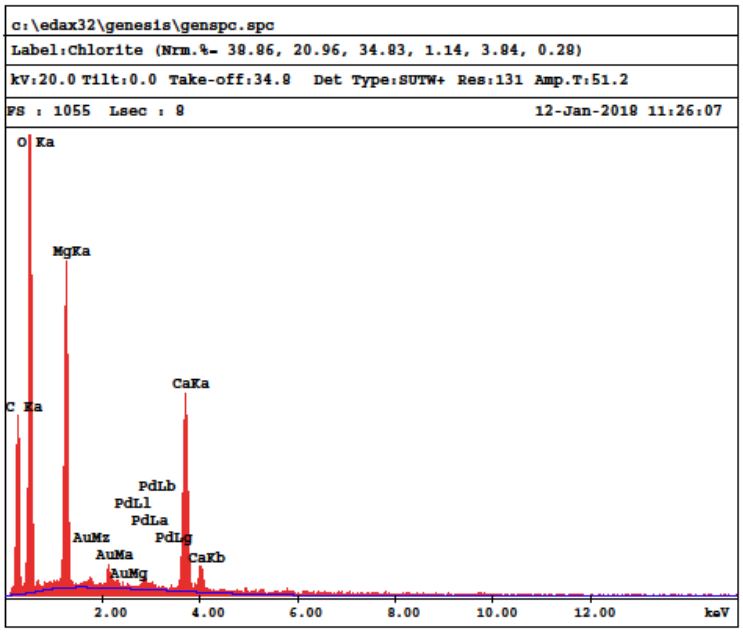

Figure 63. SEM EDAX results of the red squared region, nanoparticle aggregates on nesquhonite.

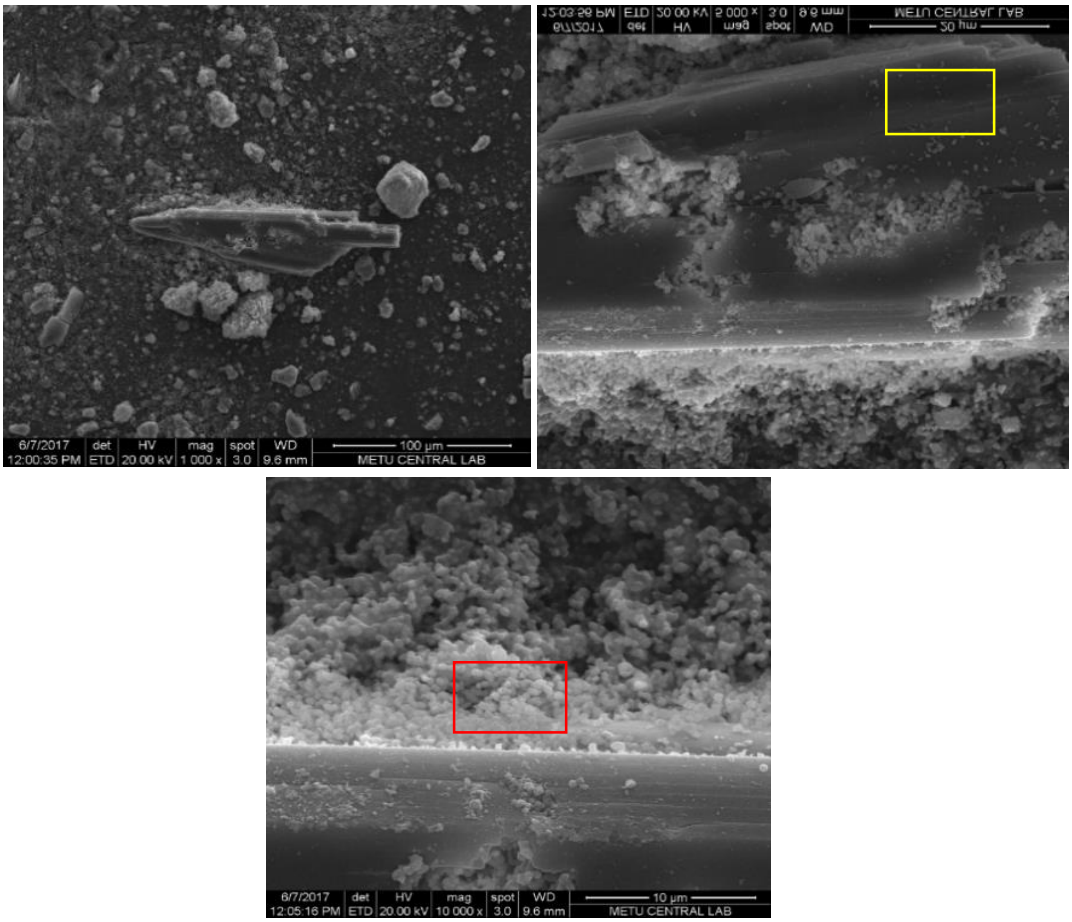

Figure 64. SEM images of carbonation products on the 21st day: general view 1000x (up, left), 5000x (up, right), closer view showing nanoparticles aggregates of dolomite having sizes around 100-500 nm10000x (down)

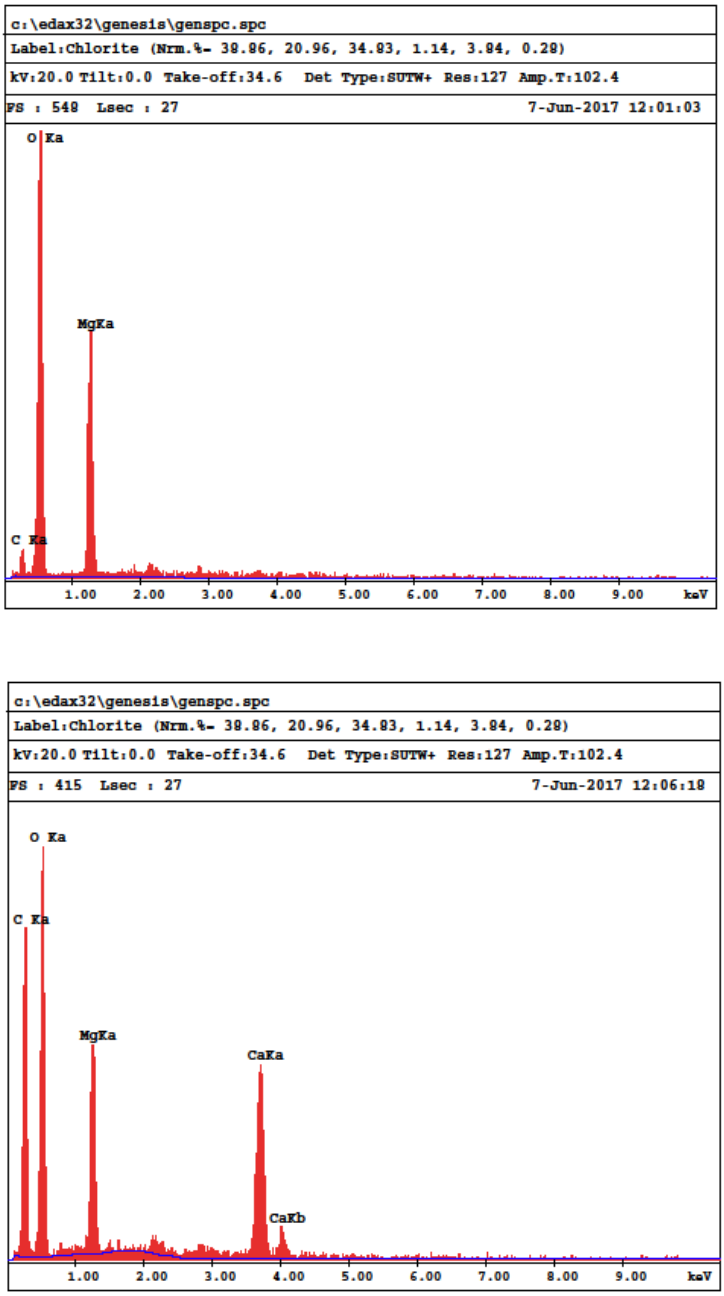

Figure 65. SEM-EDAX analysis of nesquehonite needle itself (up, yellow squared part of Fig.63), and of the aggregates of nanoparticles next to nesquehonite needle (down, red squared part of Fig 63) on the 21st day.

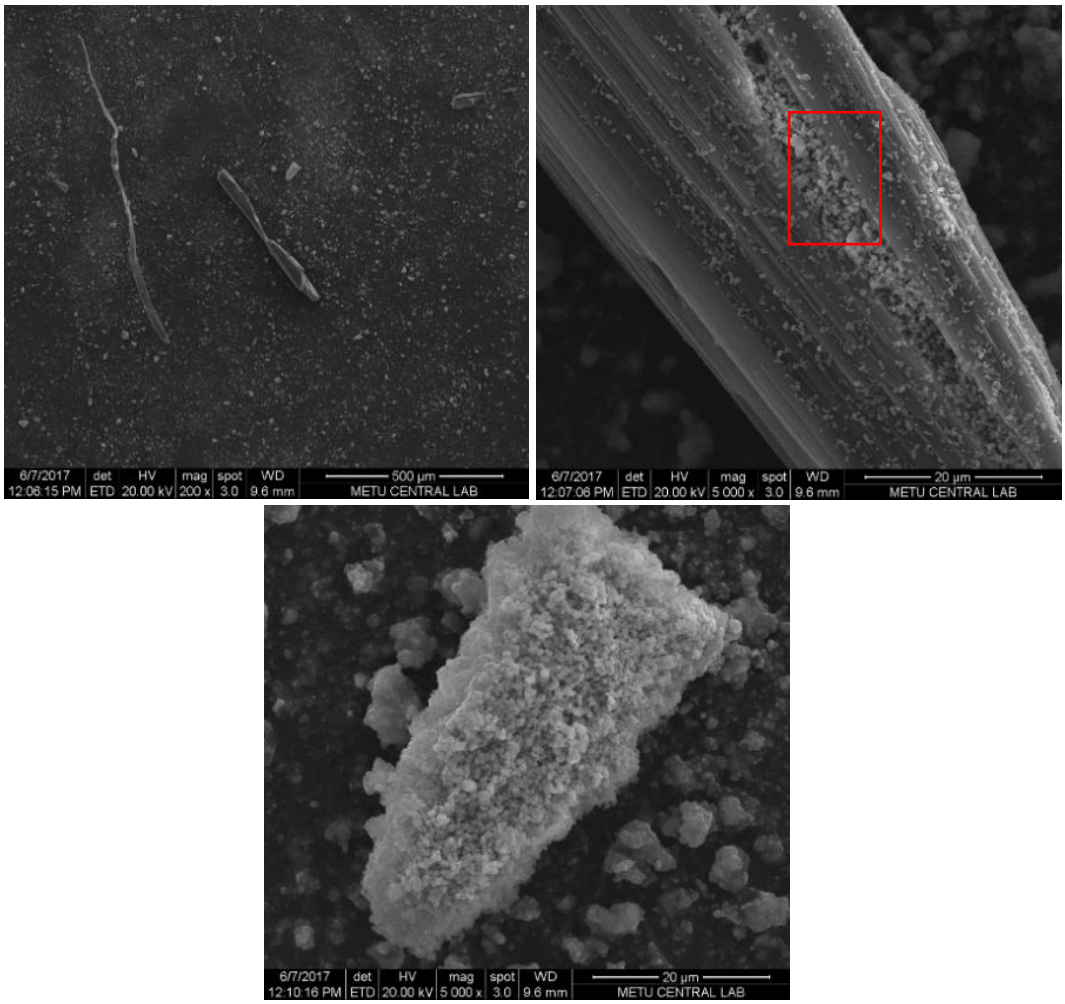

Figure 66. SEM images of carbonation products at 28th day 200x (up, left), 5000x of elongated aggregate (up, right) showing newly formed crystals on nesquehonite, 5000x of smaller aggregates belonging to calcite or dolomite (down).

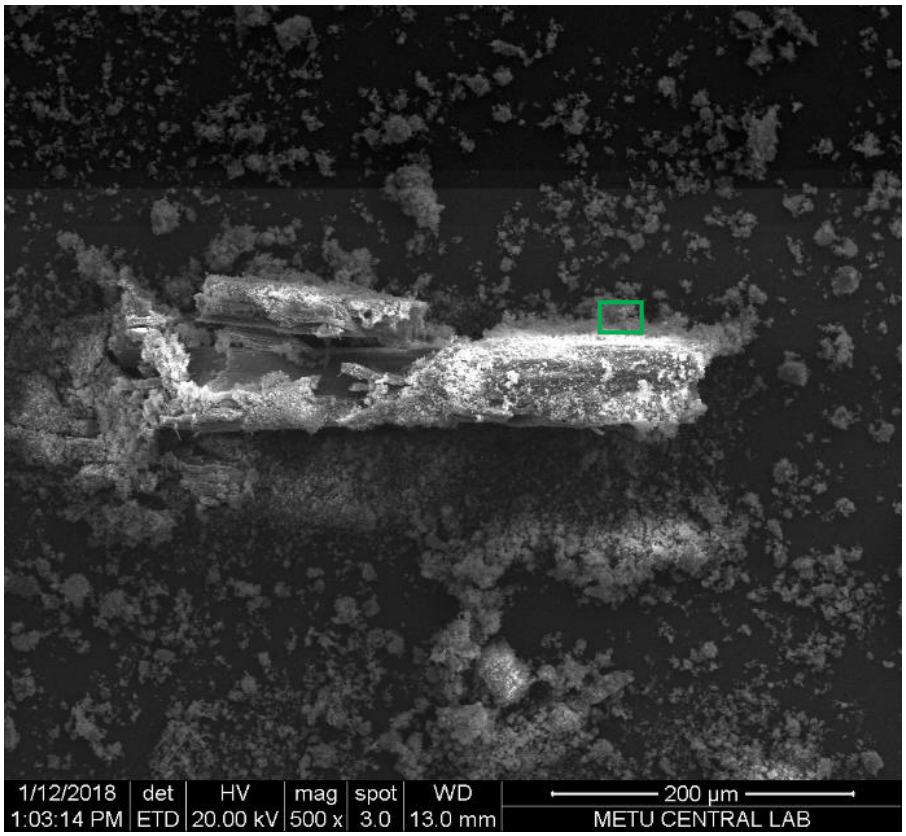

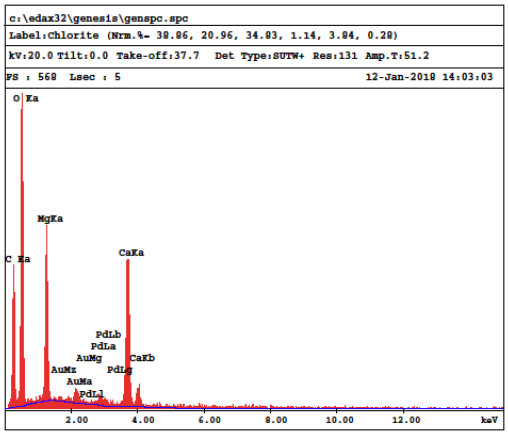

EDAX ZAF Quantification (Standardless)
Element Normalized
SEC Table : Default

Element	Wt %	At %	K-Ratio	Z	A	F
C K	29.63	40.88	0.1097	1.0295	0.3594	1.0005
O K	45.89	47.54	0.1008	1.0123	0.2169	1.0002
MgK	9.45	6.44	0.0491	0.9714	0.5350	1.0005
AuM	2.28	0.19	0.0187	0.6809	1.1996	1.0006
PdL	1.24	0.19	0.0105	0.7645	1.0901	1.0148
CaK	11.50	4.76	0.1067	0.9412	0.9859	1.0000
Total	100.00	100.00				

Figure 67. SEM image of carbonation products at 58th day: A dissociated nesquehonite aggregate 500x(up), SEM-EDX analysis of crystals near nesquehonite (green squared part) showing very close Mg:Ca ratio (down).

4.5.4 XRD and FTIR Analyses of Control Mixtures

In this section, the aim is to find out the relative amounts of carbonation products of any sample taken from the petri dish by comparing with XRD traces or FTIR spectra of control mixtures with known ratios. It was noticed that carbonation products showed heterogeneous distribution in petri dish as layers. Therefore, random sampling of carbonation products does not reflect the whole product. Control mixtures can help to make semi-quantitative interpretation of carbonation products in the layers but not in the whole sample. On the other hand, XRD and FTIR analyses of control mixtures are used as reference data for the identification of individual carbonation products in the mixture with their variable amounts.

XRD traces of standard mixtures of Calcite (Ca) and Nesquehonite (Nes) with the ratios: Ca:Nes-0.2:0.8; Ca:Nes-0.4:0.6; Ca:Nes-0.6:0.4; Ca:Nes-0.8:0.2 are given in Figure 68.

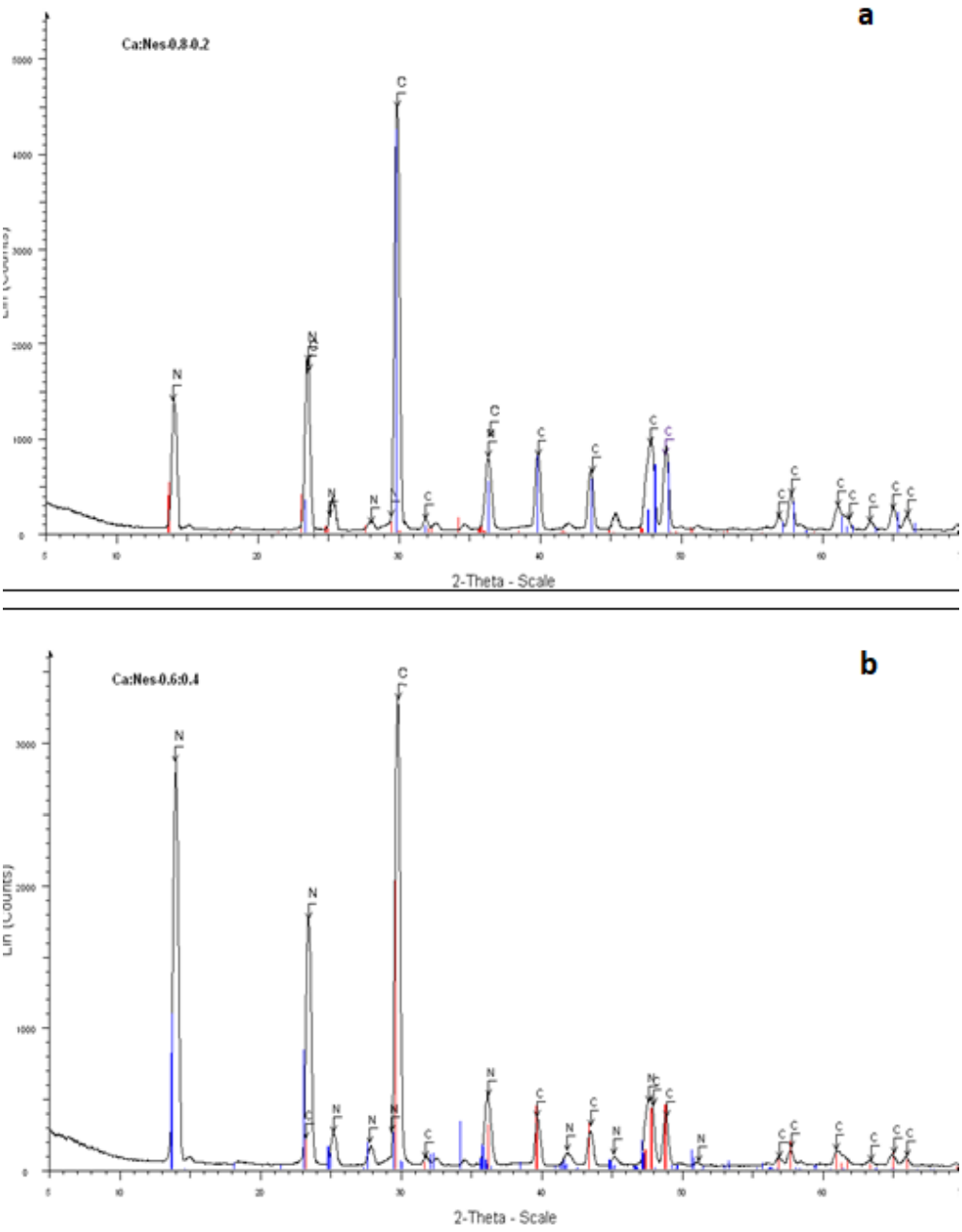

Figure 68. XRD traces of Calcite and Nesquehonite mixtures with the ratios a) Ca:Nes-0.8:0.2, b) Ca:Nes-0.6:0.4

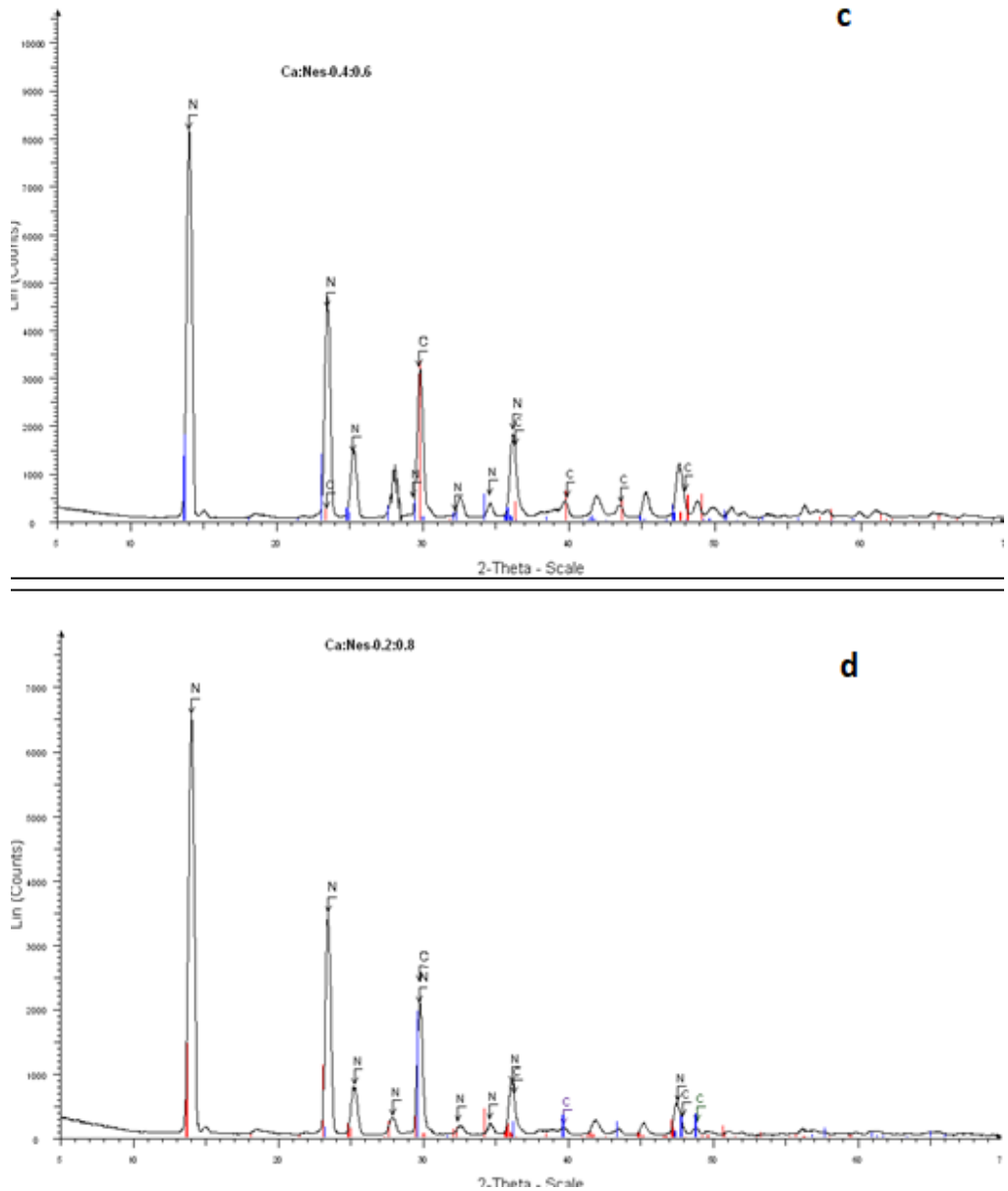

Figure 68 (continued). XRD traces of Calcite and Nesquehonite mixtures with the ratios c) Ca:Nes-0.4:0.6, d) Ca:Nes-0.2:0.8

FTIR spectra of control mixtures of Calcite (Ca) and Dolomite (Dol) with the ratios: Ca:Dol-0.2:0.8; Ca:Dol-0.4:0.6; Ca:Dol-0.5:0.5; Ca:Dol-0.6:0.4; Ca:Dol-0.8:0.2 are given in Figure 69-Figure 73. FTIR analyses of those mixtures have been carried out for the possibility of dolomite identification in the mixture even if it is present in

very small amounts. FTIR absorption bands at 712 and 728 cm^{-1} show symmetric deformation of carbonate groups that could help to identify and separate calcite and dolomite crystals, respectively. However, those peaks for calcite and dolomite were overlapping. Although, it is difficult to identify individual peaks, the presence of dolomite in the mixture can be proved by FTIR analyses by its specific band at 728 cm^{-1} even if the percentage of dolomite is low in the mixture, such as FTIR of Ca:Dol ratio 0.8:0.2 (Figure 73).

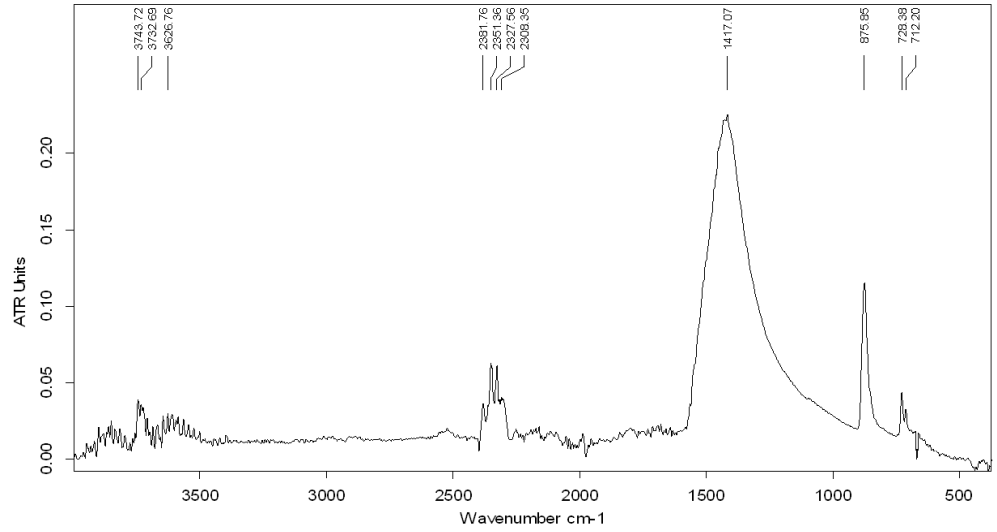

Figure 69. FTIR of Calcite and Dolomite mixture with a ratio of 0.2:0.8.

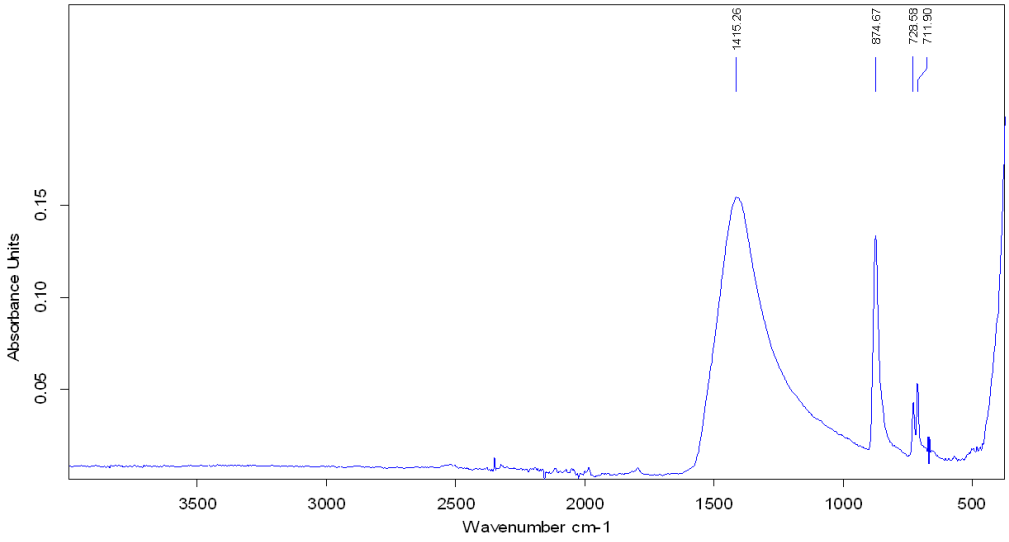

Figure 70. FTIR of Calcite and Dolomite mixture a the ratio of 0.4:0.6

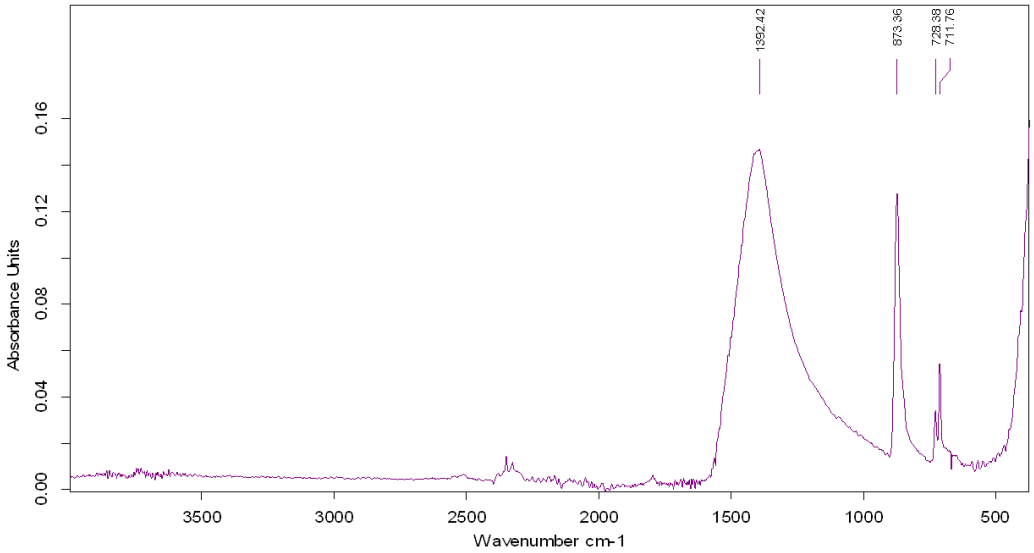

Figure 71. FTIR of Calcite and Dolomite mixture with a ratio of 0.5:0.5.

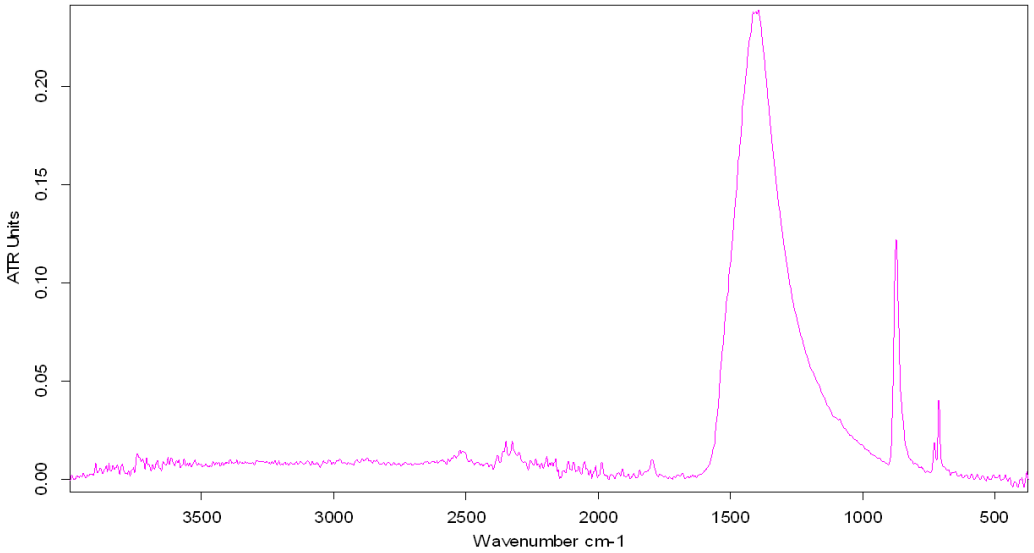

Figure 72. FTIR of Calcite and Dolomite mixture with a ratio of 0.6:0.4

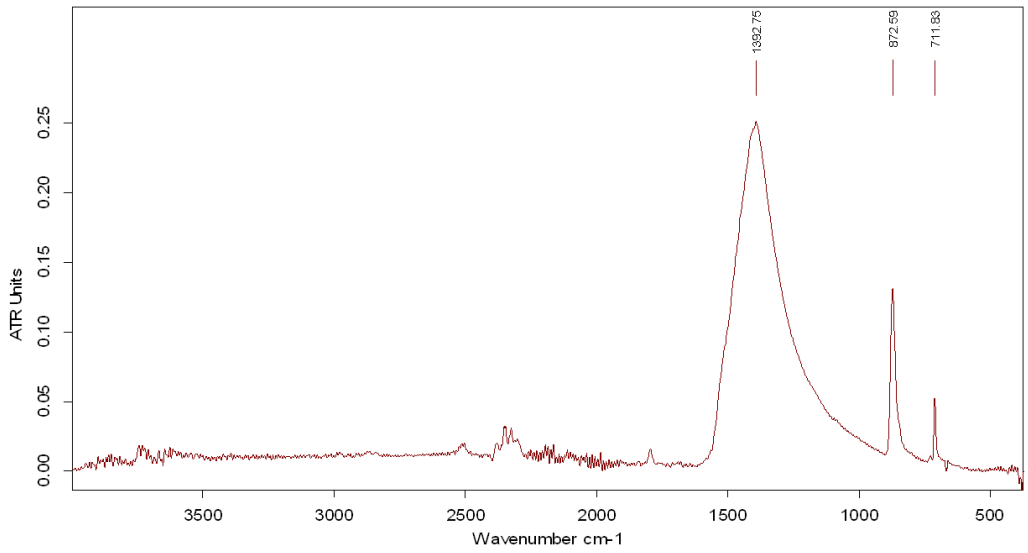

Figure 73. FTIR of Calcite and Dolomite mixture with a ratio of 0.8:0.2.

4.6 Carbonation of $Ca(OH)_2$ and $Mg(OH)_2$ Nanoparticles at High Relative Humidity and High CO_2 Partial Pressure Conditions Using Alcohol Dispersion with Mg:Ca ratio ~1: Set 2

The carbonation products of set-2 were analyzed in this section by consideration of the following points: Firstly, the alcohol dispersion of $Ca(OH)_2$ and $Mg(OH)_2$ nanoparticles was used immediately, right after the termination of stirring process (at the 0th hour) without allowing any settlement of the nanoparticles. Secondly, the products were examined in two layers (upper and bottom layers) in petri dish precipitate (deposit). The upper layer of the deposit was assumed to have air-solution interphase and the bottom layer had solution-solution interphase relative to each other.

For early stage analyses (1,2,3,4 days) the lid of the desiccator was opened each day to take samples from petri dish. CO_2 was supplied at each opening. Separate desiccators were used for the experimental run at the 5^{th} and 10^{th} days. Those two desiccators were only opened at the day of sampling. In that way, the set stayed

undisturbed in equlibrium with relative humidity and CO_2 concentration till the day of sampling.

Under high RH (90-95%), and high $p(CO_2)$ (0.4 atm) conditions, the carbonation products of set-2 experiments were followed by XRD and SEM. In addition, the stereomicroscope image and FTIR spectra are also given for the upper layer at 10^{th} day of carbonation.

4.6.1 XRD Analyses

XRD traces of carbonation products of $Ca(OH)_2$ and $Mg(OH)_2$ nanoparticles dispersed in ethanol at the 1st, 2nd, 3rd, 4th, 5th, and 10th days are given for upper and bottom layers in Figure 74-Figure 85. When the sample on the glass lamalla is in small amount, XRD traces of glass is more pronounced along with the traces of the sample as high background around 20-35 2θ values.

At the first day, the products at the upper layer (air-solution interphase) are portlandite ($Ca(OH)_2$), brucite ($Mg(OH)_2$), calcite, and nesquehonite (Figure 74). At the bottom layer (solution-solution interphase), portlandite and brucite remained uncarbonated (Figure 75).

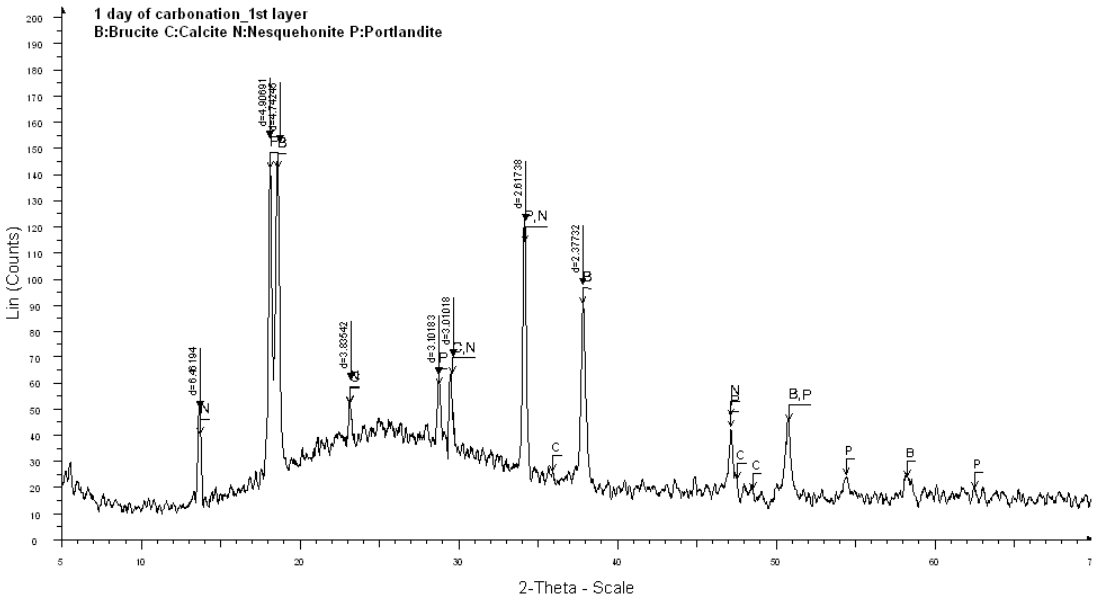

Figure 74. XRD traces of carbonation products in petri dish, upper layer, 1 day of carbonation

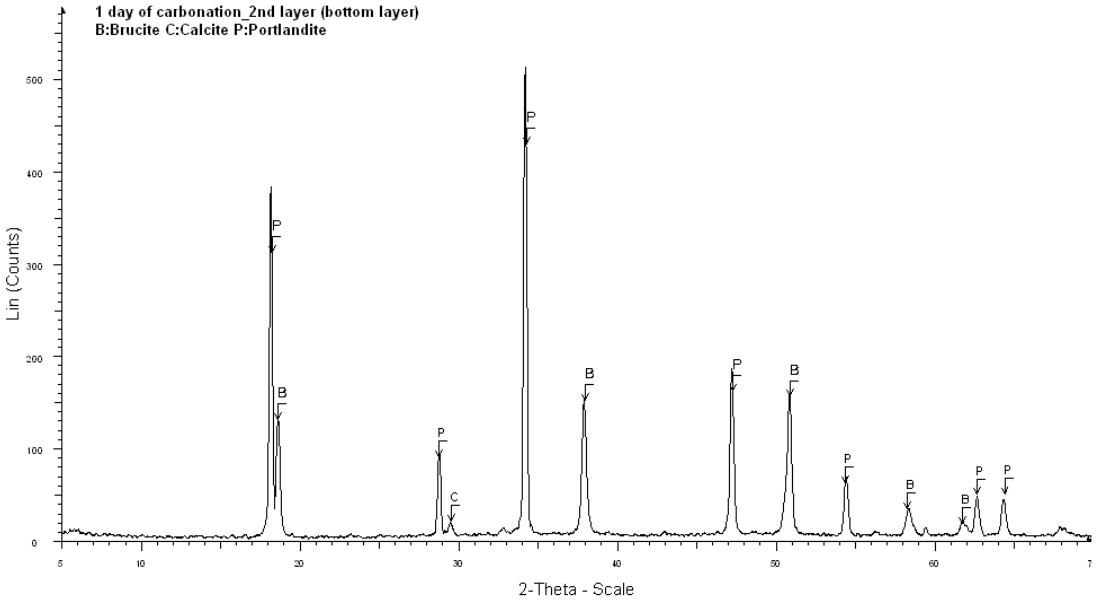

Figure 75. XRD traces of carbonation products in petri dish, bottom layer, 1 day of carbonation

At the 2nd day, at the upper layer, the main peak dolomite appears together with nesquehonite and calcite. The other characteristic peaks of dolomite start to appear, e.g., the twin peaks at 2θ-around 50 values-d=2.78&2.80) (Figure 76). At the bottom layer, the products are mostly a mixture of portlandite, brucite, calcite, and nesquehonite. Dolomite main peak can also be observed in that layer (Figure 77).

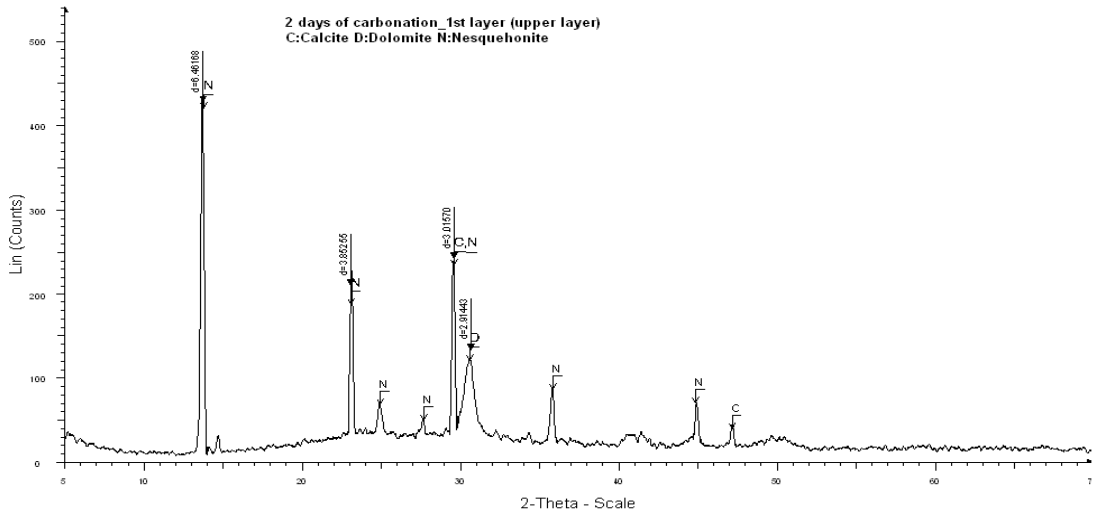

Figure 76. XRD traces of carbonation products in petri dish, upper layer, 2 days of carbonation

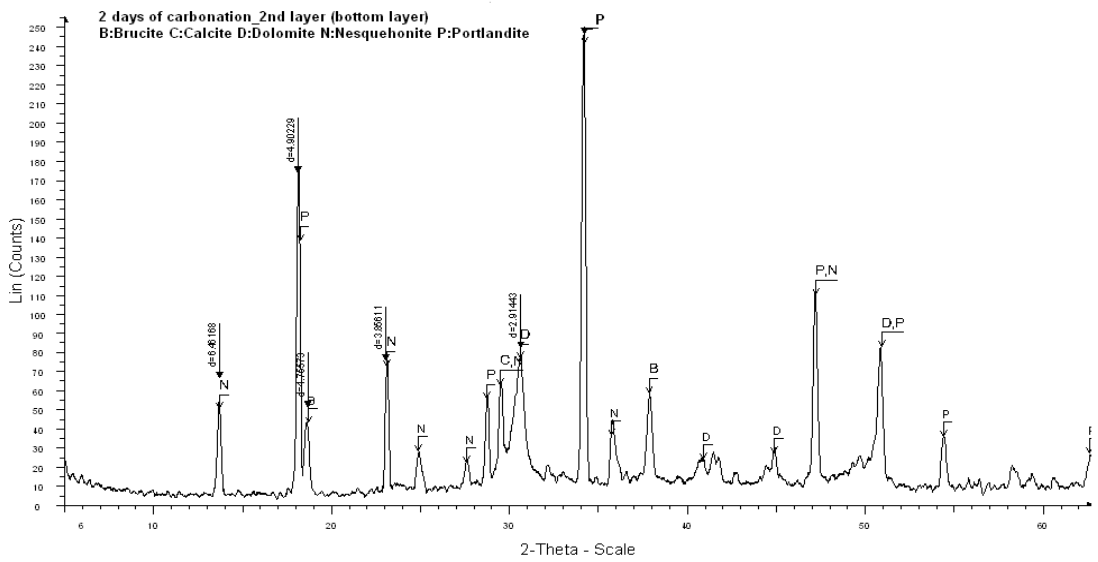

Figure 77. XRD traces of carbonation products in petri dish, bottom layer, 2 days of carbonation

At the 3rd day, dolomite peaks are clearly observed in the XRD traces of the upper layer together with most of its characteristic peaks. Some nesquehonite, calcite and aragonite are present (Figure 78). At the bottom layer, the products seemed to be similar to those in the upper layer (Figure 79).

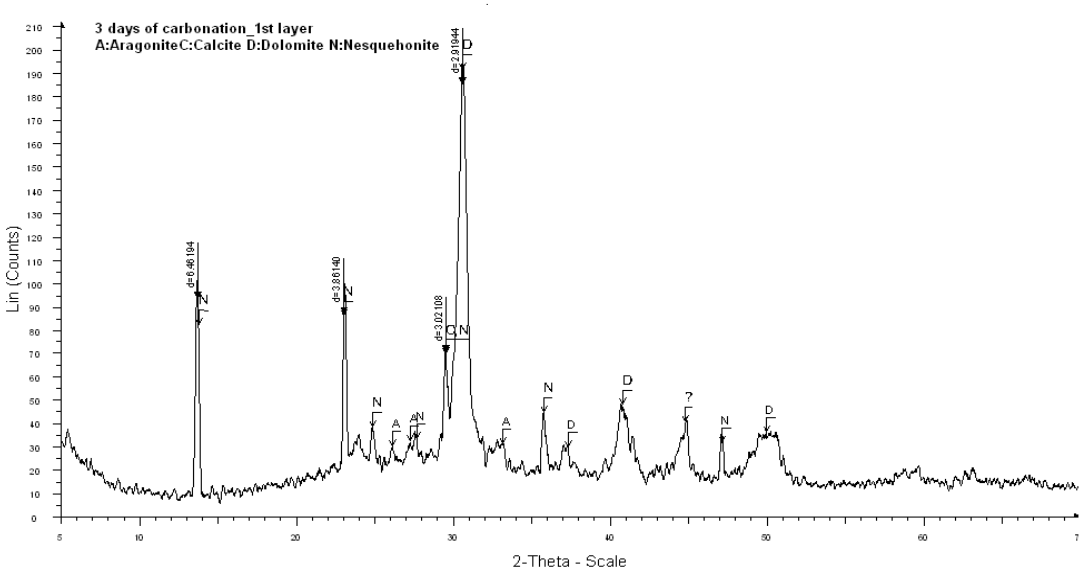

Figure 78. XRD traces of carbonation products in petri dish, upper layer, 3 days of carbonation

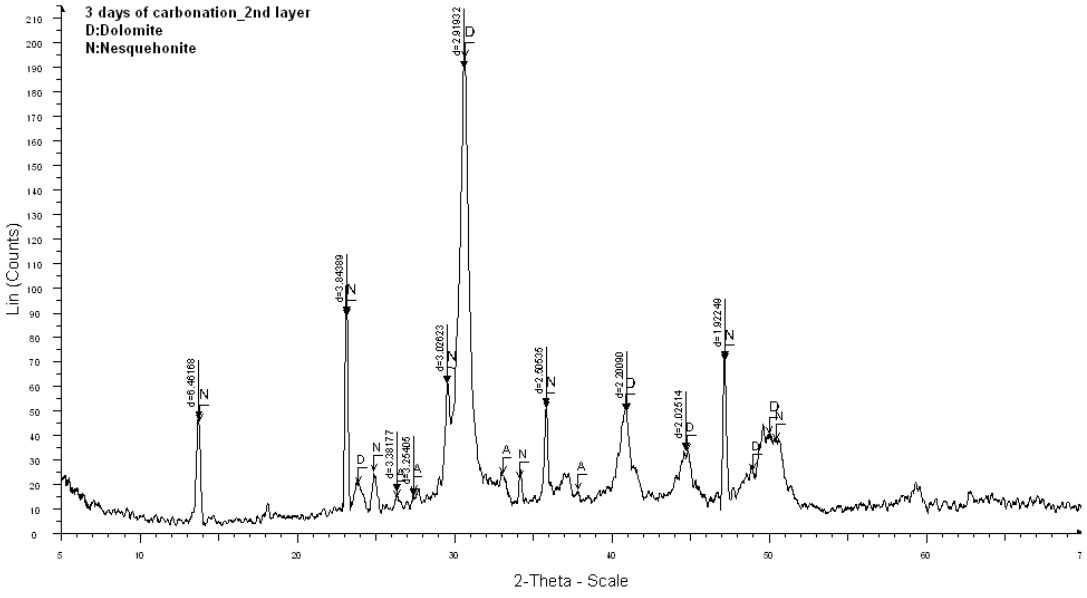

Figure 79. XRD traces of carbonation products in petri dish, bottom layer, 3 days of carbonation

At the 4th day, there are mainly dolomite and nesquehonite at the upper layer and bottom layers (Figure 80 & Figure 81).

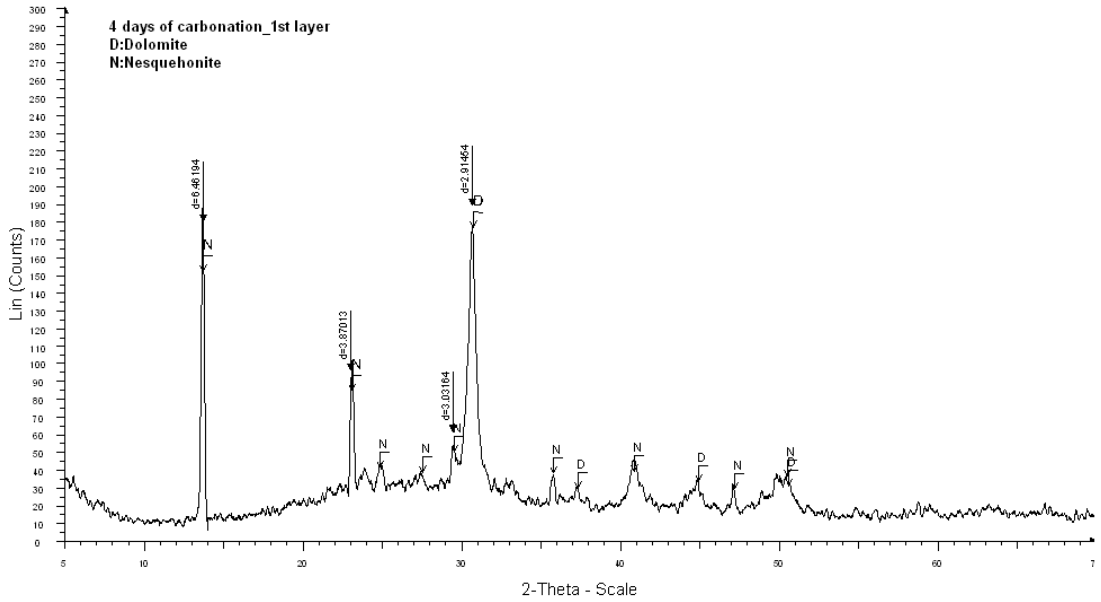

Figure 80. XRD traces of carbonation products in petri dish, upper layer, 4 days of carbonation

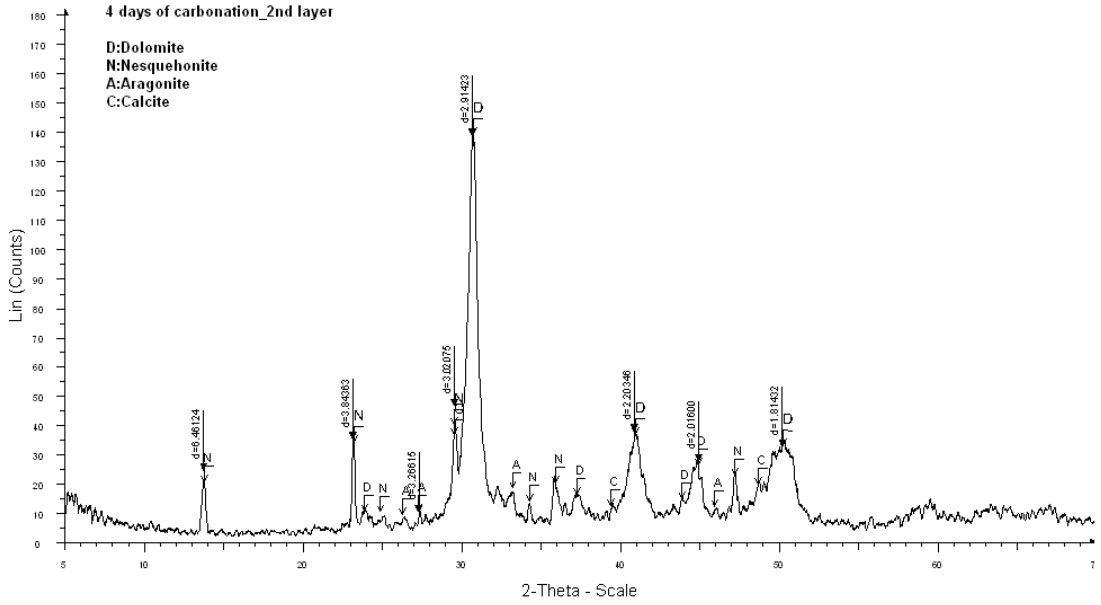

Figure 81. XRD traces of carbonation products in petri dish, bottom layer, 4 days of carbonation

At the 5th day, both the upper and bottom layers show mostly dolomite with traces of nesquehonite (Figure 82-Figure 83)

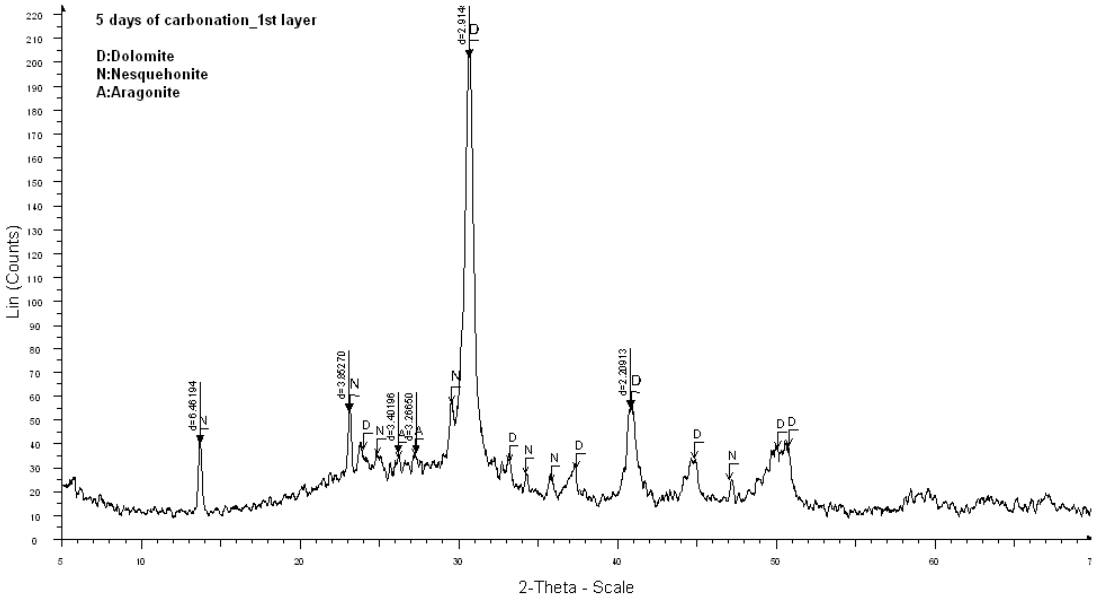

Figure 82. XRD traces of carbonation products in petri dish, upper layer, 5 days of carbonation

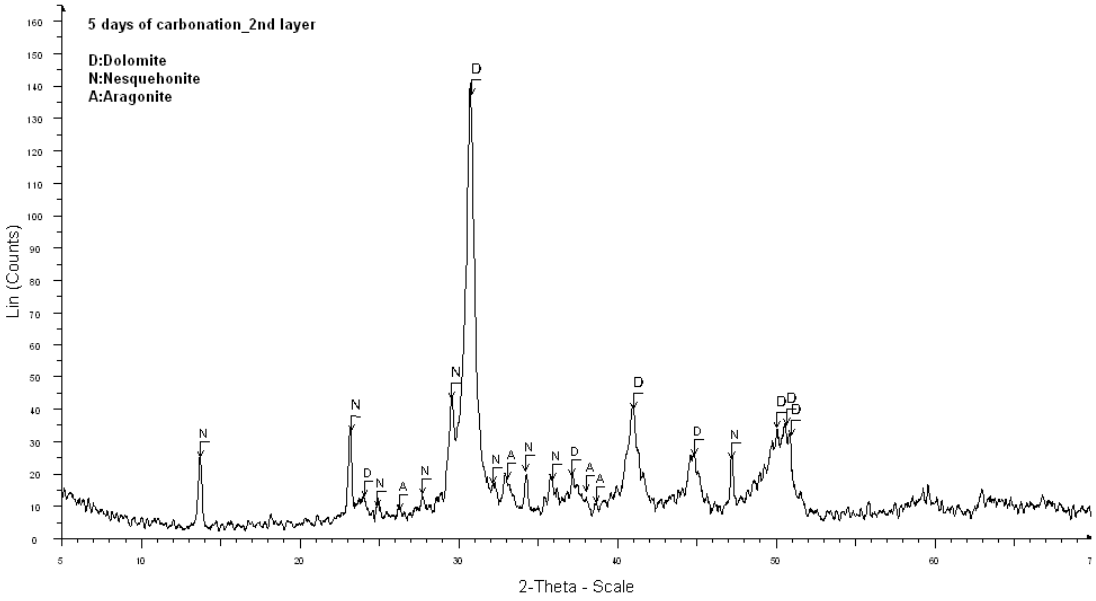

Figure 83. XRD traces of carbonation products in petri dish, bottom layer, 5 days of carbonation

At the 10th day, at the upper layer, dolomite can be best isolated with negligible amounts of calcite whose main peak appeared weak at the left of the main dolomite peak. At the bottom layer, again, dolomite is the dominant product with some nesquehonite or calcite (Figure 84-Figure 85).

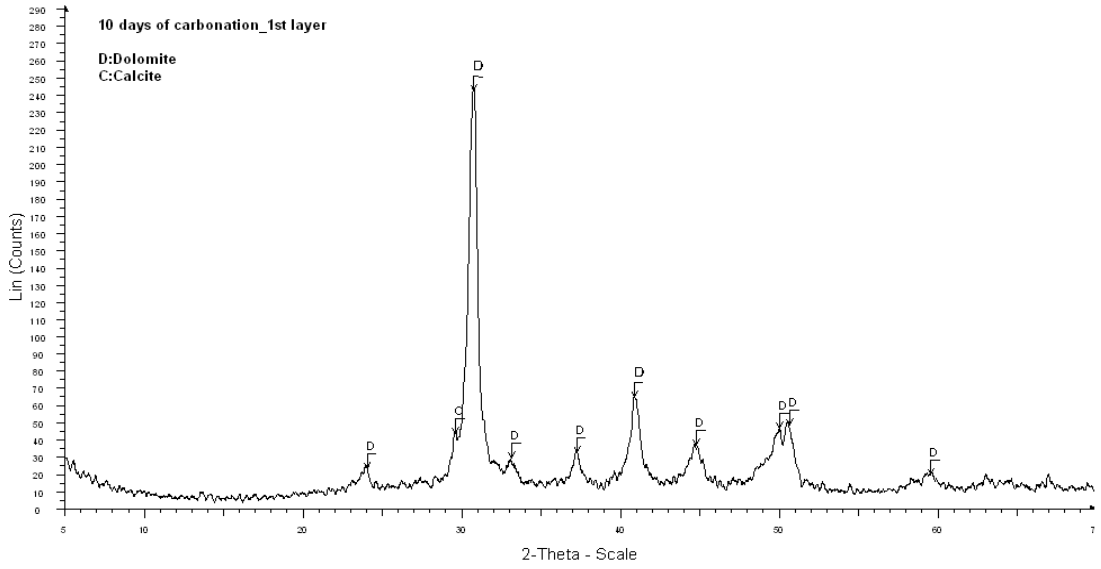

Figure 84. XRD traces of carbonation products in petri dish, upper layer, 10 days of carbonation

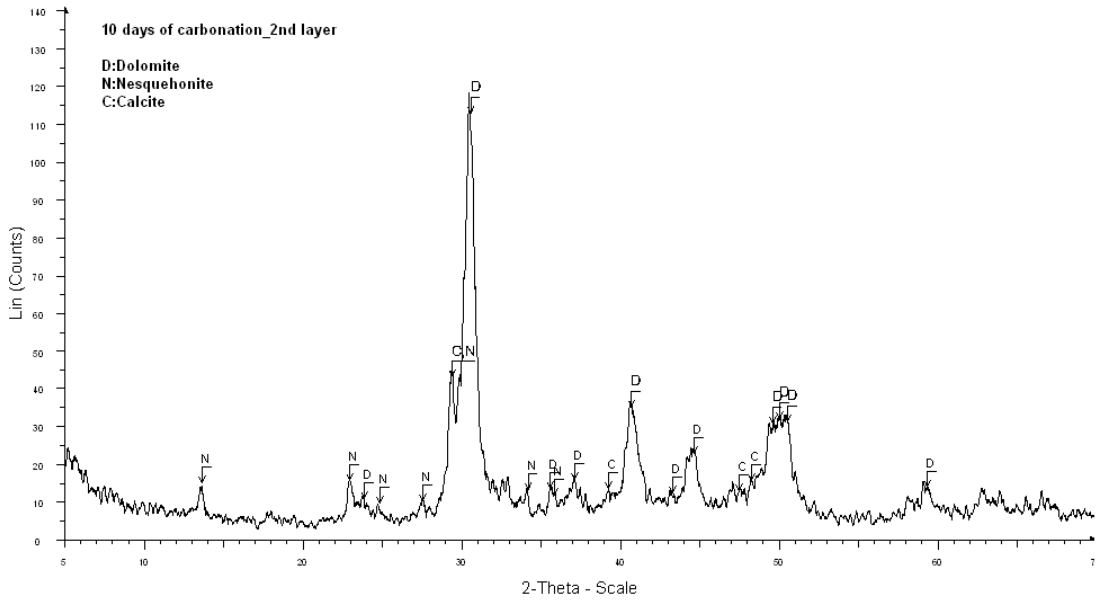

Figure 85. XRD traces of carbonation products in petri dish, bottom layer, 10 days of carbonation

XRD traces of the sample taken from the upper layer of carbonation products at the 10th day (synthesized dolomite) was compared with the original dolomite sample, i.e., Midyat dolomite, that will be consolidated. The synthesized dolomite at the laboratory (black) and original dolomite (Midyat dolomite) (red) traces have been found to be quite similar (Figure 86) (Table 10). However, it is realized that one peak of original dolomite is missing (the peak at 2θ-between 35 and 36) in the synthesized product, and the peak at 2θ-22.15 seem to be lost in the background signals. The peaks at 2θ-43.93 and 49.47 are not sharp, but integrated with the nearest peaks at 2θ-45.92 and 50.67, respectively.

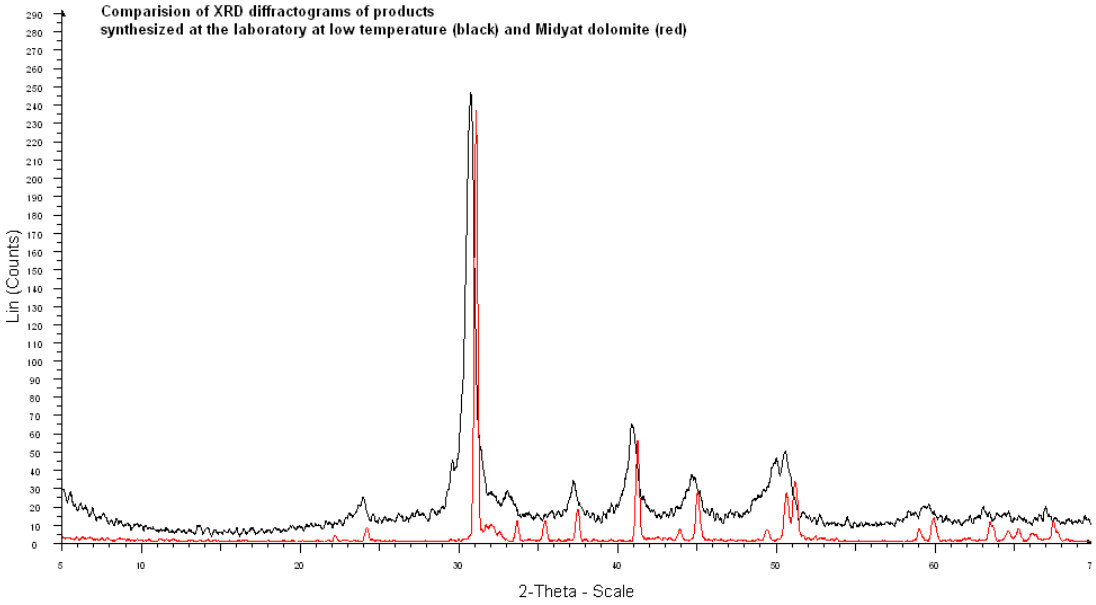

Figure 86. XRD traces of synthesized dolomite compared with the Midyat dolostone sample(red).

Table 10. Comparision of XRD traces of Midyat Dolomite(MD) versus Synthesized Dolomite (SD)

~XRD peak location ($^o2\theta$ values)		XRD hkl indices	d-Spacing (Angstroms)		Relative XRD peak intensity	
MD	SD	MD-SD	MD	SD	MD	SD
22.15*	doesn't appear	101*	4.00	-	3.3	-
24.11	23.91	012	3.69	3.71	11.9	10.3
31.17	30.76	104	2.87	2.90	100	100
33.67	33.07	006	2.66	2.71	8.5	11.7
35.41*	doesn't appear	015*	2.53	-	6.5	-
37.58	37.23	110	2.39	2.41	9.9	14
41.27	40.92	113	2.19	2.20	26.5	26.6
43.93*	43.77 (?)	021*	2.06	2.06	4.7	8.7
45.02	44.77	202	2.01	2.02	15.4	15.3
49.47	48.72	024	1.84	1.86	4.1	11
50.67	49.87	018	1.80	1.83	13.7	18.1
51.27	50.61	116	1.78	1.80	16.9	20.6
59.09	58.67		1.56	1.57	4.2	6.7
59.96	59.78		1.54	1.55	7.0	9.1

4.6.2 FTIR Analyses

FTIR spectra of upper layer at 10^{th} day show the distinctive band of dolomite that separate it from other carbonates (Figure 87). The synthesized dolomite's symmetric deformation band of carbonate group appears at 726 cm^{-1}. The band at 874 cm^{-1} belongs to the asymmetric deformation of carbonate group. The stretching bands of carbonate group are usually observed around 1400-1500 cm^{-1}. Here it is observed as a band at 1426 cm^{-1}.

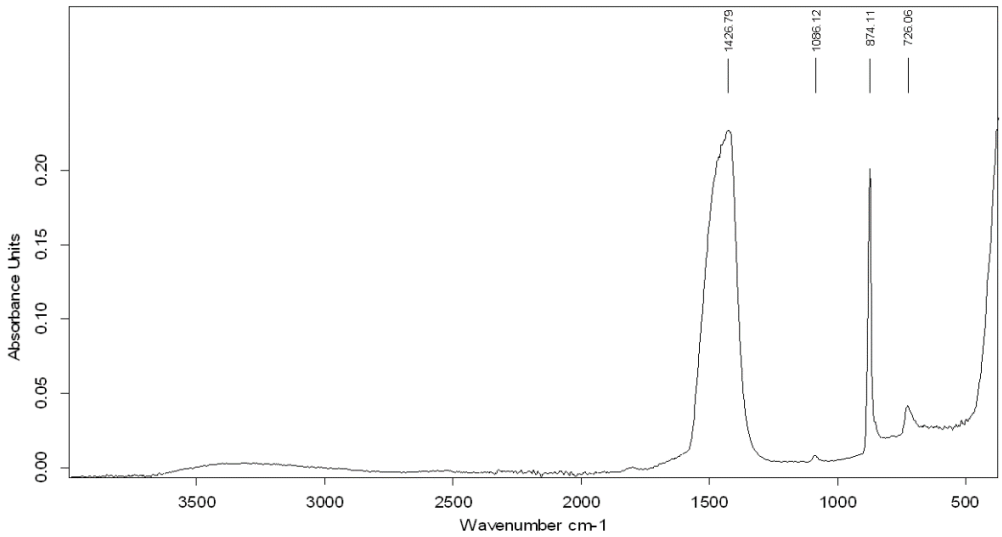

Figure 87.FTIR spectra of dolomite formed at the upper layer at the tenth day.

FTIR spectra of Midyat dolomite and synthesized dolomite are shown together in Figure 88. It is seen that the bands coincide with each other. The peak at 728 cm^{-1} is sharp for Midyat dolomite, whereas that peak for synthesized dolomite at 726 cm^{-1} is observed to be broader.

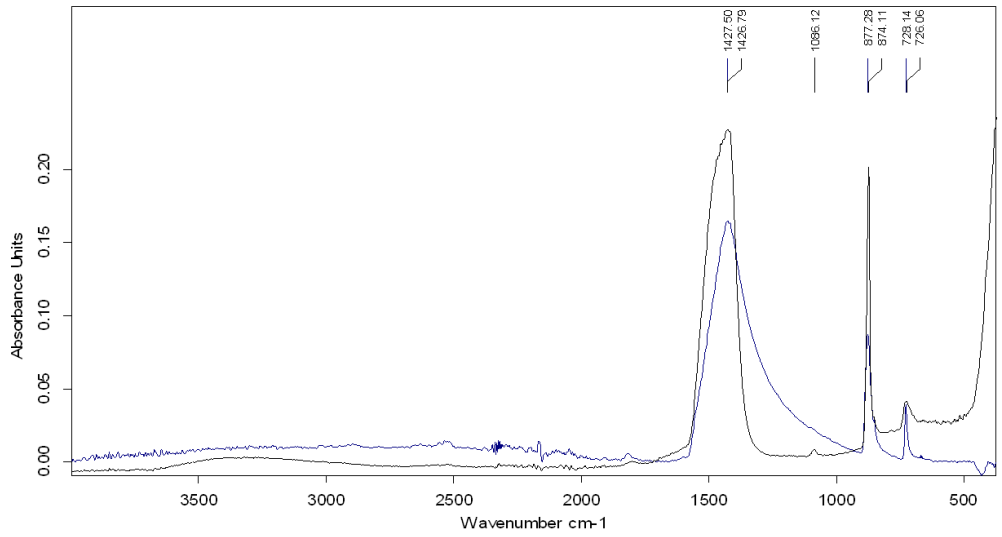

Figure 88. FTIR spectrum of dolomite formed at the upper layer (black) and FTIR spectrum of Midyat dolomite (blue)

4.6.3 Stereomicroscope Images

Stereomicroscope images of the products formed in petri dish at 10x and 50x magnifications are observed as white deposits on the surface at the 10th day of carbonation products (Figure 89). It is observed that the white deposit on the surface has some cracks that occurred probably during the drying process of alcohol.

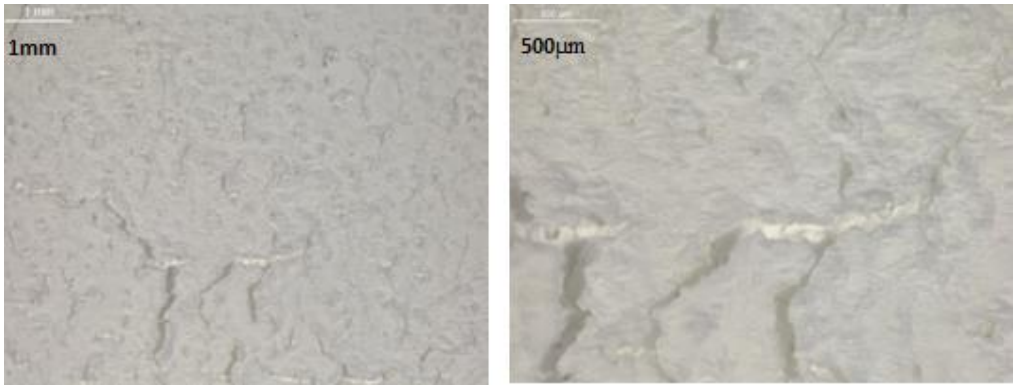

Figure 89. Stereomicroscope images of carbonation products in petri dish (left: 10x, right: 50x magnification)

4.6.4 SEM Analyses

SEM images of carbonation products formed at the upper layer at the 1st,2nd, and 10th days, which were mineralogically identified by XRD, are given in Figure 90-Figure 98.

At the first-day of carbonation, in the upper-layer SEM view, hydroxide aggregates are seen quite different from the SEM view of uncarbonated hydroxide nanoparticles (Figure 34 and Figure 90). Individual clusters of $Ca(OH)_2$ or $Mg(OH)_2$ are not seperated, but integrated with each other. Some carbonation products revealed in XRD traces as calcite and nesquehonite, cannot be well differentiaed in SEM views (Figure 90).

At the second-day, upper-layer SEM image, knowing that all hydroxide nanoparticles carbonated as calcite, nesquehonite, and some dolomite, any of

carbonation products cannot be identified individually, they show up aggregates integrated with each other (Figure 91 & Figure 92).

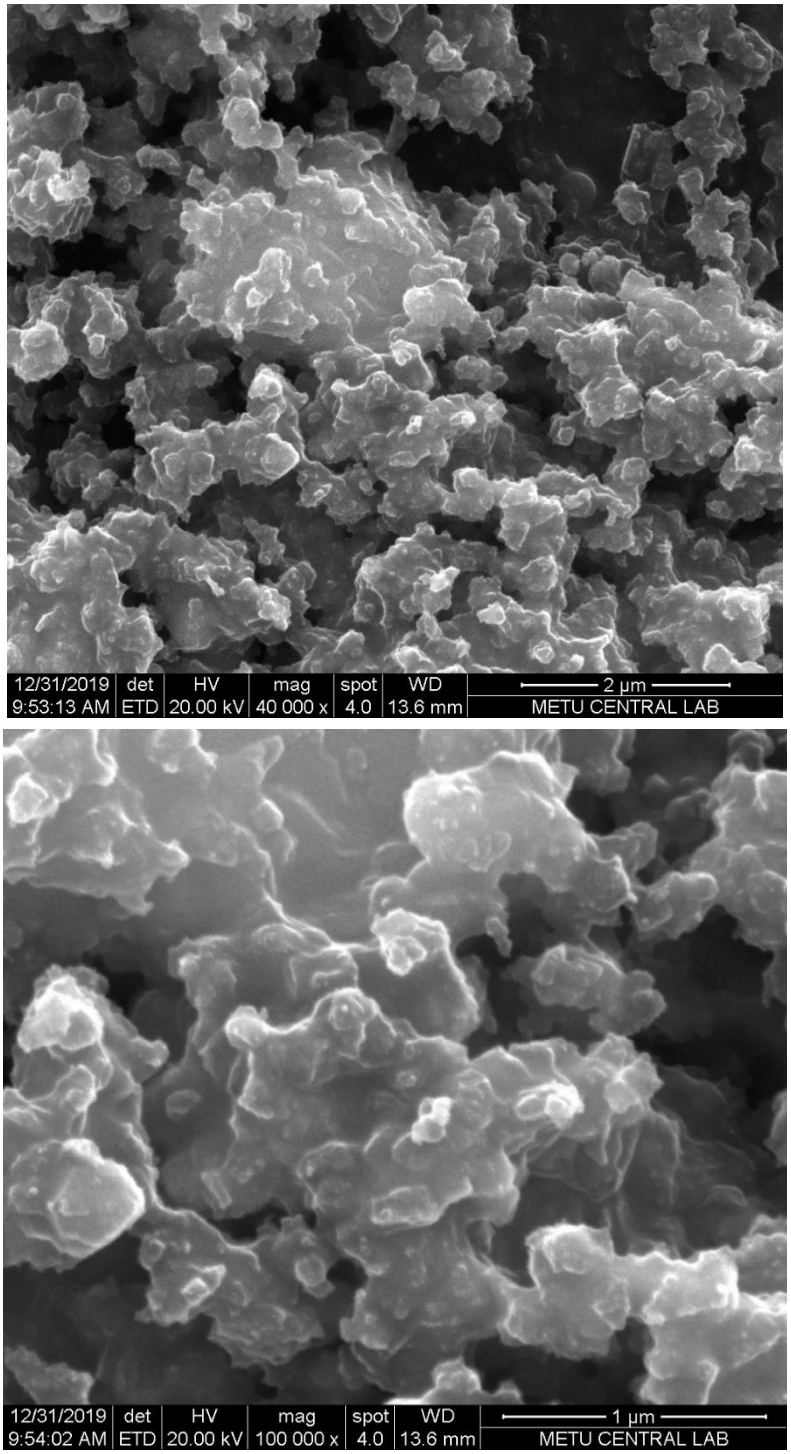

Figure 90. SEM image of carbonation products of upper layer at the first day. Hydroxide particles seems as aggregates integrated within each other (40000x-up and 100000x-down)

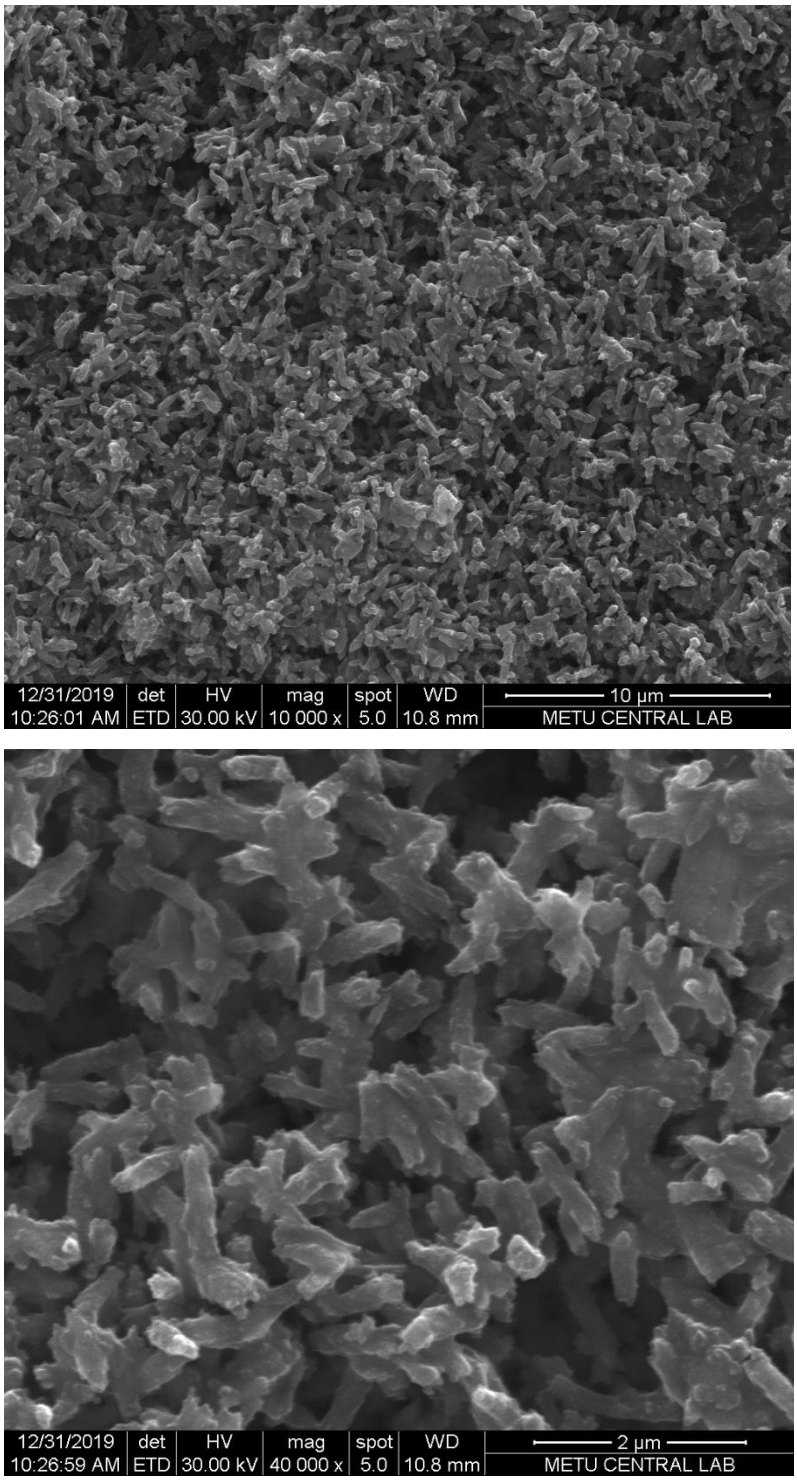

Figure 91. SEM image of carbonation products of upper layer at the second day. In that layer hydroxide nanoparticles seems to be carbonated as aggregates of calcite, dolomite (or maybe magnesium calcite) and nesquehonite (10000x-up and 40000x-down)

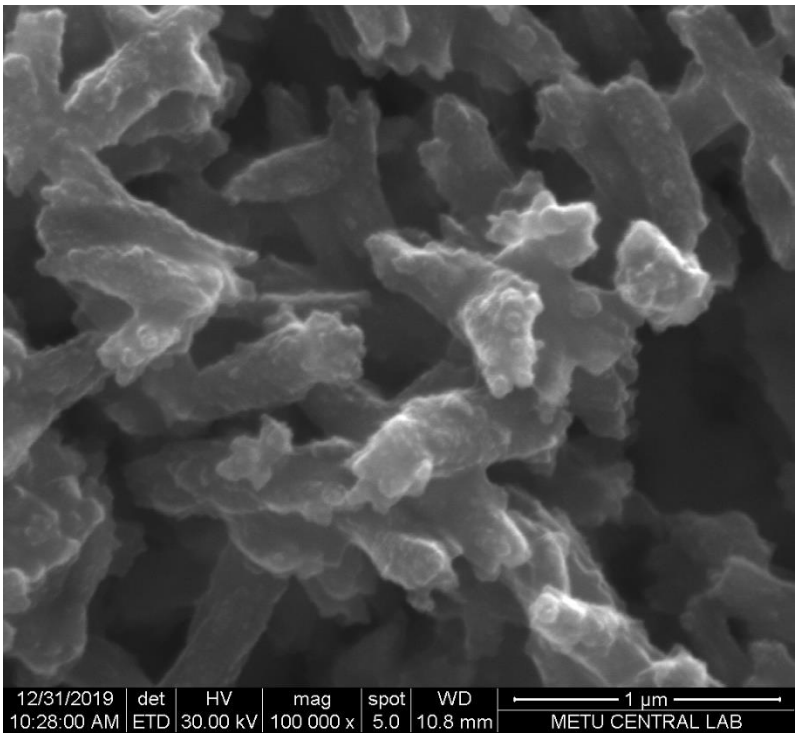

Figure 92. Closer view of aggregates having calcite, dolomite and nesquehonite aggregates integrated within each other (100000x magnification)

At the tenth-day, upper-layer SEM image, carbonation products appear more uniform, which are identified as dolomite by XRD traces. Dolomite nanoparticles appear as aggregates around 500 nm, as well as smaller-size aggregates of nanoparticles down to around 100 nm (Figure 93&Figure 94) and 25-50 nm (Figure 95&Figure 96). EDAX analysis shows the composition of dolomite with Mg and Ca peaks similar to the EDAX of the original dolomite referring to Mg:Ca ratio close to 1 (Figure 97).

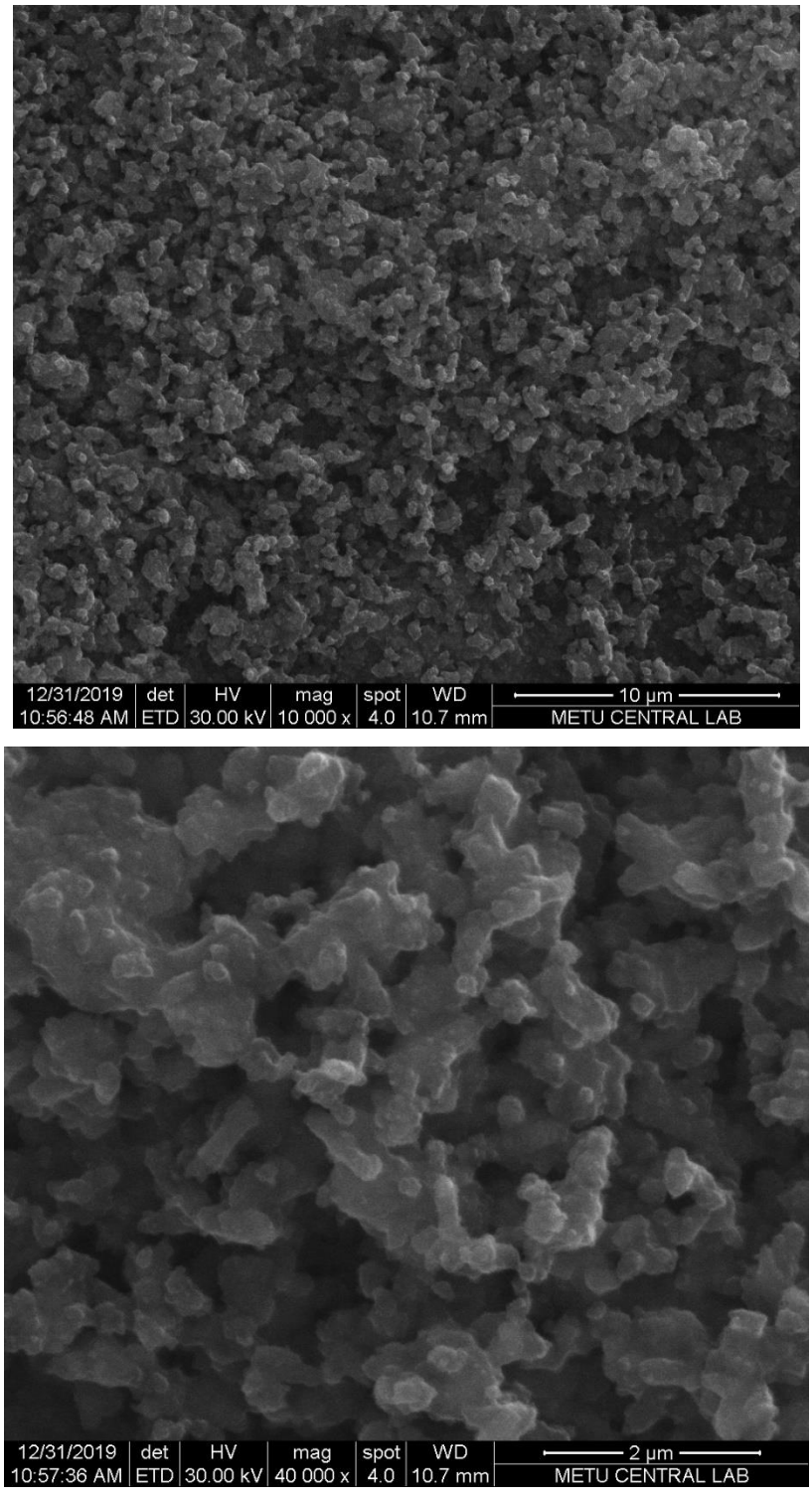

Figure 93. SEM image of carbonation products of upper layer at the tenth day. showing dolomite aggregates (at 10000x magnification)

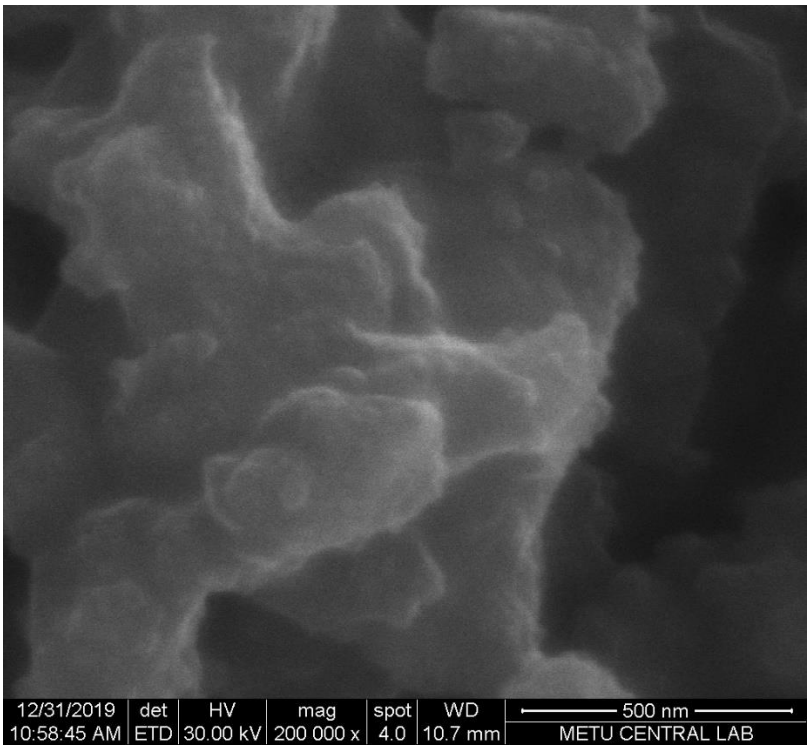

Figure 94. Closer view showing dolomite aggregates around 500 nm and smaller ones down to around 100 nm (200000x magnification)

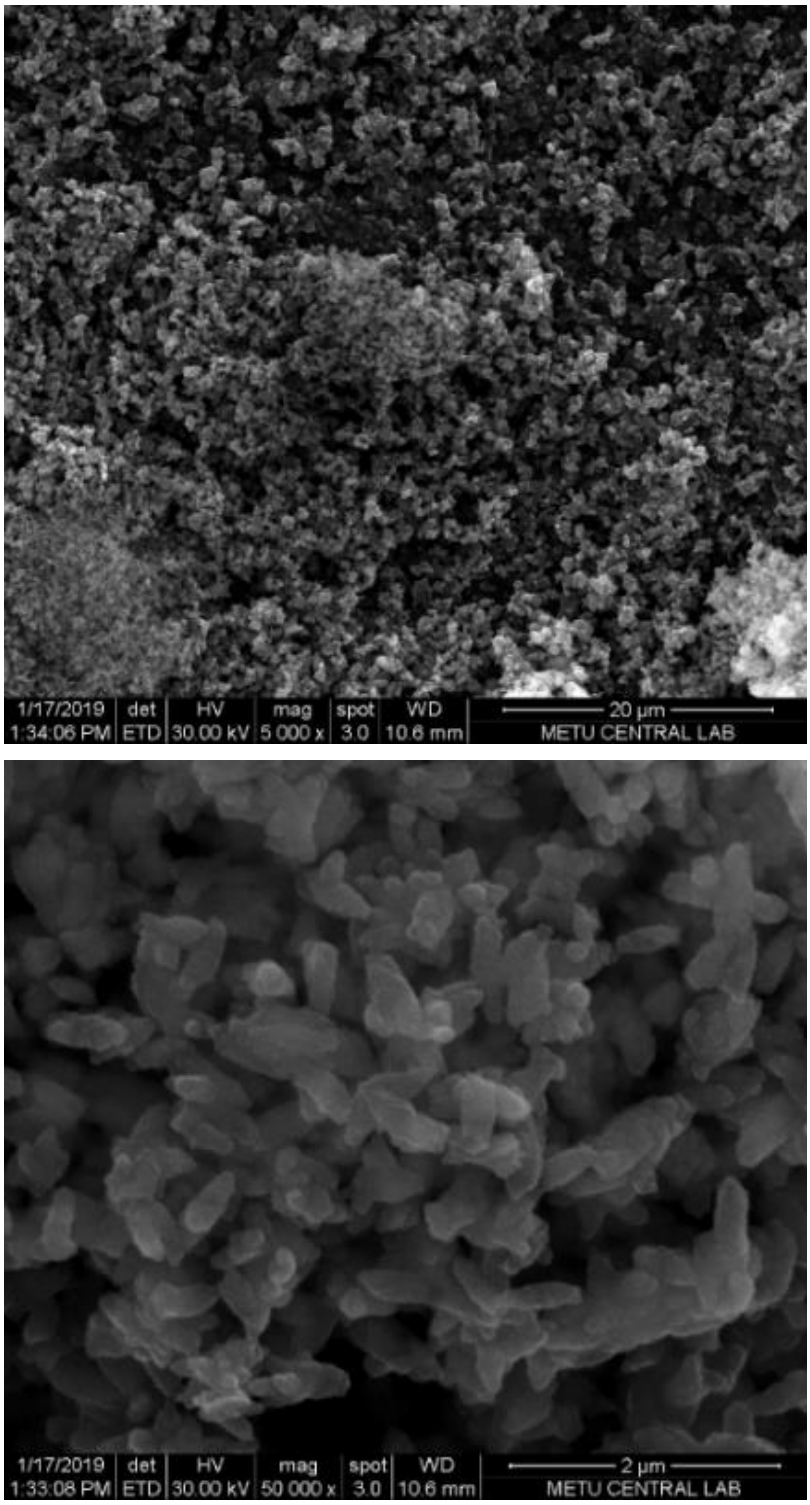

Figure 95. Another view of the upper layer at the tenth day: SEM images of carbonation products showing dolomite aggregates (up:5000x, down: 50000x magnification).

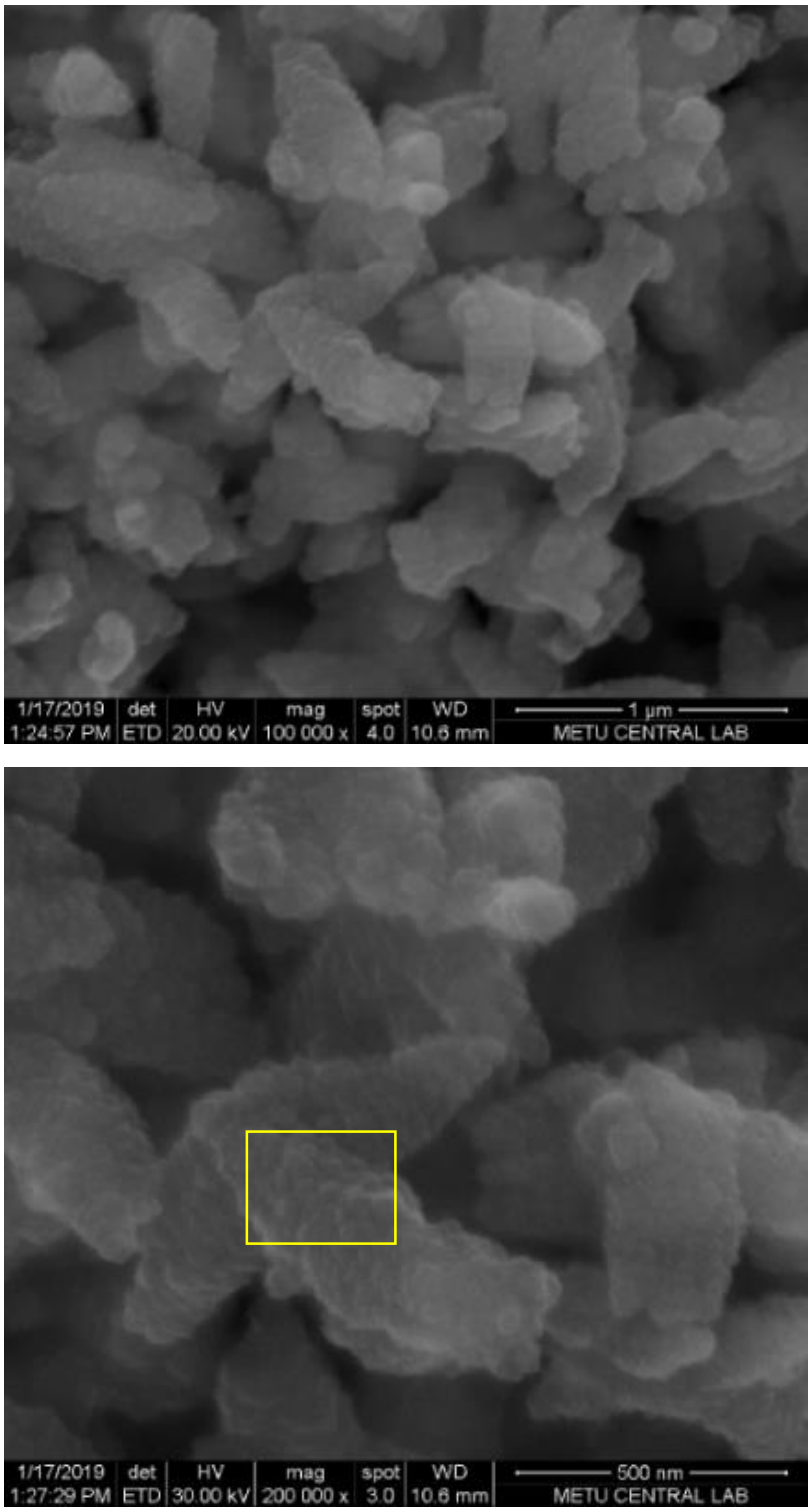

Figure 96. Closer SEM view showing dolomite aggregates around 500 nm and smaller ones having down to around 25-50 nm particles.

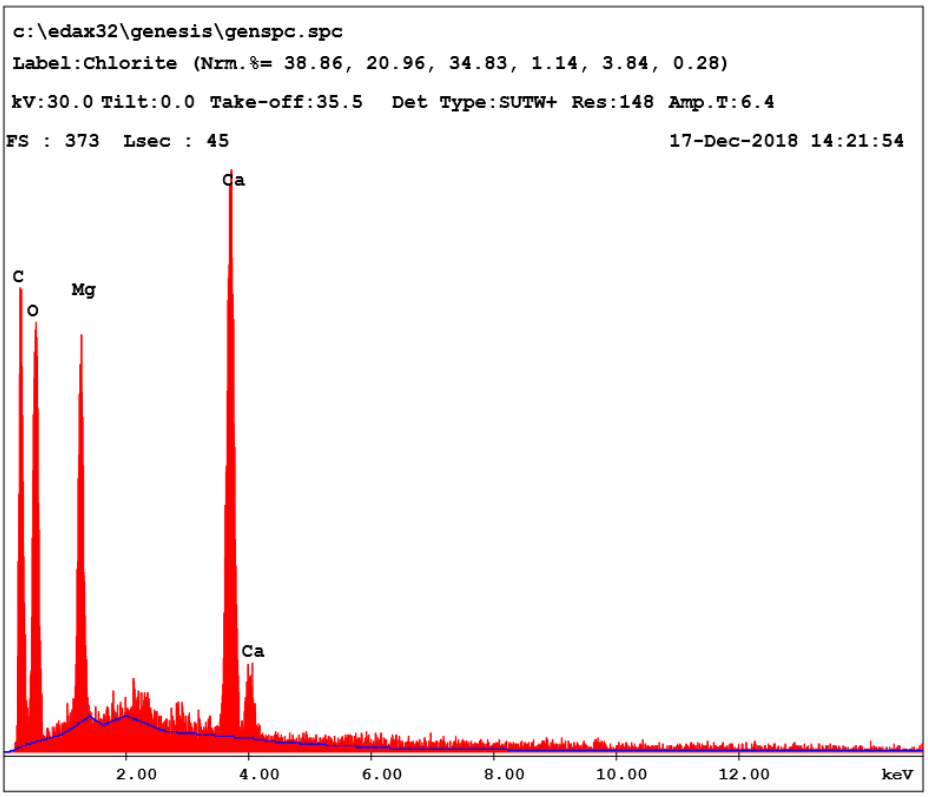

Figure 97. EDAX analysis of nanoparticle aggregates at the upper layer (at 200000x) (yellow squared part).

At the tenth-day, bottom-layer SEM images, a mixture of dolomite, nesquehonite, and calcite is observed (Figure 98). SEM-EDAX analysis of the view at 100000x magnification shows higher content of Ca than Mg. So those small aggregates are likely to be calcite on dolomite (Figure 99).

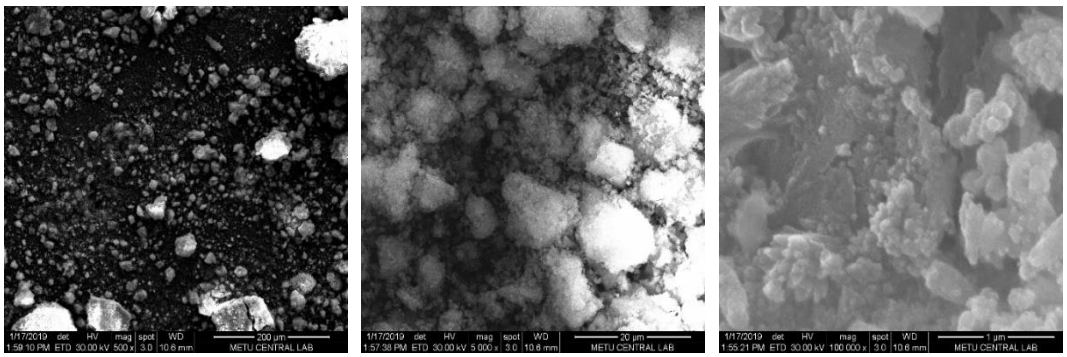

Figure 98. SEM images of carbonation products in petri dish at the bottom layer at the tenth day: 500x (left), 5000x (middle), 100000x (right).

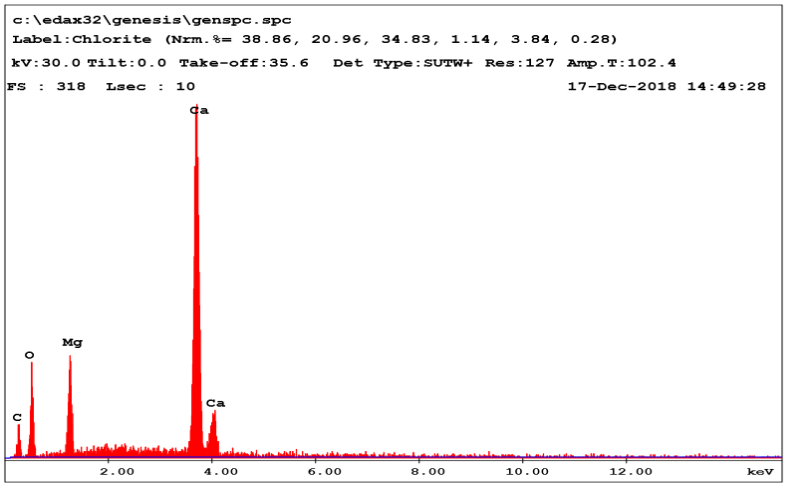

Figure 99. EDAX analysis of aggregates at the bottom layer (at 100000x).

4.7 Carbonation of $Ca(OH)_2$ nanoparticles on Nesquehonite

Under high RH and high $p(CO_2)$, carbonation products of $Ca(OH)_2$ nanoparticles on nesquehonite crystals are calcite and nesquehonite, as followed from XRD after two months. It is observed that even calcite and nesquehonite interact, there is no dolomite formation (Figure 100).

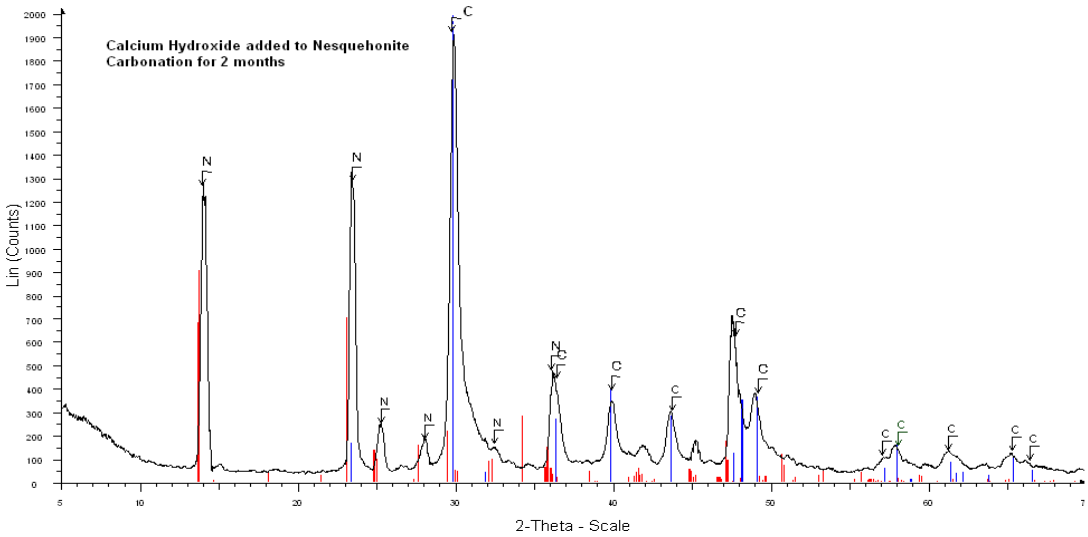

Figure 100. XRD traces of carbonation products of $Ca(OH)_2$ nanoparticles added onto nesquehonite crystals for two months.

4.8 Consolidation Treatment of Deteriorated Dolomite with Alcohol Dispersion of $Ca(OH)_2$ and $Mg(OH)_2$ Nanoparticles

In this part, a deteriorated Midyat dolostone sample was examined for the changes in its microstructure and physicomechanical properties before and after the consolidation treatment with alcohol dispersion of $Ca(OH)_2$ and $Mg(OH)_2$ nanoparticles. The microstructure was examined by SEM and Stereomicroscope, and physicomechanical properties by UPV measurements. Additionally, the adhesive property of carbonation products of $Ca(OH)_2$ and $Mg(OH)_2$ nanoparticles for a broken dolostone sample was tested by visual analysis.

4.8.1 Microstructure of Dolomite Before and After Consolidation Treatment

The stereomicroscope image of untreated deteriorated dolomite shows its porous and heterogeneous nature, together with white dolomite crystals observed in the cracks (Figure 101). After consolidation treatment, the carbonation products of $Ca(OH)_2$ and $Mg(OH)_2$ nanoparticles are seen as a very thin and white layer on the surface, in the pores and the cracks (Figure 102).

Figure 101. Stereomicroscope images of the main crack of dolostone sample before treatment: 10x (up) and 145x (down).

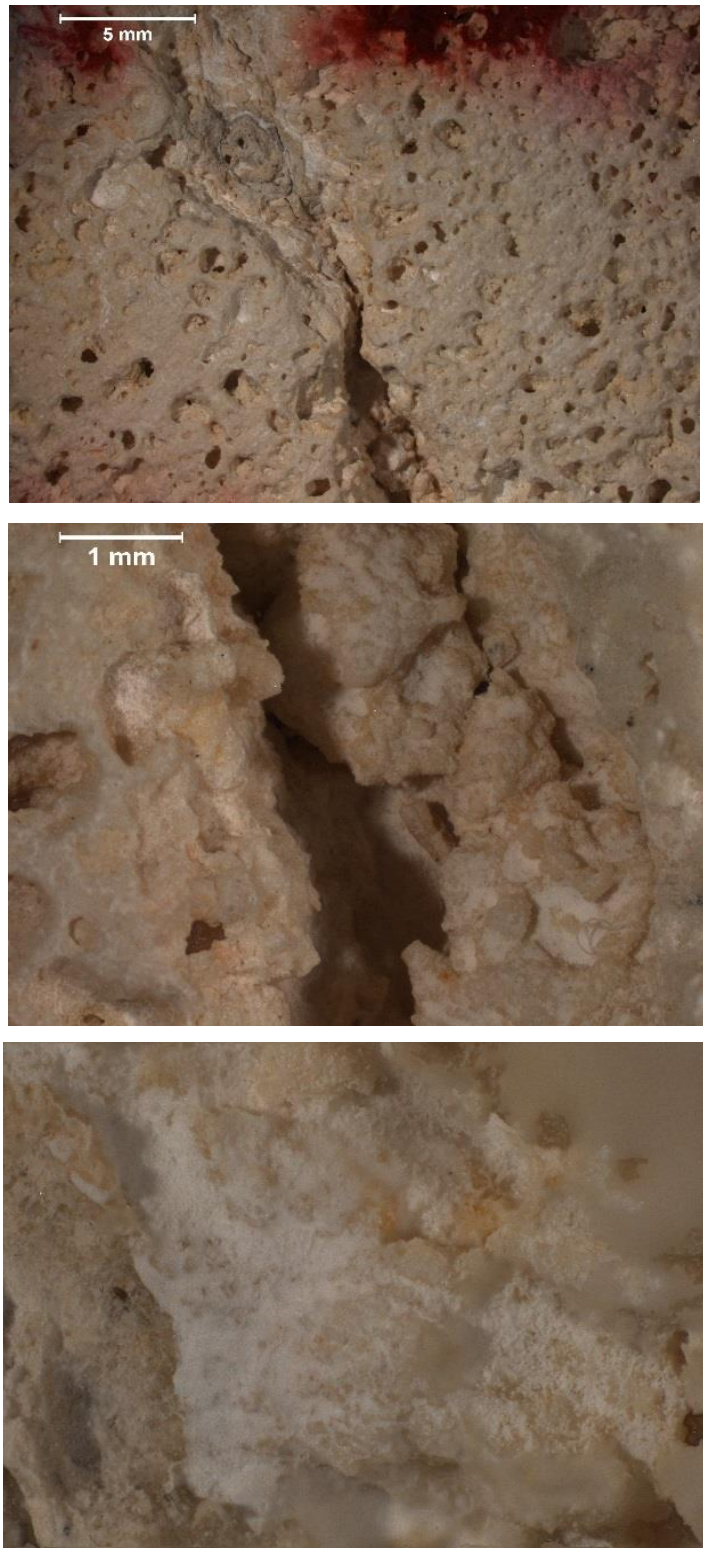

Figure 102. Stereomicroscope images of cracks of dolostone sample after treatment: 10x (up), 40x (middle), 145x (bottom).

SEM view at 50.000 magnification from the cross-section of dolomite before treatment shows the image of dolomite grain (Figure 103). The elemental composition composes similar amounts of Ca and Mg as observed from SEM-EDAX analysis (Figure 104).

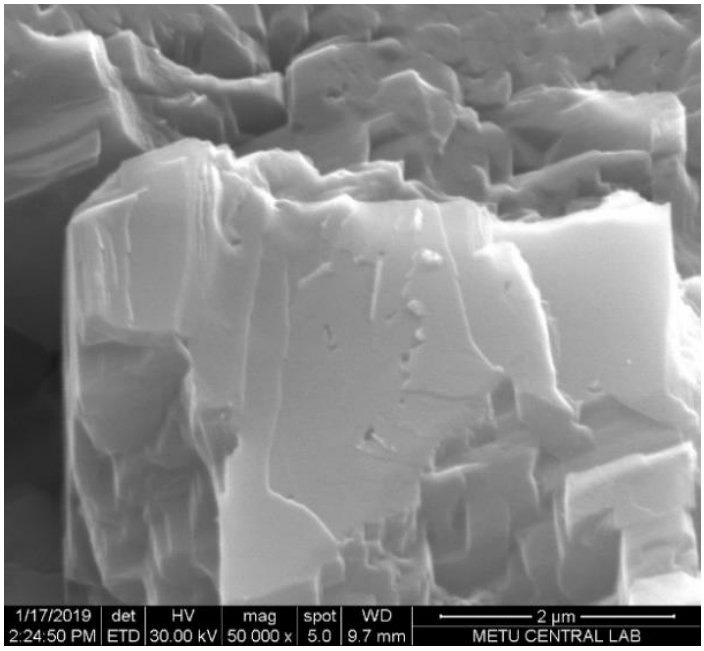

Figure 103. SEM image of dolostone sample before treatment: 50000x (dolomite grain, from cross-section).

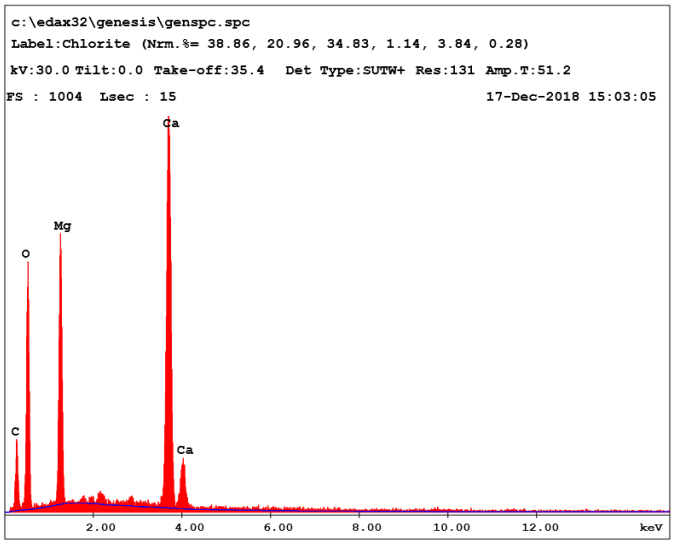

Figure 104. EDAX analysis of dolomite grain of untreated dolostone (at 50000x).

In the SEM view of the treated dolomite surface, newly formed carbonation products are observed as a thin layer at 2000x magnification (Figure 105). At 10000x and 40000x magnification, newly formed dolomite crystals are recognized in a similar form as observed in petri dishes (Figure 106). Their sizes are around 500nm. However, there are smaller or bigger aggregates, as well.

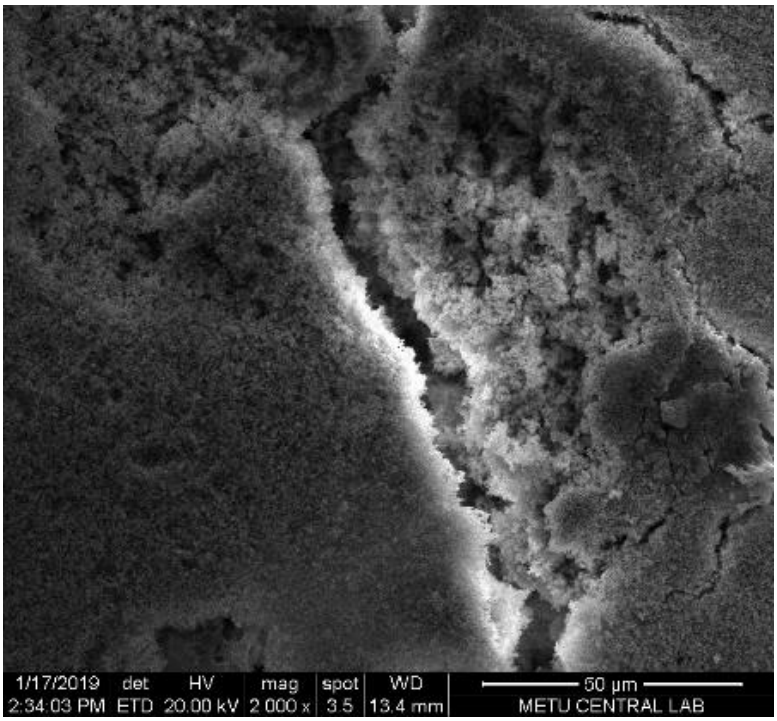

Figure 105. SEM image of dolostone surface after consolidation treatment: 2000x (dolomite layer)

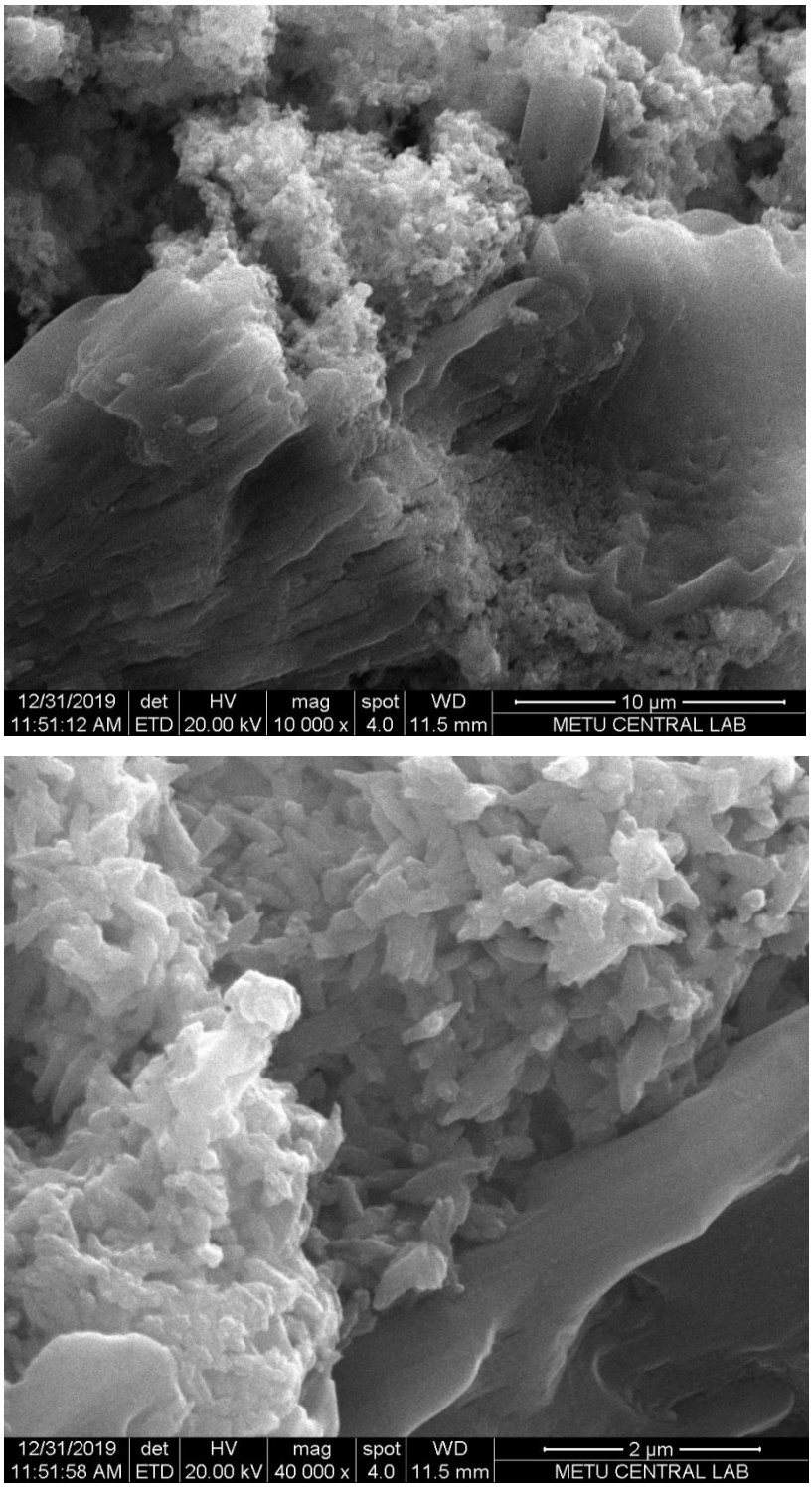

Figure 106. Closer view to the surface of treated dolomite sample (up-10000x and down-40000x)

SEM views of the cross-section surface of treated dolomite are shown in Figure 107-Figure 111. The line at the right of the SEM image corresponds to the side from where alcohol dispersion of $Ca(OH)_2$ and $Mg(OH)_2$ nanoparticles was applied. Newly formed dolomite aggregates are observed within the original dolomite matrix at 1000x magnification (Figure 107).

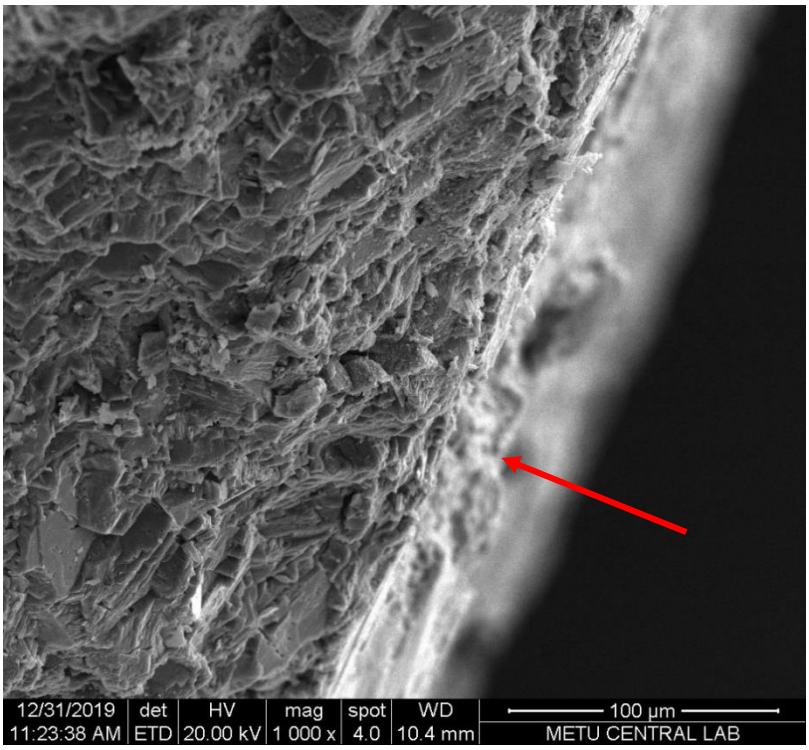

Figure 107. A general view from the cross-section surface of the treated dolostone sample. The red arrow at the right of the image corresponds to the side from where alcohol dispersion was applied: 1000x

In the closer SEM views at 10000x, 20000x, and 50000x magnifications, newly formed dolomite aggregates are better recognized within dolostone matrix (Figure 108-Figure 110). At higher magnifications, 100000x & 200000x, sizes of those newly formed dolomite aggregates are observed to be around 100-200 nm, and they appear well integrated with the original dolomite (Figure 111).

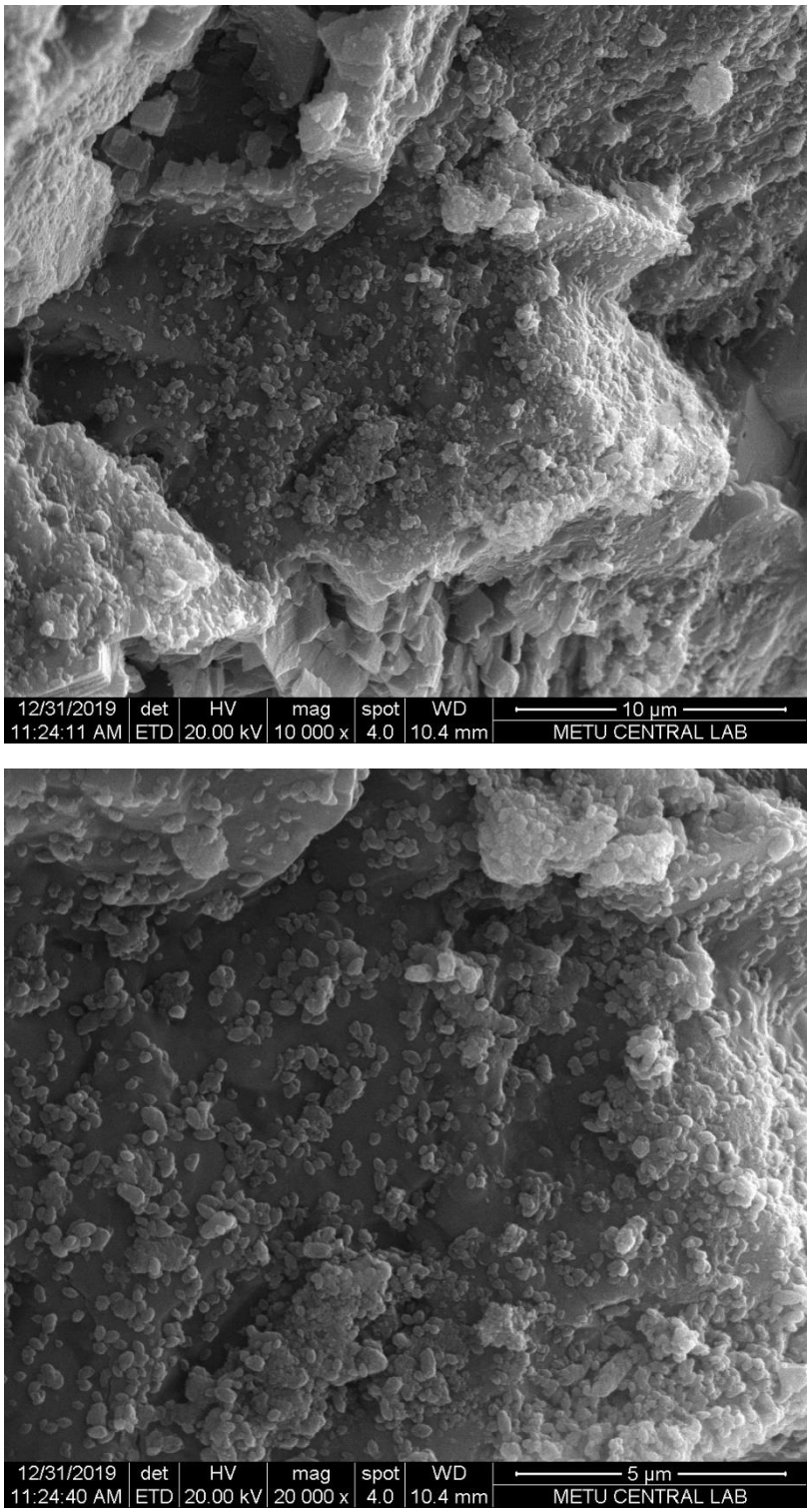

Figure 108. SEM view of the cross-section surface from the area close to the treatment surface (10000x-up, 20000x-down)

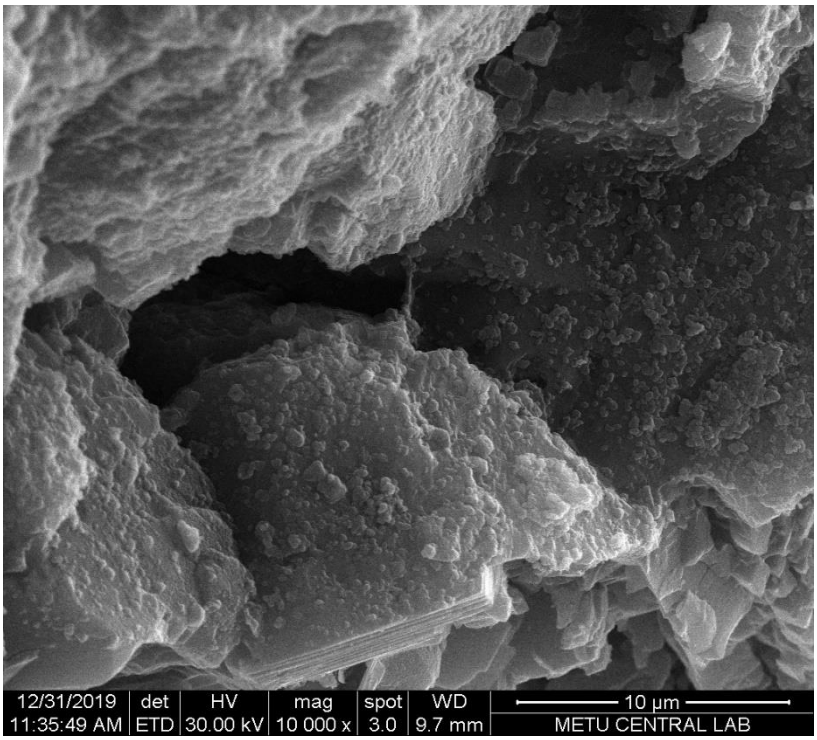

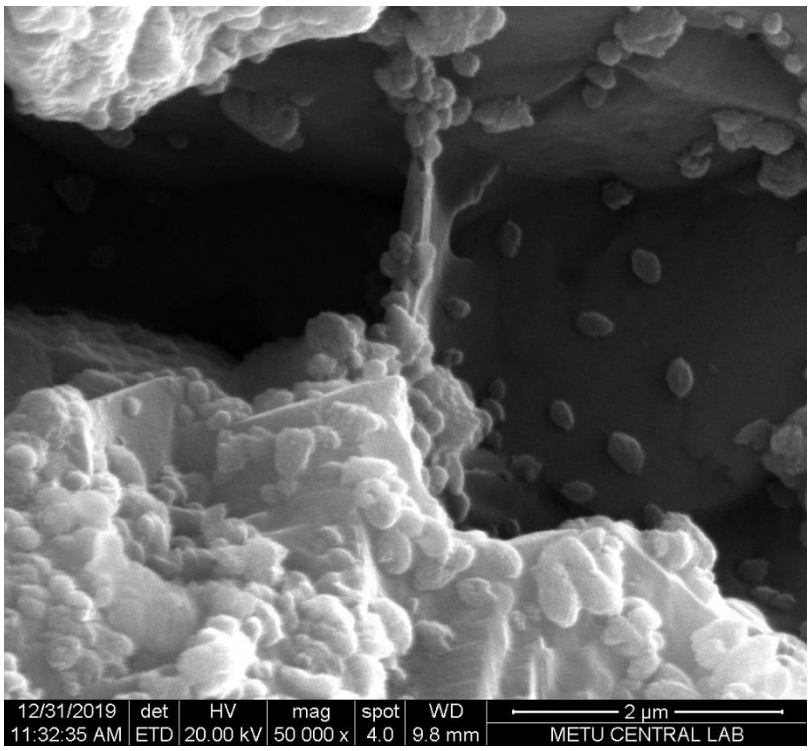

Figure 109. Another SEM view from the cross-section surface of treated dolostone sample:10000x-up, 50000x-down)

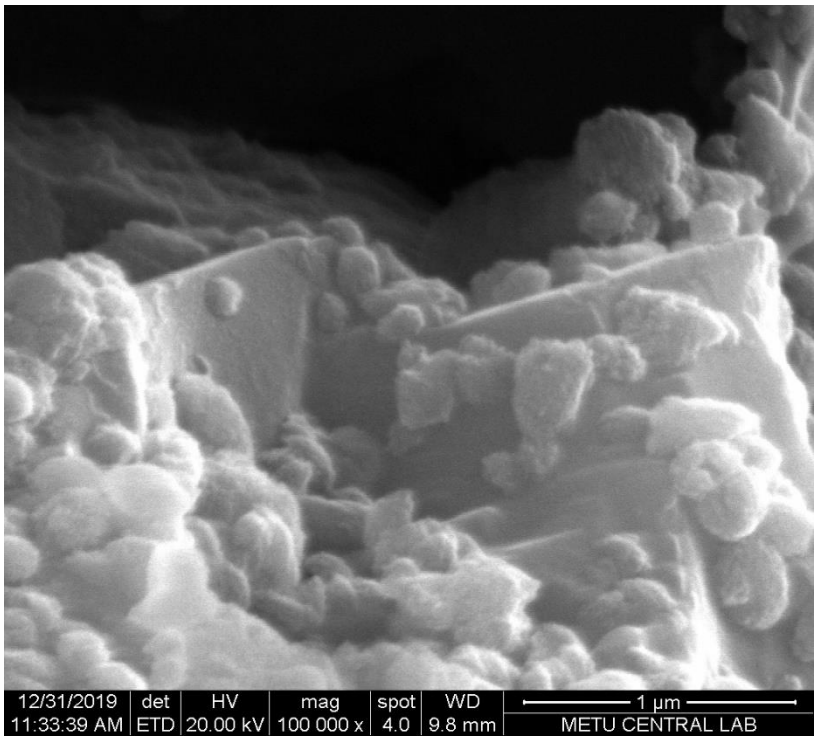

Figure 110. SEM view of the cross-section surface of treated dolostone sample showing the newly formed dolomite crystals on original dolomite crystals' edges and integration of them at 100000x magnification.

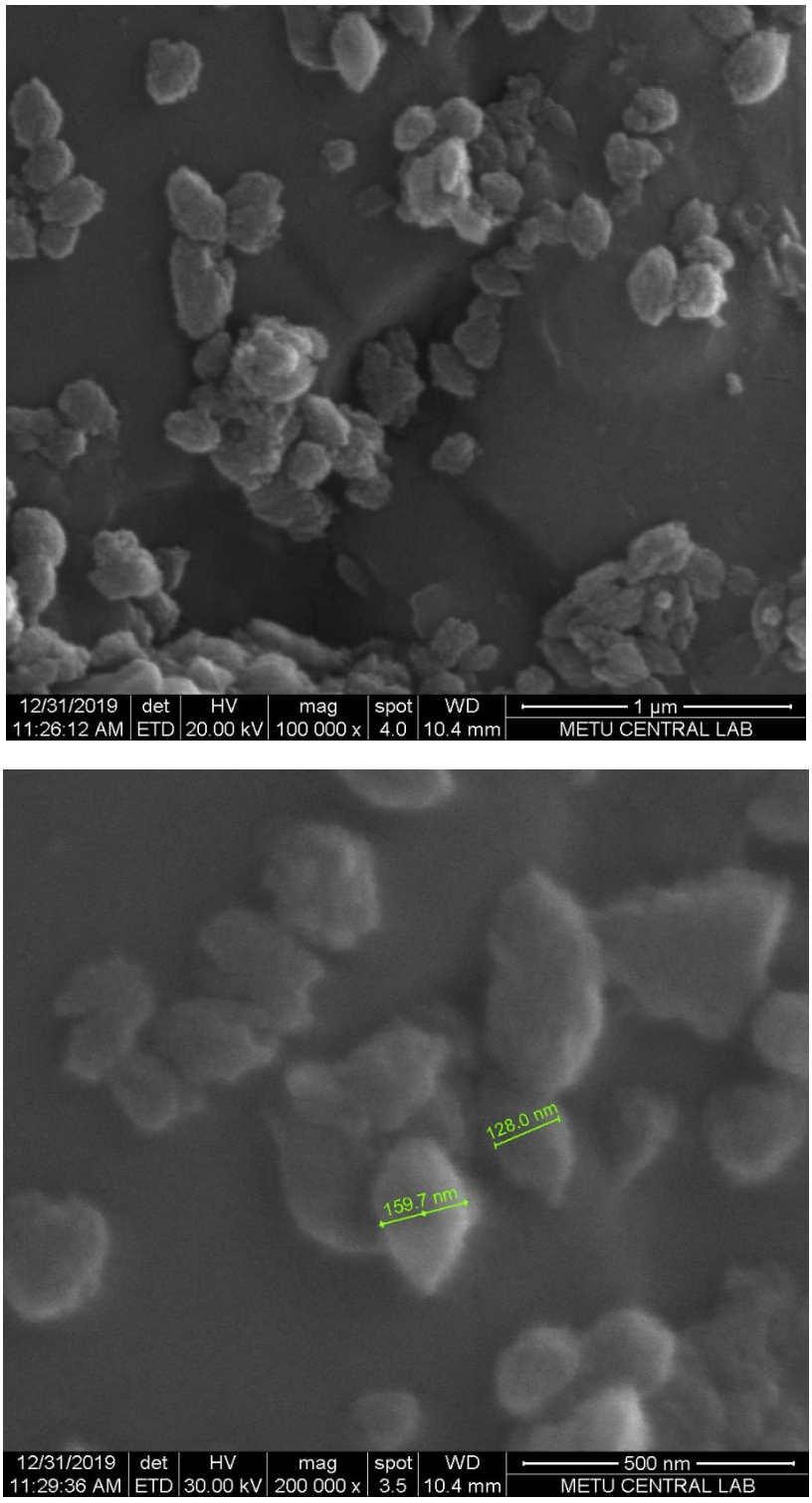

Figure 111. SEM view of the cross-section surface from the area close to the treatment surface (100000x-up, 200000x-down showing newly formed dolomite particles around 100-200nm)

4.8.2 Basic Physico-mechanical Properties of Deteriorated Dolomite Before and After Consolidation Treatment

Ultrasonic Pulse Velocity (UPV) values of a deteriorated dolomite sample are given before and after the consolidation treatment. Before consolidation treatment, it was observed that UPV values are not consistent. Interpretation of those inconsistent values are made as follows:

- The dolostone cube has cracks, impurities, and pores within the matrix. Those parts are called the weak parts where the UPV_{direct} value is minimum.
- Ultrasonic waves may find a better way to travel at the same point. Those parts are called stronger parts where the UPVdirect value is maximum.
- The average of all UPV readings at one point is accepted as the average UPV value of that point.
- Characteristic UPV readings of original Midyat dolostone is accepted as the average UPV value of the parts where there are no visible cracks (x-x' (2b) and x-x' (3a))
- The effectiveness of consolidation was evaluated by comparing the average UPV_{direct} value after treatment with the UPV value of characteristic parts before treatment.

In short, before consolidation treatment, there are three UPV values considered; minimum, maximum, and average ones (Table 11).

After consolidation treatment, UPV_{direct} values increase significantly with more consistent readings (Table 11), which implies an effective consolidation.
The results of UPV measurements are as allows:

- Before treatment, the average UPV value of the characteristic readings of the dolostone sample (x-x' (2b) and x-x' (3a)) is around 2400 $m.s^{-1}$.
- Before treatment, the average of minimum UPV values is 1756 $m.s^{-1}$
- Before treatment, the average of maximum UPV values is 1931 $m.s^{-1}$

- Before treatment, the average of UPV values is 1844 ± 64 $m.s^{-1}$
- After treatment, the average of UPV values is 2158±70 $m.s^{-1}$

The results of UPV measurements are also evaluated from each face individually. In general, the face perpendicular to the settlement of the quarry has the maximum UPV_{direct} value. However, this dolomite sample had cracks and impurities at each face. Therefore, the settlement direction couldn't be identified.

- x-face average UPV value increased from 2009 $m.s^{-1}$ to 2254 $m.s^{-1}$ after treatment
- y-face average UPV value increased from 1556 $m.s^{-1}$ to 1847 $m.s^{-1}$ after treatment
- z-face average UPV value increased from 1969 $m.s^{-1}$ to 2372 $m.s^{-1}$ after treatment

As a result, after treatment, the average UPV_{direct} value increased from 1844 $m.s^{-1}$ to 2158 $m.s^{-1}$. It became closer to the value of characteristic UPV_{direct} readings of the original dolostone before treatment (the average UPV_{direct} value of x-x' (2b) and x-x' (3a) is ~2400 $m.s^{-1}$).

Table 11. Direct UPV Measurement of a weathered dolostone sample with 5x5x5 cm^3 dimensions before (bt) and after (at) treatment.

point	$UPV_{bt,dry,\ min}$* $m.s^{-1}$	$UPV_{bt,dry,\ max}$** $m.s^{-1}$	$UPV_{bt,dry,\ average}$ $m.s^{-1}$	$UPV_{at,dry,\ average}$ $m.s^{-1}$
x-x' (1a)	1657	1780	1735±47	2267±13
x-x' (1b)	1536	2015	1693±186	2074±23
x-x' (1c)	1608	1685	1660±21	1769±12
x-x' (2a)	1839	2172	1984±136	2213±6
x-x' (2b)	**2099**	**2133**	**2116±13**	**2367±14**

point	$UPV_{bt,dry,\ min}$* $m.s^{-1}$	$UPV_{bt,dry,\ max}$** $m.s^{-1}$	$UPV_{bt,dry,\ average}$ $m.s^{-1}$	$UPV_{at,dry,\ average}$ $m.s^{-1}$
x-x' (3a)	**2568**	**2799**	**2689±106**	**3022±13**
x-x' (3b)	1705	2692	2374±374	2017±13
x-x' (3c)	2023	2071	2048±21	2450±15
y-y' (1a)	1440	1596	1531±45	1730±4
y-y' (1b)	1429	1529	1496±24	1568±5
y-y' (1c)	1599	1665	1631±23	1758±11
y-y' (2a)	1688	1807	1746±37	1615±106
y-y' (2b)	1121	1167	1143±14	1887±319
y-y' (2c)	1537	1815	1665±87	1884±9
y-y' (3a)	1929	1983	1955±16	2021±11
y-y' (3b)	1264	1630	1353±156	2081±9
y-y' (3c)	1309	1691	1481±95	2081±9
z-z' (1a)	1549	1636	1588±40	2274±102
z-z' (1b)	1685	1880	1774±59	1969±197
z-z' (1c)	1940	2031	1998±50	2034±127
z-z' (2a)	2048	2116	2085±28	2348±106
z-z' (2b)	2276	2296	2286±10	2442±8
z-z' (2c)	1684	1760	1727±28	2181±29

point	$UPV_{bt,dry,\ min}$* $m.s^{-1}$	$UPV_{bt,dry,\ max}$** $m.s^{-1}$	$UPV_{bt,dry,\ average}$ $m.s^{-1}$	$UPV_{at,dry,\ average}$ $m.s^{-1}$
z-z' (3b)	1602	1659	1623±20	2794±79
z-z' (3c)	2075	2197	2137±53	2508±8
x-x' average	1862	2130	2009±104	2254±49
y-y' average	1480	1654	1556±55	1847±54
z-z' average	1927	2011	1969±33	2372±74
Average	1736	1931	1844±64	2158±70

4.8.3 Adhesive Property of the Treatment by Injection of Alcohol Dispersion Through the Crack of Broken Dolomite Cube

Alcohol dispersion of $Ca(OH)_2$ and $Mg(OH)_2$ nanoparticles was injected through the crack of the broken dolostone cube and left for carbonation for 7 months. The broken parts were joined together and bonded firmly by the newly formed carbonation products. One piece of the cube holds the other piece when it is held by hand (Figure 112).

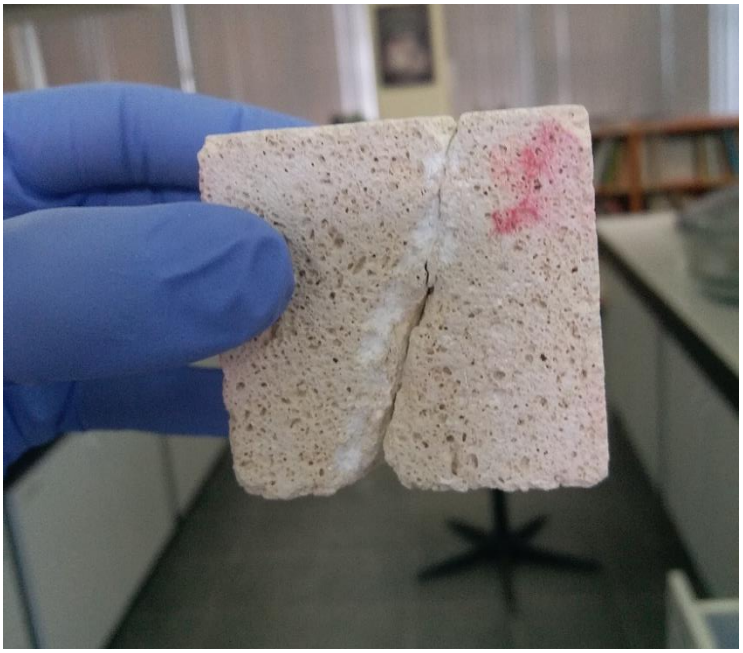

Figure 112. Broken dolostone sample after consolidation treatment with alcohol dispersion of nanoparticles; broken parts joined together.

CHAPTER 5

DISCUSSION

In this section, the results of conducted experiments and analyses were evaluated and discussed with the supportive background knowledge in the literature. The first important part was the preparation of a proper $Ca(OH)_2$ and $Mg(OH)_2$ nanoparticles' dispersion from the dolomite itself. Later on, the assessment of its use for the consolidation treatment of deteriorated dolomite. The carbonation process was examined to discover the best experimental conditions for dolomite formation. Therefore, experimental conditions that favor or restrict dolomite formation were tested, and carbonation products were identified. Therefore discussion was done under those headings that reflect the details, and the progress of experimental work towards dolomite formation, and the use of that knowledge for the consolidation treatment of deteriorated dolostone.

- Carbonation characteristics of $Mg(OH)_2$ nanoparticles dispersed in ethanol
- Characteristics of alcohol dispersion of $Ca(OH)_2$ and $Mg(OH)_2$ nanoparticles
- Carbonation characteristics of $Ca(OH)_2$ and $Mg(OH)_2$ nanoparticles dispersed in ethanol in relation to the changes in relative humidity and CO_2 partial pressure
- Carbonation process of $Ca(OH)_2$ and $Mg(OH)_2$ nanoparticles in alcohol dispersion with Mg:Ca ratio 2 (set-1)
- Carbonation process of $Ca(OH)_2$ and $Mg(OH)_2$ nanoparticles in alcohol dispersion with Mg:Ca ratio 1 (set-2): Towards dolomite formation
- Effect of Mg:Ca ratio on dolomitization
- Consolidation of deteriorated dolomite samples
- Production specifications of alcohol dispersion of $Ca(OH)_2$ and $Mg(OH)_2$ nanoparticles

The overall data was discussed to understand the point of success for the formation of dolomite within dolostone cracks and pores which will help to understand if consolidation treatment is compatible. Moreover, dolomite formation was questioned with respect to reaction mechanisms, phase diagrams, and metastable phases suggested in the literature. Comparative and combined results of analytical data were discussed in light of related literature.

5.1 Carbonation Characteristics of $Mg(OH)_2$ Nanoparticles Dispersed in Ethanol

Carbonation of $Mg(OH)_2$ nanoparticles was investigated to find out the final product/mineral phase when $Mg(OH)_2$ nanoparticles carbonate individually at high RH (90-95%) and high CO_2 partial pressure (pCO_2~0.4 atm) at room temperature. At those conditions, Nesquehonite ($MgCO_3.3H_2O$) is the only carbonation product obtained as confirmed by XRD and FTIR (Figure 28&Figure 29). That result is in accordance with the phase diagram of MgO-CO_2-H_2O system in relation to the variations in the temperature and partial pressure of CO_2 (Figure 2). Nesquehonite is readily formed at room temperature at higher CO_2 partial pressure. The shape of nesquehonite crystals appeared as cauliflower-like aggregates of around 2 mm size- a collection of around 1 mm sized needles (Figure 27). As the temperature increases, and partial pressure decreases, hydromagnesite formation can be expected at atmospheric conditions. Magnesite, on the other hand, can be observed at elevated temperatures and CO_2 partial pressure conditions. In the experimental conditions of this study, only nesquehonite is observed.

5.2 Characteristics of Alcohol Dispersion of $Ca(OH)_2$ and $Mg(OH)_2$ Nanoparticles

Alcohol dispersion of $Ca(OH)_2$ and $Mg(OH)_2$ nanoparticles which was used throughout experimental work, was prepared as described in section 3.5. It is

advantageous to start the preparation of dispersion by using dolostone to obtain both nanoparticles together and in a well-mixed form with a proper concentration ratio for dolomite formation. XRD measurements of the dispersion extracts at different time intervals show that the dispersion is composed of portlandite and brucite nanoparticles (Figure 37-Figure 41), where Mg:Ca ratio changes in time while the dispersion is at rest. Second intense peaks of portlandite and brucite in XRD traces of the solution is a measure to see the change in Mg:Ca ratio in time. In the beginning, Mg:Ca ratio is 1, at 24 hour the ratio is 2.15, and the ratio increases up to 5 at the 72nd hour (Table 9). The change in Mg:Ca ratio shows that $Ca(OH)_2$ nanoparticles start to settle first, and the solution becomes rich in $Mg(OH)_2$ nanoparticles. That phenomena is an expected property since $Mg(OH)_2$ is a smaller molecule than $Ca(OH)_2$ molecule, and $Mg(OH)_2$ nanoparticles stay in dispersion for a longer period of time in comparison to $Ca(OH)_2$ nanoparticles.

In the SEM images, $Ca(OH)_2$ and $Mg(OH)_2$ nanoparticles appear integrated in the form of aggregates at dry state before dispersion into alcohol. Their sizes vary between 1-5 μm (Figure 34). Two groups of aggregates are observed with respect to their sizes. EDAX analysis confirms that large aggregates (around 500nm-1μm) are composed of $Ca(OH)_2$ clusters (Figure 35) and smaller aggregates (around 100nm) are composed of $Mg(OH)_2$ clusters (Figure 36).

Depending on the time that passes after mixing of the alcohol dispersion, its carbonation characteristics is expected to change due to the change in Mg:Ca ratio. To see the effect of Mg:Ca ratio on carbonation products, two sets of experiments were conducted with alcohol dispersion having Mg:Ca ratio 2, and 1 respectively. The resulting carbonation products are discussed in the following headings.

5.3 Carbonation Characteristics of $Ca(OH)_2$ and $Mg(OH)_2$ Nanoparticles Dispersed in Ethanol in Relation to Changes in Relative Humidity and CO_2 Partial Pressure

Carbonation of $Ca(OH)_2$ and $Mg(OH)_2$ nanoparticles dispersed in ethanol is affected by the changes in relative humidity, and CO_2 partial pressure. At laboratory conditions, where the average relative humidity is around 45%, and estimated CO_2 partial pressure (pCO_2) is around 0.3 mmHg, some $Ca(OH)_2$ carbonates to calcite, and $Mg(OH)_2$ doesn't carbonate even after 4 weeks (Figure 43). It is seen that low RH conditions don't encourage carbonation.

When relative humidity increases up to 95%, and CO_2 partial pressure is the same as in laboratory condition (around 0.3 mmHg), $Ca(OH)_2$ carbonates to calcite($CaCO_3$) and $Mg(OH)_2$ carbonates to nesquehonite ($MgCO_3.3H_2O$). Increasing relative humidity influences the carbonation of $Mg(OH)_2$. However, under those conditions, no sign of dolomite formation is observed (Figure 44). Therefore, in addition to the increase in relative humidity, an increase in the partial pressure of CO_2 was also considered to achieve dolomite formation.

When alcohol dispersion of $Ca(OH)_2$ and $Mg(OH)_2$ nanoparticles (set-1-Mg:Ca ratio~2) carbonates at high relative humidity (~90-95%) and high CO_2 partial pressure (pCO_2~0.4 atm), the major products are nesquehonite and calcite. Moreover, dolomite is also observed in minor amounts. It is understood that high CO_2 partial pressure and RH are essential for dolomite formation. Detailed information on carbonation characteristics at those conditions is given in section 5.4.

Since the intention is to lead dolomite formation by carbonation, this set helps to improve experimental conditions for an effective dolomite formation. Therefore, at high relative humidity (~90-95%) and high CO_2 partial pressure (pCO_2~0.4 atm), another set of experiments was conducted with alcohol dispersion of $Ca(OH)_2$ and $Mg(OH)_2$ nanoparticles having Mg:Ca ratio 1. Finally, with this set and conditions, dolomite could be isolated. The detailed discussion of this set is given in section 5.5.

This is not a systematic study to follow carbonation products at different RH or partial pressure but to find the practical conditions for efficient carbonation towards dolomite formation (Figure 4).

5.4 Carbonation of $Ca(OH)_2$ and $Mg(OH)_2$ Nanoparticles in Alcohol Dispersion with Mg:Ca ratio ~2 (set-1)

Carbonation of $Ca(OH)_2$ and $Mg(OH)_2$ nanoparticles in alcohol dispersion at high relative humidity (~90-95%) and high CO_2 partial pressure (pCO_2~0.4 atm), when Mg:Ca ratio is ~2, produce mainly calcite and nesquehonite with some dolomite.

Although carbonation products were analyzed by random sampling at certain time intervals without considering layering of the products, some predictions can be made about the carbonation process in those conditions in semi-quantitative way by using XRD traces of the products (Figure 45-Figure 53).

It is observed that portlandite carbonates first to form calcite. Only after all portlandite is carbonated, brucite starts to carbonate to form nesquehonite. Formation of nesquehonite was observed together with some dolomite at the end of 3rd day (Figure 47). Follow up the carbonation process continued until 7 months shows that relative amounts of calcite, nesquehonite, and dolomite don't change in time. Dolomite is always minor product. Dolomite and calcite main peak height ratio stays quite similar in XRD traces.

Calcite formation before nesquehonite formation is expected in aqueous solution due to higher solubility of portlandite than brucite (Table 2). In alcohol dispersion, at high RH conditions, higher solubility of portlandite seems to be important to lead first to the formation of calcite. When the dispersion medium becomes rich in Mg^{2+}, while formed calcite precipitate, nesquehonite is formed together with some dolomite.

Detection of dolomite is first done by the appearance of its major XRD peak (d=2.89; hkl=104) as a broad and low intensity peak. The other important peaks that reflect

the dolomite structure are missing in XRD traces (such as; hkl=113, 018, 116 at d=2.19, 1.80, 1.78 respectively) (Table 6) due to dolomite's being in low amount in the carbonation products. In addition, the broad major peak in XRD traces is an indication of dolomite's being in nano-size. Another evidence for dolomite existence in small amounts at nano size in the carbonation products is FTIR spectra of the same sample (Figure 58). The symmetric deformation bands of carbonate groups belonging to calcite and dolomite are expected to appear at 711-728 cm^{-1}, respectively. Here, they overlap and show a weak and broadband instead of two individual sharp peaks.

In the SEM views of randomly picked up carbonation products (Figure 59-Figure 67), nesquehonite crystals as large as 100-500 μm can be distinguished by their unique needle-like shape. On the other hand, calcite and dolomite nanoparticles' aggregates look alike each other, and it is hard to distinguish them. Dolomite aggregates are observed around nesquehonite needles. Their sizes are around 100-500 nm (Figure 64). SEM-EDAX analyses confirm that those aggregates belong to dolomite by having almost 1:1 Mg:Ca ratio (Figure 65). SEM samples of this study are randomly picked up powdered samples that are stuck on carbon tape. Later on, nitrogen gas was blown over them to eliminate the loosely attached particles in order to prevent damage to the microscope. Therefore, interpretation of SEM views should be done accordingly. Some nesquehonite needles seem to be dissociated, and dolomite nanoparticles are located on those regions (Figure 67). That is why those images should be interpreted carefully to say whether nesquehonite loses some of its magnesium during dissociation, and the liberated Mg^{2+} cations incorporate into calcite structure to form dolomite (Reaction 1) (Barthust, 1975) or it is just the way of sampling forming that impression.

It may be assumed that as the carbonation process continues, nesquehonite dissociates in time to release its Mg^{2+}, and react with calcite for further dolomite formation. However, that probability is unlikely, since dolomite stays in the samples in small amounts even after 7 months of carbonation process.

As introduced in section 2.2, in nature, dolomite is found together with some other minerals that can be formed in Ca-Mg-CO_2-H_2O system. Dolomite may be formed through direct precipitation in cave, or sea waters, or by the transformation of metastable mineral phases like aragonite ($CaCO_3$), huntite ($CaMg_3(CO_3)_4$), amorphous Ca-Mg carbonates or hydromagnesite ($3MgCO_3.Mg(OH)_2.3H_2O$) (Alonso-Zarza and Martin-Perez, 2008; Martin-Perez *et al*., 2015). Aragonite and huntite transformations at high Mg/Ca ratio were reported for the formation of dolomite (Martin-Perez *et al*., 2012). Specifically, in the systems including low Ca^{2+}, high Mg^{2+}, relatively high CO_3^{2-}, and H_2O, hunite and dolomite formation may be observed (Davies *et al*., 1975). However, in set-1 experiments of the thesis, no huntite, aragonite, or hydromagnesite formations were observed at room temperature under high RH and high CO_2 partial pressure. Phase diagrams support those results (Figure 2). In literature, nesquehonite formation is favoured at room temperature, while hydromagnesite is favoured at higher temperatures above 52^oC. Based on thermodynamic properties such as free energy of formations (Table 2), favourable phases are expected to be hydromagnesite and huntite rather than nesquehonite. However, in the experimental conditions of this study, the carbonation of alcohol dispersion having nanoparticles with Mg:Ca ratio 2 yields nesquehonite, calcite, and some dolomite.

In short, XRD, SEM, and FTIR analyses prove that there is dolomite formation in minor amount and in nano-size when Mg:Ca ratio is ~2 in the dispersion under those experimental conditions. It is also worthy to note that the dispersion is alcohol dispersion, not water dispersion. Therefore, carbonation proceeds at high RH conditions. Study continued to get efficient dolomite formation to be used for consolidation purposes of dolostone.

5.5 Carbonation of $Ca(OH)_2$ and $Mg(OH)_2$ Nanoparticles in Alcohol Dispersion with Mg:Ca ratio ~1 (set-2): Towards Dolomite Formation

Carbonation of $Ca(OH)_2$ and $Mg(OH)_2$ nanoparticles in alcohol dispersion where Mg:Ca ratio is about 1 as in original dolomite, produce mainly dolomite, provided that high relative humidity (~90-95%) and high CO_2 partial pressure (pCO_2~0.4 atm) conditions in equilibrium with alcohol dispersion is not disturbed by opening the lid of the desiccator. Here dolomite formation is explained in the light of the undisturbed system at the 1st, 5th, and 10 days of carbonation.

In the closed desiccator, alcohol dispersion tries to establish an equilibrium with high RH and high CO_2 concentration conditions. During the sampling of early carbonation products at the 1st, 2nd, 3rd, and 4th days, the present equilibrium is disturbed by opening the lid of the desiccator at each time due to the fluctuations in RH and CO_2 partial pressure. It is observed that the efficiency of the dolomite formation process decreases since considerable amounts of nesquehonite and calcite are found accompanying dolomite. However, in the undisturbed system, dolomitization seems to continue at the 5th day. Although there is abundance of dolomite formation in XRD traces, there exists some nesquehonite along with it. On the other hand, when the desiccator is opened for the first time at the end of 10th day, complete dolomite formation is observed in the XRD traces (Figure 84). It is concluded that carbonation duration of 10 days in an undisturbed system starting with those conditions above yields dolomite.

Since the layering of carbonation products was found to be important during sampling, carbonation products were investigated in the upper (the layer having air-solution interphase) and bottom layers (the layer having solution interphase) of the precipitate having a thickness of about 1 mm. The types and the amounts of carbonation products produced in petri dish show differences in the upper and bottom layers of the precipitate. In the upper layer, carbonation is faster, and dolomite appears as the only product in this layer after 10 days of carbonation (Figure 84). In

the bottom layer, dolomite is still the main product, with minor amounts of nesquehonite and calcite (Figure 85).

The dispersion forms a thin precipitate in paste form in the early days. The picking up of the samples from the upper and bottom layers is not easy. The precipitate dries up in later days by the loss of alcohol, and layers can be better separated by scraping.

In the following section, the stages of the carbonation process will be discussed that end with dolomite formation at the 10^{th} day together with characteristics of dolomite synthesized.

5.5.1 Towards Dolomitization

An undisturbed system is a requirement for effective dolomite formation. However, the disturbed system gave some clues about the process towards dolomite formation. Unlike from carbonation pattern when Mg:Ca ratio is 2 in alcohol dispersion (set-1), in the carbonation pattern when Mg:Ca ratio is 1 (set-2), dolomite formation increases with time even in a disturbed system starting from the 2^{nd} day.

Dolomitization in an undisturbed system is followed starting from the first day. At the first day, it is possible to see the interaction of portlandite and brucite that make preparation for dolomite formation. In the upper layer, there is some carbonation. XRD traces show the products, calcite and nesquehonite, along with unreacted brucite and portladite (Figure 74). When SEM images of the first day samples are examined, brucite and portlandite nanoparticles appear as aggregates integrated within each other, and not observed separately, but distributed in a homogeneous manner (Figure 90). That SEM view is different from the image of those nanoparticles before carbonation (Figure 34 and Figure 90 compared). Before carbonation, they are well differentiated in the SEM images where smaller ones (~100nm) are brucite and larger ones (~500 nm-1μm) are portlandite (Figure 34). Presence of calcite and nesquehonite aggregates observed by XRD can not be differentiated in SEM images of 1^{st} day carbonation products.

Bottom layer product at the first day show no signs of carbonation in XRD traces. Carbonation in that layer seems not started yet. At the same time, the bottom layer is observed rich in portlandite in comparision to brucite (Figure 75) most likely due to its differential settlement from the upper layer.

At the second day of disturbed system in the upper layer, the main peak of dolomite appears in XRD traces. However, the other characteristic peaks of dolomite are absent (Figure 76). In the SEM images, crystal-like-aggregates are observed. These aggregates are probably the first stages of dolomite formation (Figure 91). In the bottom layer, products are mixture of brucite, portlandite, calcite, nesquehonite together with the main peak of dolomite as seen in XRD traces (Figure 77).

At the third and fourth days of the disturbed system, more dolomite peaks are observed indicating increasing amount of dolomite in the products, together with some nesquehonite and calcite. In the bottom layer, XRD traces reveal similar mixture of minerals (Figure 78-Figure 81).

Those results show that disturbed system doesn't help to the formation of high percentage of dolomite. On the other hand, in the undisturbed system, at the fifth day of dolomitization, dolomite formation is more than the previous days in disturbed system with minor amounts of nesquehonite both in the bottom and upper layers (Figure 82&Figure 83). Since high yield of dolomite is expected, it is concluded that carbonation should continue a few more days in an undisturbed system. Finally, at the tenth day of undisturbed system, almost pure dolomite is obtained in the upper layer as seen in XRD traces (Figure 84).

While interpreting XRD results for nanoparticles, the following issues should be taken into consideration: First one is the size effect; the synthesized dolomite is nano-sized, and nanomaterials have relatively broader peaks compared with materials in bulk state. In a recent study, it is shown that as the size gets smaller as 10-50 nm, XRD peaks diffuse in x-axis, the half width (the width at the half of the peak height) increases and the peaks get broader. The peak positions stay the same. Below 10 nm, peak broadening is so significant that signal intensity is low and peaks cannot be

detected (Holder and Schaak, 2019). Considerable broadening in XRD peaks of synthesized dolomite in comparision to Midyat dolomite shows the presence of nanoparticles with the sizes 50 nm-25 nm. In addition, some smaller particles may exist as well. Secondly, in the same study, it is explained that when nanoparticles precipitate in a solution, they may show some preferred orientations depending on the shape of nanocrystallite, such as being spherical, cubic or rods. Particles tend to orient with their flat faces parallel to the drying surface. According to level of alignment, some peaks belonging to parallel oriented planes may become more significant. In addition, peak shifts of the nanomaterials in XRD traces are demonstrated in a study for nanoparticles smaller than 15 nm due to some changes in the cell dimensions (Vorontsov and Tsybulya, 2018). In short, peak intensities in XRD data can look different for particles of the same material that have different morphologies in terms of size, orientation, and shape of nano-crystals. In this study, peak locations of the obtained dolomite matches well with the pattern of dolomite structure, and its peak locations are the same with Midyat dolomite with a slight shift of the main peak being around 0.4 ($^{o}2\theta$) (Figure 86 and Table 10). Since all the peak height and positions follow the dolomite structure, it is concluded that obtained dolomite has similar cell dimensions with typical dolomite, and has broader peaks due to being in nano-size.

In nature, dolomite is formed under very special circumstances (mainly in ancient marine sediments) throughout thousands of years by the transformation of some minerals (like calcite or aragonite, huntite, nesquehonite, hydromagnesite) to dolomite or by direct precipitation. Many scientists study the synthesis of dolomite at the laboratory. There is still no agreement about its synthesis at ambient temperatures. Sibley *et al*. (1994) claimed high temperature helps to overcome the kinetic barrier. On the other hand, Vasconcelos *et al*. (1995) claim that it is possible to synthesize dolomite at room temperature by microbial mediation. However, Kaczmerek *et al*. (2017) and Greg (2015) claim the products that Vasconsoles obtained are not dolomite but high magnesium calcite or protodolomite which has calcite symmetry $R\bar{3}c$, and is the precursor for ordered dolomite since those products

don't show the XRD ordering reflections of dolomite. For perfectly ordered dolomite, that is in bulk state, it could be possible to identify the XRD peaks which are characteristic peaks of ordering reflections (with hkl indices 101,015 and 021, and XRD peak location ($^o2\theta$) at 22.04, 35.31, and 43.78 respectively) (Table 5). In this study, the XRD traces of the dolomite matches with $R\bar{3}$ symmetry group, and not with $R\bar{3}c$ symmetry group. Some ordering reflections of synthesized dolomite may not be observable in XRD traces due to broadening of the peaks in nano-size, and its being a mixture with variable nano-sized particles, although low crystallinity or some degree of disorder may also be affecting those observations.

FTIR spectrum of synthesized dolomite reflects a standard dolomite sample's FTIR spectrum and its peaks overlap quite well with the FTIR spectrum of Midyat Dolomite (Figure 88). The symmetric deformation of carbonate groups' absorbance peak at 728 cm^{-1} is sharp for Midyat dolomite, whereas that peak for synthesized dolomite at 726 cm^{-1} is observed to be broader, due to its smaller crystal size. It is worthy to note that calcite has this peak at 711 cm^{-1}. Therefore, FTIR results support that the synthesized product is dolomite, but not calcite.

In the SEM view of synthesized dolomite sample from the upper layer of carbonation products at the 10^{th} day, the dolomite crystals appear as aggregates around 100-500nm size (Figure 93-Figure 97). On those aggregates, much smaller nanoparticles with sizes around 5 to 20 nm are also observed. On the other hand, Midyat dolomite is crystalline dolomite having relatively bigger crystals in μm size (TUBITAK-CNR–Bilateral Project 213M554) (Figure 103).

The mechanisms for the formation of dolomite is tried to be explained in the light of suggested reaction mechanisms for dolomite formation in literature, and experimental results of this study. There are two main reaction mechanisms suggested in the literature. The first reaction mechanism is suggesting incorporation of Mg^{2+} ions into calcite (Reaction 1) (Barthust, 1975), and the second reaction mechanism is suggesting coprecipitation of Ca^{2+} and Mg^{2+} together with CO_3^{2-}(Reaction 2) (Lippman, 1973). For the first set (Mg:Ca ratio 2), in XRD traces,

dolomite main peak appeared only after nesquehonite and calcite formation completed. It was thought that nesquehonite dissociates first to give its Mg^{2+} which then reacts with calcite as in Reaction 1. Since, dolomite crystals were found located around the dissociated nesquehonite crystals in SEM images, that type of reaction mechanism was thought to be possible. However, in the experiment described in section 4.7, the addition and carbonation of $Ca(OH)_2$ on nesquehonite crystals didn't lead to any dolomite formation. Instead, calcite was formed (Figure 100).

In the second set (Mg:Ca ratio 1), combined results of XRD and SEM suggest that $Ca(OH)_2$ and $Mg(OH)_2$ nanoparticles integrate and carbonate together to yield dolomite as in Reaction 2. The obtained dolomite at the 10^{th} day of carbonation doesn't seem to have the presence of nesquehonite or calcite in SEM images (Figure 84). Therefore in that set, dolomitization follows dissolution-precipitation mechanism. Dolomite main peak appeared in XRD traces of the 2^{nd} day of carbonation products. However, the other major peaks were absent. Therefore, it can be said that the carbonation process follows Ostwald's ripening-step rule which states formation of intermediate phases that leads to the final precipitate.

Although dolomite formation is thermodynamically favoured in terms of free energy of formation and solubility product, its formation is inhibited by kinetic factors (due to the requirement of the perfect ordering of Ca^{2+} and Mg^{2+} cations between CO_3^{2-} anions, respectively) (Lippman, 1973; Folk, 1974) as described in section 2.4. In this study, it can be said that dolomite formation is achieved by overcoming kinetic factors by using nanoparticles in alcohol dispersion.

In the light of those results obtained, it is concluded that the alcohol dispersion of $Ca(OH)_2$ and $Mg(OH)_2$ nanoparticles will be a compatible consolidation material for deteriorated dolomite.

5.5.2 Effect of Mg:Ca Ratio on Dolomitization

Mg:Ca ratio of the solution affects the carbonation characteristic of $Ca(OH)_2$ and $Mg(OH)_2$ nanoparticles. Although, in nature, dolomite is observed in Mg-rich mediums like marine sediments or evaporites, in this thesis, the increase in Mg ratio results in nesquehonite formation and inhibits dolomite formation. There might be several reasons for this inhibition. It is probable that strong hydration behaviour of Mg^{2+} ions inhibits dolomite formation. In literature, the inhibitory effect of magnesium ions on growing calcite crystal, which affect the chemical composition and mineralogy of the phases formed, is mentioned (Loste *et al*., 2003).

5.6 Consolidation of Deteriorated Dolostone with the Alcohol Dispersion of $Ca(OH)_2$ and $Mg(OH)_2$ Nanoparticles

In the thesis, the main purpose was the consolidation of deteriorated dolomite with a compatible material. Dolomite formation was achieved in petri dishes by the use of alcohol dispersion involving $Ca(OH)_2$ and $Mg(OH)_2$ nanoparticles in special carbonation conditions. Therefore, the use of that dispersion, and those special carbonation conditions will be a proper consolidation method for deteriorated dolomite.

In the consolidation process of deteriorated dolomite samples, the alcohol dispersion was injected through cracks and pores, also by capillary suction through the selected surface of stone samples. Since the dispersion has penetrated through the capillaries and pores, layering of the carbonation products was assumed to be minimized in comparison to layering in petri dish. In SEM images, newly formed nano-dolomite aggregates, which are in 100-200 nm size, and mostly in oval shape can be observed on the dolomite crystals of the sample (Figure 108&Figure 109).

One of the non-destructive techniques to understand the effect of consolidation is ultrasonic velocity measurements. The average UPV value of deteriorated dolomite sample was 1844±64 m/s. It increased to 2158±70 m/s after treatment (Table 11).

Additional experiment was done to control the adhesive property of the carbonation products for broken dolomite sample. After application of alcohol dispersion, and its carbonation for a long time, strong joining of broken pieces confirms the adhesive property of the carbonation products (Figure 112). Since dolomite crystals of the stone provide the sites for the adhesion of newly formed dolomite aggregates, it is possible that dolomite nucleation and formation within dolostone might be easier.

To sum up, dolomite formation was achieved within dolostone cracks or pores which were confirmed by SEM images. Increase in the average UPV values of consolidated dolostone samples confirm the improvement in physico-mechanical properties. Besides, broken pieces of dolostone was strongly joined together after the treatment with alcohol dispersion of $Ca(OH)_2$ and $Mg(OH)_2$ nanoparticles prepared from the dolostone itself. Therefore, the produced alcohol dispersion of nanoparticles will be a proper consolidation material for deteriorated dolomite. It is a medication for deteriorated stone that is prepared from the stone itself, which will be advantageous in restoration works.

5.7 Production Specifications of the Alcohol Dispersion of $Ca(OH)_2$ and $Mg(OH)_2$ Nanoparticles from Dolostone

As the outcome of the research, the preparation procedure of alcohol dispersion of $Ca(OH)_2$ and $Mg(OH)_2$ nanoparticles from dolostone itself is described in steps below

- Obtaining dolostone samples (from Midyat-Mardin Yolbaşı quarries in the thesis),
- Crushing large dolostone sample into small pieces,
- Powdering small dolostone pieces by the help of pulverizer,
- Sieving the powdered sample,
- Collection of the powdered sample under 125μ,

- Thermal decomposition of powdered sample that is smaller than 125μ and to obtain CaO (lime) and MgO (periclase) at 900 ºC for 4 hours in the oven,
- Slaking of CaO and MgO to obtain $Ca(OH)_2$ (portlandite) and $Mg(OH)_2$ (brucite) nanoparticles,
- Dispersion of $Ca(OH)_2$ and $Mg(OH)_2$ nanoparticles in ethyl alcohol to obtain nanodispersive solution (consolidant) with 5g/100ml concentration,
- 2 hours of ultrasonic vibration and 24 of hours magnetic stirrer,
- Verification of mineralogical composition of nanodispersive solution by XRD,
- Follow up of the change in Mg:Ca ratio in time by measuring the concentrations of $Mg(OH)_2$ and $Ca(OH)_2$ in the nanodispersive solution by comparing their XRD traces (Figure 42 and Table 9).

CHAPTER 6

CONCLUSION

There are two main purposes of the study. The first aim is to prepare a compatible consolidation material for the historical structures whose building stone is dolostone, and the second aim is to propose a consolidation treatment method for dolostone conservation.

In the first part of the study, starting from the dolostone itself, an alcohol dispersion of $Ca(OH)_2$ and $Mg(OH)_2$ nanoparticles was prepared. In the second part, the formation of dolomite within deteriorated zones of dolostone was studied for a compatible consolidation treatment. Prior to consolidation treatment, synthesis of dolomite was studied in petri dishes. It is seen that relative humidity, CO_2 partial pressure, and Mg:Ca ratio of the solution play important role in the carbonation process of $Ca(OH)_2$ and $Mg(OH)_2$ nanoparticles. Together with the key factors listed below, it is shown that dolomite is synthesized at room temperature by overcoming the kinetic barrier that inhibits dolomite formation at the laboratory.

- To study at nanoscale by using $Ca(OH)_2$ and $Mg(OH)_2$ nanoparticles (sizes were 500nm-1μm and around 100nm respectively),
- To produce $Ca(OH)_2$ and $Mg(OH)_2$ nanoparticles from dolostone itself. So they were well integrated together.
- Use of alcohol dispersion right after its preparation when Mg:Ca ratio was 1,
- Carbonation of nanoparticles together at high relative humidity (90-95%) and high CO_2 partial pressure (pCO_2~0.4 atm),
- To let the carbonation system, stay calm without disturbing the equilibrium established between RH, CO_2, and dispersion until the carbonation process is complete (at least 10 days in this thesis).

Towards dolomitization, the combination of SEM, XRD, and FTIR analyses suggest that portlandite and brucite in the dispersion integrate together and carbonate together, i.e., they follow coprecipitation reaction. When they integrate together, they form aggregates and form an intermediate phase (Figure 91). This phase transforms to dolomite upon further carbonation. The synthesized dolomite in petri dish appears as aggregates around 100-500nm size in SEM views. On those aggregates, much smaller nanoparticles with sizes around 5 to 20 nm are also observed. XRD reflections of synthesized dolomite match well with those of Midyat dolomite.

Deteriorated dolostone sample was consolidated with the prepared alcohol dispersion of $Ca(OH)_2$ and $Mg(OH)_2$ nanoparticles by injection through the cracks and pores, and by capillary suction, followed by carbonation process. The effectiveness of the consolidation treatment was followed through UPV_{direct} measurements and SEM. Average UPV_{direct} value of treated dolostone sample increased from 1844 m/s to 2158 m/s, quite close to characteristic UPV readings of the same dolostone sample (2400 m/s) measured from the sound parts of the sample. In the SEM images, newly formed dolomite nanoparticle aggregates could easily be identified and distinguished from its bulk state. They settled with a well adhesion within capillaries and pores.

In conclusion, at the start of the study, the research questions were “Is it possible to consolidate dolostone by producing dolomite within deteriorated zones (in the cracks or pores) of the stone?” and “How can we integrate nanotechnology into stone conservation studies?”. Those questions were answered by introducing a new nano-consolidation material and treatment method of this consolidation material, for deteriorated dolostone, to the field of cultural heritage conservation.

All experiments conducted at the Materials Conservation Laboratory and this study explains the experimental results obtained at the laboratory. The development of practical application solutions for on-site consolidation practices and in-situ monitoring the effectiveness of the treatments necessitate further detailed and multidisciplinary studies involving non-destructive methods.

REFERENCES

Alderman, A.R., von der Borch, C.C., 1963. Dolomite reaction series, Nature, 198 (4879), 465–466.

Althoff P. L., 1977, Structural refinements of dolomite and a magnesian calcite and implications for dolomite formation in marine-environment. Am. Mineral. 62 (7–8), 772–783.

Alonso-Zarza, A. M. and Martin-Perez, A., 2008, Dolomite in caves: Recent dolomite formation in oxic, non-sulfate environments. Castaar Cave, Spain, Sedimentary Geology, 205, 160-164.

ASTM, 1990. D 2845-90. Standard Test Method for Laboratory Determination of Pulse Velocities and Ultrasonic Elastic Constants for Rock, in American Society for Testing and Materials, (p. 361-365).

Badiozamani, K., 1973, The Dorag dolomitization model-application to the Middle Ordovician of Wisconsin: Jour. Sed. Petrology, 43, 965-984.

Baker PA, Kastner M. 1981. Constraints on the formation of sedimentary dolomite. Science, 213, 214–216.

Baron, G., 1960. Sur la synthese de la dolomie. Application au phenomene de dolomitization. Rev. Inst. Fr. Pet. Ann. Combust Liq, 15 (1), 3-68

Bathurst, R.G.C., 1975, Carbonate sediments and their diagenesis: Development in sedimentology, NO.12. Amsterdam, Elsevier, 658 p.

Behre, C.H. Jr., 1947. Geochemistry and localization of dolomitization. J. Geol., 42, 540–542.

Berner, R.A., 1975, The role of magnesium in the crystal growth of calcite and aragonite from sea water, Geochimica et Cosmochimica Acta, 39 (4), 489-494.

Bischoff, W.P., Bishop, F.C. and Mackenzie, F.T., 1983, Biologically produced magnesian calcite: Inhomogenities in chemical and physical properties, comparision with synthetic phases, American Mineralogist, 68, 1183-1188.

Blee, A., Matisons, J.G., 2008, Nanoparticles and the conservation of cultural heritage, Materials Forum, 32, 121-128.

Busenberg E. and Plummer L. N., 1989, Thermodynamics of magnesian calcite solid-solutions at 25-degrees-C and 1-atm total pressure. Geochim. Cosmochim. Acta 53 (6), 1189–1208.

Caner E .N, Demirci, S., Turkmenoglu, A.G., l985, Deterioration of Dolomite by Soluble Salts in Divrigi Great Mosque Turkey VtH. International Congress on Deterioration and Conservation of stone, Lousane.

Caner Saltık, E.N., 2009, Divriği Ulu Camii ve Darüşşifası Koruma Projesi Kapsamı: Anıtın Sorunlarının Teşhisi ve Koruma Uygulamalarını Belirleyecek Araştırmalar, Kagir Yapılarda Koruma ve Onarım Semineri.

Caner E., 2011, Limestone decay in historic monuments and consolidation with nanodispersive calcium hydroxide solutions. Middle East Technical Univeristy, Phd Thesis, Ankara.

Chave, K.E., 1952, A solid solution between calcite and dolomite, J. Geol., 60, 190–192.

Chelazzi, D., Poggi, G., Jaidar, Y., Toccafondi, N., Giorgi, R., Baglioni, P., 2013, Hydroxide nanoparticles for cultural heritage: Consolidation and protection of wall paintings and carbonate materials, Journal of Colloid and Interface Science, 392, 42-49,

Daehne, A., Hern, C., 2013, Calcium hydroxide nanosols for the consolidation of porous building materials, Heritage Science, v. 1:11.

Daniele, V., Taglieri, G., Quaresima, R., 2008, The Nanolimes in cultural heritage conservation: characterization and analysis of the carbonation process, Journal of Cultural Heritage, 9 (3), 294-301.

Davies, P.J., Bubela, B., 1973, The transformation of nesquehonite to hydromagnesite, Bureau of mineral resources, geology and geophysics.

Davies P. J., Bubela, B., Ferguson, J., 1975, Simulation of Carbonate Diagenetic Processes: Formation of dolomite, huntite and monohydrocalcite by the reactions between nesquehonite and brine, Bureau of Mineral Resources, Geology and Geophysics.

Davis K. J., Dove P. M. and De Yoreo J. J., 2000, The role of Mg^{2+} as an impurity in calcite growth. Science, 290 (5494), 1134– 1137.

Davis K. J., Dove P. M., Wasylenki L. E. and De Yoreo J. J., 2004, Morphological consequences of differential Mg^{2+} incorporation at structurally distinct steps on calcite, Am. Mineral, 89 (5–6), 714–720.

Dei, L., Salvadori, B., 2006, Nanotechnology in Cultural Heritage Conservation: Nanometric Slaked Lime Saves Arcitectonic and Artistic Surfaces from Decay, Journal of cultural heritage, 7, 110-115.

Doehne, E., Price, C.A., 2010, Stone Conservation: An Overview of Current Research, Getty Publications, LA, p:176.

Dowty E, 1999, ATOMS 5.0, a computer program for displaying atomic structures. Kingsport, TN.

Dupraz S, Parmentier M, Menez B, Guyot F. 2009. Experimental and numerical modeling of bacterially induced pH increases and calcite precipitation in saline waters, Chemical Geology, 265, 44–53.

Fairbridge, R.W., 1957. The dolomite question. In: LeBlanc, R.J., Ž. Breeding, J.G. Eds. , Regional Aspects of Carbonate Deposition. Spec. Publ.-SEPM, 5, 125–178.

Faust, G. T., 1953, Huntite, $Mg_3Ca(CO_3)_4$, a new mineral, Am. Mineralogist, 38, 4-24

Fernandez-Diaz, L., Putnis, A., Prieto, M., Putnis, C.V., 1996, The role of magnesium in the crsytallization of calcite and aragonite in a porous medium, Journal of sedimentary research, 66 (3), 482-491.

Folk, R.G., 1974, The natural history of crystalline calcium carbonate: effect of magnesium content and salinity: Jour. Sed. Petrology, 44, 40-53.

Folk, R. L., and Land, L. S., 1975, Mg/Ca ratio and salinity: two controls over crystallization of dolomite: American Assoc. Petroleum Geol. Bull., 59, 60-68.

Friedman, G.M., Sanders, J.E., 1967, Origin and occurrence of dolostones. In: Chilingar, G.V., Bissell, H.J., Fairbridge, R.W. Ž. Eds. , Carbonate Rocks, Origin, Occurrence, and Classification. Elsevier, Amsterdam, pp. 267–348.

Friedman, G.M., 1991, Methane-generated lithified dolostone of Holocene age; eastern Mediterranean, Journal of Sedimentary Research, 61 (2), 188–194.

Gaines, A. M., 1974, Protodolomite synthesis at 1008 C and atmospheric pressure, Science, 183, 518–520.

Gaines, A. M., 1977, Protodolomite redefined, J. Sed. Petrol., 47, 543–546.

Garcia, E.; Alfonso, P.; Tauler, E.; Gali, S., 2003, Surface alteration of dolomite in dedolomitization reaction in alkaline media, Cement and concrete Research, 33, 1449-1456.

Garrels, R.M., Thompson, M.E., Siever, R., 1960, Stability of some carbonates at 25 ^oC and 1 atmosphere total pressure, Am, J. Sci, 258, 402-418.

Garrels, R.M., Thompson, M.E., 1962, A chemical model for sea water at 25 ^oC and one atmosphere total pressure, Am. J. Sci, 260, 57-66

Gieseler, J., Quidant, R., Dellago, C., Novotny, L., 2014, Dynamic relaxation of a levitated nanoparticle from a non-equilibrium steady state, Nature Nanotechnology, doi:10.1038/nnano.2014.40

Giester, G., Langauer, L. C., Rieck, B., 2000, The Crystal Structure of nesquehonite, $MgCO_3.3H_2O$ from Lavrion, Greece, Mineralogy and Petrology, 70, 153-163.

Gilliott, J. E.; Swenson, E. G., 1969, Mechanism of the alkali-carbonate rock reaction, Engineering Geology, 2, 7-23

Giorgi, R., Bozzi, C., Dei, L., Gabbiani, C., Ninham, B. W., Baglioni, P., 2005, Nanoparticles of $Mg(OH)_2$: synthesis and application to paper conservation, Langmuir, 21, 8495-8501.

Goldsmith J. R. and Graf D. L., 1958, Relation between lattice constants and composition of the Ca–Mg carbonate, Am. Mineral, 43, 84–101.

Goldsmith J. R., Graf D. L. and Heard H. C., 1961, Lattice constants of the calcium–magnesium carbonates, Am. Mineral, 46, 453–459.

Gomez-Villalba, L.S., Lopez-Arce, P., Zornoza-Indart, A., Alvarez de Buergo, M., Fort, R., 2012, Modern Restoration products based on nanoparticles: The case of Nano-Lime, Interaction and compability with limestone and dolostone surfaces, advantages and limitations. In EGU General Assembly Conference Abstracts, vol 14, p:2418.

Gordey, W. G., 1971, Stratigraphy and Sedimentation of the Cretaceous Mardin Formation in Southeastern Turkey, 13th Annual Conference of Petroleum Exploration Society of Libya, in Geology and History of Turkey, p:317-348, edited by Campbell, A.S.

Graddy, M. M., Gibson, E. K., Wright, J. P., Pillinger, C. T., 1989, Meteoritics, 24, 1.

Graf, D.L., Goldsmith, G.R., 1956, Some hydrothermal syntheses of dolomite and protodolomite, J. Geol, 64, 173–186.

Gregg, J.M., Howard, S.A., Mazzullo, S.J., 1992. Early diagenetic Ž.recrystallization of Holocene -3000 years old peritidal dolomites, Ambergis Cay, Belize, Sedimentology, 39, 143–160.

Gregg, J. M., Bish, D. L., Kaczmarek, S. E., and Machel, H. G., 2015, Mineralogy, nucleation and growth of dolomite in the laboratory and sedimentary environment: A review, Sedimentalogy, 62, 1749-1769.

Gunasekaran, S., Anbalagan, G., Pandi, S., 2006, Raman and Infrared spectra of carbonates of calcite structure, Journal of Raman Spectroscopy, 37, 892-899.

Hadley, D. W., 1961, Alkali reactivity of carbonate rocks- expansion and dedolomitization, Symposium Highway Reseasrch. Board. 40, 462-474.

Hanchen, M., Prigiobbe, V., Baciocchi, R., Mazzotti, M., 2007, Precipitation in the Mg-carbonate systems-effects of temperature and CO_2 pressure, Chemical Engineering Sciences, 63, 1012-1028.

Hardie, L.A., 1987, Dolomitization; a critical view of some Ž. current views. J. Sediment. Petrol, 57 (1), 166–183.

Hewett, D.F., 1928, Dolomitization and ore deposition. Econ. Geol, 23, 821–863.

Holder, C.F., Schaak, R.E., 2019, Tutorial on Powder Diffraction for Characterizing Nanoscale Materials, ACS Nano, 13 (7), 7359-7365.

Horn, G., 1969, Löslichkeitskonstanten und Freie Bildungsenthalpien von Magnesit, Brucit und Dolomit. Radex-Rundschau, 439-459.

Hummel, W., Berner, U.R., Curti, E., Pearson, F. J., 2002, Nagra/PSI Chemical Thermodynamic Data Base 01/01, Radiochimica Acta, 90, 9-11.

Jie, Z., Jianfeng, S., Yigang, W., Yingchu, W., Xingping, Z., Anping, H., 2011, Dedolomitization: types, mechanism and its releasionship to carbonate reservoir properties, AAPG Annual Covention and Exhibiton, Houstan, Texas, USA, 10-13.

Jull, A. J. T., Cheng, S., Gooding, J. L., Velbel, M. A., 1988, Rapid Growth of Magnesium-Carbonate Weathering Products in a Stony Meteorite from Antarctica, Science, New Series, 242 (4877), 417-419.

Kaczmarek, S.E., Sibley, D. F., 2007, A comparison of nanometer-scale growth and dissolution features on natural and synthetic dolomite crystals: Implications for the origin of dolomite, Journal of Sedimentary Research, 77, 424–432.

Kaczmarek, S.E., Sibley, D. F., 2011, On the evolution of dolomite stoichiometry and cation order during high-temperature synthesis experiments: An alternative model for the geochemical evolution of natural dolomites, Sedimentary Geology, 240, 30–40.

Kaczmarek, S.E., Sibley, D. F., 2014, Direct physical evidence of dolomite recrystallization, Sedimentology, 61, 1862–1882.

Kaczmarek, S. E., Gregg, J. M., Bish, D. L., Machel, H. G., and Fouke, B.W., 2017, Dolomite, very high-magnesium calcite, and microbes-implications for the microbial model of dolomitization, Society for Sedimentary Geology, 109, 7-20.

Katz, A., Matthews, A., 1977, The dolomitization of $CaCO_3$, Geochimica et Cosmochimica Acta, 41, 297–308.

Kenward, P.A., Fowle, D.A., Goldstein, R.H., Ueshima, M., Gonza ´lez, L.A., Roberts, J. A., 2013, Ordered low-temperature dolomite mediated by carboxyl-group density of microbial cell walls, American Association of Petroleum Geologists Bulletin, 97, 2113–2125.

Kinsman, D.J.J., 1967, Huntite from a Carbonate Evaporite Environment. Am. Mineralogist, 52, 1332-1340.

Kloprogge, J. T., Martens, W. N., Nothdurft, L., Duong, L.V., Webb, G. E., 2003, Low Temperature Synthesis and Characterization of Nesquehonite, Journal of Materials Science Letters, 22, 825-829.

Konigsberger, E. and Gamsjager, H., 1992, Solid-solution aqueoussolution equilibria – thermodynamic theory and representation, Am. J. Sci., 292(3), 199–214.

Kulik, D. A., 2006, Dual-thermodynamic estimation of stoichiometry and stability of solid solution end members in aqueoussolid solution systems. Chem. Geol. 225 (3–4), 189–212.

Land, L. S., 1967, Diagenesis of skeletal carbonates, Journal of Sedimentary Petrology, 37, 914–930.

Land, L.S., 1985, The origin of massive dolomite. J. Geol. Educ. 33, 112–125.

Land, L.S., 1998, Failure to precipitate dolomite at 25 degrees C from dilute solution despite 1000-fold oversaturation after 32 Ž. Years, Aquat. Geochem., 4 (3–4) , 361–368.

Landes, K.K., 1946, Porosity through dolomitization, Am. Assoc. Petrol. Geol. Bull., 30, 305–318.

Langmiur, D., 1965, Stability of Carbonates in the System $MgO-CO_2-H_2O$, The Journal of Geology, 73 (5), 730-754.

Lenntech calculator, Converter Parts Per Million (ppm) from https://www.lenntech.com/calculators/ppm/converter-parts-per-million

Lippman, F., 1960, Versuche zur Aufklarung der Bildungsbedingungen von Calcit und Aragonite: Fortschritte der Mineralogie, 38, 156-161.

Lippman, F., 1973, Sedimentery carbonate minerals: New York. Springer Werlag, 228p.

Lopez- Arce, P., Gomez- Villalba, L.S., Pinho, L., Fernandez-Valle, M.E., Alvarez de Buergo, M., Fort, R., 2010, Influence of porosity and relative humidity on consolidation of dolostone with calcium hydroxide nanoparticles: Effectiveness assessment with non-destructive techniques, Materials Characterization, 61, 168-184.

Lopez-Arce, P., Gomez-Villalba, L.,Martinez-Ramirez, S., Alvarez de Buergo, M., 2011, Powder Technol., 205 (1), 263-269.

Lopez-Arce, P., Zornoza-Indart, A., Gomez-Villalba, L., Fort, R., 2013, Journal of Mater. Civ. Eng., 25 (11), 1655-1665.

Lopez-Arce, P., Zornoza-Indart, A., 2015, Carbonation acceleration of calcium hydroxide nanoparticles:induced by yeast fermentation, Appl. Phys. A, 120, 1475–1495

Loste, E., Wilson, R. M., Seshadri, R., and Meldrum, F. C., 2003, The role of magnesium in stabilising amorphous calcium carbonate and controlling calcite morphologies, J. Cryst. Growth, 254 (1–2), 206–218.

Machel, H.G., 2004, Concepts and models of dolomitization-A critical reappraisal. In Braithwaite CJR, Rizzi, G., Darke, G. (Editors), The Geometry and Petrogenesis of Dolomite Hydrocarbon Reservoirs, Special publication 235: Geological Society, London, p:7-63.

Martin-Perez, A., Kosir, A., Otonicar, B., 2015, Dolomite in Speleothems of Snezna Jama Cave, Slovenia, Acta Carsologica, 44 (1), 81-100.

Martin-Perez, A., Martin-Garcia, R. And Alonso-Zarza, A. M., 2012, Diagenesis of a Drapery Spleothem from Castanar Cave: from Dissolution to Dolomitization, International Journal of Speleology, 41(2), 251-266.

Medlin, W.L., 1959. Preparation of synthetic dolomite, Am. Mineral, 44, 979–986.

Morrow, D.W., 1982, Diagenesis 1. Dolomite-Part 1. The chemistry of dolomitization and dolomite precipitation, Geosicience Canada, 9 (1), 5-13.

Morrow, D.W., 1982, Diagenesis 2. Dolomite-Part 2. Dolomitization Models and Ancient Dolostones, Geosicience Canada, 9 (2).

Morrow, D. W., Ricketts, B.D., 1988, Experimental investigation of sulfate inhibition of dolomite and its mineral analogues. In Shukla V, Baker PA (Editors). Sedimentology and Geochemistry of Dolostones, Special Publication 43: SEPM (Society for Sedimentary Geology), Tulsa, Oklahoma. p. 25–38.

Morse, J.W., Casey, W.H., 1988, Ostwald processes and mineral paragenesis in sediments, Am. J. Sci, 288, 537–560.

Mucci, A. and Morse, J.W., 1983, The incorporation of Mg^{2+} and Sr^{2+} into calcite over growths: Influences of growth rate and solution composition, Geochimica et Cosmochimica Acta, 47, 217-233.

Neher, J., Rohrer, E., 1958, Dolomitbildung unter mitwirkung von bacterien, Eclogae Geologicae Helvetiae 51, 213–215.

Noyes, R. M., 1962, Thermodynamics of ion hydration as a measure of effective dielectric properties over water, J. Am. Chem, Soc., 84, 513-522.

Palache, C., Berman, H., Frondel, C., 1951, The System of Mineralogy, v:2 (7th ed.), New York, John Wiley & Sons, 1124 p.

Paquette, J. and Reeder, R. J., 1990, New type of compositional zoning in calcite – insights into crystal-growth mechanisms, Geology, 18(12), 1244–1247.

Reeder, R. J., 1983, Crystal chemistry of the rhombohedral carbonates. In: Carbonates: Mineralogy and Chemistry (Ed. R.J. Reeder), Mineral. Soc. Am. Rev. Mineral., 11, 1–47.

Ries, J.B., 2010, Review: geological and experimental evidence for secular variation in seawater Mg/Ca (calcite-aragonite seas) and its effects on marine biological calcification, Biogeosciences, 7, 2795–2849

RILEM. 1980a. Tentative Recommendations, Commission – 25 – PEM, Recommended Test to Measure the Deterioration of Stone and to Assess the Effectiveness of Treatment Methods. Materials and Structures, 13 (73), 173-253.

Riviere, A., 1939, Sur la dolomitization des sediments calcaires. Comptes Rendus 209, 597–599.

Rodriguez-Navarro, C., Suzuki, A., Ruiz- Agudo, E., 2013, Alcohol dispersions of calcium hydroxide nanoparticles for stone conservation, Langmuir, 29, 11457-11470.

Sa´nchez-Roma´n M., Vasconcelos C, Schmid T, Dittrich M, McKenzie JA, Zenobi R, Rivadeneyra MA., 2008, Aerobic microbial dolomite at the nanometer scale: Implications for the geologic record, Geology, 36, 879–882.

Sayles, F.L., Fyfe, W.S., 1973, Crystallization of magnesite from aqueous solution, Geochimica et cosmochimica acta, 37 (1), 87-99.

Shannon, R. D., 1976, Revised effective ionic-radii and systematic studies of interatomic distances in halides and chalcogenides. Acta Crystallogr. Sect. A 32(SEP1), 751–767.

Sherwood, W. C. and Newlon, N. H., 1964, Studies on the mechanisms of alkali-carbonate rock reaction. Part 1- Chemical reactions. Washington Symposium Highway Reseasrch. Board, 45, 41-56.

Sibley, D.F., Dedoes, R.E., Bartlett, T.R., 1987, Kinetics of dolomitization, Geology 15, 1112–1114.

Sibley, D. F., 1990, Unstable to stable transformations during dolomitization, Journal of Geology, 98, 739–748.

Sibley, D. F., Nordeng, S.H., Borkowski, M.L., 1994, Dolomitization kinetics in hydrothermal bombs and natural settings, Journal of Sedimentary Research A, 64, 630–637.

Sierra-Fernandez, A., Gomez- Villalba, L.S., Rabanal, M.E., Fort, R., 2017, New Nanomaterials for applications in conservation and restoration of stony materials: A review, Materiales de Construccion, 67,325.

Simona, E., Murph, H., Coopersmith, K. J., Larsen, G. K., 2017, Nanoscale Materials: Fundamentals and Emergent Properties, in Anisotropic and Shape-Slective Nanomaterials, ch: 2, p: 7-28, Springer International Publishing AG.

Skeats, E.W., 1905, The chemical and mineralogical evidence as to the origin of dolomites of southern Tyrol. Q, J. Geol. Soc., London 61, 97–141.

Steidtmann, E., 1926, The origin of dolomites. In: Twenhofel, Ž. W.H. Ed. , Treatise on Sedimentation. Williams and Wilkins, Baltimore, MD, pp. 256–265.

Strakhov, N.M., 1958, Facts and hypotheses in the problem of the formation of dolomite rocks. Izv. Akad. Nauk S.S.S.R. Ser. Geol. 6, 3–22.

TUBITAK-CNR–Bilateral Project 213M554: Stone consolidation with innovative nanodispersive products for the conservation of cultural heritage in the Mediterranean Basin. Projects funded within the scope of TUBITAK International Academic Support Programs Projects to support the integration to international projects and research networks (1011 etc.) Tübitak-İtalya Ulusal Araştırma Konseyi(CNR) İşbirliği proje, 1 JUNE 2014 - 1 JULY 2017.

Usdowski, E., 1994, Synthesis of dolomite and geochemical implications. In Purser BH, Tucker ME, Zenger D (Editors). Dolomites: A Volume in Honour of Dolomieu, International Association of Sedimentologists Special Publication 21: Blackwell, Oxford, UK. p. 345–360.

Van Tuyl, F.M., 1918, Depth of dolomitization, Science 48, 350–352.

Vasconcelos, C., McKenzie J.A., Bernasconi S., Grujic D., Tiens A.J., 1995, Microbial mediation as a possible mechanism for natural dolomite formation at low temperatures. Nature, 377, 220–222.

Vasconcelos, C., McKenzie, J.A., 1997, Microbial mediation of modern dolomite precipitation and diagenesis under anoxic conditions (Lagoa Vermelha, Rio de Janeiro, Brazil). Journal of Sedimentary Research 67 (3), 378–390

Vasconcelos C., McKenzie J.A., 2008, Dolomite as a biomineral and possible implications. Revista de la Sociedad Espa˜nola de Mineralog´ıa, 9, 21–22.

Von Morlot, A., 1847, Uber die dolomit und seine kunstliche darstellung aus kalkstein. Haidinger Naturwiss, Abhandl. 1, 305.

Vorontsov, A. V. and Tsybulya, S.V., 2018, influence of nanoparticles size on XRD patterns for small monodisperse nanoparticles of Cu^0 and TiO_2 Anatase, Ind. Eng. Chem. Res., 57 (7), 2526-2536.

Warren, J., 2000, Dolomite: occurrence, evolution and economically important associations, Earth-Science Reviews, 52, 1-81.

Warthmann, R., Van Lith, Y., Vasconcelos, C., McKenzie, J. A., Karpoff, A. M., 2000, Bacterially induced dolomite precipitation in anoxic culture experiments. Geology, 28, 1091–1094.

Wautelet, M., Shiriyan, A.S., 2009, Thermodynamics: Nano vs. macro, pure applied chemistry, 81 (10), 1921-1930.

Wells, A.J., 1962, Recent dolomite in the Persian Gulf, Nature, 194, 274–275.

Wenk, H.R., Hu, M., Frisia, S., 1993, Partially disordered dolomite: microstructural characterization of Abu Dhabi sabkha Ž. carbonates. Am. Mineral. 78 (7–8) , 769–774.

Wigley, T.M.L. and Plummer, L.N., 1976, Mixing of carbonate waters: Geochim. Cosmochim, Acta, 40, 989-995.

Winland, D., 1969, Stability of calcium carbonate polymorphs in warm, shallow seawater, Journal of Sedimentary petrology, 39 (4), 1579-1587.

Woods, T. L. and Garrels, R. M., 1987, Thermodynamic Values at Low Temperature for Natural Inorganic Materials: An Uncritical Summary.

Wright, D. T., Wacy, D., 2005, Precipitation of dolomite using sulphate-reducing bacteria from the Coorong region, South Australia: Significance and implications, Sedimentology, 52, 987–1008.

Young, R.B., 1933, Conditions of deposition of the Dolomite Series. Trans. Geol. Soc. S. Afr. 36, 135–1221.

Zenger, D.H., Dunham, J.B., Ethington, R.L., 1980, Concepts and models of dolomitization. Spec. Publ.-SEPM 28, 320 pp.

Zhao, L., Sang, L., Chen, J., Ji., J.,2010, Aqueous carbonation of natural brucite: relevance to CO_2 sequestration, Environ Science Technology, 44 (1), 406-411.

Zhang, F., Xu, H., Konishi, H., Shelobolina, E. S., Roden, E.E., 2012, Polysaccharidecatalyzed nucleation and growth of disordered dolomite: A potential precursor of sedimentary dolomite. American Mineralogist, 97, 556–567.

Zhang, X.; Glasser, F. P.; Scrivener, K. L., 2014, Reaction kinetics of dolomite and portlandite, Cement and Concrete Research, 66, 11-18.

CURRICULUM VITAE

PERSONAL INFORMATION

Surname, Name : Karahan Dağ, Fulya
Nationality : Turkish (TC)
Date and Place of Birth : 12 August 1985, Ankara
E-mail : flykarahan@gmail.com

EDUCATION

Degree	Institution	Year of Graduation
PHD	METU-Archaeometry	2021
MS	METU Chemistry	2011
BS	METU Chemistry	2008
High School	Ankara Atatürk High School	2003

WORK EXPERIENCE

Year	Place	Enrollment
2015-Present	METU-GSNAS	Academic
2014-2015	METU Central Laboratory	Research Assistant
2009-2014	METU-GSNAS	Research Assistant

FOREIGN LANGUAGES

Advanced English

APPLIED PATENT

Turkish Patent (applied on 15th August 2019)**,** Dolostone Consolidation.

PCT Patent (Applied on 13rd August 2020), Dolomite Consolidation.

PROJECTS INVOLVED

Researcher: METU Scientific Research Project (2018): GAP-201-2018-2811. Consolidation of Deteriorated Dolomite Compatible with Its Own Structure by Using Alcohol Dispersion of Nanoparticles

Scholar: TUBITAK-CNR–Bilateral Project 213M554: Stone consolidation with innovative nanodispersive products for the conservation of cultural heritage in the Mediterranean Basin. 1 JUNE 2014 - 1 JULY 2017.

CONFERENCE PUBLICATIONS

1. Karahan Dağ, F., Caner-Saltık, E.N., Tavukçuoğlu, A. (2018). Assesing the Usage of Calcium and Magnesium Hydroxide Nanoparticles as Consolidant for Dolostones. In: Koui M., Zezza F., Kouis D. (eds): *10th International Symposium on the Conservation of Monuments in the Mediterranean Basin- Natural and Anthropogenic Hazards and Sustainable Preservation – MONUBASIN 2017* (pp. 135-142), 20-22 September 2017, Athens, Greece. Springer, Cham. URL: https://link.springer.com/chapter/10.1007/978-3-319-78093-1_13

2. Karahan-Dag, F., Caner-Saltık, E.N., Tavukçuoğlu, A. (2018). Dolostone conservation with nanodispersive solutions. In, A. Macchia, N. Masini, M.F. La Russa, F. Prestileo (Eds.): Dialogues in Cultural Heritage - *Books of Abstracts of the 6th YOCOCU Conference (Youth in Conservation of Cultural Heritage)*, 22-26 May 2018, Matera, Italy (p. 309-311s). Matera: YOCOCU.

3. Karahan Dağ, F., Mısır, Ç.T., Çömez, S., Erdil, M., Tavukçuoğlu, A., Caner-Saltık, E.N., Güney, B.A. & Caner, E. (2016). Assessment of Dolomite Conservation by Treatment with Nano-Dispersive Calcium Hydroxide Solution. In J.J. Hughes, T. Howind (Eds.): Science and Art: A Future for Stone: *Proceedings of the 13th Int. Congress on the Deterioration and Conservation of Stone, Vol. 2*, 6 - 10 September 2016, Paisley, Scotland (pp. 839-846). University of the West of Scotland, Paisley, Scotland. http://researchportal.uws.ac.uk/portal/files/397446/13th_ICDCS_Paisley_2016_VOL_II.pdf.